Design and Evaluation of Novel Lipid-based Nanocarrier Systems of Tofacitinib for Better Treatment of Rheumatoid Arthritis

THESIS

Submitted in partial fulfillment
of the requirements for the degree of

DOCTOR OF PHILOSOPHY

by

Ms. GORANTLA SRIVIDYA

ID. No. 2018PHXF0414P

Under the Supervision of

Dr. GAUTAM SINGHVI

and

Co-Supervision of

Prof. RANENDRA N. SAHA

BITS Pilani
Pilani | Dubai | Goa | Hyderabad | Mumbai

BIRLA INSTITUTE OF TECHNOLOGY AND SCIENCE, PILANI

2023

DECLARATION

I declare that the thesis entitled "**Design and Evaluation of Novel Lipid-based Nanocarrier Systems of Tofacitinib for Better Treatment of Rheumatoid Arthritis"** work has been done by me under the guidance of Dr. Gautam Singhvi and Prof. Ranendra N. Saha, Department of Pharmacy, Birla Institute of Technology and Science, Pilani. No part of this thesis has previously formed the basis for the award of any degree or fellowship.

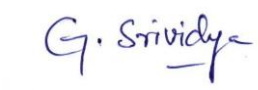

Srividya Gorantla,

2018PHXF0414P

Department of Pharmacy**,**

Birla Institute of Technology and Science, Pilani

Vidya Vihar, Pilani, Rajasthan 333031

DATE:

BIRLA INSTITUTE OF TECHNOLOGY AND SCIENCE, PILANI

CERTIFICATE

This is to certify that the thesis entitled **"Design and Evaluation of Novel Lipid-based Nanocarrier Systems of Tofacitinib for Better Treatment of Rheumatoid Arthritis**" and submitted by **Ms. Srividya Gorantla** ID No**. 2018PHXF0414P** for the award of Ph. D. of the institute embodies original work done by her under my supervision.

Signature of the Supervisor

Dr. Gautam Singhvi

Associate Professor,

Department of Pharmacy,

BITS-Pilani,

Pilani Campus, Rajasthan.

Signature of the Co-Supervisor

Prof. Ranendra N. Saha

Former Vice Chancellor (Acting) of BITS-Pilani, Pilani Campus,

Former Director of BITS-Pilani, Dubai campus, UAE

Date:

Acknowledgments

I would like to present my wholehearted gratitude to my Ph. D. supervisor, **Dr.Gautam Singhvi, Associate Professor, Department of Pharmacy, BITS Pilani**, Pilani Campus for giving me an opportunity to learn and grow under his guidance. He is one of those teachers who believe in bringing out the best of his students. As the saying goes, "*The best teachers are those who show you where to look but don't tell you what to see*". He always followed this approach and that helped me to learn and explore things beyond the routine lab work which I believe is going to help me soon. Apart from research, he taught us the value of punctuality, planning, ethics, and humility by example. He trained us to think, think and think some more before starting any work. He believed in extensive thought processes and planning before beginning any work. Besides, he was always there to help and advise regarding work or personal issues whenever required. It won't be wrong to say that words would not suffice in describing his contribution to my Ph. D.

I would take the opportunity to express my feelings through humble prayer as a mark of respect for my research co-supervisor **Prof. Ranendra N. Saha,** Senior Professor, Department of Pharmacy, Birla Institute of Technology Sciences - Pilani, Pilani Campus. I am thankful for his kind, cooperative, valuable help, guidance, and continuous encouragement during every phase of the dissertation. His way of sharing knowledge during crucial times are memorable.

It has been a matter of pride and honour for me to be a student of BITS Pilani. This thesis would not have seen the light of the day without the infrastructural and administrative support from the institute for which I owe a special thanks to **Prof. V Ramgopal Rao** Vice-Chancellor, BITS Pilani, **Prof. Sudhir Kumar Barai,** Director, BITS Pilani, Pilani Campus, Prof. Shamik Chakraborty, Associate Dean, Administration, Research (AGSR) Division, BITS Pilani for their administrative support.

I sincerely thank **Prof. Gaikwad Anil Bhanudas,** Professor & Head, and **Prof. Anil Jindal,** Convener of the Departmental Research Committee (DRC), Department of Pharmacy, BITS Pilani, Pilani Campus, for their timely suggestions, intellectual guidance, and support during various stages of my doctoral program. This thesis work would not have been the same without the scientific inputs, enthusiastic discussions, and evaluation from my DAC members, **Prof. Aniruddha Roy** and **Dr. Murli Monohar Pandey**, Department of Pharmacy, BITS Pilani, Pilani Campus.

I would also like to extend my sincere gratitude to the faculty members **Prof. R. Mahesh, Prof. Hemant R Jadhav, Prof. Sankaranarayanan Murugesan, Prof. Rajeev Taliyan, Prof. Deepak Chitkara, Prof. Anupama Mittal, Prof. Aniruddha Roy, Dr. Sunil Kumar Dubey, Dr. Sandeep Sundriyal, Dr. Richa Srivatsawa** who have supported me during my research and teaching practice. I wish to thank all non-teaching staffs **Mr. Rampratap Suthar, Mr. Puran, Mr. Lakshman, Mr. Navin, Mr. Tarachand, Mr. Surendar, Mr. Mukesh,** and **Mr. Mahender** for their direct and indirect help and support during my doctoral program.

I will always be grateful to, **Dr. V.G.M.Naidu**, Professor, and **Mr. Eswar Rao Puppala,** Department of Pharmacology & Toxicology, National Institute of Pharmaceutical Education and Research, Guwahati (NIPER-Guwahati). Involved in the collaboration of the proposed research work. Without them, I would not have completed the proposed work.

I would like to make a special mention to **Dr. Vamsi Krishna Rapalli** for taking out time of his busy schedule and helping in setting up the experiments and analyzing results whenever I was stuck. I also received great support and motivation from **Ms. Tejasree Waghule** in the lab for the timely completion of the academic tasks.

I would also like to extend my sincere thanks to my Teammates and cherished juniors **Mr. Prem Prakash Singh, Mr. Rupesh Kumar Jain, Ms. Manisha Choudary, Mr. Mahipal Reddy Donthi, Ms. Sakshi Priya, and Ms. Yashika Tomar** for their immense support. I want to thank graduates and postgraduates with whom I worked closely for exploring things. I thank Ms. Sailaja Jain, Ms. Arisha Mahmood, Ms.Neha Dabolkar, Mr. Sarath Chandra, Ms. Unnati Batra, Ms. Samshrita RN, and Ms. Shreya Maheshwari. We had fruitful discussions regarding each other's work, and they made sure that the lab is running smoothly. They also ensured that the lab environment remained jovial, and we enjoyed working together.

I wholeheartedly thank **Ms. Karanam Swetha and Ms. Aishwarya Ramesh** for being my roommates besides being my colleagues who made my stay in BITS-Pilani, a wonderful experience. Special thanks to the persons **Ms. Kanika Moonga, Mr.Karan Kumar Banoth, Ms. Kavya sree M, Mr. Rajesh Kumar Bheem, Ms. Ravali, Mrs. Urmila Rajesh and Mr. Sai Pradhyut who helped to** relieve our frustrations at times with full fun and sarcasm. Steadfast supporters of my personal life are **Dr. Ganesh and Ms. Kavya Sri** who encouraged me from the very beginning to successful completion of the work.

I would also like to thank my other colleagues in the department **Mr. Kedar, Mr. Imran, Mr. Arihant Kumar, Mr. Rajesh Pradhan, Mr. Prabhjeet, Ms. Nisha Yadav, and Ms.Moumita** for all the memorable moments we spent on the campus. I am happy to acknowledge my senior colleagues, **Dr. Krishna Kothavarapu, Dr. Kishan, Dr. Nisha, Dr. Ginson, Dr. Sudeep, Dr. Pracheta, Dr. Himanshu, Dr. Saurabh, Dr. Dhanashree, Mr. Sharath, Mrs. Paramita Vishal, Ms. Swati, Ms. Violina, Ms. Nikita, Mr. Amritansh, and Mr. Samrat** who helped with fruitful suggestions during my Ph.D. and survival at the department and BITS. I will also like to mention my juniors **Ms. Chandu Ala, Ms. Giriprasad, Mr. Prashant, Ms. Sharayu, Ms. Shreya, Mr. Atharva, Mr. Ajinath, Mr. Mukesh, Mr. Shrikanth, Mr. Shubham, Mr. Shivanshu, Mr. Amit, Ms. Sonia and Mr. Ela** for their bright smiles and positive attitudes with which they met me each day and inspired me to keep working.

I am thankful to and grateful for the Ph.D. fellowship provided by DST-INSPIRE, Govt. of India [#IF190259], in granting me financial assistance for my doctoral research.

Thanks to the unwavering support and blessings of my family. Everything I own is due to their support. In first place, I would like to thank my parents, Shri. **Gorantla Haribabu**, and Mrs. **Gorantla Siva Lakshmi,** for their loyalty, support, and encouragement. Having my father, and teachers as inspiration have always been a great source of motivation for me. Special acknowledgment goes to my supporting brother **Dr. Ganesh Gorantla**, and lovely sister Ms. Gorantla Kavya Sri without which my life would not be what it is. Also, I want to give my thanks to my other family members as well.

Srividya Gorantla

Abstract

Tofacitinib (TF), an oral JAK inhibitor, has been recently approved by USFDA to treat moderate to severe rheumatoid arthritis (RA). The delivery of TF to specific inflammation site at joint via topical route using nano formulations helps in managing the potential adverse effects better. The topical delivery of novel TF-loaded liquid crystal nanoparticles (TF-LCNP) can provide a controlled release, and also site-specific drug delivery to inflamed synovium. Also, CD44 receptors are highly expressed on the macrophages or other immune cells in the dermal region. Thus, the high affinity of the natural ligands hyaluronic acid (HA) and chondroitin sulphate (CS) to CD44 can enhance the therapeutic efficacy of TF. Therefore, the present research work was inspired by the possibility to develop and evaluate the potential of LCNP, uncoated cationic proglycosomes (N-TF-PG), hyaluronic acid-coated proglycosomes (HA-TF-PG), chondroitin sulphate coated proglycosomes (CS-TF-PG) as the carrier for site-specific dermal delivery of TF to treat RA condition.

In the dissertation work, we have developed and validated a simple and sensitive spectrophotometric method for the quantitative determination of TF in methanol and phosphate buffer saline. The linearity range in both media was 5-30 µg/mL (methanol) and 5-40 µg/ mL (10% methanol in pH 7.4 phosphate buffer saline containing 0.15% sodium lauryl sulphate) with a high correlation coefficient value (>0.9998). This indicates the clear correlation between TF concentrations and their absorbance within the test ranges. The repeatability and intermediate precision articulated by the relative standard deviation were less than 2 % in the developed method. The method specificity and applicability were also ascertained by performing recovery studies using quality control samples by spiking method, which was 95.85 ± 1.98% with % RSD 1.24 ± 0.045. The method developed in methanol was successfully applied to determine the entrapment efficiency of TF in developed LCNP formulation. The method developed in pH 7.4 phosphate buffer saline was applied to quantify TF from LCNP in *in vitro* drug release samples.

Further, we developed and validated a simple, specific, and sensitive stability-indicating HPLC method for the quantification of TF in N-TF-PG, HA-TF-PG, and CS-TF-PG formulations. A 3^2 factorial 'Design of Experiments' was applied to optimize process variables and to understand the effect of variables on peak properties. The calibration curve showed a regression coefficient (R^2) of 0.9999 and linearity in the concentration range of 50 to 15000 ng/mL, which is suitable for the analysis of conventional dosage forms and nanoformulations. Method validation was performed as per ICH guideline Q2 (R1). The accuracy by recovery studies

ranged between 98.09% and 100.82%. The % relative standard deviations in intraday and interday precisions were in the range of 1.16-1.72 and 1.22-1.80% respectively. Forced degradation studies indicated the specificity of the method and showed stability indicating the potential for a TF peak. The validated method provides a quantification method of TF in the presence of formulation excipients, dissolution media, and skin tissues in detail. In addition, the method was successfully utilized for the determination of various dermatokinetics profiles of TF.

TF-LCNP gel was formulated using a quality by design driven approach to enhance the delivery of TF to skin layers. The present work investigated the impact of two different liquid lipids on different critical quality attributes of LCNP. The optimized lyotropic liquid crystals system was constructed with the glyceryl monooleate, myristol, Lutrol®, and water system. The optimized TF - LCNP showed particle size of 74.82 ± 4.26 nm, polydispersity index of 0.124 ± 0.024, and entrapment efficiency of 68.29 ± 5.24 %. The TF-LCNP showed sustained release for 24 h and followed quasi-Fickian diffusion from non-swellable matrix diffusion with an n value of 0.197. The *ex vivo* permeation studies exhibited that amount of TF permeated through TF-LCNP gel and TF loaded gel (FD-gel) after 24 h were found to be 63.81 ± 4.32 µg/cm^2 and 38.5 ± 2.78 µg/cm^{2,} respectively. The dermal pharmacokinetic studies revealed that the LCNP showed a steady equilibrium state in 5-8 h in the epidermis and dermis layers. The total amount of TF permeated with the developed LCNP formulation was 3.9 times and 3.1 times higher in the epidermis and dermis compared to the FD-gel). The developed formulation exhibited good spreadability and rheology and has not shown any significant changes in stability and scale-up studies. In a nutshell, the developed TF-LCNP strategy poses excellent potential in targeting the viable skin layer.

Also, this dissertation work aimed to enhance the therapeutic efficacy of TF by HA, CS coated N-TF-PG through the anchoring of high-affinity of HA and CS to CD44 receptors on immune cells in the inflammatory region. Initially, the N-TF-PG was prepared by the thin-film hydration (TFH) method. Then the N-TF-PG was coated with HA and CS. The developed N-TF-PG, HA-TF-PG, and CS-TF-PG showed particle sizes of less than 250 nm. The developed formulations were evaluated for *in vitro* drug release, *ex vivo* (permeation, dermatokinetics), and *in vivo* efficacy studies. Ex-vivo studies of N-TF-PG gel, HA-TF -PG, and CS-TF-PG gels exhibited 2.56-fold, 3.15-fold, and 3.39-fold high dermal retention compared to FD gel.
The *in vivo* pharmacodynamic study, cytokines, and radiographic study on Complete Freud's adjuvant-induced arthritic rat model revealed that HA-TF-PG and CS-TF-PG exhibited a

significant ($P < 0.001$) reduction in inflammation in arthritic rat's paw compared to TF oral and FD gel. The obtained data confirmed that the developed TF-LCNP has lowered the CD44 levels compared to FD gel and TF-oral ($p< 0.05$). Whereas the developed HA-TF-PG treated groups showed significantly lowered CD44 levels compared to FD gel and N-TF-PG i.e., 2.28 and 1.32-fold respectively ($p<0.001$). In the present thesis work among the formulation approaches for TF topical delivery, HA-TF-PG, and CS-TF-PG improved skin retention in dermal layers and exhibited a stronger downregulation of the assayed cytokines and CD44 expression marker on macrophages than the N-TF-PG and TF-LCNP ($p < 0.001$). The current study ensured that the developed nanocarrier-embedded topical gel systems would provide a safe and effective formulation for localization and site-specific delivery of TF at the RA site and overcome the adverse effects associated with the TF.

List of Tables

List of Figures

List of symbols and abbreviations

%	Percentage
µg	Microgram
cm	Centimeter
mg	milligram
g	Gram
h	Hour
min	Minutes
g/mol	Gram per mole
mL	Milliliter
°C	Degree Celsius
V_d	Volume of distribution
C_{max}	Maximum concentration
T_{max}	Time taken to reach maximum concentration
$t_{1/2}$	Half-life
L	Liter
mV	Milli volts
Nm	Nanometer
µm	Micrometer
mm	Millimetre
cm	Centimeter
µL	Microliter
ng	Nanogram
M	Molar
mM	millimolar
µM	micromolar
nM	Nanomolar
λ_{max}	Lambda max
SD	Standard deviation
rpm	revolutions per minute
s	Seconds
Jss	Steady-state flux

Kp	permeability coefficient
K_e,	Elimination rate constant
w/v	Weight per volume
w/w	Weight per weight
mPa.s	millipascal-second
KDa	KiloDaltons
<	Less than
>	More than
≤	Less than equal to
≥	More than equal to
=	Equal to
α	Alpha
β	Beta
γ	Gamma
AUC	Area under concentration
AUC0-t	Area under the curve from zero to the last measurable point
AUC0-∞	Area under curve from time 0 extrapolated to infinity
AIA	Adjuvant Induced Arthritis
ACPA	anti-citrullinated protein antibodie
AIC	Akaie information criterion
APCs	Antigen–presenting cells
ANOVA	Analysis of variance
ATR	Attenuated total reflection
bDMARDs	biologic DMARDs
BBD	Box-Behnken design
CS	Chondroitin sulphate
CD44	Cluster Determinant 44
cDNA	Complementary Deoxyribonucleic acid
CFA	Complete Freund's Adjuvant
CMAs	Critical material attributes
CPPs	Critical process parameters

CPCSEA	Committee for the Purpose of Control and Supervision of Experiments on Animals
CS-TF-PG	Chondroitin sulphate coated proglycosomes
CQAs	Critical quality attributes
DoE	Design of Experiment
DC	Disease control / RA induced Rat
DSC	Differential scanning calorimetry
DNA	Deoxyribonucleic Acid
DMARDs	Disease-modifying anti-rheumatic drugs
DLS	Dynamic light scattering
EBV	Epstein - Barr virus
EDTA	Ethylenediaminetetraacetic acid
EPR	Enhanced permeation and retention
FD-gel	Tofacitinib loaded sepineo gel
FMEA	Failure mode evaluation and analysis
FTIR	Fourier transform infrared spectroscopy
FESEM	Field Emission Scanning Electron Microscopy
GRAS	Generally recognized as safe
GMO	Glyceryl mono oleate
HA	Hyaluronic acid
HLA	Human leukocyte antigen
HA-TF-PG	Hyaluronic acid coated proglycosomes
HPLC	High-pressure liquid chromatography
IL	Interleukin
ICH	The International Council for Harmonisation of Technical Requirements for Pharmaceuticals for Human Use
IFN	Interferon
JAK	Janus kinases
LVE	Linear Viscoelastic
LOD	Limit of detection
LOQ	Limit of quantification
LCNPs	Lyotropic liquid crystalline nanoparticles

LC/LC-MS	liquid chromatography–liquid chromatography-mass spectrometry
mRNA	Messenger Ribonucleic acid
miRNA	Micro Ribonucleic acid
NC	Normal Control
NF- κβ	Nuclear factor κβ
N-TF-PG	Normal proglycosomes
MHC-II	Major histocompatibility complex molecule -II
NSAIDs	Non-steroidal anti-inflammatory drugs
PBS	Phosphate buffer saline
PG	Propylene glycol
PRESS	Prediction error sum of squares
PRRs	Pattern-recognition receptors
QC	Quality control
OA	Orthogonal array
PDI	Polydispersity index
PXRD	Powder X-ray diffraction
QbD	Quality by design
QTPP	Quality target product profile
REM	Risk estimation matrix
RA	Rheumatoid arthritis
RSD	Relative standard deviation
RT-PCR	Real time-quantitative polymerase chain reaction
STAT	Signal transducer and activator of transcription proteins
SLS	Sodium lauryl sulfate
S/N	Signal to Noise
TFH	Thin Film Hydration
Th	T-helper (CD4) / T-cytotoxic cells (CD8)
TF	Tofacitinib
TLRs	Toll-like receptors
TNF	Tumor necrosis factor
TYK	Tyrosine kinase
USFDA	United States Food and Drug Administration

1 Rheumatoid arthritis

Rheumatoid arthritis (RA) is an inflammatory-mediated chronic and pathologically complex autoimmune disease that is characterized by synovial dysplasia, progressive joint destruction, and bone erosion [1]. According to recent statistics from Global RA networks, and World Health Organization (2019), globally, 23 million people are affected by RA among these 12.6 million are Indians [2]. The prevalence rate of RA varies between 0.5% to 1% globally, whereas 0.92% in Indians, which varies regionally [2]. RA is a chronic disabling condition of skeletal muscles, fibrous tissue, and connective tissue, and principally affects the synovial joint lining which causes pain and deformity. This leads to a socio-economic burden while compromising quality of life in RA patients. So, for desirable outcomes, an early diagnosis of the disease is required [1]. Recent advances in science have been investigating the specific etiology of RA, but still, it requires more understanding and investigation. In general, RA is a heterogeneous disease that can be caused by environmental and genetic factors. The HLA-DRB1 alleles that code shared epitopes (conserved sequence of amino acids in positions 70–74 of HLA-DRβ chains) are associated with the structural severity of RA. It was reported that more than 80% of the RA-affected individuals carry the HLA-DRB1*04 cluster, in which *04 signifies the allele group which corresponds to the serological type [3].

The environmental factors trigger the anti-citrullinated protein antibodies and epigenetic regulation at the gene expression stage. The genetic and environmental interaction impacts the autoantibodies subtlety to citrullinated antigens in RA. Hence, these anti-citrullinated protein antibodies (ACPA) can be identified in RA patients before the starting of joint destruction symptoms. As per available information, 67% of RA patients have shown the presence or absence of anti-citrullinated protein antibodies. Therefore, these can be used as a diagnostic tool for the early identification of RA [4]. Regarding autoimmunity, the joint may not be the only triggering smudge. Other triggering agents like exposing the lungs to deleterious agents like tobacco smoke, alcohol, obesity, nanomaterials derived from carbon, silica dust, Epstein - Barr virus (EBV) infection, Porphyromonas gingivalis, and Aggregatibacter actinomycetemcomitans increase the risk of RA [5]. Mostly tobacco smoking is considered a risk factor because it modulates cell death and triggers mucosal toll-like receptors. All the above factors stimulate the antigen-presenting cells like dendritic cells and B cells. Moreover, tobacco smoking causes a very high concentration of free radicals, which interact with Deoxyribonucleic Acid (DNA) and leads to mutation [6]. The environmental and genetic

factors activate macrophages, mast cells, dendritic, and natural killer cells, and recruit them to the affected joint site. Besides this the activated synovial macrophages, synoviocytes, $CD4^+$, and $C8^+$ T cells play a crucial role in inflammation by continuously releasing the pro-inflammatory cytokines such as Interleukin-1 (IL-1), and Interleukin-6 (IL-6), Tumor necrosis factor – α (TNF-α), receptor activator of nuclear factor κβ (NF- κβ) [6]. Figure 1 represents the etiology of RA.

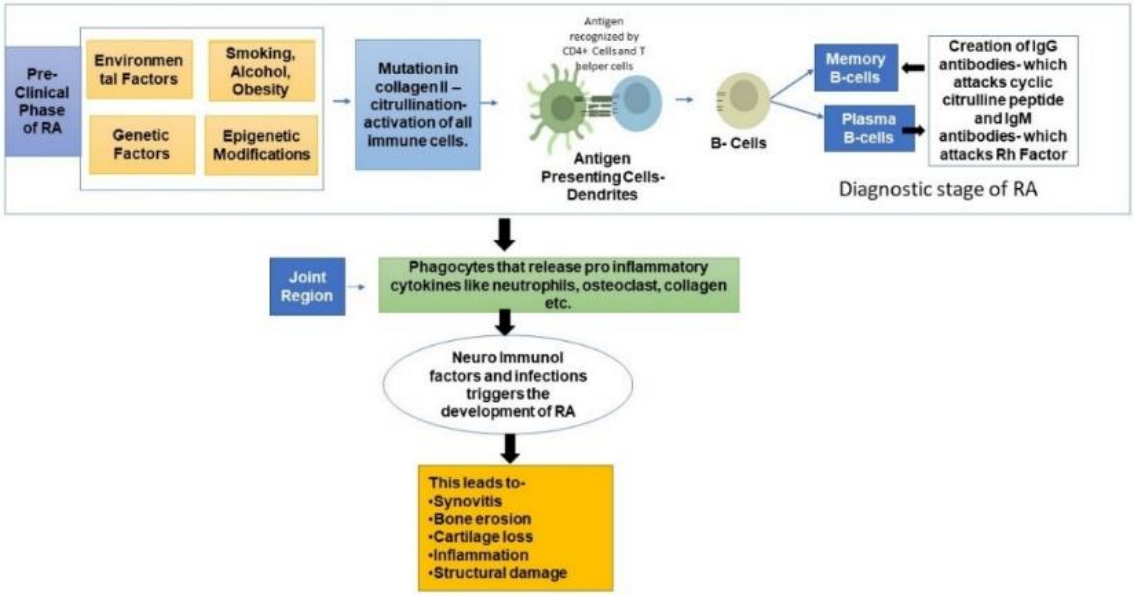

Figure 1.1. Etiology of Rheumatoid arthritis [7]

1.1 Pathophysiology of rheumatoid arthritis

RA is an auto immune disorder and thus T-cells, B-cells, macrophages, and immune cells plays an important role in pathogenesis. The T-cells activate macrophages and fibroblasts and turns them into tissue-destructive cells. The RA pathogenesis mainly involves the activation of macrophages in the synovial inflammatory joint through the production of the pro-inflammatory cytokines such as interleukin (IL)-6, IL - 1, and tumor necrosis factor (TNF-α). TNF-α induces abnormal differentiation and proliferation of osteoclasts. Further, TNF-α together with IL-6 stimulates the synovial cells to release tissue degrading enzymes, notably matrix metalloproteinases, which lead to bone erosion. In addition, the synovial fibroblasts of both the synovial lining and sub-lining layers undergo significant proliferation in RA. As macrophages and fibroblasts tend to be the most active cells in the RA synovium, their interaction is particularly appealing; ultimately resulting in inflammation and tissue damage. These cells provoke the production of granulocyte-macrophage colony-stimulating factor, IL-

6, and IL-8 [3]. Also, anti-citrullinated protein bodies are responsible for the initiation of degradation in bones [8]. Figure 2 presents the pathogenesis of RA.

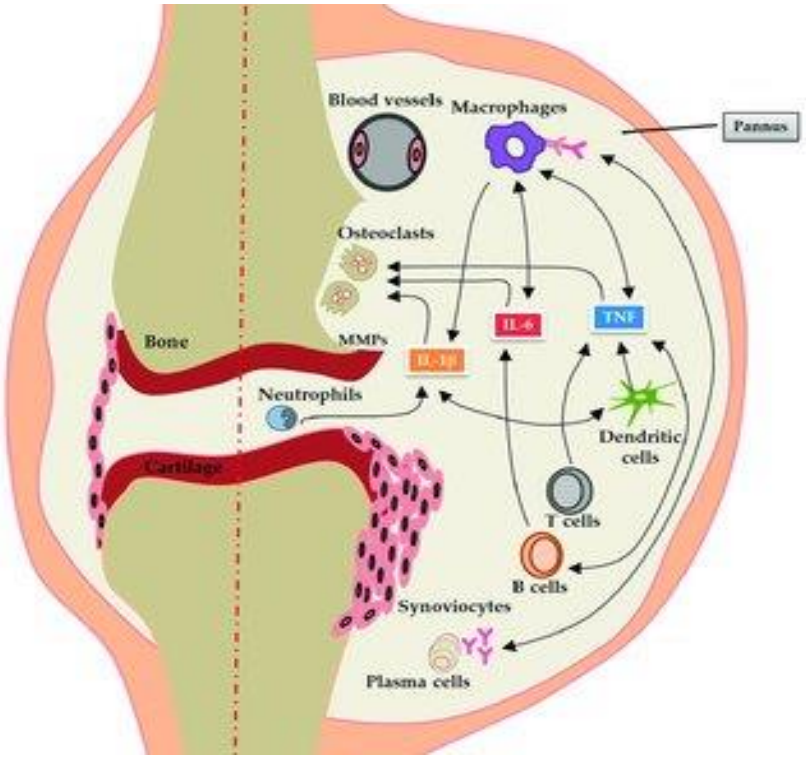

Figure 1.2. Pathogenesis of RA [9]

Reported studies support that lymphocyte mediate RA pathological process by releasing the pro-inflammatory cytokines. Janus kinases (JAK) mediates the intracellular signaling transduction of the lymphocytes. The JAK-STAT (signal transducer and activator of transcription proteins) pathway modulates cytokine-mediated signals. JAK is a family of intracellular, cytoplasmic tyrosine kinases. The JAK enzymes (JAK1, JAK2, JAK3, and TYK2) produced by this JAK-STAT pathway activate cell signaling and signaling for gene transcription. The impairment of the JAK-STAT pathway in T helper cells may leads to several immune disorders.

1.2 Role of intracellular signaling Janus kinases pathway in causing pain during rheumatoid arthritis condition

Janus Kinases play a key role in the JAK–STAT pathways and exhibited its implication in autoimmune disorders [10]. It has been reported that JAK-STAT signaling is a universal and vital intracellular pathway for cytokines' action. The JAK-STAT pathway constituted of four intracellular protein kinases (JAK1, JAK2, JAK3, and tyrosine kinase2 (TYK2) and seven STATs (STAT1, STAT2, STAT3, STAT4, STAT5a, STAT5b, STAT6) [11]. The signaling

pathway in RA is initiated by the binding of proinflammatory cytokine to specific cytokine receptors, which enables the recruitment of specific protein kinases and binds in pairs to the intracellular domain of the receptor [11]. Then the receptor contributes to dimerization and activation of associated JAKs. Activated JAKs phosphorylates specific residues on the intracellular domain of cytokine receptors i.e. autophosphorylation, which serves as a docking site for recruited STAT proteins. The activated receptor-associated JAKs phosphorylate STATs upon STAT docking before dissociating from the receptor. The dissociated STATs dimerize with each other and translocate to the cell nucleus which recognizes and binds to specific DNA sequence and regulates gene transcription [12]. The JAKs are associated with different receptors, including JAK1 (interferon and interleukin (IL) -6 and IL-10), JAK2 (IL-3, erythropoietin, growth hormone, and prolactin), whereas dimers of JAK2 and TYK2 are associated with IL-12 and IL-23 receptors. Whereas, JAK3 has been mostly expressed on the hematopoietic cells i.e., lymphocytes. The JAK3 in coexistence with JAK1 binds to IL-2, IL-4, IL-7, IL-9, IL-15, and IL-21 receptors. All these play a key role in intracellular signal transduction [13]. Hence, we can conclude that the JAK/STAT pathway being an intracellular signaling pathway can be activated by a variety of cytokines, resulting in the emergence of additional pro-and anti-inflammatory cytokines as well as locally damaging enzymes. The multiple cytokines are directly or indirectly activated by the JAK/STAT pathway. The IL-6, IL-1, L-10, and (IFN)- γ are the cytokines that signal directly through JAK/STAT pathway whereas interleukin (IL)-1 and TNF-α are indirectly activated [14]. Cytokine interactions with the JAK/STAT pathway and possible involvement in pain are presented in Table 1.1. This pathway offers a similar role in the pathogenesis of RA. Therefore, in RA, inhibition of JAKs results in inhibition of signal transduction and gene transcription at the intracellular level, as a consequence reduction of inflammation at the joint region. The overview of various cytokines that are mediated by JAK/STAT pathway are presented in Figure 3. The cytokines with a red arrow and green arrow represent the pro-nociceptive (increase pain sensation) and anti-nociceptive (decrease pain sensation) respectively.

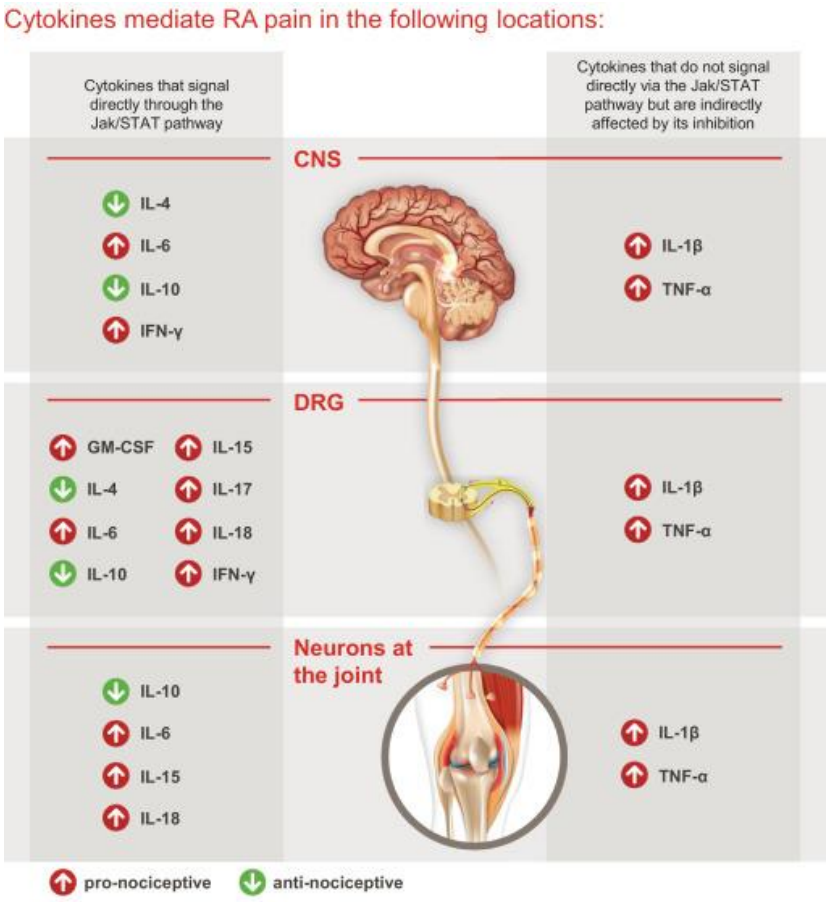

Figure 1.3. Overview of various cytokines that are mediated by JAK/STAT pathway [15]

Table 1.1. Cytokine interactions with the JAK/STAT pathway and likely involvement in pain [15]

Cytokine (ligand/receptor)	**Elements of JAK/STAT pathway affected**	**Association with pain mechanisms**
GM-CSF/GM-CSFR	JAK 2, STAT 3, STAT 5	Induces hyperalgesia and upregulates sodium channel expression
IFN-γ/IFN- γ R	JAK 1 and JAK 2, STAT 1, STAT 3	IFN- γ and IFN- γ receptor-deficient mice show social dysfunction can signal through inhibitory (GABAergic-specific) neurons for the initiation or maintenance of pain.
IL-1b/IL-1R	Indirect via IL-6/STAT 3	The initiation of pain may negatively impact cognitive performance.
IL-4/IL-4R	JAK 1, JAK 3, STAT 1, STAT 3, STAT 6	IL-4 overexpression can reduce hyperalgesia Mice deficient in IL-4 have improved social behaviour, a

		possible mechanical allodynia, and cognitive impairments
IL-6/IL-6R, sIL-6R	JAK 1and JAK 2, TYK 2	Pro-nociceptive factor subsidize to the progress of hyperalgesia/allodynia in rats can have a damaging effect on cognitive function
IL-10/IL-10R	JAK1, STAT 3	Mitigates pain (anti-nociceptive effects)
IL-12/IL-12R	TYK 2 and STAT 4	Leads to the release of pro-nociceptive cytokines TNF and IFN- γ
IL-15/IL-15Ra, IL-2Rb, γ C	JAK1and JAK 3, STAT 5	Associated with the severity of pain in osteoarthritis, Induces neuropathic pain
IL-17/IL-17RA	JAK 2, STAT 1, STAT 3	Causes allodynia
IL-18/IL-18R	TYK 2 and STAT 4	Pro-nociceptive factor
IL-22/IL-22R	JAK1, STAT 3	Improved expression level is noted in experimental arthritis Impeding IL-22 decreases pain
IL-27/gp130	TYK 2, STAT 1, STAT 3, STAT 5a/b, gp130signaling subunit	Reduced expression of gp130 can lessen pain
TNF-a/TNFR1, TNFR2	Indirect via IFN-b–Jak/STAT expression and STAT1	Initiate pain and induce pain-receptor sensitization (both mechanical and thermalhyperalgesia), It is accompanying with neuropathic pain and has a negative effect on cognitive function

1.3 Currently available therapies to treat rheumatoid arthritis

There is no complete cure for rheumatoid arthritis, but the currently available therapies give only symptomatic relief. The approved therapies for treating RA include, corticosteroids, Non-steroidal anti-inflammatory drugs (NSAIDs), Disease-modifying anti-rheumatic drugs (DMARDs) through oral, systemic, and intra-articular routes. NSAIDs and corticosteroids fight inflammation and reduce pain with a high risk of side effects and cannot retard disease progression [16]. The conventional DMARDs and biologic DMARDs (bDMARDs) minimize joint damage only through remission. Besides, loss of response upon bDMARDs administration due to the immunogenicity of administered protein [17]. Currently, bDMARDs are administered through intra-articular injections. The main side effects associated with intra-

articular injections are muscle pain, trouble walking, infection, and local site reactions, which lead to poor patient compliance [18]. In case of moderate to severe arthritis condition, if the patient is not responding to the DMARDs like methotrexate, they are treated with a combination of bDMARDs or biological agents or with a potent small-molecule inhibitor of selective oral Janus kinases. The biological agents have a shorter half-life upon oral administration and exhibit toxic effects on long-term treatment. In addition to this, the currently available drugs act at the extracellular region, however intracellular genetic factors like kinases play a crucial role in RA progression. Hence, the treatment with intracellular kinase inhibitors can be more efficacious [19]. Therefore, the intracellular signaling pathways inhibiting therapeutics have been developed and are currently available in the market for the effective treatment of RA [20].

Some of the new chemical entities like vagus nerve stimulants (NCT03437473) and anti-TNF-alpha therapies via intra-articular delivery with etanercept (Enbrel®), adalimumab (Humira®) and infliximab (Remicade®), consist of soluble TNF receptors, fully human anti-TNF-alpha monoclonal antibodies, and chimeric human-mouse anti-TNF-alpha monoclonal antibodies have gained importance due to their positive results in clinical trials like inhibition of structural damage (NCT00126724) [21,22]. A combination of TNF-alpha inhibitors along with Synthetic DMARDs (NCT01881308) is in phase IV clinical trial [23]. In addition to this, the use of TNF-blocking therapy in combination with DMARDs in patients with early RA (Trexan + Salazopyrin + Oxiklorin + Prednisolone + Infliximab) (NCT00908089), are potent therapeutic combinations undergoing clinical trials to treat moderate to severe arthritis [24].

1.4 Drug delivery systems for the treatment of rheumatoid arthritis

A variety of therapeutics are available for the treatment of RA, but still, there is no complete cure for RA. To achieve the goal of a close-to-ideal RA treatment, the delivery strategy for antiarthritic drugs should fulfil three main requirements including, the anti-rheumatic drug should afford stabilization and extended bioavailability, site-specific and targeted delivery of drug to the inflamed joint with high specificity and efficacy. These requirements can be attained using a drug delivery vehicle or molecular modification of the drug. Currently, to improve the therapeutic efficacy, advanced drug delivery systems and nanotechnology driven preparations such as polymer-drug conjugates, micelles, liposomes, niosomes, lipidic nanocarrier drug delivery systems, gold nanoparticles, microneedles technology and flare responsive drug delivery systems have gained importance [25]. Table 1.2 presents the summary of reported drug delivery vehicles with the route of administration to treat RA conditions.

The delivery of anti-rheumatic drugs using nanoparticle-based systems has made enormous advancements. In addition, to enhance the therapeutic efficacy of the drugs, passive and active targeting approaches for inflamed synovial sites have been explored [26]. The passive targeting approach implies targeting the anatomical and physiological changes in injured tissues, which occurred due to inflammation. The enhanced permeation and retention (EPR) are the basis for passive targeting strategy. Due to the EPR effect, white blood cell extravasations and nanoparticle retention arise in the inflammatory tissue. Therefore, the leaky vasculature in RA can be used as a potential target for selective drug delivery [26]. The nanoparticles with a size less than 250 nm can reside at the inflammatory site due to the enhanced permeation effect and release the drug in a sustained manner.

In RA condition, the formation of endothelial gaps allows leakage of plasma to the inflammation site, ensuring entry of monocytes, and the overexpression of antigen-presenting cells or inflammatory presenting cells. Therefore, the drug delivery via the joint blood barrier is increased by 6-40 folds due to the inflammatory cell infiltration and abnormal blood vessels at the affected site. All these become an advantage to the nanoparticles due to their small size, i.e., of less than 250 nm to reside at the inflammatory site and release the drug in a sustained manner [27]. Therefore the leaky vasculature in RA can be utilized as a potential passive targeting approach for selective drug delivery [28,29].

1.5 Targets for site-specific drug delivery for treating rheumatoid arthritis

However, this passive targeting approach lacks site-specific targeted drug delivery [30]. The way to wrestle with this confrontation is to screen inflammatory cells for structural entities expressed on their surface that are engaged in pathological functions; apart from normal cells involved in physiological activities. The active targeting strategy involves the identification of the target receptors and the selection of a suitable ligand for drug delivery that can firmly bind to specific cells at the target site. In RA pathogenesis, the overexpression of particular cells like T cells, vascular endothelial cells, and activated macrophages are reported. The overexpression of folate, E-Selectin, Cluster Determinant 44 (CD44) receptors, alpha V, beta 3 and integrins vasoactive intestinal peptides are identified in the inflammatory cells compared to the normal cells [31–35]. Among all the cells at the inflammatory site, macrophages are activated and play a vital role at the inflammatory synovial membrane. On the surface of activated macrophages, folate receptor- β and CD44 (glycoprotein) overexpress at the pannus and synovial region in RA conditions. Hence the molecules that can particularly bind to these can be used as potential ligands for drug targeting [31]. Commonly utilised targeted ligands for

the folate receptor and CD44 receptor are folic acid and hyaluronic acid respectively [32]. Nogueira et al. investigated on targeted delivery of liposomes loaded with methotrexate to folic acid receptors using SP-DS3 peptide linker for the treatment of RA. The results revealed that folic acid-targeted liposomes enhanced discrete internalization in activated macrophages compared to macrophages that deprivate folic acid receptors [36]. Similarly, E-Selectin is a glycoprotein that is expressed on the vascular endothelium and upregulated at the inflamed RA. The overexpression of vasoactive intestinal peptides on the synoviocytes and macrophages during the proliferating stage can be selected as an active targeting approach [33,34]. Further, overexpression of other markers such as alpha V and beta 3 integrins during the hypoxia condition at the inflamed synovium can be targeted to prevent angiogenesis and bone resorption [35]. Figure 4 illustrates the inflamed synovial joint with pro-inflammatory cytokines such as IL-6, IL-1, and tumor necrosis factor (TNF-α) along with the key targets for site-specific delivery of therapeutics to RA site. The application of the advanced nanocarriers with their drug delivery target in treating RA is discussed thoroughly in Table1.2 [38-56].

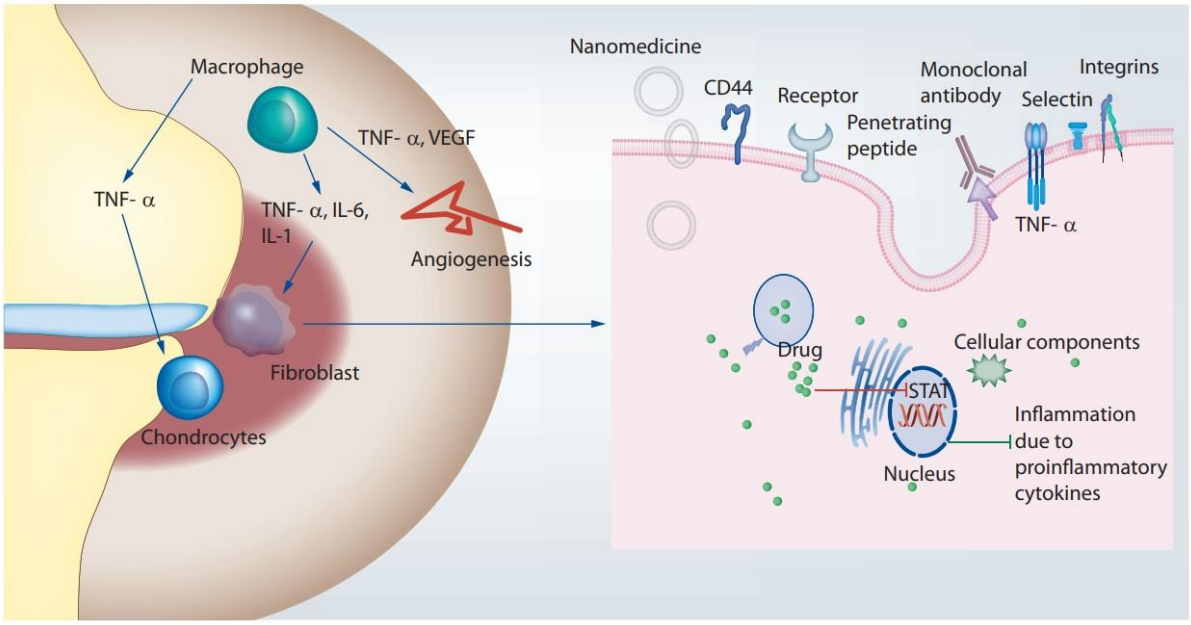

Figure 1.4. The inflamed synovial joint with pro-inflammatory cytokines and the key targets for site-specific delivery of therapeutics for the treatment of rheumatoid arthritis [3]

Among all the cells at the inflammatory site, macrophages are activated and play a crucial role at the inflammatory synovial membrane. A hallmark of the inflammatory responses like RA synovitis involves the overexpression of adhesion molecules including vascular cell adhesion molecule, intercellular adhesion molecule-1, and CD44. The adhesion molecules play a important role in inflammatory processes by modulating leukocyte endothelial cell adhesion

and migration, and T cell-antigen presenting cell interactions. Compared to normal cells, the inflammatory cells express higher levels of CD44 receptors, folate, E-selectin, alpha V and beta 3 integrins, and vasoactive intestinal peptides on their surface. Additionally, overexpression of other markers like alpha V and beta 3 integrins can be targeted to prevent angiogenesis and bone resorption during the hypoxic condition at the inflamed synovium. [3].

Table 1.2: Summary of drug delivery vehicles in treating rheumatoid arthritis

Drug	**Delivery system**	**Target delivery**	**Ligand**	**Route of administration**	***In vitro*/ animal model**	**Beneficial outcome**	**Ref**
Withaferin-A	Liposome	Synovial Macrophages	*p*-Aminophenyl-D mannopyranoside	Intravenous	AIA rat	Inhibited TNFα, IL-1β, IL-6, MCP-1, and VEGFs	[37]
Betamethasone	Liposome	FR β-expressing macrophages & EPR effect	Folic acid	Intravenous	AIA rat	Enhanced therapeutic efficacy by reducing splenomegaly and reduction of folate immune cells	[38]
Methotrexate	Ultra deformable liposome gel	Passive	NA	Topical	AIA rat	Suppression in mRNA levels of TNF-α and IL-1β.	[39]
p-Coumaric acid	Liposome	Synovial macrophages (CD86) & pre-/osteoclast (CD51)	4-aminophenyl α-D-mannopyranoside	Intravenous	AIA rat	Downregulation of the MMP-9 and NFATc1 expression and inflammatory cytokines.	[40]
Loperamide	Liposome	-	-	Topical	AIA rat	Accelerated disease progression in comparison to the diclofenac gel.	[41]

Interleukin-27	Liposome	Activated endothelial cells	ART-1lipopeptide	Intravenous	AIA rat	High efficacy and reduced side effects	[42]
MCL-1 siRNA	Neutral PEGylated liposomes	FR β-on Activated macrophages	Folic acid	-	RAW 264.7	Slow release into cells and sensitizes cells to apoptosis.	[43]
Dexamethasone palmitate	Liposome	Peripheral blood neutrophils	Sialic acid	Intravenous	AIA rat	Enhanced anti-inflammatory activity& targeted delivery	[44]
Methotrexate	Micelles	E-selectin on lymphocytes	Sialic acid-dextran-octadecanoic acid	Intravenous	CFA rat	Reduced alanine aminotransferase, aspartate aminotransferase, creatinine, and urea nitrogen levels	[45]
Methotrexate & microRNA-124	Hybrid micelles	FR β –on activated macrophages	PEI-LA and mPEG-LA	Intravenous	AIA Rat	Synergistic efficacy and successful delivery of microRNA-124 by escape from the endosome	[46]
Co-delivery of Dexamethasone and siRNA	Polymeric hybrid micelles	p65 in macrophages	Polycaprolactone-polyethyleneimine (PCL-PEI) and polycaprolactone-polyethylene glycol (PCL-PEG)	Intravenous	CIA	Suppressed nuclear translocation of p65 and pro-inflammatory cytokines.	[47]

Dexamethasone palmitate	Mixed micelles	Passive targeting	NA	Intravenous	CFA	Enhanced bioavailability	[48]
Dexamethasone	Mixed micelles	FR β –on activated macrophages	Folic acid	Intravenous	AIA Rat	Compared to commercial Dexamethasone injection 4 to 5-fold longer elimination half-life and a 2 to 3 folds higher bioavailability.	[49]
Dexamethasone	Acid labile micelle	Macrophages	Hydrazone linkers	Intravenous	AIA Rat	Prolonged circulation time and promote the bioavailability	[50]
Piroxicam	Solid lipid nanoparticles	Passive	No ligand	Percutaneous	-	Avoided gastric irritation problem by delivering through topical route	[51]
Triptolide	Nanostructured lipid carriers	Passive	No ligand	transdermal drug delivery	CFA	Avoiding the f liver first-pass effect and gastrointestinal reaction	[52]
Methotrexate	Cubosomes	Inflamed joint site (Passive)	NA	Transdermal delivery	CFA	Enhanced anti-inflammatory activity compared to diclofenac sodium.	[53]
Indomethacin	Ethosomes	Passive	NA	Transdermal delivery	NA	Enhanced skin disposition and permeation.	[54]

AIA: Adjuvant Induced Arthritis; CFA: Complete Freund's Adjuvant

1.6 Modes of drug delivery for the treatment of rheumatoid arthritis

In severe arthritis conditions intra-articular, systemic, and oral therapy are preferred. Currently, these bDMARDs are administered as intra-articular injections. The main side effects associated with intra-articular injections are muscle pain, trouble walking, infection and local site reactions. The oral administration of TF was associated with extensive first-pass metabolism, gastrointestinal degradation, enzymatic degradation, limited bioavailability, and food-based interactions. The injectable formulation imparts immediate action as well as higher bioavailability but require skilled personnel and it is also invasive and painful. Moreover, injectable formulations must be sterile and stable, making their manufacturing, transportation, and storage conditions costly. Locally administrating injection at every affected joint is neither practicable nor comfortable for the patient. Most of the concerns outlined above eventually depends on the mode and route of delivery. During these conditions the topical administration with appropriate delivery vehicles can provide improved stability, and optimized delivery to inflamed synovium. The topical administration provides a promising alternative for effective delivery of drugs. Application of drug incorporated nanocarrier-loaded hydrogels has several advantages over oral and parenteral systems. Topical administration can be efficacious over oral and intra-articular administration, apart from the outermost stratum corneum which acts as a physiological barrier and limits the drug penetration [55].

1.7 Shortcomings of conventional formulation on topical administration

Traditionally, various dosage forms like creams, lotions, ointments, liniments, patches, and hypodermic needles are being used for topical and transdermal drug delivery [56]. These formulations have been widely used for relief from skin diseases and inflammatory diseases. However, they possess certain disadvantages such as differential drug-carrying capacity, efficiency, bioavailability, and patient compliance issues [57]. Conventional topical drug delivery systems portray reduced drug availability to the target site. Transdermal patches are also popular for transdermal delivery. But there are a few disadvantages associated with transdermal patches; that is the restricted ability of the drug to cross skin barrier and the rate of drug release. These problems lead to a slow and less desirable suboptimal effect [58]. Conventional hypodermic needles have been a popular choice for transdermal drug delivery. Nonetheless, patient acceptance becomes an important parameter when it comes to needles, as it requires the assistance of an expert for administration, and the pain associated with them leads to fewer patients accepting needles as a mode of drug delivery [59].

1.8 Skin as a protective barrier

Human skin is a protective barrier that only allows one-way channelization. It prevents the entry of external matter into the body. Hence, it also resists absorption of chemicals that come in contact with it; making drug delivery through the skin cumbersome [60]. Skin is the largest organ in the human body, consisting of three major layers; epidermis, dermis, and hypodermis. The large surface area of the skin provides an excellent opportunity for the delivery of different molecules to elicit both local and systemic action. The stratum corneum of the epidermis is the outermost layer that forms a barrier between the external environment and the body. It is composed of keratinized cells with intracellular spaces filled with cholesterol, saturated lipids, and fatty acids [61]. Also, it is having a 10-15 μm thick dead layer which is considered as a primary barrier for transport of hydrophilic low molecular weight compounds and macromolecules. The layer below this outermost layer is the epidermis which is about 50-150 μm thick containing cells, nerves and devoid of blood vessels. Deeper to the epidermis is the dermis layer accommodating cells, nerves, blood vessels along with pain receptors. Due to the presence of these barriers in the skin, the drug cannot reach the site at the effective rate to elicit the therapeutic effect [62].

Additionally, the drugs administered through topical formulations are expected to penetrate in a therapeutic quantity into the skin layers to treat various inflammatory disorders. On the other hand, drug molecules administered via transdermal formulations are expected to be absorbed in sufficient amounts to maintain therapeutic concentration in the blood, which will elicit a pharmacological response to the target sites.

1.8.1 General mechanisms of drug delivery through skin

There are two routes of penetration of drug across the intact skin; trans epidermal route and transappendegeal route (Figure 5). In the trans epidermal route, the molecules pass through the stratum corneum; intracellularly through the corneocytes and intercellularly through the intercellular spaces. Intracellular route allows penetration of polar or hydrophilic solutes, whereas intercellular route allows penetration of non-polar or hydrophobic solutes. In the transappendegeal route, the molecules pass across the hair follicles, and *via* sweat glands [63,64]. Understanding the kinetics is necessary to design a TDDS. Percutaneous absorption is an important step in transdermal delivery. The penetration of molecules into various layers of skin and their permeation into the systemic circulation is termed as percutaneous absorption. It is a step-wise process that involves (i) penetration, (ii) partitioning from the stratum corneum

into the epidermis, (iii) diffusion into upper dermis, (iv) permeation, and (v) absorption into systemic circulation [65].

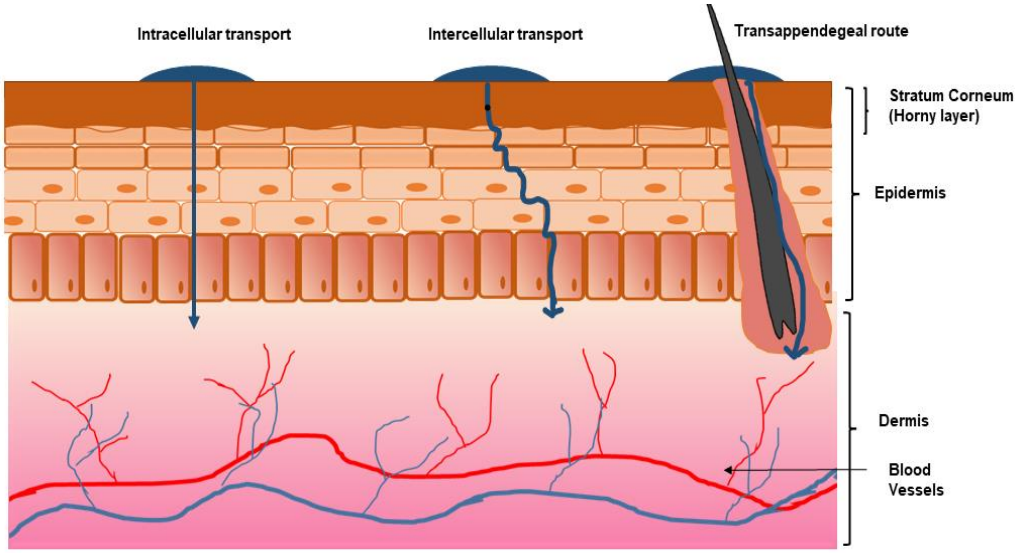

Figure 1.5. General mechanisms of drug delivery through skin

1.8.2 Immune system of the skin

Immunity can be classified broadly as innate immunity and adaptive immunity. The innate immunity is formed by the stratum corneum in the skin. When the stratum corneum is breached, the adaptive immune system responds. Overall skin immune system consists of molecular, cellular components and stratum corneum [66]. The cellular components include T lymphocytes, Langerhans cells, keratinocytes, macrophages, mast cells, dermal dendritic cells and melanocytes. The epidermal Langerhans cells (dendritic cells) and keratinocytes are the initial line of defence for the skin immune system. The key immune cells in the dermis are dermal Langerhans cells, T – lymphocytes, B-lymphocytes, Natural killer cells and mast cells. The keratinocytes and dendritic cells possess Toll-like receptors (TLRs). These TLRs are pattern-recognition receptors (PRRs) detect pathogens conserved molecules and trigger an inflammatory response. Whereas the antigen–presenting cells (APCs) i.e. (dendritic cells, monocytes/macrophages and B cells) identify the antigens and present them to immature T cells [66]. Initially, APCs internalize the pathogen, process inside the cell and then exhibit a short peptide on the surface of a major histocompatibility complex molecule -II (MHC-II). T cells are categorized as T- helper cells (CD4) and T- Cytotoxic cells (CD8). The T helper cells are of two types Th1 and Th2. In these, Th 1 promote inflammation, produce IFN-γ, secrete and activates the macrophages and NK cells, while Th 2 cells stimulate B cells to produce antibodies and produce the cytokines such as IL-4, IL-5, IL-6, and IL-10 [67]. The cellular components of the skin immune system are presented in Figure 6. However, macrophages play

a crucial role in RA pathogenesis by generating cytokines that enhance inflammation and contribute to the destruction of cartilage and bone. The surface of activated macrophages shows the presence of CD44 (cluster of differentiation) as a marker [68] .

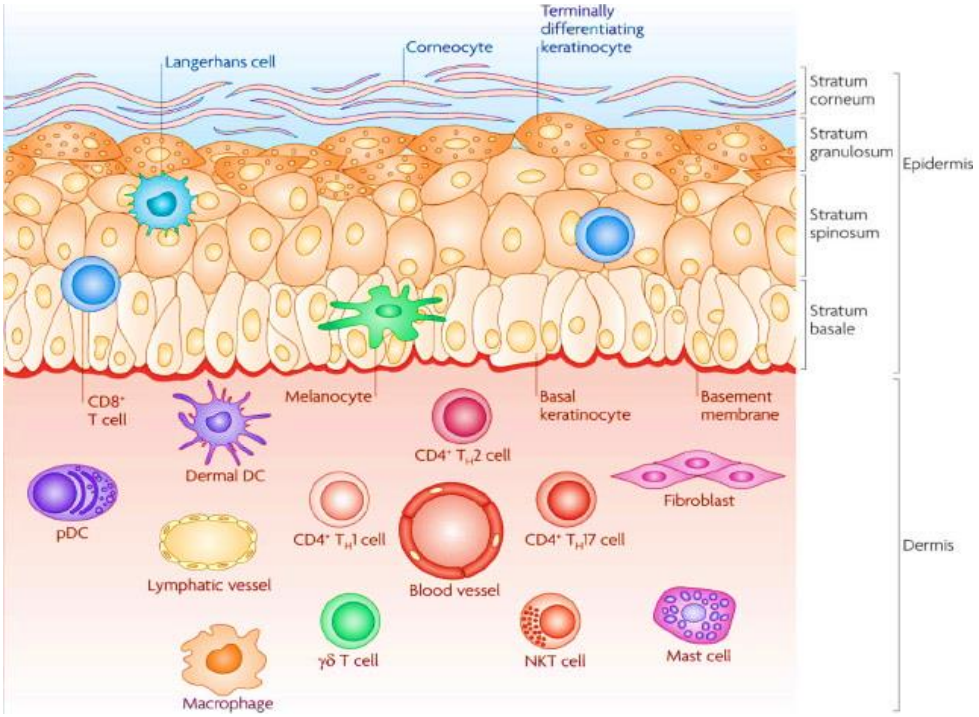

Figure 1.6. Cellular components of the skin immune system [69]

1.9 Cluster Determinant 44 (CD44) receptors

Among the receptors that have been discussed earlier, CD44 has been reported to be over-expressed in the sites of inflammation in RA proportionate to the inflammation intensity [70]. The levels of CD44 in the synovium of patients with RA are 3.5-fold and 10.7-fold higher than that of patients with osteoarthritis and joint trauma, respectively. According to histochemical immunostaining, CD44 expression was greater in RA and osteoarthritis synovium, than in the normal synovium [71]. Thus, there has been a surge in the research that focuses on the CD44 targeted drug delivery strategies to treat RA. CD44 targeting has been attempted using anti-CD44 monoclonal antibodies, DNA vaccines, and CD44 siRNA nanoparticles.

CD44 is a multi-structural cell surface glycoprotein for the ligand hyaluronan, which is a major polysaccharide present in the synovium. CD44 can potentially produce over 800 isoforms. The alternatively spliced versions of CD44 like CD44v3, v6–v10 were highly expressed in fibroblasts from RA synovium. These results indicate that joint inflammation activates

fibroblasts expressing CD44 variants or CD44 alternatively spliced versions [71]. Also, CD44 expression was found to be higher on synovial lymphocytes and macrophages in rats with adjuvant arthritis. There have been reports of the role of CD44 and hyaluronan in the upregulation of Fas receptor on the RA synovial cells, and the implication of the involvement of CD44 in the pathogenesis of RA [72]. The CD44 receptor, which is overexpressed in synovial macrophages and fibroblasts binds to hyaluronic acid (HA) [71]. CD44 receptor-mediated active targeting drug delivery systems have been immensely explored among the various targeted delivery systems [73]. CD44 can recognize and bind glycosaminoglycan-based biomaterials such as HA and chondroitin sulphate (CS). Glucosaminoglycans are polysaccharides that typically consist of repeating disaccharide units that have been modified to contain an amino group and negatively charged groups. CD44 consists of binding sites for HA and CS where HA binds to N- terminal of the CD44 and CS binds to the variant stem fibrin region.

1.9.1 Hyaluronan based CD44-targeted drug delivery

Hyaluronan or hyaluronic acid is a natural, water-soluble, linear, non-sulphated anionic glycosaminoglycan. It consists of repeating β-1, 3-N-acetyl glucosamine, and β-1, 4-glucuronic acid disaccharide units [74]. HA is found in epithelial and connective tissue, synovial fluid, and vitreous humor of the eye. It possesses exclusive properties including, excellent biocompatibility, biodegradability, ease of chemical modification, satisfactory safety for enduring clinical use in human subjects, and less immunogenicity. It also possesses cartilage protective and lubricant effects in synovial fluid [75]. Besides the structural role, HA is a principal counter molecule to HA receptors on CD44 (Figure 7A and Figure 7B). The synovium of the healthy subject contains the highest concentrations of hyaluronan in the entire human body. During the inflamed joint condition, the depletion of hyaluronan occurs. It was reported that 0.71 ± 0.1 mg/cm^3 is found in rheumatoid synovial tissue, whereas 1.07 ± 0.16 mg/cm^3 in healthy subject.

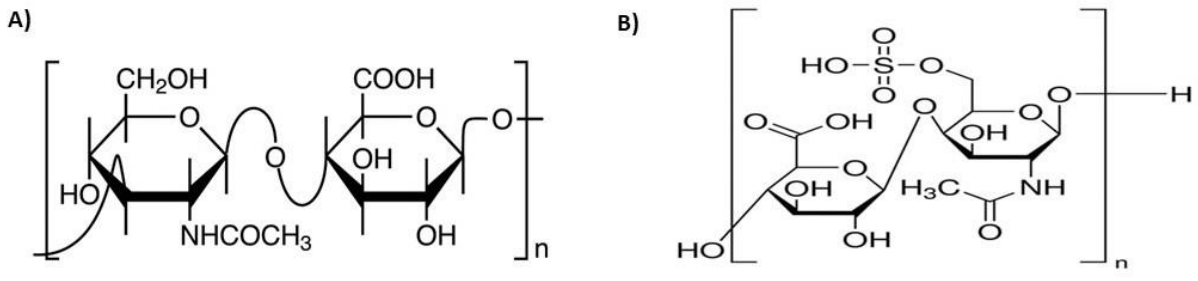

Figure 1.7. A) Structure of hyaluronic acid; B) Structure of chondroitin sulphate [68]

Targeting techniques using HA-modified nanocarriers rely on their preferential binding to the CD44 cell receptor, which is overexpressed in synovial activated cells and plays a role in autoimmune response control. The off-target distribution of the drug could be reduced by targeted delivery to CD44.

1.9.2 Chondroitin sulphate based CD44-targeted drug delivery

CS is a water soluble, unbranched sulphated anionic glycosaminoglycan composed of alternating 4-linked β- d-glucuronic acid and, 3-linked *N*-acetyl galactosamine disaccharide units with varied sulphate positions [76]. The sulphate group imparts hydrophilicity, and was found on the fourth and sixth positions in CS, which are named CS A and CS C, respectively [77].

CS is distributed in cartilage around the joint and ligament. It shows good biocompatibility and biodegradability, and low toxicity. Moreover, it is well known that during arthritis conditions, the CS present at the knee joint decreases the joint space's discomfort and narrowing. It also protects the joint by lowering the matrix in enzymes in chondrocytes [73]. In addition, CS has chemical structural similarity to HA (Figure 7A); thus, CS can specifically target the CD44 receptor (Figure 7B). Due to these reasons, the CS-based nanocarriers were used for passive and active targeted drug delivery.

1.10 Lipid based nanocarriers for topical drug delivery and importance of nanocarriers

Nanocarriers gained importance due to small size, which can reduce the reticuloendothelial clearance and achieve passive targeting to inflamed RA site. The in-vivo fate of nanocarriers depends on the size, charge, and surface properties. Lipid nanocarriers systems have been found to be a suitable choice for topical delivery due to their increased resemblance to the skin, and enhanced penetration by polarity and fluidization [78,79]. Vesicular drug delivery systems can easily permeate through the skin, but the percutaneous permeability depends on the elasticity of vesicles [80]. Among these nanocarriers, lyotropic liquid crystalline nanoparticles (LCNP), proglycosomes gained huge attention due to their effective topical delivery.

1.10.1 Liquid crystalline nanoparticles

LCNP designed with self-assembling lipid based systems like bicontinuous cubic and hexagonal mesophases mimic the curvature of the cellular membrane and possess unique properties of infinite swelling, sustained drug release, and protects the drug from physical and enzymatic degradation [81]. These LCNP can be used for the delivery of hydrophilic, lipophilic, and amphiphilic therapeutics with high loading capacity. Mono oleins are mostly

used in the preparation of LCNP. These mono oleins fluidize the stratum corneum and promote easy penetration through the skin. In addition to this, these exhibit skin adhesion nature. Hence these can be promising drug delivery carriers for the delivery of anti-inflammatory drugs on topical administration [82]. In addition, the use of non-toxic, biocompatible, and Generally Recognized As Safe (GRAS) approved permeation enhancer i.e. glyceryl monooleate (GMO) - as a liquid crystal structure forming material makes this delivery system suitable for topical drug delivery. GMO is an amphiphilic molecule with a hydrophilic head group and a hydrophobic hydrocarbon tail [83]. Under varying conditions of temperature from room temperature to 80^0C, and in the presence of excess aqueous phase, it exhibits cubic crystal morphology. The GMO based mesophases have proven its application in enhancing the permeation into the skin matrix [84]. GMO is majorly composed of oleic acid, which can easily interact with skin lipids, and enhances permeation through the stratum corneum [84].

1.10.2 Proglycosomes

Vesicular drug delivery systems can easily permeate through the skin, but the percutaneous permeability depends on the elasticity of vesicles [80]. Proglycosomes are the modified liposomes consisting of propylene glycol as an edge activator. Liposomes are phospholipid bilayered vesicles composed of naturally occurring phospholipids along with cholesterol surrounding the distinct aqueous core. Cholesterol is used as the main component to reduce the fluidity of the liposomal bilayer membrane and improve stability [85]. Liposomes can encapsulate both hydrophilic and lipophilic drugs. The modified liposomes with ethanol and propylene glycol have shown more skin permeability compared to the conventional liposomal formulations. The use of propylene glycol in place of ethanol acts as an edge activator on liposomes, and these are named ‘proglycosomes’. The edge activators helps to soften the phospholipid membrane by which its deformability is increased. These proglycosomes have excellent encapsulation efficiency [86]. Further facilitated by their small size (less than 200 nm) proglycosomes can penetrate through leaky endothelium and accumulate at RA site. Along with permeation, site specific active targeting is desirable for effective delivery of tofacitinib (TF) loaded proglycosomes to synovial fluid.

1.10.3 Surface coated Proglycosomes for targeted drug delivery

The proglycosomes can be modified by attaching a ligand onto the surface to target a specific tissue or organ. Targeting ligands are molecules that recognise and bind to specific receptors on the surface of target cells. During RA disease conditions, the inflamed skin layers and synovial fluid shows the presence of CD44 (cluster of differentiation) on the surface of

activated macrophages [68]. Diagrammatic illustration of the CD44 receptor mediated endocytosis of glycosaminoglycan coated nanoparticles by the activated macrophages or lymphocytes and the drug release are presented in Figure 8.

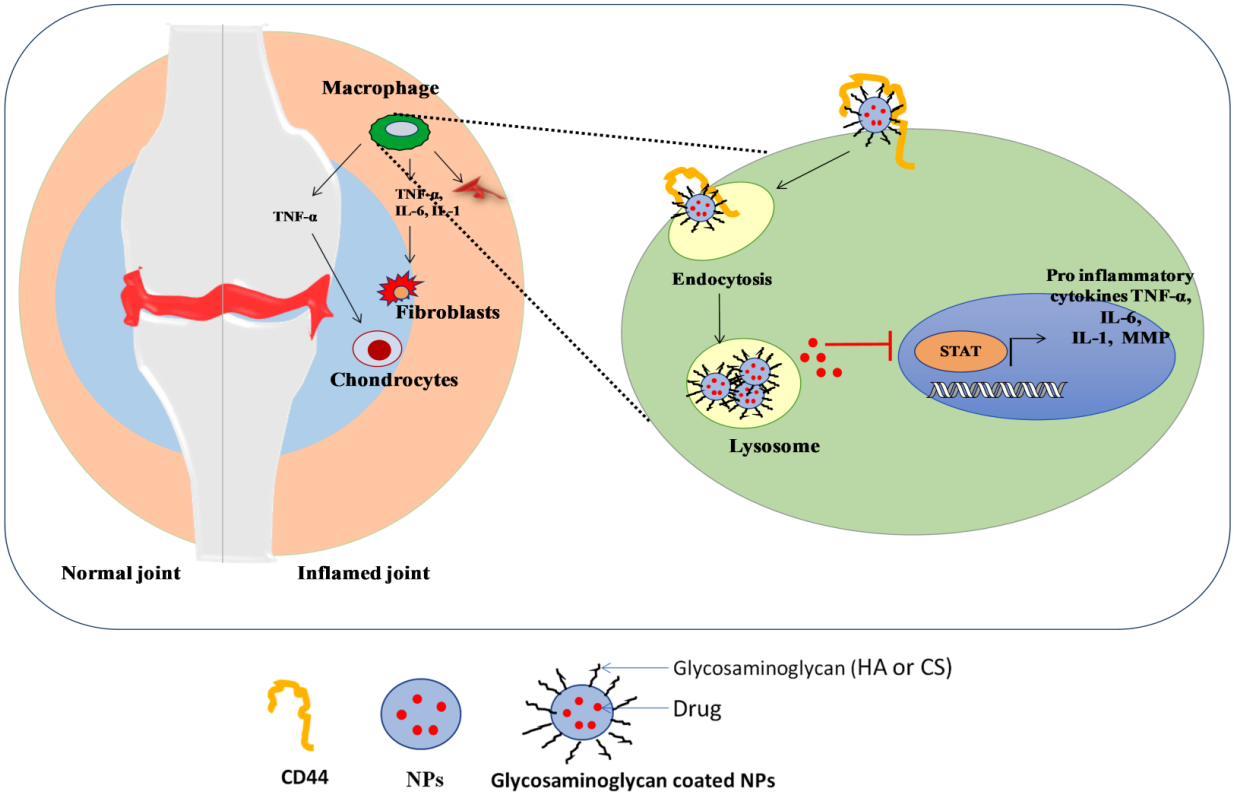

Figure 1.8. Diagrammatic illustration of the CD44 receptor mediated endocytosis of glycosaminoglycan coated nanoparticles by the activated macrophages or lymphocytes and the drug release [68]

1.10.4 Mechanism of coating of nanocarrier with glycosaminoglycans

These polyelectrolytes (or) glycosaminoglycans are polymers, consists of charged monomers. The charge is then related to the degree of ionisation in solution. These are distinguished based on the chemical composition. The monomers that contain quaternary ammonium group (permanent charges) and monomers containing ionisable primary amines and carboxylic acids that can dissociate in solution based on the pH and ionic strength. The pKa of the ionisable group is determined as the pH at which 50% of the ionisable monomer groups are charged. Polyelectrolytes are divided into anionic and cationic based on their charge [87].

The coating of polyelectrolytes/glycosaminoglycans onto the nanocarriers is driven by the electrostatic attraction between the oppositely charged constituents. The interactions responsible for this self-assembly are non-covalent forces, such as electrostatic, hydrophobic,

hydrogen bonding, van der Waal interactions. These influence the stability, morphology of particles/nanocarriers and permeation properties of the developed nanocarrier system. The attractive features of this technique include low cost, simplicity and versatility made researchers to develop novel delivery carriers. Generally, the process is as follows: (1) A charged nanocarrier formulation is added onto the solution of an oppositely-glycosaminoglycans solution to adsorb (2) a washing cycle follows to remove unbound glycosaminoglycan i.e., by centrifugation method [88].

The coating material concentration should be high enough for successful adsorption and to prevent depletion. To obtain the optimum adsorption layer around the nanocarrier, the glycosaminoglycan/polyelectrolyte concentration should be greater than the minimum threshold concentration for attachment and to reverse charge polarity. The threshold is determined by the coating material's solubility and charge density [89].

1.11 Permeation mechanisms of Liquid crystalline nanoparticles and proglycosomes on topical administration

Elias postulated bilayer in the stratum corneum is composed of lipids. Stratum corneum is represented as a two-compartment system like brick and mortar in which cells are related as a brick whereas inter- cellular lamellae equate to mortar. The skin cells which surround the intercellular matrix mainly help in preventing the water loss. Liquid crystals and lipids cover the skin to provide lubrication and to prevent loss of moisture from the skin. When the lipid content of the skin becomes less, it leads to roughness, wrinkles, and fine lines. Indeed, many chemicals contribute to healthy skin like cholesterol, triglycerides, glycerine, phospholipid, and fatty acids [90]. There are mainly two pathways for permeation through skin i.e., either transcellular or intercellular pathway. In general liquid crystals take the intercellular path to permeate into the skin. Due to the structural similarities between liquid crystals and stratum corneum, formulations based on liquid crystals have higher levels of hydration and easier distribution than emulsions. When applied topically, the cubic phase system demonstrates strong bio-adhesive properties and develops a biological membrane-like structure across the skin. It is expected that stratum corneum and the cubic phase will collaborate to form a cubosomal lipid stratum corneum and a cubosome depot, which releases the drug slowly. The liquid crystals consisting of amphiphilic lipid and the surfactant favour increase the drug permeability. The drugs encapsulated in LCNP interact with the skin tissue and localize in the stratum corneum resulting in the controlled release of the drug. This attributes to the minimal systemic absorption thus reducing the adverse effects. The presence of water in liquid crystals

acts as reservoir and provides hydration to the tissue [90]. On the topical application of the cubosomal gel, they interact with skin lipids specific to stratum corneum. The cubosomal gel undergoes transition to ordered hexagonal or orthorhombic lipids and further to the disordered fluid lamellar liquid crystalline phase. This further helps in permeation through paracellular gaps in the skin, the disorder liquid crystals exhibit more permeation over ordered lipid phases of the skin [91]. The permeation mechanism of LCNP through skin is presented in Figure1.9.

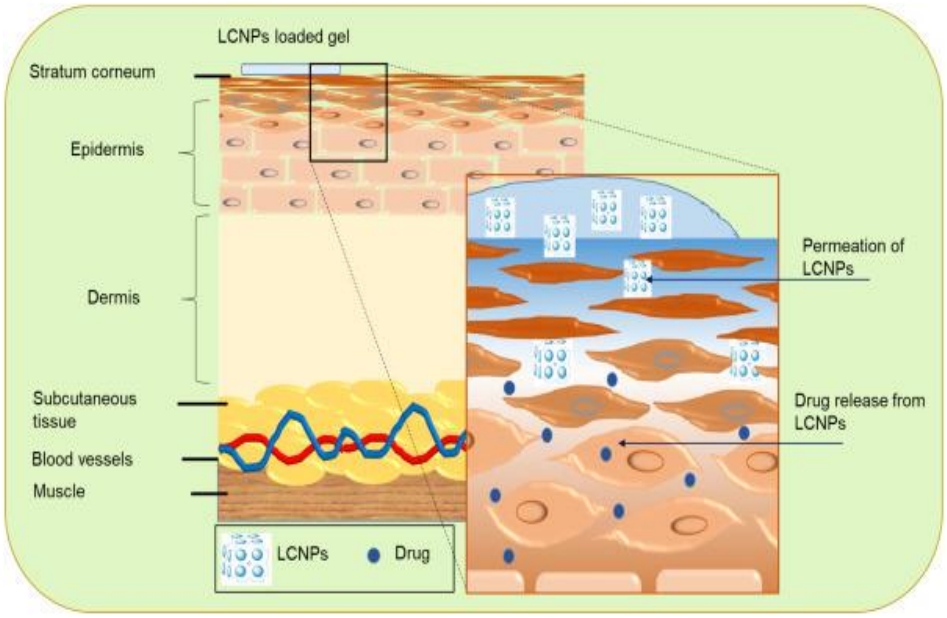

Figure 1.9. Permeation mechanism of LCNP through skin [92]

Skin permeability and retention were found to be more with modified liposomes i.e., reported ethosomes when compared to the conventional liposomal formulations. Use of ethanol for long time causes toxic effects on skin hence use of propylene glycol (named as proglycosomes) in place of ethanol act as edge activator on liposomes and also enhances the permeation through skin.

The vesicular carriers can exhibit high permeation profile because the Phospholipid molecules and propylene glycol improve molecular transport over the skin by changing lipid tight packing. In general, modified liposomes that is proglycosomes take the trans appendageal and intercellular pathway to permeate into the skin [86]. Thus, these LCNP and proglycosomes can be used for epidermal, dermal and transdermal drug delivery.

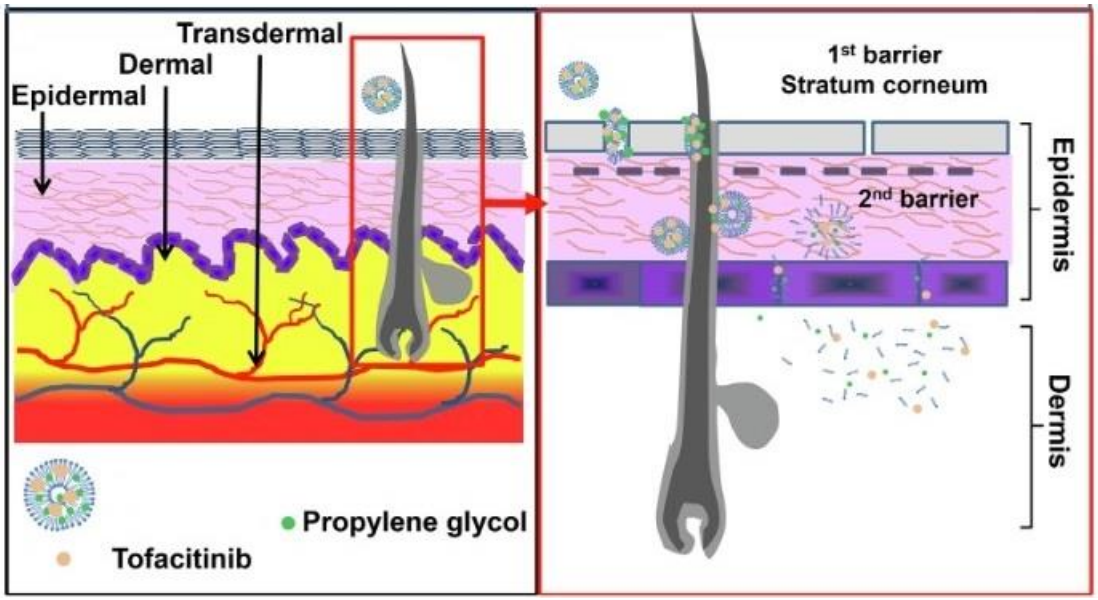

Figure 1.10. Permeation mechanism of proglycosomes through skin [86]

1.12 The problem statement and objectives of current research work

Worldwide 23 million people are affected by RA. The treatment of RA with other biologic agents exhibits disease suppression, but only approximately 30% accomplish complete remission and greater part of the RA population exhibits exacerbation following the cessation of treatment. Therefore, targeting the cytokines outside the cell is not enough. Thus, the design of small molecule or biological agent that can target multiple cytokines intracellularly could be a potential approach to overcome the complications in RA. The thorough literature survey revealed that continuous activation of Janus kinase (JAK) / signal transducers and activators of the transcription (STAT) pathway plays a crucial role in the pathogenesis and progression of inflammation in rheumatoid arthritis. Also, activated macrophages play a crucial role in RA pathogenesis by generating cytokines that enhance inflammation and contribute to the destruction of cartilage and bone. The above literature suggests that specific inhibition of the JAK/STAT pathway in macrophages is required to enhance the efficacy and minimize the cytotoxicity of JAK inhibitors. TF is a first approved potent inhibitor of the JAK 1 and JAK 3 by the United State Food and Drug Administration (USFDA) in 2012 for the treatment of moderate to severe arthritis.

TF, inhibits intracellular signaling from the receptor to the cellular nucleus, i.e., JAK1 and JAK3, which results in the dramatic improvement of pain and reducing swelling and the inflammation. The safety and efficacy data were examined for TF up to 9.5 years from 2007 to 2016 with 5 mg and 10 mg twice daily through the oral route in RA patients. A total of 4481

patients were enrolled, and efficacy data are reported for up to 8 years for TF 5 mg, and 6 years for 10 mg two times daily [93]. Overall, 52% of patients discontinued the treatment, i.e., 24% due to adverse actions and 4% due to inadequate clinical response. The long-term oral administration of TF has been linked to serious side effects such as a rise in cholesterol level, a decline in neutrophil count (upon 3 months of continuous usage), gastrointestinal perforations, systemic effects, and immunological suppression. In addition to this, dose escalation was a major limitation with this and the distribution of the drug to non-specific tissues. To overcome the systemic side effects and limitations of oral therapy site-specific delivery of TF via topical application can be one of the good approaches. However, permeation through the skin and selective action at the site is a big challenge. TF is a small hydrophobic molecule with a log P of 1.15 (neutral free base), and pKa of 5.2. Thus, it will be an un-ionized at acidic condition that allows it to accumulate at the skin tissues and synovial lining of joints. The properties confirms that TF is a suitable candidate for topical delivery to maintain improved concentration of TF in the synovial region and skin layers as compared to the plasma concentrations. However, these properties restrict the TF permeation through the stratum corneum. The conventional delivery systems fail to cross this stratum corneum passively and cannot provide the depot effect by residing at the epidermal and dermal region for prolonged action. Thus, there is a need of a TF delivery using vehicle which can penetrate the outermost stratum corneum barrier and exhibits the depot effect. The intense literature search has given a hope for effective delivery of rheumatic drugs using lipid-based nanoparticle-based systems with enormous advancements in recent days. The nanoparticles with a size less than 250 nm can reside at the inflammatory site due to the enhanced permeation effect and release the drug in a sustained manner. The lipid-based nanocarriers, especially LCNP, can enhance the permeation due to their similarity with the skin composition. The LCNP can also enhance the permeation by altering the skin polarity and interacting with the intercellular skin lipids and promote percutaneous absorption, i.e., penetration of stratum corneum, accumulation at the deeper skin layers. Also, the vesicular drug delivery systems can easily permeate through the skin, but the percutaneous permeability depends on the elasticity of vesicles. However, the modified liposomes with ethanol and propylene glycol smoothens the phospholipid bilayer and exhibits more skin permeability compared to the conventional liposomal formulations or ordinary topical applications.

Considering these benefits, for site specific delivery of TF we have utilized RA disease condition in animal i.e., targeting CD44 on the surface of the macrophages at the RA site for effective targeted delivery better therapeutic efficacy.

Therefore, the objectives of this research work was to design and investigate the effectiveness of TF loaded LCNP, TF loaded proglycosomes, hyaluronic acid coated proglycosomes and chondroitin sulphate coated proglycosomes for improved permeation and site specific delivery. Further, the optimized formulations were evaluated for *in vitro, ex vivo* and *in vivo* efficacy studies in the RA induced animal model.

In this research work, the aim was to deliver TF via topical route to the epidermal, dermal and synovial regions using LCNP, proglycosomes, proglycosomes coated with hyaluronic acid (HA) and chondroitin sulphate (CS) for targeting CD44 in the inflamed skin layers which may benefit progress in RA condition. The TF loaded proglycosomes were prepared by using biocompatible and biodegradable lipids LIPOID S 75 (Soya phosphatidyl choline with 70 % phosphatidyl choline), LIPOID S100 and cholesterol. The proglycosomes coated with HA and CS are also biocompatible and biodegradable.

In the current research work we have developed and optimized TF loaded LCNP using systematic QbD principles and investigated the effect of liquid oils on critical quality attributes (CQA) i.e., entrapment efficiency, particle size, and polydispersity index (PDI). Also, developed and optimized modified liposomes i.e., proglycosomes, were prepared by thin film hydration technique and further coated with hyaluronic acid and chondroitin sulphate for-TF delivery to targeted dermal region. All these formulations were evaluated for physico-chemical characterization, *In vitro* drug release studies, *ex vivo* skin retention, permeation, and dermatokinetics. Majorly, the *In vivo* evaluation of the all the designed formulations was performed in complete Freund's adjuvant RA diseased model and compared with oral administration. Finally, serum analysis was performed for the determination of the pro-inflammatory cytokines levels in disease control (DC) and post treatment with developed formulations. Also, the changes in hematological parameters, radiographic and histological analysis of ankle joints of rats and accessed the efficacy of developed formulations. All the formulations were studied for their stability.

Also, the above-mentioned objectives clearly signifies that there is a need for the analysis of the *in vitro* release samples, skin samples and plasma samples need to be analyzed. Thus, analytical and bioanalytical methods were developed and validated to quantify TF.

References

1. Guo Q, Wang Y, Xu D, Nossent J, Pavlos NJ, Xu J. Rheumatoid arthritis: Pathological

mechanisms and modern pharmacologic therapies. *Bone Res.* 6(1), 1-14 (2018).

2. WHO | Chronic rheumatic conditions. https://www.who.int/chp/topics/rheumatic/en/.

3. Gorantla S, Singhvi G, Rapalli VK, Waghule T, Dubey SK, Saha RN. Targeted drug-delivery systems in the treatment of rheumatoid arthritis: recent advancement and clinical status. *Ther. Deliv.* 11(4), 269–284 (2020). https://www.future-science.com/doi/10.4155/tde-2020-0029.

4. McInnes IB, Schett G. The pathogenesis of rheumatoid arthritis. *N. Engl. J. Med.* 365(23), 2205–2219 (2011).

5. Liao KP, Alfredsson L, Karlson EW. Environmental influences on risk for rheumatoid arthritis. *Curr. Opin. Rheumatol.* 21(3), 279–283 (2009). http://www.ncbi.nlm.nih.gov/pubmed/19318947.

6. McInnes IB, Schett G. Pathogenetic insights from the treatment of rheumatoid arthritis. *Lancet.* 389(10086), 2328–2337 (2017). http://dx.doi.org/10.1016/S0140-6736(17)31472-1.

7. Gorantla S, Batra U, SR, *et al*. Emerging trends in microneedle-based drug delivery strategies for the treatment of rheumatoid arthritis. *Expert Opin Drug Deliv.* 19(4), 395–407 (2022). https://www.tandfonline.com/doi/abs/10.1080/17425247.2022.2053674.

8. Qindeel M, Ullah MH, Fakhar-ud-Din, Ahmed N, Rehman A ur. Recent trends, challenges and future outlook of transdermal drug delivery systems for rheumatoid arthritis therapy. *J. Control. Release*. 327, 595–615 (2020).

9. Chuang SY, Lin CH, Huang TH, Fang JY. Lipid-Based nanoparticles as a potential delivery approach in the treatment of rheumatoid arthritis. *Nanomaterials*. 8(1), 42-48 (2018).

10. Rapalli VK, Singhvi G, Dubey SK, Gupta G, Chellappan DK, Dua K. Emerging landscape in psoriasis management: From topical application to targeting biomolecules. *Biomed. Pharmacother.* 106, 707–713 (2018). https://linkinghub.elsevier.com/retrieve/pii/S0753332218336667.

11. Schwartz DM, Kanno Y, Villarino A, Ward M, Gadina M, O'Shea JJ. JAK inhibition as a therapeutic strategy for immune and inflammatory diseases. *Nat. Rev. Drug Discov.*16(12), 843–862 (2017).

12. Hsu L, Armstrong AW. Review Article JAK Inhibitors: Treatment Efficacy and Safety Profile in Patients with Psoriasis. *J Immunol Res*. 283617 (2014). http://dx.doi.org/10.1155/2014/283617.

13. Szilveszter KP, Németh T, Mócsai A. Tyrosine kinases in autoimmune and inflammatory skin diseases. Front. Immunol.10, 1862 (2019).

14. Simon LS, Taylor PC, Choy EH, *et al.* The Jak/STAT pathway: A focus on pain in rheumatoid arthritis. *Semin. Arthritis Rheum.* 51(1), 278–284 (2021). https://pubmed.ncbi.nlm.nih.gov/33412435/.

15. Simon LS, Taylor PC, Choy EH, *et al.* The Jak/STAT pathway: A focus on pain in rheumatoid arthritis. *Semin. Arthritis Rheum.* 51(1), 278–284 (2021).

16. Nissen SE, Yeomans ND, Solomon DH, *et al.* Cardiovascular Safety of Celecoxib, Naproxen, or Ibuprofen for Arthritis. *N. Engl. J. Med.* 375(26), 2519–2529 (2016). http://www.nejm.org/doi/10.1056/NEJMoa1611593.

17. Wilsdon TD, Hill CL. Managing the drug treatment of rheumatoid arthritis. *Aust. Prescr.* 40(2), 51–58 (2017).

18. Ayhan E, Kesmezacar H, Akgun I. Intraarticular injections (corticosteroid, hyaluronic acid, platelet rich plasma) for the knee osteoarthritis. 5(3), 351 (2014). http://dx.doi.org/10.5312/wjo.v5.i3.351.

19. Fragoulis GE, Mcinnes IB, Siebert S. JAK-inhibitors. New players in the field of immune-mediated diseases, beyond rheumatoid arthritis. *Rheumatol.* 58, i43–i54 (2019).

20. Alunno A, Carubbi F, Giacomelli R, Gerli R. Cytokines in the pathogenesis of rheumatoid arthritis: new players and therapeutic targets. *BMC Rheumatol.* 1(1), 1-13 (2017).

21. Safety and Efficacy of Vagus Nerve Stimulator in Patients With Rheumatoid Arthritis (RA) - ClinicalTrials.gov. https://clinicaltrials.gov/ct2/show/NCT03437473?term=implants&cond=Rheumatoid+Arthritis&phase=0345&draw=2&rank=5.

22. Study of Intra-articular Delivery of tgAAC94 in Inflammatory Arthritis Subjects - ClinicalTrials.gov.https://clinicaltrials.gov/ct2/show/NCT00126724?term=intra+articular&cond=Rheumatoid+Arthritis&phase=0345&draw=2&rank=16.

23. Assessing Withdrawal of Disease-Modifying Antirheumatic Drugs in Rheumatoid Arthritis - ClinicalTrials.gov. https://clinicaltrials.gov/ct2/show/NCT01881308?term=intra+articular&cond=Rheumatoid+Arthritis&phase=0345&draw=2&rank=18.

24. TNF-blocking Therapy in Combination With Disease-modifying Antirheumatic Drugs in Early Rheumatoid Arthritis - ClinicalTrials.gov. https://clinicaltrials.gov/ct2/show/NCT00908089.

25. Rapalli VK, Waghule T, Gorantla S, Dubey SK, Saha RN, Singhvi G. Psoriasis: pathological mechanisms, current pharmacological therapies, and emerging drug delivery systems. *Drug Discov. Today*. 25(12), 2212-2226 (2020). https://linkinghub.elsevier.com/retrieve/pii/S1359644620303809.

26. Mostafavi SH. Nano-Sized Drug Delivery. *J. Mol. Pharm. Org. Process Res.* 1(3), 1–2 (2013).

27. Levick JR. Permeability of Rheumatoid and Normal Human Synovium to Specific Plasma Proteins. *Arthritis Rheum*. 24(12), 1550–1560 (1981). http://www.ncbi.nlm.nih.gov/pubmed/7326067.

28. Wardwell PR, Forstner MB, Bader RA. Investigation of the cytokine response to NF-KB decoy oligonucleotide coated polysaccharide based nanoparticles in rheumatoid arthritis in vitro models. *Arthritis Res. Ther.* 17(1),1-11 (2015).

29. Quan L, Zhang Y, Crielaard BJ, *et al.* Nanomedicines for inflammatory arthritis: Head-to-head comparison of glucocorticoid-containing polymers, micelles, and liposomes. *ACS Nano*. 8(1), 458–466 (2014). http://www.ncbi.nlm.nih.gov/pubmed/24341611.

30. Heo R, Park JS, Jang HJ, *et al.* Hyaluronan nanoparticles bearing γ-secretase inhibitor: In vivo therapeutic effects on rheumatoid arthritis. *J. Control. Release*. 192, 295–300 (2014). https://pubmed.ncbi.nlm.nih.gov/25109660/.

31. Naor D, Nedvetzki S. CD4 in rheumatoid arthritis. *Arthritis Res. Ther.*5(3), 105–115 (2003).

32. Nagayoshi R, Nagai T, Matsushita K, *et al.* Effectiveness of anti-folate receptor β antibody conjugated with truncated Pseudomonas exotoxin in the targeting of rheumatoid arthritis synovial macrophages. *Arthritis Rheum*. 52(9), 2666–2675 (2005). http://www.ncbi.nlm.nih.gov/pubmed/16142741.

33. Jubeli E, Moine L, Vergnaud-Gauduchon J, Barratt G. E-selectin as a target for drug delivery and molecular imaging. *J. Control. Release.*158(2), 194–206 (2012). http://www.ncbi.nlm.nih.gov/pubmed/21983284.

34. Delgado M, Abad C, Martinez C, *et al.* Vasoactive intestinal peptide in the immune system: Potential therapeutic role in inflammatory and autoimmune diseases. *J. Mol. Med.*80(1), 16–24 (2002). http://www.ncbi.nlm.nih.gov/pubmed/11862320.

35. Wilder RL. Integrin alpha V beta 3 as a target for treatment of rheumatoid arthritis and related rheumatic diseases. In: *Annals of the Rheumatic Diseases,* 61(2), 96-99(2002).

36. Nogueira E, Lager F, Le Roux D, *et al.* Enhancing methotrexate tolerance with folate tagged liposomes in arthritic mice. *J. Biomed. Nanotechnol.* 11(12), 2243–2252 (2015).

37. Sultana F, Neog MK, Rasool MK. Withaferin-A, a steroidal lactone encapsulated mannose decorated liposomes ameliorates rheumatoid arthritis by intriguing the macrophage repolarization in adjuvant-induced arthritic rats. *Colloids Surfaces B Biointerfaces*. 155, 349–365 (2017).

38. Poh S, Chelvam V, Kelderhouse LE, *et al.* Folate-conjugated liposomes target and deliver therapeutics to immune cells in a rat model of rheumatoid arthritis. *Nanomedicine*. 12(20), 2441–2451 (2017).

39. Zeb A, Qureshi OS, Yu CH, *et al.* Enhanced anti-rheumatic activity of methotrexate-entrapped ultradeformable liposomal gel in adjuvant-induced arthritis rat model. *Int. J. Pharm.* 525(1), 92–100 (2017).

40. Neog MK, Rasool M. Targeted delivery of p-coumaric acid encapsulated mannosylated liposomes to the synovial macrophages inhibits osteoclast formation and bone resorption in the rheumatoid arthritis animal model. *Eur. J. Pharm. Biopharm.* 133, 162–175 (2018).

41. Hua S, Dias TH, Pepperall D-G, Yang Y. Topical Loperamide-Encapsulated Liposomal Gel Increases the Severity of Inflammation and Accelerates Disease Progression in the Adjuvant-Induced Model of Experimental Rheumatoid Arthritis. *Front. Pharmacol*. 8, 503 (2017). http://journal.frontiersin.org/article/10.3389/fphar.2017.00503/full.

42. Meka RR, Venkatesha SH, Acharya B, Moudgil KD. Peptide-targeted liposomal delivery of dexamethasone for arthritis therapy. *Nanomedicine*. 14(11), 1455–1469 (2019).

43. Nogueira E, Freitas J, Loureiro A, *et al.* Neutral PEGylated liposomal formulation for efficient folate-mediated delivery of MCL1 siRNA to activated macrophages. *Colloids Surfaces B Biointerfaces*. 155, 459–465 (2017). http://www.ncbi.nlm.nih.gov/pubmed/28472749.

44. Hu L, Luo X, Zhou S, *et al.* Neutrophil-mediated delivery of dexamethasone palmitate-loaded liposomes decorated with a sialic acid conjugate for rheumatoid arthritis treatment. 36(7), 1-5 (2019). https://doi.org/10.1007/s11095-019-2609-4.

45. Xu X-L, Li W-S, Wang X-J, *et al.* Endogenous sialic acid-engineered micelles: a multifunctional platform for on-demand methotrexate delivery and bone repair of rheumatoid arthritis. *Nanoscale*. 10, 2923 (2018).

46. Hao F, Lee RJ, Zhong L, *et al.* Hybrid micelles containing methotrexate-conjugated polymer and co-loaded with microRNA-124 for rheumatoid arthritis therapy. *Theranostics*. 9, 18 (2019). http://www.thno.org//creativecommons.org/licenses/by/4.0/.

47. Wang Q, Jiang H, Li Y, *et al.* Targeting NF-kB signaling with polymeric hybrid micelles that co-deliver siRNA and dexamethasone for arthritis therapy. *Biomaterials*. 122, 10–22 (2017). http://www.ncbi.nlm.nih.gov/pubmed/28107661.

48. Wang X, Feng Y, Fu J, *et al.* A Lipid Micellar System Loaded with Dexamethasone Palmitate Alleviates Rheumatoid Arthritis. *AAPS PharmSciTech*. 20(8), 1–10 (2019).

49. Zhang N, Xu C, Li N, *et al.* Folate receptor-targeted mixed polysialic acid micelles for combating rheumatoid arthritis: In vitro and in vivo evaluation. *Drug Deliv*. 25(1), 1182–1191 (2018).

50. Wang Q, Li Y, Chen X, Jiang H, Zhang Z, Sun X. Optimized in vivo performance of acid-liable micelles for the treatment of rheumatoid arthritis by one single injection. *Nano Res.* 12 (2), 421-428 (2019). https://doi.org/10.1007/s12274-018-2233-3.

51. Mohammadi-Samani S, Zojaji S, Entezar-Almahdi E. Piroxicam loaded solid lipid nanoparticles for topical delivery: Preparation, characterization and in vitro permeation assessment. *J. Drug Deliv. Sci. Technol.* 47, 427–433 (2018).

52. Gu Y, Tang X, Yang M, Yang D, Liu J. Transdermal drug delivery of triptolide-loaded nanostructured lipid carriers: Preparation, pharmacokinetic, and evaluation for rheumatoid arthritis. *Int. J. Pharm*. 554, 235–244 (2019).

https://linkinghub.elsevier.com/retrieve/pii/S0378517318308421.

53. Janakiraman K, Krishnaswami V, Sethuraman V, Rajendran V, Kandasamy R. Development of methotrexate-loaded cubosomes with improved skin permeation for the topical treatment of rheumatoid arthritis. *Appl. Nanosci.*9(8), 1781-1796 (2019).

54. Sakdiset P, Amnuaikit T, Pichayakorn W, Pinsuwan S. Formulation development of ethosomes containing indomethacin for transdermal delivery. *J. Drug Deliv. Sci. Technol*. 52, 760–768 (2019). https://linkinghub.elsevier.com/retrieve/pii/S1773224719300772.

55. Singhvi G, Patil S, Girdhar V, Dubey SK. Nanocarriers for Topical Drug Delivery: Approaches and Advancements. *Nanosci. &Nanotechnology-Asia*. 9(3), 329–336 (2019). http://www.eurekaselect.com/160578/article.

56. Singh Malik D, Mital N, Kaur G. Topical drug delivery systems: a patent review. *Expert Opin. Ther. Pat.* 26(2), 213–228 (2016).

57. Tuma J & Pratt JM. Clinical child psychology practice and training: A survey. Journal of Clinical Child & Adolescent Psychology. *Adolescent Psychology*. 11(1), 27-34(1982).

58. Al Hanbali OA, Khan HMS, Sarfraz M, Arafat M, Ijaz S, Hameed A. Transdermal patches: Design and current approaches to painless drug delivery. *Acta Pharm.*69(2), 197-215(2019).

59. Waghule T, Singhvi G, Dubey SK, *et al.* Microneedles: A smart approach and increasing potential for transdermal drug delivery system. *Biomed. Pharmacother.*109, 1249–1258 (2019).

60. Mishra DK, Dhote V, Mishra PK. Transdermal immunization: Biological framework and translational perspectives. *Expert Opin. Drug Deliv*.10(2),183-200 (2013).

61. Rapalli VK, Singhvi G. Dermato-pharmacokinetic: assessment tools for topically applied dosage forms. *Expert Opin. Drug Deliv.*18(4),423-426(2020). https://www.tandfonline.com/doi/full/10.1080/17425247.2021.1856071.

62. Matriano JA, Cormier M, Johnson J, *et al.* Macroflux Microprojection Array Patch Technology : A New and Intracutaneous Immunization. *Pharma res.* 19(1),63-70 (2002).

63. Schoellhammer CM, Blankschtein D, Langer R. Skin permeabilization for transdermal drug delivery: Recent advances and future prospects. *Expert Opin. Drug Deliv.* 11(3), 393-407 (2014).

64. Shahzad Y, Louw R, Gerber M, Du Plessis J. Breaching the skin barrier through temperature modulations. *J. Control. Release*. 202, 1-13(2015).

65. Alkilani AZ, McCrudden MTC, Donnelly RF. Transdermal drug delivery: Innovative pharmaceutical developments based on disruption of the barrier properties of the stratum corneum. *Pharmaceutics*.7(4),438-470(2015).

66. Marshall JS, Warrington R, Watson W, Kim HL. An introduction to immunology and immunopathology. *Allergy, Asthma Clin. Immunol.* 14(2), 1–10 (2018). https://aacijournal.biomedcentral.com/articles/10.1186/s13223-018-0278-1.

67. Ploegh HL. Dendritic Cells: Biology and Clinical Applications. *Nat. Med.* 5(9), 970–979 (1999). https://www.nature.com/articles/nm0999_979a.

68. Gorantla S, Gorantla G, Saha RN, Singhvi G. CD44 receptor-targeted novel drug delivery strategies for rheumatoid arthritis therapy. *Expert Opin. Drug Deliv.* 18(11), 1553–1557 (2021). https://pubmed.ncbi.nlm.nih.gov/34190674/.

69. Matejuk A. Skin Immunity. *Arch. Immunol. Ther. Exp.* 66(1), 45–54 (2018).

70. Badghaish MMO, Qorban GNM, Albaqami AS. Rheumatoid Arthritis, Pathophysiology and Management. *Egypt. J. Hosp. Med.* 70(11),1898-1903(2018).

71. Teriete P, Banerji S, Noble M, *et al.* Structure of the regulatory hyaluronan binding domain in the inflammatory leukocyte homing receptor CD44. *Mol. Cell*. 13(4), 483–496 (2004).

72. Shin JM, Kim SH, Thambi T, *et al.* A hyaluronic acid–methotrexate conjugate for targeted therapy of rheumatoid arthritis. *Chem. Commun*. 50(57), 7632–7635 (2014). www.rsc.org/chemcomm.

73. Mahtab A, Rabbani SA, Neupane YR, *et al.* Facile functionalization of Teriflunomide-loaded nanoliposomes with Chondroitin sulphate for the treatment of Rheumatoid arthritis. *Carbohydr. Polym.* 250, 116926 (2020).

74. Gouveia VM, Lopes-De-Araújo J, Costa Lima SA, Nunes C, Reis S. Hyaluronic acid-conjugated pH-sensitive liposomes for targeted delivery of prednisolone on rheumatoid

arthritis therapy. *Nanomedicine*. 13(9), 1037–1049 (2018). http://www.ncbi.nlm.nih.gov/pubmed/29790395.

75. Lee H, Lee MY, Bhang SH, *et al.* Hyaluronate-gold nanoparticle/Tocilizumab complex for the treatment of rheumatoid arthritis. *ACS Nano*. 8(5), 4790–4798 (2014). https://pubs.acs.org/doi/full/10.1021/nn500685h.

76. Shilpi S, Upadhaye S, Shivvedi R, *et al.* Chondroitin sulphate mediated targeted delivery of methotrexate and aceclofenac to the joints for effective management of rheumatoid arthritis. *Asian J. Pharm. Pharmacol.* 5(3), 495–502 (2019).

77. Toyama-Sorimachi N, Kitamura F, Habuchi H, Tobita Y, Kimata K, Miyasaka M. Widespread expression of chondroitin sulfate-type serglycins with CD44 binding ability in hematopoietic cells. *J. Biol. Chem*. 272(42), 26714–26719 (1997). https://pubmed.ncbi.nlm.nih.gov/9334256/.

78. Waghule T, Gorantla S, Rapalli VK, *et al.* Emerging Trends in Topical Delivery of Curcumin Through Lipid Nanocarriers: Effectiveness in Skin Disorders. *AAPS PharmSciTech*. 21(7) (2020). https://pubmed.ncbi.nlm.nih.gov/33058071/.

79. Parekh K, Mehta TA, Dhas N, Kumar P, Popat A. Emerging Nanomedicines for the Treatment of Atopic Dermatitis. *AAPS PharmSciTech.* 22(2), 1–14 (2021). https://link.springer.com/article/10.1208/s12249-021-01920-3.

80. Hussain A, Singh S, Sharma D, Webster TJ, Shafaat K, Faruk A. Elastic liposomes as novel carriers: Recent advances in drug delivery. *Int. J. Nanomedicine*.12, 5087–5108 (2017).

81. Rapalli VK, Waghule T, Hans N, *et al.* Insights of lyotropic liquid crystals in topical drug delivery for targeting various skin disorders. *J. Mol. Liq.*315 (2020). https://doi.org/10.1016/j.molliq.2020.113771.

82. Singhvi G, Banerjee S, Khosa A. Lyotropic liquid crystal nanoparticles. In: *Organic Materials as Smart Nanocarriers for Drug Delivery*, Elsevier, 471–517 (2018). https://linkinghub.elsevier.com/retrieve/pii/B9780128136638000117.

83. Lim DG, Jeong WW, Kim NA, *et al.* Effect of the glyceryl monooleate-based lyotropic phases on skin permeation using invitro diffusion and skin imaging. *Asian J. Pharm. Sci.* 9(6), 324–329 (2014).

84. Guo C, Wang J, Cao F, Lee RJ, Zhai G. Lyotropic liquid crystal systems in drug delivery. *Drug Discov. Today*.15(23–24), 1032–1040 (2010).

85. Akbarzadeh A, Rezaei-Sadabady R, Davaran S, *et al.* Liposome: Classification, preparation, and applications. *Nanoscale Res. Lett.* 8(1), 1–9 (2013).

86. Kathuria H, Nguyen DTP, Handral HK, Cai J, Cao T, Kang L. Proposome for transdermal delivery of tofacitinib. *Int. J. Pharm*. 585 (2020). https://pubmed.ncbi.nlm.nih.gov/32565283/.

87. Ferjaoui Z, Nahle S, Chang CS, Ghanbaja J, *et al*. Layer-by-layer self-assembly of polyelectrolytes on superparamagnetic nanoparticle surfaces. *ACS omega*.5(10):4770-4777(2020).

88. Bantchev G, Lu Z, Lvov Y. Layer-by-layer nanoshell assembly on colloids through simplified washless process. *J. Nanosci. Nanotechnol.* 9(1), 396–403 (2009). https://pubmed.ncbi.nlm.nih.gov/19441325/.

89. Szarpak A, Pignot-Paintrand I, Nicolas C, Picart C, Auzély-Velty R. Multilayer assembly of hyaluronic acid/poly(allylamine): Control of the buildup for the production of hollow capsules. *Langmuir*. 24(17), 9767–9774 (2008). https://pubs.acs.org/doi/abs/10.1021/la801274z.

90. Suhaimi H, Rose LC. Skin and liquid crystal: A brief review on their similarities. *Orient. J. Chem.* 32(4), 2073–2078 (2016).

91. Hasnain MS, Nayak AK. Alginates : versatile polymers in biomedical applications and therapeutics. CRC Press. (2019).

92. Rapalli VK, Waghule T, Hans N, *et al.* Insights of lyotropic liquid crystals in topical drug delivery for targeting various skin disorders. *J. Mol. Liq.*315, 113771 (2020).

93. Boyce E, Vyas D, Rogan E, Valle-Oseguera C, O'Dell K. Impact of tofacitinib on patient outcomes in rheumatoid arthritis – review of clinical studies. *Patient Relat. Outcome Meas.*7,1-10(2016).

2 Drug profile

JAK inhibitors

JAK inhibitors are new small-molecule drugs of the immunosuppressant class. The JAK inhibitors are currently being tested in clinical trials to target various JAKs. Tofacitinib, a small molecule, inhibitor of JAK1, JAK2, JAK3, and TYK2 is on the market for the treatment of rheumatoid arthritis, psoriatic arthritis, and ulcerative colitis [1].

2.1 Drug properties

Name	:	Tofacitinib (TF)
Chemical Name	:	3-[(3R, 4R)-4-methyl-3-[methyl ({7H-pyrrolo[2,3-d]pyrimidin-4-yl})amino]piperidin-1-yl]-3- oxopropanenitrile
Structural Formula:		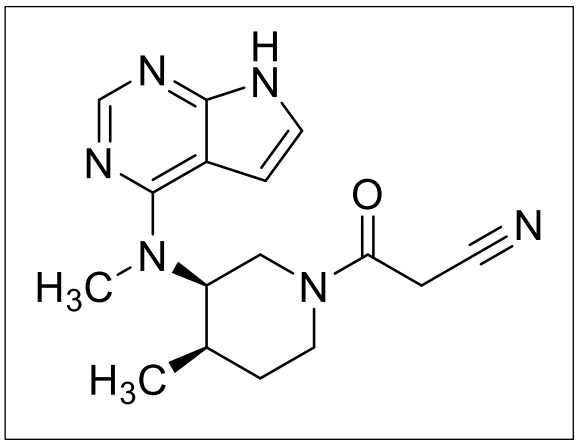
Molecular Formula		$C_{16}H_{20}N_6O$
Molecular Weight:		312.369 g/mol
Physical state:		Powder
Solubility:		Aqueous solubility (0.155 mg/mL), pH 7.4 (720-770 µg/mL), Tofacitinib in its citrate form exhibits pH-dependent solubility.
pK_a:		5.82
Log P:		1.81 (citrate form), 1.15 (neutral free base)

Log D (pH):	1.9
Melting Point:	154.5°C
Half-life:	3 to 3.2 h
Mechanism of Action:	TF is a JAK inhibitor. TF modulates the signaling pathway at the point of JAKs, preventing the phosphorylation and activation of STATs [2].

2.2. Pharmacokinetics

Absorption:	The absolute bioavailability with 10 mg dose was 74%. The peak plasma concentrations (Cmax) occurring at a T_{max} of approximately 0.5 – 1 h. TF co-administration with high fat meal shows a significant reduction in Cmax by 32% whereas no change in the extent of absorption (AUC0-∞).
Distribution:	TF exhibit approximately 40% of human plasma protein binding. TF binds mostly to albumin and does not appear to bind to α1-acid glycoprotein. On intravenous administration, the apparent volume of distribution (V_d) of TF was 87 L in average adult.
Metabolism:	TF undergoes extensive metabolism by CYP3A4 enzyme with minor contribution from CYP2C19.

TF undergoes extensive metabolism by liver microsomes in the presence of nicotinamide adenine dinucleotide phosphate. It was prone to approximately 70% hepatic metabolism.

The obtained metabolites have less than ≤10% of the potency of tofacitinib for JAK1/3 inhibition.

Elimination: TF administration on single- or multiple-doses, the terminal elimination half-life was found to be approximately 3 h.

Next to oral administration of radio-labelled tofacitinib, about 65% and 35% of the total circulating radioactivity is due to the unchanged TF and 8 metabolites respectively.

In a mass balance study, on oral administration 94% of the drug was recovered in urine (29% as TF; 51 % as tofacitinib metabolite) and feces (1% as TF; 13 % as TF metabolite) [3].

Table 2.1. Pharmacokinetic parameters of oral dosing of XELJANZ Solution and XELJANZ XR [4]

PK Parameters[a] (CV%)	XELJANZ		XELJANZ XR	
Dosing Regimen	5 mg Twice Daily	10 mg Twice Daily	11 mg Once Daily	22 mg Once Daily
AUC_{24} (ng.hr/mL)	263.4 (15)	539.6 (22)	269.0 (18)	596.6 (19)
C_{max} (ng/mL)	42.7 (26)	84.7 (18)	38.2 (15)	83.8 (25)
C_{min} (ng/mL)	1.41 (40)	3.10 (54)	1.07 (69)	3.11 (43)
T_{max} (hours)	1.0 (0.5 to14.0[b])	0.8 (0.5 to 14.0[b])	4.0 (3.0 to 4.0)	4.0 (2.0 to 4.0)

[a] Values represent the geometric mean, except T max, for which is the median (range) is shown.

2.3. Dosage forms and strengths

XELJANZ Tablet: 5 mg and 10 mg

XELJANZ XR Tablet: 11 mg and 22 mg

XELJANZ Oral solution: 1 mg/ mL solution

2.4. Limitations of Use

Administration of TF oral solution in combination with bDMARDs or potent immunosuppressants such as azathioprine and cyclosporine is not recommended

2.5. Adverse effects

Oral administration of TF is associated with severe adverse effects such as decreased neutrophil count, increased cholesterol level, gastrointestinal perforations, and immune suppression. Additionally, TF undergoes extensive metabolism by liver microsomes in the presence of nicotinamide adenine dinucleotide phosphate. Other adverse effects that are reported in >2% during clinical trials are include upper respiratory tract infections, nasopharyngitis, diarrhoea, malignancies, blood clots and serious infections.

References

1. Hosking A-M, Juhasz M, Mesinkovska NA. Topical Janus kinase inhibitors: A review of applications in dermatology. *J. Am. Acad. Dermatol*. 79(3), 535–544 (2018). http://www.ncbi.nlm.nih.gov/pubmed/29673776.
2. Dowty ME, Lin J, Ryder TF, *et al.* The pharmacokinetics, metabolism, and clearance mechanisms of tofacitinib, a janus kinase inhibitor, in humans. *Drug Metab. Dispos.* 42(4), 759–773 (2014). https://pubmed.ncbi.nlm.nih.gov/24464803/.
3. Pharmacology Reviewer Lokesh Jain C, Reviewer Lokesh Jain P, Bhattaram A, *et al.* Clinical pharmacology review NDA. 203214.
4. XELJANZ / XELJANZ XR Clinical Pharmacology (tofacitinib) | Pfizer Medical Information - US [Internet]. https://www.pfizermedicalinformation.com/en-us/xeljanz/clinical-pharmacology.

3 Introduction

The analytical methods play a pivotal role in formulation development. A suitable sensitive and precise analytical method is essential for analysis of pure drug, formulations, drug release, stability studies. During development of topical TF-loaded nanocarriers, it needs to be characterized for entrapment efficiency, *in vitro* drug release, assay, *ex vivo* permeation, and quantification of TF in the skin layers, pharmacokinetic studies.

There are few methods such as liquid chromatography-tandem mass spectrometry (LC-MS/MS), a dual-pump LC/LC-MS, and HPLC methods are reported for routine quantification of TF in in-vitro release samples, stability samples, and skin matrix samples. The reported LC-MS/MS, and LC/LC-MS are sensitive, but involve complex procedures. These methods are time-consuming and require a large amount of organic solvent [1–6].

The determination of drug substances using the UV spectrometric method and HPLC are most preferred in the industrial and academic sectors for routine analysis in a cost-effective way. However, Sankar et al. reported a spectrometric assay method for the determination of TF but the method applicability was limited to physical admixtures only [7]. Although the spectrometric methods were not explored for nanogram sensitivity, purity of target peak, and stability studies. Recently, a fully automated in situ ultraviolet fiber-optic system with 10 mm arch probes for the estimation of TF has been reported [8]. However, this is quite expensive, requires accurate installation, a trained operator, and it might be difficult to design acceptable measurement systems for routine analysis [7,9].

Thus, there is a need for a simple and economical validated UV spectrophotometric method to assess TF in API, formulations and in drug release samples. Therefore, a spectrophotometric method is developed and validated using methanol and 10% methanol in pH 7.4 phosphate buffer saline (PBS) containing 0.15% sodium lauryl sulfate (SLS). The developed method was validated as per International Conference on Harmonization (ICH) guidelines Q2 (R1) and USFDA [10]. The developed method in methanol was successfully applied to determine the entrapment efficiency of TF in LCNPs. Additionally, the developed method in 7.4 phosphate buffer saline (PBS) with 0.15% sodium lauryl sulphate (SLS) was substantially utilized as media for in-vitro release studies.

In consideration of the above discussion, we aimed to develop a method to determine the drug in nanogram level with high accuracy and precision. Few HPLC methods have been developed for the determination of TF. The reported HPLC methods for TF determination showed a lower

limit of quantification at microgram level only and were not fully validated as per ICH guidelines concerning stability studies and robustness [16–24]. Therefore, we developed and validated a rapid, accurate, and precise stability-indicating reverse phase HPLC method for the estimation of TF up to 50 nanogram levels in nanocarrier formulations and skin tissues. Further, the Design of Experiment (DoE) was applied to study the factor interaction and their impact on chromatographic properties [15]. The developed method is suitable for industry and academia for quantification of TF in lipid-based formulations, with ease and economic way. The % recovery of TF in the skin matrix was calculated and the method was successfully applied for dermatokinetics profiling of TF on topical application.

3.1 Materials, reagents, and chemicals

Analytical grade methanol and acetonitrile were procured from Merck Limited (Mumbai, India). Potassium dihydrogen phosphate, sodium chloride, potassium chloride, and disodium hydrogen phosphate were acquired from Merck. Glyceryl monooleate was procured as a gift sample from Mohini Organics Pvt Ltd. Poloxamer 407 was received as a gift sample from BASF (Mumbai). Oleic acid was procured from CDH (P) Ltd, Carbopol® 974P NF was obtained as a gift sample from Lubrizol, India. Milli-Q water from a Milli-Q water purification system, Millipore, USA. TF was received from Dr. Reddy's Laboratories as a generous gift sample.

3.1.1 Instrumentation

The analysis was performed using Jasco V-750 UV/VIS spectrophotometer (Tokyo, Japan). All the measurements are carried out at medium sensitivity using a 1 cm quartz cell. The equipment was supported by Jasco Spectra Manager software for the analysis of spectra.

3.2 Spectrophotometric method for the quantification of tofacitinib

3.2.1 Experimental requirements

3.2.1.1 Preparation of stock and standard solutions

TF (1 mg/mL) stock solution was prepared by dissolving an accurately weighed 5 mg of TF in 2 mL methanol. The volume was made up to 5 mL with the same solvent. Further, the standard stock solution (100 µg/mL), and secondary stock solutions were prepared separately using the solvent system such as absolute methanol and 10% methanol in pH 7.4 PBS containing 0.15% SLS. These 10 µg/mL working standards were prepared separately in the solvent system mentioned above to determine the λ_{max} of TF in both the solvent systems.

3.2.1.2 Determination of absorption maxima

The prepared working standard 10 µg/mL in both the solvent system were scanned on spectrum mode using Jasco V-750 UV spectrophotometer between 200 - 800 nm using respective solvent system as blank and the absorption maximum (λmax) in the solvent systems was determined.

3.2.2 Method development

3.2.2.1 Construction of calibration curve

The working standard of 100 µg/mL was diluted with methanol to obtain the final concentrations of 5 - 30 µg/mL. The absorbance of the prepared concentrations was determined at 285 nm. Additionally, the working standard 100 µg/mL was diluted with 10% methanol in pH 7.4 PBS containing 0.15% SLS to obtain the final concentrations in the range of 5 - 40 µg/mL. The absorbance of the prepared concentrations was determined at 287 nm.

3.2.2.2 Validation of the developed spectrophotometric method

The developed spectrophotometric methods in both the solvent systems were fully validated as per ICH Q2 R1 guidelines for system suitability, linearity, range, limit of detection (LOD), limit of quantification (LOQ), accuracy, precision, specificity, and repeatability [10].

3.2.2.3 Linearity, Range, Limit of Detection, and Limit of Quantification

The linearity was executed for six concentrations within the range of 5- 30 µg/mL and 5-40 µg/mL in methanol and 10% methanol in pH 7.4 PBS containing 0.15% SLS, respectively. The experiment was performed on three consecutive days in both the solvent system. The linearity was obtained by plotting analyte absorbance against drug concentration. Further, the regression equations representing these linear correlations were determined. These can be written as y = mx + c, where y is instrument response, and x is analyte level; m is the line's gradient, and c is its intercept with the y-axis. The LOD and LQ were calculated by using the below-mentioned formulas.

$$\boldsymbol{LOD = 3.3\ \frac{\sigma}{S}}$$

$$\boldsymbol{LOQ = 10\ \frac{\sigma}{S}}$$

where; σ denotes the standard deviation of absorbance of the sample; S denotes calibration curve slope.

3.2.2.4 Accuracy

Accuracy is the measurement of the closeness of the observed value to a real value. In contrast, precision refers to the consistency of measurement values to each other. Accuracy was determined by using quality control standards of TF (LQC: 7 µg/mL; MQC: 14 µg/mL; HQC: 28 µg/mL) for both the solvent systems. The accuracy was determined by calculating the % bias and % recovery of absorbances of quality control samples (LQC, MQC, and HQC) within a day. Each QC sample was analyzed in triplicate and sample concentration was determined by linearity curve.

3.2.2.5 Precision

The precision was established in both the solvent systems by using the quality control standards (LQC: 7 µg/mL; MQC: 14 µg/mL; HQC: 28 µg/mL) on intra and interday. The intra and inter day precision was performed by determining % RSD of the quality control samples on three consecutive days (a total of nine determinants). As per the regulatory guidelines, the acceptance criterion for accuracy and precision of quality control samples $\leq \pm$ 2%RSD.

3.2.2.6 Specificity

The specificity of TF was determined in the presence of nanoparticle excipients, including glyceryl monooleate, oleic acid, and poloxamer 407. A dispersion of liquid crystalline nanoparticles formulation was prepared, and a standard solution (10 µg/mL) of TF was spiked and vortexed. Further, it was filtered through a 0.22 µ filter and analyzed using the validated spectrometric methods in the presence of respective solvent systems as blanks.

The method was tested on another laboratory condition with the Shimadzu system (model number: 2800).

3.2.3 Results and discussion

3.2.3.1 Linearity, Range, Limit of detection, and Limit of Quantification

The calibration graph was constructed by plotting the absorbance against concentration (µg/mL) to measure TF by the validated spectrophotometric method. The Linearity plot of TF in methanol and 10% methanol in pH 7.4 PBS containing 0.15% SLS was presented in Figure 3.1. The LOD and LOQ were calculated in the solvent system (methanol and 10% methanol in pH 7.4 PBS containing 0.15% SLS) by using the equations recommended by the ICH guidelines. The statistical data of the regression equations and validation parameters for the spectrophotometric determination of TF is illustrated in Table 3.1.

Table 3.1. Statistical data of the regression equations and validation parameters (n = 3)

Solvent system	**Methanol**	**10% methanol in pH 7.4 PBS containing 0.15% SLS**
Regression analysis		
Regression coefficient (R^2)	0.9990	0.9999
Intercept (C)	0.001 ± 0.01056	-0.0045 ± 0.00289
Slope (M)	0.0419 ± 0.000585	0.0313 ± 0.000122
Validation parameters		
Linearity	5 - 30 µg/ml	5 - 40 µg/ml
LOD (µg/mL)	1.54 µg/ml	1.32 µg/ml
LOQ (µg/mL)	4.67 µg/ml	4.01 µg/ml

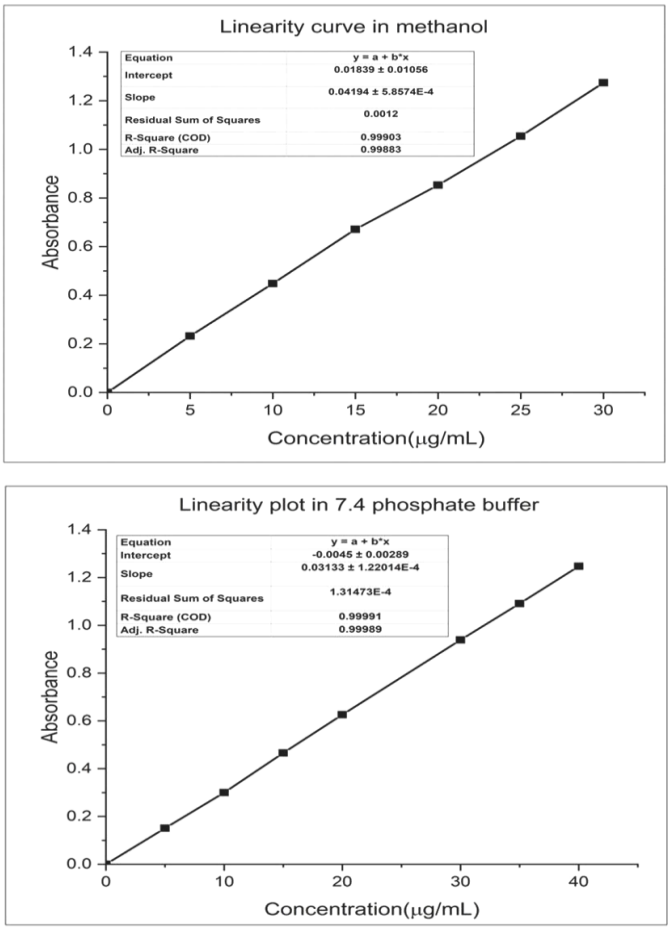

Figure 3.1. Linearity plot of TF in methanol and Phosphate buffer saline with 0.15% SLS

3.2.3.2 Accuracy

The accuracy of the developed methods was determined by calculating the % bias and % recovery of the quality control samples. The quality control samples of TF (LQC, MQC, and HQC) with methanol and **PBS with 0.15% SLS, and methanol in the ratio of 4:1 were** 7 µg/mL, 14 µg/mL, 28 µg/mL and 9 µg/mL, 18 µg/mL, and 36 µg/mL, respectively. The data of the recovery studies were tabulated in Table 3.2 and 3.3. The results indicated that the % recovery was found to be 99.49 ± 0.909 % to 101.40 ± 0.4331 % in methanol and 99.00 ± 0.271 % to 104.94 ± 1.492 % in pH 7.4 PBS with 0.15% SLS.

3.2.3.3 Precision

The precision of the quality control samples of TF in methanol (7 µg/mL, 14 µg/mL, 28 µg/mL) and **PBS with 0.15% SLS, and methanol in the ratio of 4:1 were** (9 µg/mL, 18 µg/mL, and 36 µg/mL) was determined. The intraday and inter-day precision data of TF are presented in Table 3.2 and 3.3. The results of % RSD of developed methods were below 2% in all media. The obtained results of % RSD in both the solvent system was <2%, which confirmed the consistency of the developed method. Figure 3.2 represents the overlay of UV spectroscopy spectrum of quality control standards of TF in methanol and **PBS with 0.15% SLS.**

Table 3.2. Accuracy and precision of TF in methanol

Sample	**Intraday**			
QC	**Mean± SD**	**% Recovery**	**%Bias**	**%RSD**
LQC	0.3266 ± 0.0015	101.40± 0.4331	1.404 ± 0.9165	0.808 ± 0.012
MQC	0.610 ± 0.0068	99.92 ± 1.336	0.9618 ± 1.7370	1.640 ± 0.226
HQC	1.182 ± 0.0026	99.49 ± 0.218	0.9630 ± 0.2840	0.2771 ± 0.040
	Inter-day			
LQC	0.3225 ± 0.0019	99.80 ± 0.776	0989 ± 0.8773	0.785 ± 0.030
MQC	0.6094 ± 0.0035	99.69 ± 1.025	0.980 ± 1.2483	1.181 ± 0.1165
HQC	1.1816 ± 0.0029	99.49 ± 0.341	0.963 ± 0.2449	0.567 ± 0.081

QC: Quality control samples; LQC: 7 µg/mL; MQC: 14 µg/mL; HQC: 28 µg/Ml

Table 3.3. Accuracy and precision of TF in 7.4 pH Phosphate buffer with 0.15% SLS

Sample	**Intraday**			
QC	**Mean± SD**	**% Recovery**	**%Bias**	**% RSD**
LQC	0.287 ± 0.004	99.49 ± 0.909	0.595± 0.282	1.386 ± 0.013
MQC	0.583 ± 0.002	101.94 ± 0.183	0.963± 0.098	1.787 ± 0.004
HQC	1.180 ± 0.009	103.78 ± 0.596	0.963 ± 0.649	0.836 ± 0.006
	Inter-day			
LQC	0.303 ± 0.002	104.94 ± 1.492	0.990 ± 0.764	1.766 ± 0.01
MQC	0.561 ± 0.004	98.03 ± 0.942	0.982 ± 0. 547	1.268 ± 0.025
HQC	1.126 ± 0.003	99.00 ± 0.271	0.964 ± 0. 243	0.334 ± 0.079

LQC: 9 µg/mL; MQC: 18 µg/mL; HQC: 36 µg/mL

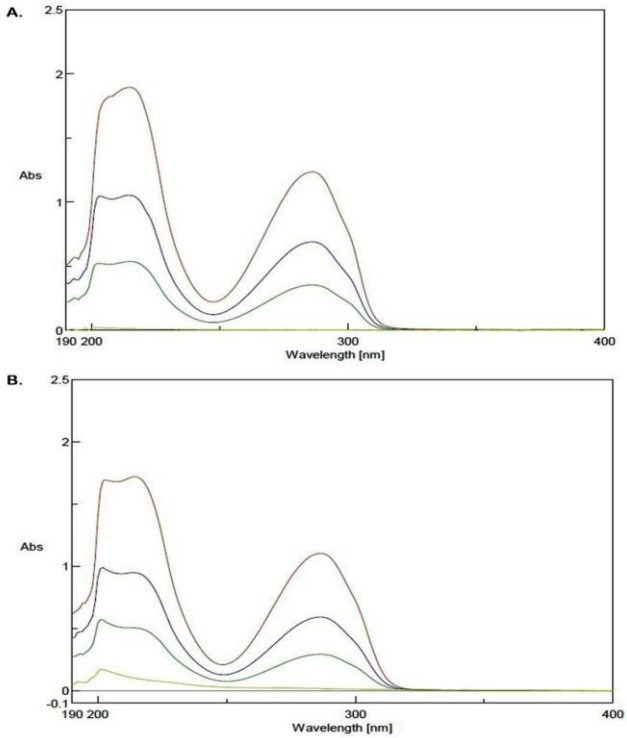

Figure 3.2. Overlay of UV-Spectroscopy spectrum of A) Quality control standards of TF in methanol B) Quality control standards of TF in 10% methanol in pH 7.4 PBS containing 0.15% SLS.

3.2.3.4 Specificity

The specificity of the TF in the presence of placebo lipid nanocarriers was determined. The recovered amount of TF from lipid nanocarrier formulation was found to be 98.85 ± 0.45%. The obtained recovery represented the specificity of the developed method in the presence of formulation excipients without interference.

Upon analyzing on the prepared standard concentration on Schimadzu UV instrument insignificant change was observed. Hence this method could be easily transferable from one laboratory to another.

3.3 Stability indicating RP-HPLC method for the determination of TF in nanoparticles and skin matrix

3.3.1 Experimental requirements

3.3.1.1 Instrumentation and chromatographic conditions

The chromatographic experiments were conducted on the HPLC system (Shimadzu, Kyoto, Japan) comprised of model LC-10AT, a binary pump, SIL-HTA autosampler (Shimadzu, Kyoto, Japan), column oven (CTO-10AS) compartment, and SPD-M20A Photodiode array (PDA) detector. Chromatographic separation was carried out at 30 ± 0.5 °C using LiChrospher ^{R} 100 RP-18 analytical column (Hibar ^{R} 250-4.6; 5 µm; Merck ^{R}). In the first instance, preliminary trials were conducted to acquire knowledge about the method performance and identification of various critical, independent parameters and their effect on dependent variables. Systematic method development strategies were applied to identify the independent parameters with a smaller number of trials. Primarily, acetonitrile and methanol were tried with various % ratios of ammonium acetate and phosphate buffers (pH 5, 10 mM) to obtain desired peak symmetry. A 3^2 full factorial experimental design was applied for the optimization of the mobile phase composition. The detection was carried out with a PDA detector with a 30 µL injection volume at a wavelength of 285 nm. The data acquisition and HPLC system were controlled by the LC solution software version 1.24 SP1.

3.3.1.2 Preparation of stock, calibration and quality control standards

A stock solution of TF (1 mg/mL) was prepared by dissolving an accurately weighed amount (5 mg) of TF in 5 mL methanol. The working standard solution (100 µg/mL) and calibration standards of 50-15000 ng/mL were prepared through serial dilution with methanol. The quality control (QC) standards were prepared from the standard stock at three concentration levels;

low QC (250 ng/mL), medium QC (8000 ng/mL), high QC (12000 ng/mL), and the lower limit of quantification (LLOQ) (50 ng/mL).

3.3.2 Method development

3.3.2.1 DoE methodology and optimization of analytical method

Using the above-executed trials, the organic phase and pH of phosphate buffer demonstrated a high impact on retention time and tailing factor. Therefore, to investigate the effect of organic phase composition and phosphate buffer pH on drug retention time and tailing factor, the Design of experiments (DoE) methodology was applied [16]. A 3^2 factorial design consisting of 2 factors at 3 levels was considered for an experimental plan with Design-Expert 8.0 Stat-Ease Inc. Minneapolis, USA. The two independent variables % organic Phase (X_1) with 3 levels (-1 (40%), 0 (50%), +1 (60%)), and pH of phosphate buffer (X_2) with 3 levels (-1 (3.5), 0 (4.5), +1 (5.5)) were confiscated as the actual value. The retention time and tailing factor were considered as dependent variables as responses Y_1 and Y_2, respectively.

3.3.3 Validation of the developed method

The validation of the analytical method was performed for system suitability, linearity, range, detection limit, quantification limit, specificity, accuracy, precision, carryover effect, and robustness according to the ICH Q2 (R1) guideline (2005).

3.3.3.1 System suitability

System suitability test was preferred for chromatographic methods to ensure that the system is efficient to give reproducible results. The performance of the system was evaluated by injecting six replicates of 10 µg/mL concentration with optimized chromatographic conditions.

3.3.3.2 Linearity, limit of detection and quantification limit

Linearity was determined with a concentration range between 50-15000 ng/mL with six calibration standards. The obtained data was fitted into linear regression analysis, and the calibration curve was plotted by the analyte peak area on the x-axis against the concentration of analyte on the y-axis. The detection limit (or) LOD and quantification limit (or) LOQ were decided based on the signal-to-noise (S/N) ratio. Initially, in the system suitability test, the signal to noise ratio was obtained based on the detector response. LOD and LOQ were calculated based on the below mentioned formula [17]. The preferred S/N values were 3 and 10 for LOD and LOQ, respectively. From these, LLOQ has been determined and considered as the lowest standard of the calibration curve.

$$LOD\ and\ LOQ = \frac{Concentration\ of\ standard}{\frac{S}{N} value\ of\ standard} * Desired \frac{S}{N} value$$

3.3.3.3 Accuracy

The measurement of the observed value's proximity to a given value is known as accuracy. Accuracy was determined by using quality control standards of TF (LLOQ: 50 ng/mL; LQC: 250 ng/mL; MQC: 8000 ng/mL; HQC: 12000 ng/mL). Accuracy was performed in six replicate and denoted as % recovery and % bias which should be ≤ ±10 % as per regulatory guidelines.

3.3.3.4 Precision

Precision, on the other hand, relates to the closeness of measurement values to one another. The precision of the quality control samples LQC (250 ng/mL), MQC (8000 ng/mL), and HQC (12000 ng/mL), as well as LLOQ, were determined in six replicates on intra and inter days. and the precision as % relative standard deviation (RSD). The acceptance requirement for precision and accuracy of quality control samples according to regulatory criteria was ≤ ±2% % RSD [18].

3.3.3.5 Carryover effect

The carryover was assessed by analyzing successive samples (10 µg/mL, 12 µg/mL, and 15 µg/mL) of the linearity curve followed by a blank carryover acceptance criterion should not be higher than 20% of LLOQ.

3.3.3.6 Robustness

Robustness can be defined as the reproducibility potential of the developed method in the same laboratory conditions with slight modification in chromatographic conditions and different HPLC systems with specified conditions. Initially, the robustness of the developed analytical method was performed by changing the column oven temperature, to ± 5 ^{0}C and mobile phase pH, to ± 0.5. Further, the optimized method was tested on another laboratory condition with the Shimadzu system (model number: LC 2010CHT).

3.3.3.7 Specificity

The specificity of the developed analytical method was studied in the presence of formulation excipients (lipids). A known concentration of TF within the linearity range was spiked into the

lipids and analyzed using the developed HPLC method. The interference of lipids with the retention time of analyte and peak purity was observed.

3.3.4 Stability indicating property of the developed method

The stability-indicating property of the developed analytical method was studied by exposing the TF solution to stress conditions as per ICH Q1A (R2) guidelines. The stress studies of TF solution were conducted under acidic hydrolysis, base hydrolysis, oxidation, and thermolytic conditions [19]. The acid hydrolysis and base hydrolysis were carried out by preparing the TF solution (200 µg /mL) using 0.5 M hydrochloric acid and 0.5 M sodium hydroxide, and kept in a water bath at 60^0C for 6 h. Similarly, for oxidative degradation**,** TF solution was prepared using 2% hydrogen peroxide and heated at 60^0C under reflux condition for 3 h. For thermal degradation, the TF solution was heated at 80^0C under reflux condition for 6 h. After subjecting TF solution (200 µg /mL) to the above-mentioned stress conditions, a concentration of 10 µg /mL was prepared using methanol. The samples of acid and base were neutralized before dilution with methanol to protect the column. All the samples were filtered through a 0.2 µm filter before injecting it into HPLC analysis [20,21]. The chromatograms of different stress conditions were recorded and compared with the normal condition. The retention time of different degradant peaks and drug peak were identified and the % degradation was calculated.

3.3.5 Applicability of the developed method for skin studies of TF and dermatokinetic assessment

The validated method for quantification of TF in the presence of a skin tissue matrix was used to evaluate TF penetration through the skin. Initially, skin tissue was homogenized using an Ultra-Turrax type homogenizer. Furthermore, the homogenized tissue was spiked with a predetermined concentration of TF solution (500 µg/mL) and centrifuged. The supernatant (1 mL) was collected and from this a concentration of 10 µg/mL was prepared. The samples were filtered through the 0.22 µ membrane filter before analysis and observed for peak specificity, and percent recovery was calculated [22]. In-house, TF cream was prepared using stearic acid as a base (0.5 mg/g) and applied topically to the skin (350 mg). After topical application, skin samples were collected for each time point at 2, 4, 6, 8, 12, and 24 h. The collected skin samples were washed with phosphate buffer and gently wiped with the cotton. Tape stripping analysis was performed to separate the epidermis and dermis layers. The collected tapes and skin were soaked for 6 h in methanol. After 6 h, the samples were filtered through a 0.25 µ filter and then stored at −20 °C until analyzed as per the validated method. TF concentration in the epidermis

and dermis-time graphs were evaluated by a non-compartmental model approach to obtain half-life ($t_{1/2}$); TF concentration in epidermis and dermis at t = 0 (C_0); area under the curve from zero to the last measurable point (AUC_{0-t}); area under curve from time 0 extrapolated to infinity ($AUC_{0-\infty}$).

3.3.6 Results

3.3.6.1 DoE methodology and optimization of analytical method

Preliminary studies were performed for the development of HPLC method. Initially, different combinations of mobile phases were explored using methanol, acetonitrile, and aqueous buffers (potassium phosphate and ammonium acetate 10mM). Peak splitting and broad peaks were observed in the case of acetonitrile, whereas peak symmetry was found acceptable in the case of methanol. Methanol was combined with different proportions of aqueous buffers and chromatogram properties (peak area, tailing factor, and retention time) were observed. The peak properties were analyzed and it was observed that methanol in combination with 10mM phosphate buffer showed acceptable peak properties. The above-mentioned preliminary studies were performed with the aqueous mobile phase in 50:50 v/v. The injection volumes of 20 µL and 30 µL were screened, and it was found that 30 µL showed a good peak area with a reduced tailing factor. The above trials revealed that the peak properties were mostly influenced by the methanol percentage and pH of the aqueous phosphate buffer. Further, to optimize these parameters, a full factorial design was applied.

A total of 11 experimental runs were performed based on a 3^2-factorial design, and obtained results were analyzed for the retention time and tailing factor. The results of the responses are specified in Table 3.4. To evaluate the relation between the dependent and independent variables, the response surface methodology plots were produced from Design expert software, as reported in Figure 3. The experimental runs responses were fitted into linear, second-order, and quadratic models. Quadratic models proved to be the best fit with $p < 0.0001$. The model summary statistics suggested the quadratic model for responses, because of the low prediction error sum of squares (PRESS) value of the quadratic model. Here, the low standard deviation and high adjusted R^2 value, specify the good correlation of the fitted model with experimental data. The model was analyzed and validated by Analysis of Variance (ANOVA) and the results are shown in Table 3.5.

Table 3.4. Suggested experiments by the design of experiments and responses

Variable 1	**Variable 2**	**Response 1**	**Response 2**
Organic phase (%)	Buffer pH	Retention time (Minutes)	Tailing factor
40	3.5	7.243	1.681
50	3.5	4.918	1.514
60	3.5	3.667	1.325
40	4.5	9.790	1.652
50	4.5	5.430	1.473
60	4.5	3.868	1.352
40	5.5	11.168	1.435
50	5.5	5.630	1.365
60	5.5	3.902	1.334
50	4.5	5.420	1.472
50	4.5	5.430	1.455

Table 3.5. ANOVA for response surface quadratic model

Parameter	**Response 1 (Retention time)**	**Response 2 (Tailing factor)**
Std. Dev.	0.38	0.024
Mean	6.04	1.46
C.V. %	6.31	1.63
R-Squared	0.9877	0.9804
Adj R-Squared	0.9755	0.9608
Pred R-Squared	0.8712	0.8210
Adeq Precision	26.389	21.688
F value	80.51	50.03
p-value	< 0.0001	0.0003

The independent variables exhibited a reasonable impact on retention time. ANOVA analysis (Table 3.5) showed model F-value of 80.51 (p-value < 0.0001), which stipulated that the model

was significant. The 3D plots, 2D contour plots and final polynomial equation 1 for actually coded variables showed the relationship between % of the organic phase (X_1), and pH of phosphate buffer (X_2), on the retention time (Y_1) (Figure 3.3). Figures 3.3a and 3.3b showed that the methanol ratio in the mobile phase had shown a notable effect on retention time. The retention time was decreased with an increase in methanol percentage in mobile phase composition. In contrast, increasing the pH of phosphate buffer resulted in increased retention time. The combination of both the variables X_1 and X_2 showed a parabolic effect on the retention time. The obtained polynomial equation 1 has confirmed the same.

The polynomial equation 1 showed that the % of the organic phase (X_1) showed a negative effect while the pH of phosphate buffer (X_2) showed a positive effect, but the combination of both the independent variables exhibited a negative effect on retention time (Y_1).

Retention time (Y_1) = +22.67376 -1.17143 X_1 +7.65975 X_2 - 0.092250 X_1 X_2 + 0.013072 X_1^2- 0.24834 X_2^2 …….. Equation (1)

The independent variables showed a reasonable impact on the tailing factor. ANOVA analysis showed model F-value of 50.03 with a p-value 0.0003, indicating that the model was significant (Table 3.5). The 3D plots and final polynomial equation 2 for actual coded variables showed the relationship between % of the organic phase (X_1), and pH of phosphate buffer (X_2) on the tailing factor (Y_2) (Figure 3.3a and 3.3b). Figure 3.3c and 3.3d showed that the methanol ratio in the mobile phase had shown a prominent effect on the tailing factor. The obtained polynomial equation 2 has proved the same. The polynomial equation 2 showed that the % of the organic phase (X_1) showed a negative effect, while the pH of phosphate buffer (X_2) exhibited a positive effect, but the combination of both the independent variables exhibited a positive effect on the tailing factor (Y_2).

Tailing factor (Y_2) = +3.42085 - 0.060278 X_1 + 8.65351E-003 X_2 + 6.37500E-003 X_1 X_2 + 1.89737E-004 X_1^2 - 0.043526 X_2^2…….. Equation (2)

The 3^2 factorial designs presented 50 solutions for the optimized chromatographic conditions, but the solutions were reduced by setting the goal values. The optimized chromatogram conditions were found to be methanol and 10mM phosphate buffer (pH 3.5) in the ratio of 50:50% v/v with a flow rate of 0.8 mL/min.

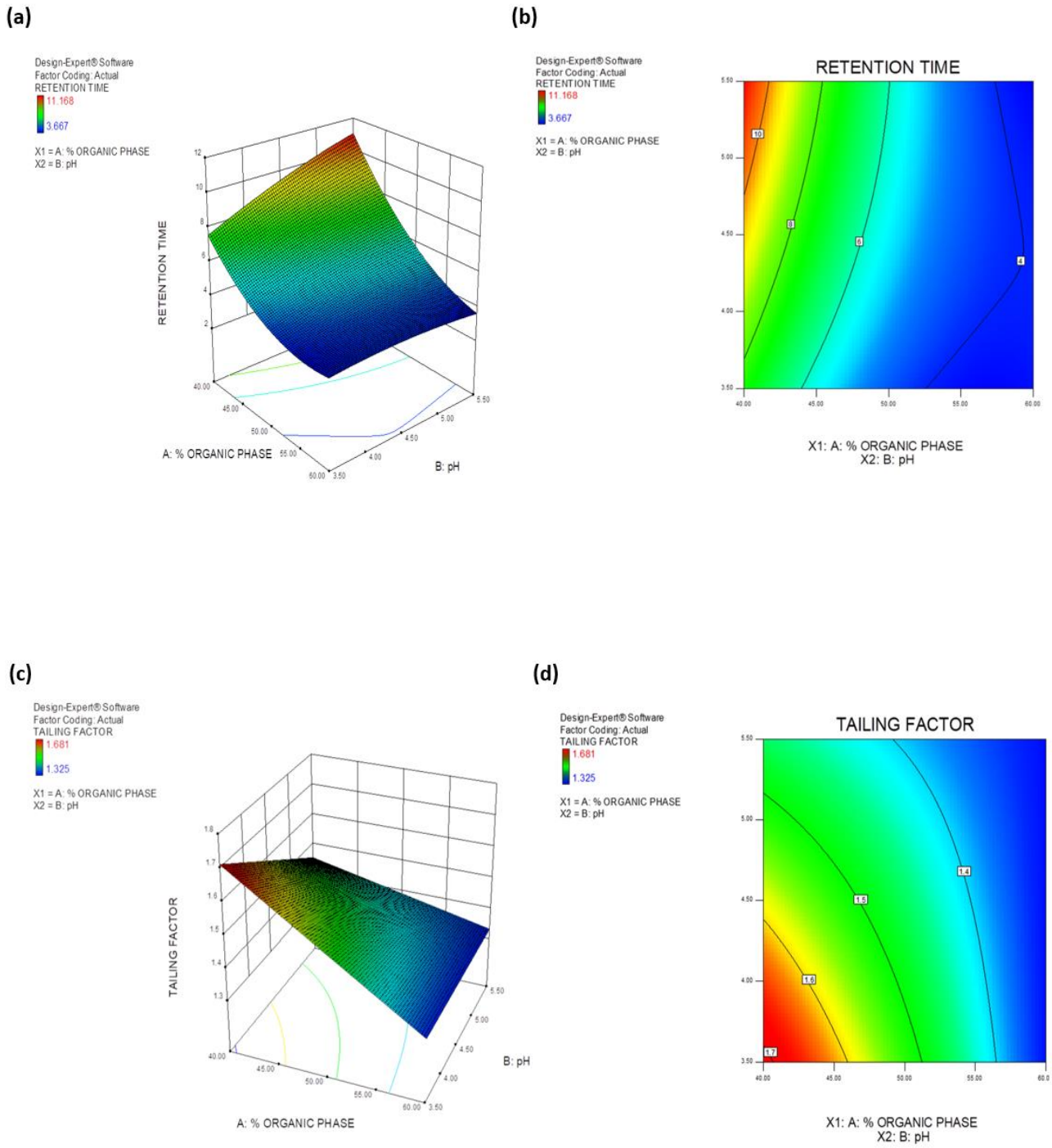

Figure 3.3. (a) and (b) represents the 3D response curve and 2D contour plots for response 1 i.e., retention time; (c) and (d) represents the 3D response curve and 2D contour plots for response 2 i.e., tailing factor

3.3.6.2 Validation of the developed method

3.3.6.2.1 System suitability

The system suitability was estimated by six replicate injections of 10 µg/mL concentration of TF with the optimized chromatographic conditions. The tailing factor was found to be 0.997, which indicated the acceptability of peak properties. The % RSD for peak area was within ≤ ± 2% indicating the suitability of the system. The standard calibration curve of TF was constructed. The linearity between the concentration of TF and peak area was obtained in the range of 50 ng/mL to 15 µg/mL with regression coefficient of 0.999. The obtained linear regression equation was y=47.34 x -749.10. In the regression equation, 'x' is the concentration of TF and 'y' is the peak area at 285 nm. The calibration curve of TF was presented in Figure 3.4. The data of calibration curve was presented in Table 3.6. The LOD and LOQ of the developed analytical method were determined using the signal to noise ratio and values were found to be 16.5 and 49.5 ng/mL, respectively. The LLOQ was found to be 50 ng/mL (n=6). The results proved that the developed method was sensitive enough to detect and quantify TF in nanogram levels. This method would be beneficial for routine analysis of TF in nano formulation where the entrapped drug is in low concentration.

Table 3.6: Data of Calibration curve peak area of analytical method

Concentration (ng/ml)	Peak area ± SD
50	4125.75 ± 483.932
100	8250.75 ± 356.129
200	11645 ± 964.746
400	24844 ± 984.496
800	54123 ± 408.834
1000	73256.75 ± 4348.161
1500	126971.8 ± 14056.89

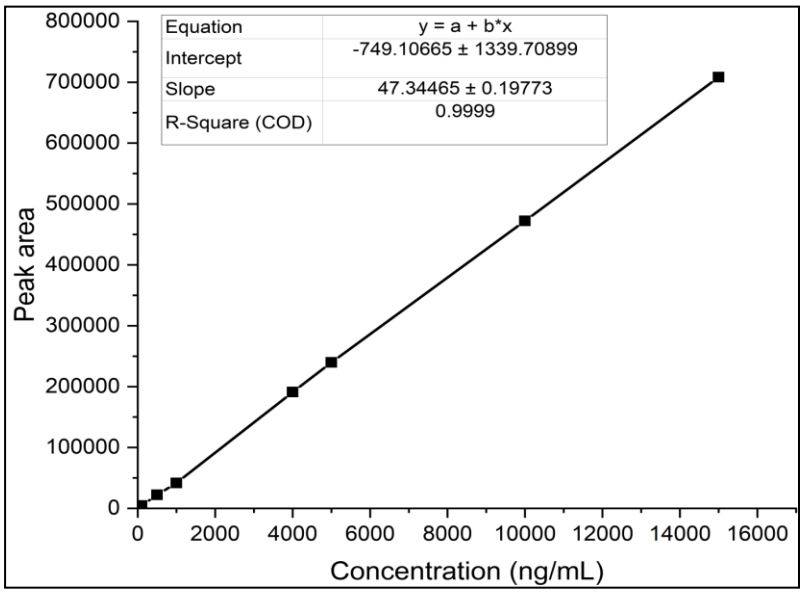

Figure 3.4. Calibration curve of TF in methanol (analytical method)

3.3.6.2.2 Accuracy

The accuracy was estimated by the quality control standards methods with three concentrations of LQC (250 ng/mL), MQC (8000 ng/mL), and HQC (12000 ng/mL). The chromatograms representing LQC and HQC are presented in Figure 3.5. The method demonstrated acceptable % recovery and reproducibility with % bias less than 10 %. The accuracy data of TF are depicted in Table 3.7.

3.3.6.2.3 Precision

The precision was estimated by the quality control standards methods with three concentrations of LQC (250 ng/mL), MQC (8000 ng/mL), and HQC (12000 ng/mL). The chromatograms representing LQC and HQC are presented in Figure 3.5. The obtained results of % RSD in both the solvent system was <2 %, which confirmed the consistency of the developed.

Table 3.7. Intra and inter-day Precision and Accuracy results of analytical method (n=6)

Sample	**Intraday Precision**			**Accuracy**
QC	**Experimental concentration (µg/ml)**	**% Recovery ± SD**	**% RSD**	**% bias**
LQC	252.06 ± 4.32	100.81 ± 1.73	1.1666 ± 0.019	0.818 ± 0.39
MQC	7847.82 ± 192.2	98.09 ±1.52	1.7295 ±0.0423	1.908 ± 0.20
HQC	11781.5 ± 213.9	98.17 ± 1.25	1.2827±0.023	1.827 ± 0.56
	Inter-day Precision			
LQC	252.06 ± 4.32	100.82 ± 1.44	1.6498± 0.027	0.824 ± 0.39
MQC	7915.25 ± 96.84	98.94 ± 1.35	1.2219 ± 0.014	1.059 ± 0.20
HQC	11797.79 ± 212.75	98.31 ± 1.43	1.8017 ± 0.032	1.685 ± 0.43

LQC: 250 ng/mL; MQC: 8000 ng/mL; HQC: 12000 ng/mL

3.3.6.2.4 Carryover effect

The carryover effect was estimated by analyzing successive samples i.e., 10 µg/mL, 12 µg/mL, and 15 µg/mL concentration of TF followed by a blank sample. There was no TF peak observed in the blank at the retention time of 6.1 minutes. The result demonstrated that no carryover effect was observed, thus this method could be utilized for an unremitting run for greater number of samples.

The optimized chromatographic conditions were evaluated for robustness with the deliberate change in oven temperature and mobile phase pH. The effect was found to be insignificant with these two variables on analysis of LQC, MQC, and HQC. The RSD (%) was less than 2 and showed good reproducibility of peak properties. The obtained result implied that the developed method was stable against small variations in intrinsic parameters.

3.3.6.2.5 Robustness

The robustness of the analytical method was performed on another Shimadzu system (model number: LC 2010CHT) with the optimized chromatogram conditions. The results demonstrated that there was no change in peak area and tailing factor. The observed changes were insignificant; hence this method could be easily transferable from one laboratory to another.

3.3.6.2.6 Specificity

The specificity study was performed with the presence of lipids used for the preparation of proglycosomes. There was no peak interference observed at the retention time of the TF peak, and the purity of peak was found to be 99.99%. The forced degradation studies such as acid hydrolysis, base hydrolysis, oxidation, and thermal were successfully carried out. The stability results of TF are shown in Table 3.8. The chromatogram of acid hydrolysis (Figure 3.5c) sample of TF showed degradation peaks at 3.67, 3.8, and 4.6 minutes. There was 14.78% degradation of TF observed under acidic hydrolysis. The chromatogram of base hydrolysis (Figure 3.5d) sample of TF showed peak splitting, and the impurity peak was prominent and eluted at the retention time of 5.5. This indicates that nearly 75% of TF was degraded. The observed base degradation result was confirmed with the reported study by Younis et al. They reported that above the pH ~ 9, TF citrate showed the highest degree of degradation [23]. In contrast, under oxidative stress conditions, the chromatogram (Figure 3.5e) of TF generated impurity peaks at 3.7 and 4.6 minutes, and 20.25% degradation of TF was observed. The thermal degradation samples of TF did not show any impurity peak (Figure 3.5f). The sample showed 1.5% degradation of TF.

The results confirmed that the developed analytical method could discriminate the degradation products from the retention time of TF. The developed method was found to be selective for TF and demonstrated the method stability-indicating property. This can be applied for stability testing of TF in-process and finished products.

Table 3.8: Stability results of TF under various stress conditions

Study performed	**Stress condition**	**% TF degraded**	**Degradation peaks with retention time (**minutes)
Acid hydrolysis	0.5M hydrochloric acid	14.78 ± 0.04%	3.67, 3.8 and 4.6
Base hydrolysis	0.5M sodium hydroxide	75 ± 0.06%	5.4
Oxidative	2% hydrogen peroxide	20.25 ± 0.04%	3.7 and 4.6
Thermal degradation	Water	1.5 ± 0.02%	-

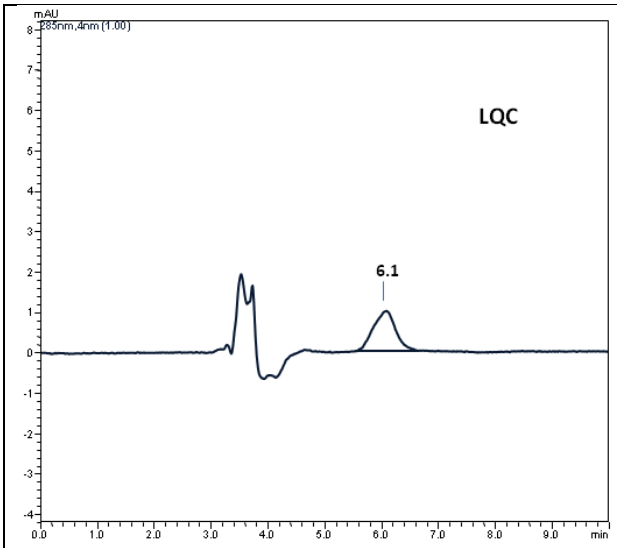

3 (a)

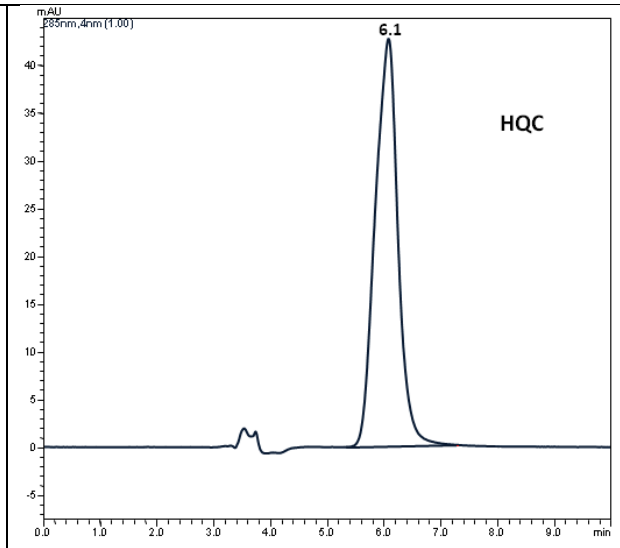

3 (b)

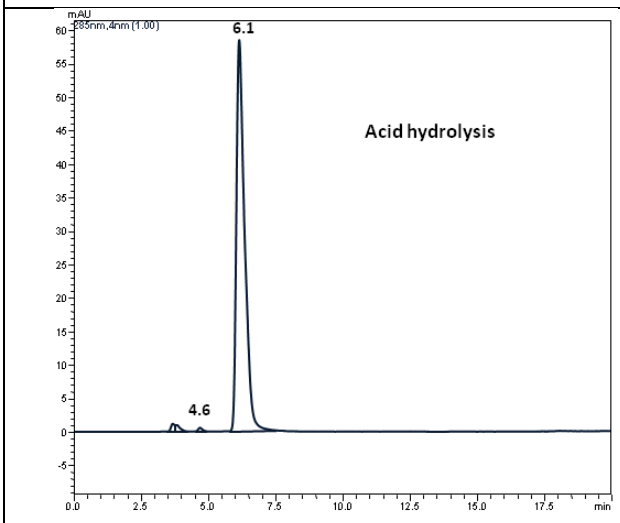

3 (c)

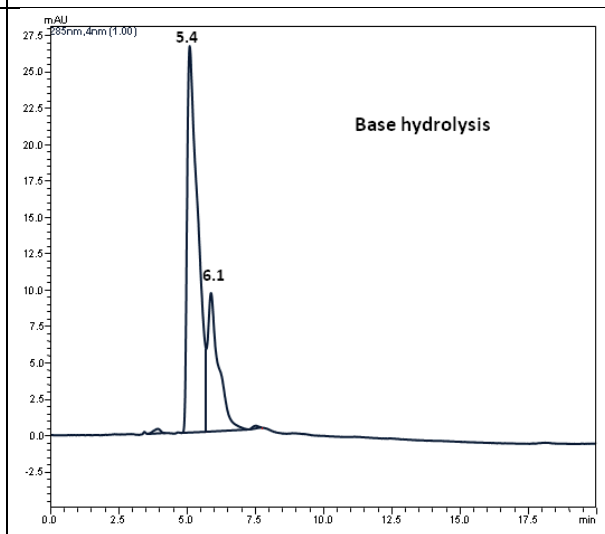

3 (d)

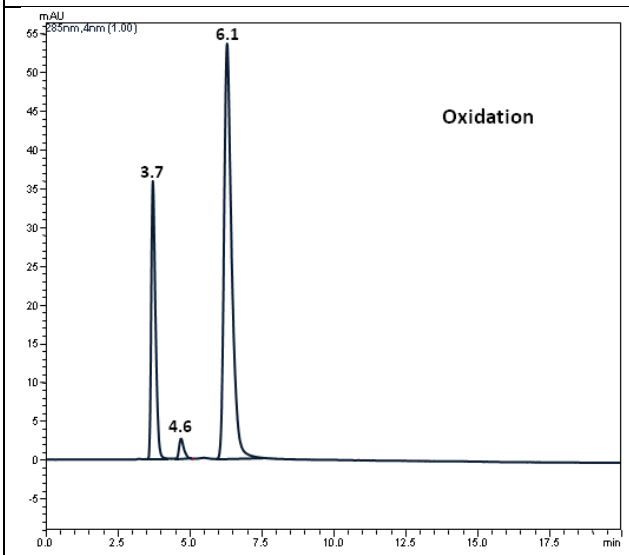

3 (e)

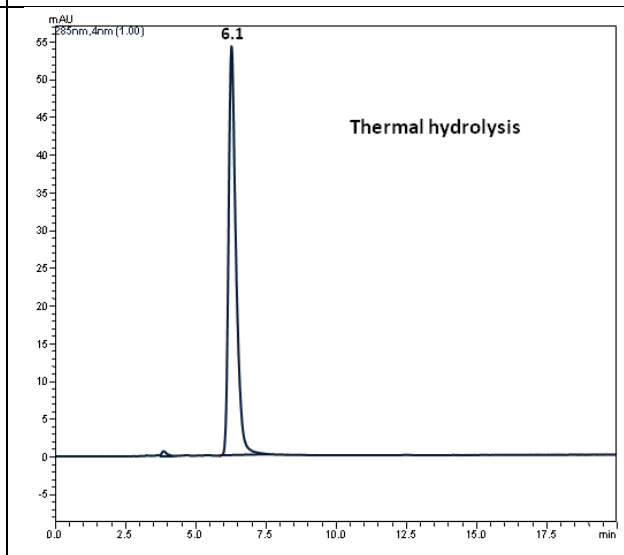

3 (f)

Figure 3.5. Representative HPLC chromatograms for (a) Lowest quality control (LQC: 250 ng/mL) (b) Highest quality control (HQC: 12000 ng/mL (c) acid hydrolysis (d) base hydrolysis (e) oxidation (f) thermal conditions

3.3.6.3 Applicability of the developed method for skin studies of TF and Dermatokinetic assessment

The suitability of the method was confirmed in dermatokinetics studies on topical administration of TF. The validated method was used for the routine analysis i.e., for understanding the in vivo dermatokinetics studies of developed nanoformulation.

3.3.6.3.1 Applicability in the characterization of nanoformulation

The applicability of the validated analytical method was appraised by determining the cumulative drug release of TF from the proglycosomes, stability, and estimation of TF from the skin tissues. The *in vitro* release is acquiring considerable interest as a surrogate test for product capability. The *in vitro* drug release samples were collected and filtered through the 0.22 µ membrane, and the concentration of TF was determined by the developed method (n=3). The developed method appropriately quantified the TF in the lipid nano formulations from the first hour until the end of the release study. The total amount of drug was found to be 98.9%. The developed method showed good agreement for the characterization of drug release in dissolution media (Figure 3.6). Therefore, the developed method can be used for the routine assessment of the effect of formulation factors and quality control parameters.

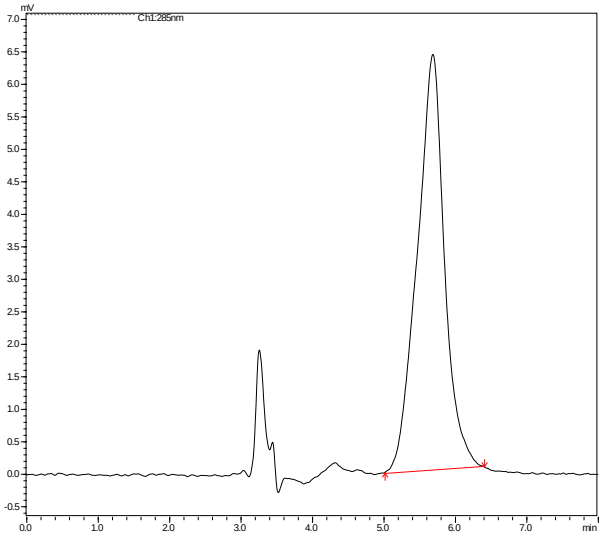

Figure 3.6. TF peak in the presence of *in vitro* release media

3.3.6.3.2 Applicability in characterization of Tape and skin tissue samples

The skin tissue samples were analyzed in six replicates for the determination of % recovery of TF. The % recovery of TF from the skin tissue was found to be 95.61 ± 0.96, with a peak purity of 99.99 ± 0.54 %. A specific peak was observed at 6.1 min without any interference with the skin matrix. The obtained results confirmed that the developed method can be applied for the quantification of TF during skin permeation and retention studies, and Dermatokinetics studies. TF in the presence of tape samples and skin samples are presented in Figures 3.7 and 3.8.

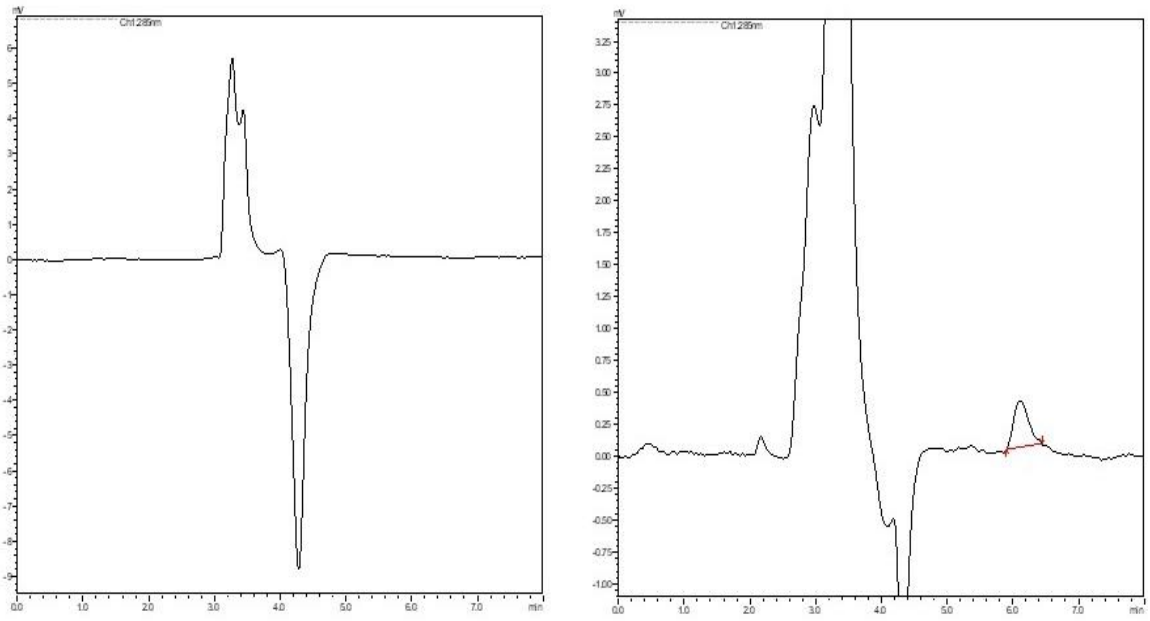

Figure 3.7. Tape samples i.e., blank (left-hand side) and TF peak in the presence of tape (right hand side).

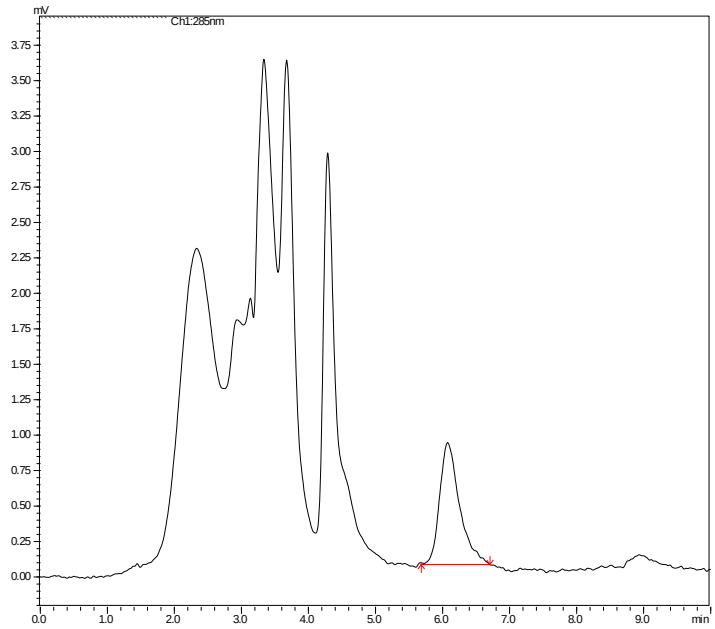

Figure 3.8. TF in the presence of skin matrix

3.4 Bioanalytical method for the determination of TF in Blood samples

3.4.1 Animals

The bio analytical method was developed by collecting the blood from Healthy Male Wistar rats with weight of 200 -250 g. Prior to the commencement of work, the current study protocol was duly approved by the Institutional Animal Ethics Committee (IAEC) registered under Committee for the Purpose of Control and Supervision of Experiments on Animals (CPCSEA) with Protocol No. IAEC/RES/31/05. The Male Wistar rats were housed in individual ventilated cages with standardized pellet food *ad libitum* and water. Also, all the animals were exposed to light and dark cycles of 12 h and relative humidity of 40–70% for one week prior to the experiment.

3.4.2 Experimental requirements

3.4.2.1 Instrumentation and chromatographic conditions

The chromatographic experiments were conducted on the HPLC system (Shimadzu, Kyoto, Japan) comprised of model LC-10AT, a binary pump, SIL-HTA autosampler (Shimadzu, Kyoto, Japan), column oven (CTO-10AS) compartment, and SPD-M20A Photodiode array (PDA) detector. Chromatographic separation was carried out at 30 ± 0.5 °C using Supelco, Ascentis C18 column, 15 cm X 4.6 mm, particle size 5 µm. The detection was carried out with

a PDA detector with 40 µL injection volume at wavelength 285 nm. The data acquisition and HPLC system were controlled by the LC solution software version 1.24 SP1.

3.4.2.2 Preparation of stock, calibration and quality control standards

Stock solutions of TF (2 mg/mL) and internal standard (pentoxyphylline; 2 mg/mL) were prepared by dissolving an accurately weighed amount of TF and pentoxyphylline in methanol. Further, the working solutions of 25, 50, 100, 200, 400, 600, and 1500 µg/mL were prepared by stepwise dilution with mobile phase. The calibration standards and quality samples were prepared by spiking 96 µL of rat plasma (without drug) with 2 µL of subsequent working standard solutions and internal standard. The calibration standards 50-1500 ng/mL were prepared through serial dilution with methanol and the internal standard concentration as 2 µg/mL. The QC standards were prepared from the standard stock at three concentration levels; low QC (150 ng/mL), medium QC (600 ng/mL), high QC (1200 ng/mL), and the lower limit of quantification (LLOQ) (50 ng/mL).

3.4.3 Sample preparation

Simple protein precipitation (PPM) method was used for extracting TF from the rat plasma. 100 µL aliquot of plasma sample with TF and pentoxyphylline (IS) was prepared and vortexed for 2 min. Into this 500 µL of methanol was added and vortexed for 5 min and centrifuged at 3500 rpm for 15 min at 8^0C. The upper supernatant was collected and filtered. Finally, 40 µL of the sample was injected into HPLC for quantification.

3.4.4 Validation of the developed method

The validation of the analytical method was performed for system suitability, linearity, range, detection limit, quantification limit, specificity, accuracy, precision, carryover effect, and robustness according to the ICH Q2 (R1) guideline (2005).

Selectivity test was performed to assess the probability of chromatographic interference from the rat plasma matrix. This was evaluated by injecting six plasma samples from 6 Wistar rats with optimized chromatographic conditions.

Linearity was determined with a concentration range between 50-1500 ng/mL with six calibration standards.

The accuracy and precision of the quality control samples LQC, MQC, and HQC, as well as LLOQ, were determined in six replicates on intra and inter days. Accuracy was denoted as %

bias and the precision as % relative standard deviation (RSD). The acceptance requirement for precision of quality control samples according to regulatory criteria was ≤ ±15%. The acceptance criteria for accuracy are within ≤ ± 15% (expressed as %bias) whereas for LLOQ the acceptance criteria was ≤ ± 20%.

3.4.5 Results

3.4.5.1 Selectivity

The developed bioanalytical method has not shown matrix interference at the retention time of the TF and IS. The representative HPLC chromatograms of rat plasma with TF and IS are presented in Figure 3.9.

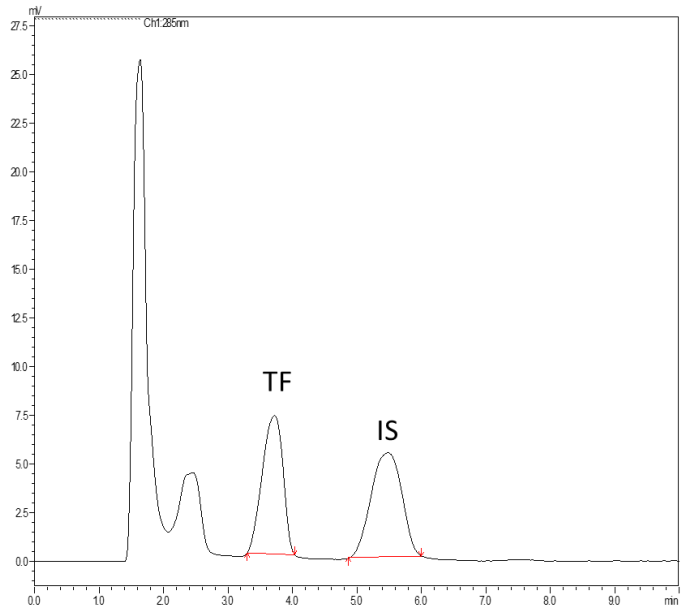

Figure 3.9. HPLC chromatograms after extraction and analysis of TF and IS

3.4.5.2 Linearity, limit of quantification

The LOQ of the developed bioanalytical method was determined using the signal to noise ratio and values and trail method. The LLOQ was found to be 50 ng/mL, respectively (n=6). This method would be beneficial for routine analysis of TF in plasma samples in nanogram concentration. The standard calibration curve of TF was constructed in a plasma matrix with internal standard. The linearity between the concentration of TF and peak area was obtained in the range of 50 ng/mL to 1500 ng/mL with an excellent regression coefficient of 0.9856. The obtained linear regression coefficient was y=81.485 x – 3463.4. In the regression equation, ‘x’ is the concentration of TF and ‘y’ is the peak area at 285 nm. The data of calibration cure peak areas were mentioned in Table 3.9. The calibration curve of TF extracted from plasma was presented in Figure 3.10.

Table 3.9. Data of Calibration curve peak areas of bioanalytical method

Concentration (ng/ml)	**Peak area ± SD**
50	4125.75 ± 483.932
100	8250.75 ± 356.129
200	11645 ± 964.746
400	24844 ± 984.496
800	54123 ± 408.834
1000	73256.75 ± 4348.161
1500	126971.8 ± 14056.89

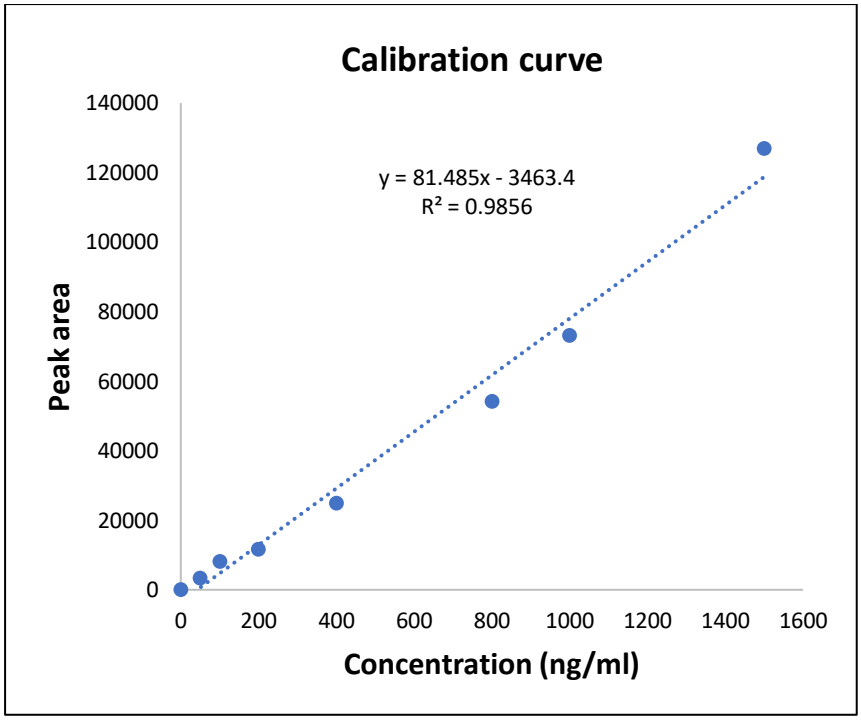

Figure 3.10. The calibration curve of TF extracted from plasma

3.4.5.3 Accuracy and precision

The accuracy and precision were estimated by standard addition method with three concentrations of LQC (150 ng/mL), MQC (600 ng/mL), and HQC (1200 ng/mL). The chromatograms representing LQC, MQC and HQC are presented in Figure 3.11. The % accuracy for TF was found in a range of -13.530 to 8.26 %. The method demonstrated

acceptable values for accuracy and precision which were within the 15 %. The intra and inter-day precision and accuracy results of TF rat plasma samples at quality control concentrations of the calibration ranges are presented in Table 3.10.

Table 3.10. Intra and inter day Precision and Accuracy results of TF rat plasma samples at quality control concentrations of the calibration ranges

Sample	**Intraday Precision**			
Quality Control standards	**Experimental concentration (ng/ml) ± SD**	**% Recovery ± SD**	**% RSD**	**% Bias**
LQC	169.934± 14.15	115.246 ± 2.76	4.355 ± 1.14	-13.289 ± 2.76
MQC	606.898 ± 8. 72	101.149 ± 2.59	2.722 ± 4.05	-1.149 ± 1.78
HQC	1225.605 ± 15.24	99.801 ± 3.29	5.784 ± 2.57	-2.134 ± 3.29
LLOQ	45.866 ± 13.99	91.73 ± 2.11	2.63 ± 1.94	8.26 ± 2.11
	Inter-day Precision			
LQC	158.280 ± 15.74	105.518 ± 8.49	5.917 ± 3.14	-5.518 ± 3.4
MQC	554.720 ± 36.89	96.801 ± 6.15	6.986 ± 2.04	7.547 ± 6.1
HQC	1142.920 ± 9.87	94.661 ± 1.82	7.594 ± 2.88	4.756 ± 0.8
LLOQ	56.786 ± 13.86	113.57 ± 25.5	12.80 ± 2.31	-13.530 ± 7.7

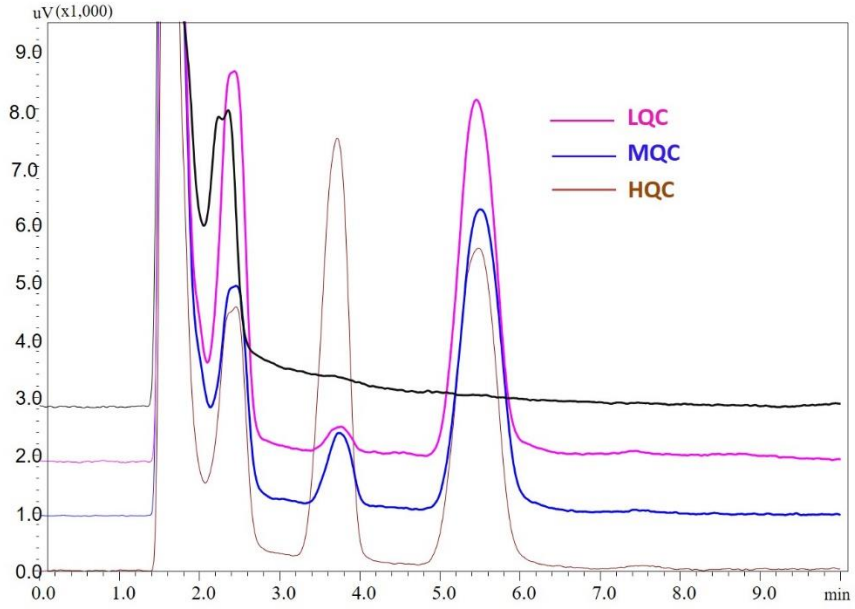

Figure 3.11. Representative HPLC chromatograms of TF in plasma blank; Lowest quality control (LQC: 150 ng/mL); Medium quality control (MQC:600 ng/mL); (d) Highest quality control (HQC: 1200 ng/mL)

3.5 Conclusion

The UV spectrophotometric method for quantification of TF was developed in methanol and 10% methanol in pH 7.4 PBS containing 0.15% SLS and validated as per ICH Q2 (R1) and USFDA guideline. The validated method in methanol could be suitably utilized for analysis of % entrapped drug and % drug loading in nanocarriers (especially LCNPs and lipid formulation excipients which has absorbance at lower UV region i.e., > 250 nm).

Thus, for the estimation of drug in other lipidic systems especially nano formulation containing high surfactant proportion there is a need for another analytical method. The validated analytical method evidenced its utility in the estimation of TF in the pharmaceutical nanoformulations and different skin layers (viable epidermis, and dermis). The method quantified the TF in skin layers after the application of topical formulation to quantify TF in *in vivo* dermatokinetics experiments.

Further, a simple reversed-phase HPLC method in rat plasma for the determination of TF was developed. The developed method ensures economical, lowest sample volume, easy extraction technique, and selectivity without matrix interference. Partial validation was performed such that it could be widely used for their routine analysis for understanding the *in vivo*

pharmacokinetic- studies. It can analyze the TF in a 100 µL plasma sample with an overall run time of less than 10 min.

References

1. Dowty ME, Jesson MI, Ghosh S, *et al.* Preclinical to Clinical Translation of Tofacitinib, a Janus Kinase Inhibitor, in Rheumatoid Arthritis. *J. Pharmacol. Exp. Ther.* 348(1), 165–173 (2014).

2. Bharwad KD, Shah PA, Shrivastav PS, Singhal P. Development and validation of a rapid and sensitive UPLC–MS/MS assay for the quantification of tofacitinib in human plasma. *Biomed. Chromatogr.* 33(4), e4458-e4464 (2019).

3. Wu X, Zeng X, Wang L, Hang T, Song M. Identification of related substances in tofacitinib citrate by LC-MS techniques for synthetic process optimization. *J. Pharm. Biomed. Anal.* 143, 17–25 (2017).

4. Paniagua R, Campbell A, Changelian PS, Reitz BA, Prakash C, Borie DC. Quantitative analysis of the immunosuppressant CP-690,550 in whole blood by column-switching high-performance liquid chromatography and mass spectrometry detection. *Ther. Drug Monit.* 27(5), 608–616 (2005).

5. Kim JE, Mun ·, Park Y, Kim SH. Simple determination and quantification of tofacitinib, a JAK inhibitor, in rat plasma, urine and tissue homogenates by HPLC and its application to a pharmacokinetic study. J. Pharm. Investig. 50(6), 603-612(2020).

6. Siva B, Kiran S, Raja S. RP-HPLC method development and validation for the quantification of tofacitinib. J Life Sci Res. 4(4), 646-53 (2018).

7. Sankar ASK, Shanmugasundaram P, Datchayani B, *et al.* Stress degradation studies and development of validated spectrometric- assay-method for determination of tofacitinib in pure and physical admixtures. *Res. J. Pharm. Technol*. 10(1), 117–120 (2017).

8. Kushner J, Lamba M, Stock T, *et al.* Development and validation of a Level A in-vitro in-vivo correlation for tofacitinib modified-release tablets using extrudable core system osmotic delivery technology. *Eur. J. Pharm. Sci*. 147, 10500 (2020).

9. Gorantla S, Saha RN, Singhvi G. Spectrophotometric method to quantify tofacitinib in lyotropic liquid crystalline nanoparticles and skin layers: Application in ex vivo dermal distribution studies. *Spectrochim. Acta - Part A Mol. Biomol. Spectrosc.* 255, 119719

(2021).

10. ICH Topic Q 2 (R1) Validation of Analytical Procedures: Text and Methodology note for guidance on validation of analytical procedures: text and methodology (cpmp/ich/381/95) approval by cpmp November 1994 [Internet]. http://www.emea.eu.int.

11. Naik P, Chandra Sekhar KB. A Novel Stability Indicating Chromatographic Method Development And Validation For The Quantification of Tofacitinib In Pure And Its Dosage Form. *IOSR J. Appl. Chem.* 11(2), 33–37 (2018).

12. Sankar ASK, Datchayani B, Balakumaran N, Rilwan M, Subaranjani R. Development of a validated reverse phase liquid chromatographic assay-method for determination of tofacitinib in pure form and in physical admixtures. *Res. J. Pharm. Technol.*10(1), 223–226 (2017).

13. S VK, Dhiman V, Giri KK, Sharma K, Zainuddin M, Mullangi R. Development and validation of a RP-HPLC method for the quantitation of tofacitinib in rat plasma and its application to a pharmacokinetic study. *Biomed. Chromatogr.* 29(9), 1325–1329 (2015).

14. Bashir S, Aamir M, Sarfaraz RM, *et al.* Fabrication, characterization and in vitro release kinetics of tofacitinib-encapsulated polymeric nanoparticles: a promising implication in the treatment of rheumatoid arthritis. *Int. J. Polym. Mater. Polym. Biomater.* 70(7), 449–458 (2021).

15. Patel PN, Karakam VS, Samanthula G, Ragampeta S. Quality-by-design-based ultra high performance liquid chromatography related substances method development by establishing the proficient design space for sumatriptan and naproxen combination. *J. Sep. Sci.*38(19), 3354–3362 (2015).

16. Shukla SK, Kadry H, Bhatt JA, Elbatanony R, Ahsan F, Gupta V. Statistical optimization and validation of a novel ultra-performance liquid chromatography method for estimation of nintedanib in rat and human plasma. *Bioanalysis* 12(3), 159–174 (2020).

17. Krishna KV, Saha RN, Puri A, Viard M, Shapiro BA, Dubey SK. Pre-clinical compartmental pharmacokinetic modeling of 2-[1-hexyloxyethyl]-2-devinyl pyropheophorbide-a (HPPH) as a photosensitizer in rat plasma by validated HPLC

method. *Photochem. Photobiol. Sci.* 18(5), 1056–1063 (2019).

18. Singhvi G, Gampa G, N. Saha R. Development and Validation of a Stability Indicating Liquid Chromatographic Method for the Determination of Milnacipran in Bulk and its Formulations. *Curr. Pharm. Anal.*9(2), 191-198 (2013).

19. Rajadhyaksha NS, Jain SP, Amin PD. Analytical Letters Carbamazepine: Stability Indicating HPLC Assay Method Carbamazepine: Stability Indicating HPLC Assay Method. *Anal. Lett.* 40(13), 2506–2514 (2007).

20. Rapalli VK, Singhvi G, Gorantla S, *et al.* Stability indicating liquid chromatographic method for simultaneous quantification of betamethasone valerate and tazarotene in in vitro and ex vivo studies of complex nanoformulation. *J. Sep. Sci.* 42(22), 3413–3420 (2019).

21. Blessy M, Patel RD, Prajapati PN, Agrawal YK. Development of forced degradation and stability indicating studies of drugs - A review. *J. Pharm. Anal.*4(3), 159–165 (2014).

22. Rapalli VK, Kaul V, Gorantla S, *et al.* UV Spectrophotometric method for characterization of curcumin loaded nanostructured lipid nanocarriers in simulated conditions: Method development, in-vitro and ex-vivo applications in topical delivery. *Spectrochim. Acta - Part A Mol. Biomol. Spectrosc.* 224, 117392 (2020).

23. Younis US, Vallorz E, Addison KJ, Ledford JG, Myrdal PB. Preformulation and Evaluation of Tofacitinib as a Therapeutic Treatment for Asthma. *AAPS PharmSciTech*. 20(5),1-11(2019).

4 Liquid Crystal Nanoparticles

Systemic administration of TF is associated with severe adverse effects such as decreased neutrophil count, increased cholesterol level, gastrointestinal perforations, and immune suppression. Additionally, TF undergoes extensive metabolism by liver microsomes in the presence of nicotinamide adenine dinucleotide phosphate [1]. The adverse effects posed by oral administration of TF can be minimized by topical delivery of TF i.e., by providing localized action, reducing systemic exposure, avoiding the first-pass metabolism, and avoidance of the risk of gastrointestinal tract-associated adverse effects [2]. The topical administration of TF elicits its action at the appropriate site and relieves pain at the intracellular level. Illustrating the potential of the topical JAK inhibitor like TF is effective in treating the RA condition. The RA topical treatment needs a high concentration of TF in the dermal and synovial regions [3]. To achieve this, the stratum corneum is considered as a rate-limiting barrier. Thus, the development of nanocarriers for topical delivery is focused on modifying drug permeation through the skin [4].

Lipid nanocarriers systems have been found to be a suitable choice for topical delivery due to their increased resemblance to the skin and enhanced penetration by polarity and fluidization [5]. Among the lipid nanocarriers, lyotropic liquid crystalline nanoparticles (LCNP) gained huge attention due to their effective topical delivery. LCNP designed with self-assembling lipid-based systems like bicontinuous cubic and hexagonal mesophases mimic the curvature of the cellular membrane and possess unique properties of swelling, sustained drug release, and protect the drug from physical and enzymatic degradation [6]. In addition, the use of non-toxic, biocompatible, and Generally recognized as safe (GRAS) approved permeation enhancer - glyceryl monooleate (GMO) - as a liquid crystal structure forming material makes this delivery system suitable for topical drug delivery [7]. GMO is an amphiphilic molecule with a hydrophilic head group and a hydrophobic hydrocarbon tail [8]. Under varying conditions of temperature from room temperature to 80^0C, and in the presence of excess aqueous phase, it exhibits cubic crystal morphology [9]. The GMO based mesophases have proven its application in enhancing the permeation into the skin matrix [10]. GMO is majorly composed of oleic acid, which can easily interact with skin lipids, and enhances permeation through the stratum corneum [11]. The available literature signifies that the liquid crystals could be potential drug delivery system carriers to improve the permeation of topically administered drugs.

Therefore, the current study focuses on the effective formulation of TF-loaded LCNP using the systematic quality by design (QbD) principles. In this study, initially, we intended to investigate the effect of liquid oils (varied composition) along with Glycerol Mono Oleate (GMO) and surfactant (Lutrol®) on critical quality attributes (CQA) i.e., entrapment efficiency, particle size, and polydispersity index (PDI). The preliminary screening of liquid oil was performed by solubility studies and Taguchi L8 orthogonal array (OA) design. The Box-Behnken design (BBD) was employed to scrutinize the effect of the critical material and process variables on the CQAs of LCNP. The optimized formulation composition was incorporated into the gelling system that controls the drug release and makes the system suitable for topical application. Additionally, this work emphasizes the potential for TF permeation and retention potential through designed LCNP. TF accumulation in various skin layers viz., epidermis, and dermis using dermal pharmacokinetics modeling have also been studied.

4.1 Materials and methods

GMO was received from Mohini organics Pvtt. Ltd as a generous gift sample. Liquid oils such as 2-octyl dodecyl myristate (myristol), Linoleoyl polyoxyl-6 glycerides (Labrafac M 2125), Oleoyl polyoxyl-6 glycerides (Labrafac M 1944), and Labrafac CC were received as gift samples from Gatteffose India. The Caprylic/Capric Triglyceride Myglol 812 and Myglol 810 were received as gift samples from Sasol Olefins & Surfactants (Germany). Methanol was procured from S.D. Fine Chemicals (India). Lutrol® F 127 was obtained as a gift sample from BASF (India). SEPINEO™ P 600 was received as a gift sample from SEPPIC. All the reagents used during the study are of analytical grade.

4.2 Formulation development, scale-up, and characterization of the TF-loaded glyceryl mono oleate– myristol self-assembled LCNP

4.2.1 Selection of excipients

4.2.1.1 Selection of liquid oil

The liquid oil was selected based on the solubility studies**.** To 1 mL of each liquid lipids (Oleic acid, Labrafac M 1944, Labrafil 2125 CS, Labrafac CC 1349, Miglyol 812, Myristol, Miglyol 810), excess TF was added and kept on an orbital shaker for 24 h. After 24 h the samples were subjected to centrifugation, and the supernatant was collected. Subsequently, lysis was performed by the addition of methanol to extract the TF. The sample was filtered through a 0.25 µ syringe and analyzed by the developed analytical method.

4.2.1.2 Screening of compatibility of liquid oil with GMO and their ratios

The phase separation study was performed to confirm the strong interaction of GMO with the selected liquid oil. The addition of liquid oil changes the thermodynamic property, which has a direct relation to the liquid lattice. These changes can also influence TF loading. Initially, GMO and liquid oil (50:50, 60:40, 80:20 ratios) were mixed at 40^0C, and observed for their miscibility. These mixtures were then kept in ice bath for 30 minutes and observed for phase separation visually.

4.2.2 Preparation of tofacitinib-loaded Lyotropic liquid crystalline nanoparticles

LCNP were prepared by hot emulsification followed by a probe sonication process. In brief, the batch quantity of lipid (alone or in combination) melted at 70 ± 2^0C. A Batch quantity of TF (5 mg) and surfactant (Lutrol® F 127) (100 mg) were added one after another to the melted lipid blend and subjected to stirring until the formation of a clear liquid. The aqueous phase (MilliQ water) was preheated to 60 ± 2^0C. The preheated aqueous phase was added to the drug lipid mix under constant stirring to form a hot emulsion. The obtained dispersion was subjected to probe sonication for size reduction. The obtained LCNP was left to cool for re-crystallization of the lipids [12].

4.2.3 Quality by design approach for LCNP development

4.2.3.1 Quality target product profile

The first step for developing a product using QbD is to predefine the Quality target product profile (QTPP). LCNP QTPP contains a prospective overview of the critical drug product quality criteria that should be achieved to ensure the quality of the finished product in terms of safety and efficacy [13].

4.2.3.2 Critical quality attributes

The second and important element of QbD - based development is to identify the CQAs. CQAs are product critical quality attributes, which are derived from QTPP. CQAs exhibit a great influence on the final product quality as they decide the limit. Due to this, they must be deliberated and controlled [14].

4.2.3.3 Quality risk assessment studies

Initial risk assessment studies were performed to identify the influence of critical material attributes (CMAs) and critical process parameters (CPPs) on the quality of topical LCNP. International Conference on Harmonisation (ICH) guideline of Q9 quality risk management

guidelines furnish an excellent high-level framework for the use of risk management in the development of nanosystems and to built-up quality decision making applications. To identify the various risk factors and cause-effect correlation, Ishikawa fish bone was established. For qualitative risk assessment, a risk estimation matrix (REM) was employed by assigning low, medium, and high levels to each material and process variable of LCNP. The risk of the obtained variables for LCNP was quantified from REM. The likelihood of failure modes was assessed using failure mode evaluation and analysis (FMEA). Based on this, a rank order score from 1 to 10 was allotted based on their occurrence (O), severity (S), and detectability (D). The final risk priority number (RPN) score was calculated using below mentioned equation prior to optimization. The obtained risk factors established the relationship between each of the CMAs and CPPs to the potential CQAs.

$$\boldsymbol{RPN\ Score = O * S * D}$$

4.2.3.4 Factor screening studies

The CMAs and CPPs that exhibited high RPN values were subjected to a quantitative screening study based on the quality risk assessment studies. The Taguchi OA Design Matrix (two-level multi-factorial design) was used for the identification of the most influential variables from a large number of questionable factors with a minimum number of experiments. Design-Expert® software Version 8.0., (U.S.A, Minneapolis, MN, Stat-Ease Inc.,) software was used to obtain the experimental run. Taguchi OA Design Matrix is preferred to prepare topical TF-LCNP and assigned low and high-level values and category types. The obtained trials were executed, and they were characterized for the CQAs (particle size, PDI, and entrapment efficiency). The obtained data was fitted into the first-order linear model, and only the coefficients for each of the given factors were analyzed. The quantitative assessment of given factors was determined by half-normal plots and Pareto charts.

4.2.3.5 DoE on formulation development and optimization

The optimization of TF-LCNP was formulated using QbD by experimental design. Employing statistically evolving CMPs and CPPs, the design of experiments recommends the batch with the fewest experiments. Response surface methodologies like central composite design and BBD are normally investigated to assess the variation among the variables. Here, in the current research work, BBD has been employed to optimize the TF-LCNP using Design-Expert® software Version 8.0. The BBD design provides data on the interactive effects of CMAs with CPPs formulation aspects.

The low and high levels of screened CMAs and CPPs were assigned, and 17 experiments were obtained. The suggested trials were executed, and the obtained data were incorporated into the Design-Expert software. Then the factor-response relationship was obtained by a second-order mathematical model. Each response can have a linear, quadratic, and two-factor interaction regression model after developing a regression model. The statistical model for each response was selected by R-square value, F-tests, and lack-of-fit tests. The analysis of variance (ANOVA) supports the significance of each factor, including the linear, quadratic, and interaction factors. ANOVA for all the responses were executed and the best fit model was statistically chosen based on adjusted multiple correlation coefficient and coefficient of variance. The optimization of TF- LCNP formulation was carried out by using numerical and graphical data generated from Design-Expert software. The interaction effects of CMAs and CPPs on the CQAs (Particle size, PDI, and Entrapment efficiency) were examined by 3D response surface plots and 2D contour plots of the fitted regression equation. In addition, the model optimization was accomplished to attain the lowest mean particle size and PDI with higher % entrapment efficiency. The validation of the obtained LCNP formulation was performed. The quantitative comparison in terms of % deviation or error between the predicted CQAs values and experimental values was used to validate the BBD model.

4.2.4 Characterization of TF-loaded LCNP

4.2.4.1 Particle size, polydispersity index and zeta potential measurements

Particle size, PDI and zeta potential were measured with Zetasizer Nano ZS (Malvern instruments, Malvern, UK). Before particle size and PDI measurements, the TF-LCNP were diluted 20 times with Milli-Q water. The diluted LCNP were measured by dynamic light scattering at a refractive index of 1.33. The measurements were performed in triplicate with 15 runs minimum. For the measurement of zeta potential, the TF- LCNP formulation was transferred into the disposable capillary cell (Malvern 1006) and the samples were measured in triplicate with minimum of 25 runs.

4.2.4.2 Entrapment efficiency

Initially, the total amount of TF in LCNP was determined. LCNP formulation was dissolved in methanol and centrifuged at 15,000 rpm for 15 min. The obtained samples were diluted and analyzed by the validated High performance liquid chromatography (HPLC) method. The amount of entrapped and free TF present in LCNP was estimated using Amicon tubes

(10 kDa, Amicon Ultra 5 mL, Millipore, USA). LCNP formulation (1 mL) was transferred to Amicon tubes and centrifuged at 10000 rpm for 30 min. The sample was filtered through a 0.22 µ-syringe and analyzed using HPLC. The entrapment efficiency was calculated using the below mentioned formulas.

$$\% \text{ Entrapment efficiency} = \frac{\text{Amount of drug entrapped}}{\text{Total amount of drug present}} x\ 100$$

4.2.4.3 Field Emission Scanning Electron Microscope and Transmission electron microscopy

Field Emission Scanning Electron Microscope (FESEM) (Apreo, Switch XT microscope, USA) was used for the imaging of developed LCNP morphology. The LCNP formulation was spread on the glass side and dried. The dried glass slide was sputter coated with gold for 60 sec (Gold sputter module, Quorum, UK). FESEM images were obtained at a magnification range of 1000x – 170000 xs at 1-20 kV.

The sample preparation of TF-LCNP for TEM analysis involved initial staining with the uranium acetate and then placing them on copper grid. Further, the dried sample were analysed using TEM at 100 kV [15].

4.2.4.4 Polarized light microscopy

The polarized light microscope (Olympus; BX53M) was used to identify optically birefringent or double refraction of the formed liquid crystal nanoparticles and to distinguish the type of either isotropic or anisotropic. The prepared LCNP was lyophilized by the addition of 5% mannitol. The obtained lyophilized formulation was redispersed by the addition of water. A drop of this was placed on a glass slide and examined for birefringence under a polarized light microscope with and without a cross polarizer.

4.2.4.5 X-ray diffraction

X-ray diffraction patterns for the lyophilized TF- LCNP, a pure drug, were performed using X-ray diffractometer (Rigaku, Miniflex) to evaluate the crystallinity. The powder X-ray diffraction (PXRD) measurements were carriedout in the scanning range from 3° to 40° angles with a data acquisition time of 1.0 s per step. A 40 kV accelerating voltage, a 40 mA beam current, and a 0.01° step size were used to run the PXRD.

4.2.4.6 In vitro drug release analysis

The in vitro release of TF-LCNP was performed by dialysis membrane using Franz diffusion cell apparatus. Freshly prepared pH 7.4 phosphate buffer saline (PBS) with 0.15% sodium lauryl sulphate was used as dissolution media. The media was selected based on drug stability and sink condition. TF-loaded LCNP formulation (1mL) equivalent to 0.5 mg of TF was taken into a dialysis bag (Hi media, MW: 12 to 14 KDa). The dialysis bag was placed into the diffusion assembly and the whole assembly was kept at 37 ± 0.5^{o}C on a magnetic stirrer at 80 rpm. An aliquot of 1 mL was collected at time intervals of 2, 4, 6, 8, 12, and 24 h and replaced by the same dissolution media to maintain the sink conditions. The collected samples were filtered through a 0.45 µ filter prior to HPLC analysis. The filtered samples were analyzed at 285 nm by the validated HPLC method. The obtained results were analyzed and the graph was plotted by taking time on the x-axis and % cumulative drug release on the y-axis. The drug release mechanism was evaluated using an Excel add-in, DD Solver. The release kinetics models (Zero order, First order, Higuchi, Korsmeyer-Peppas, and Hixon Crowell) were investigated. Later the best fit model was selected based on the correlation coefficient value, Akaie information criterion (AIC), and Model selection criteria (MSC) values.

4.2.5 Incorporation of TF-LCNP into the TF-LCNP loaded SEPINEO P 600

The optimized TF-LCNP was loaded into the SEPINEO P 600 to make it feasible for topical application. SEPINEO P 600 i.e., 3.5 % was added to the TF-LCNP formulation, continued stirring for 20 min on magnetic stirring at 500 rpm, and kept aside overnight. The gel was further characterized for viscosity, and rheology data (amplitude and frequency test).

4.2.6 Characterization of TF-LCNP gel

4.2.6.1 pH and physical appearance

The pH of the LCNP gel was determined using a digital pH meter. The gel was examined visually for the evaluation of appearance.

4.2.6.2 Rheological Behavior of TF-LCNP gel

The flow behavior and the effect of formulation, storage time and temperature on the quality and acceptability of a developed LCNP-loaded gel can be evaluated based on rheological tests. The rheological properties of LCNP-loaded gel and free drug loaded gels (FD gel)

were measured with an Anton Paar rheometer. The rheometer setup includes MCR equipment (Model no. MCR92) with P-PTD 200 and PP25 fixture.

4.2.6.2.1 Amplitude sweep test

The mechanical stability was determined by performing the amplitude sweep test in a short time. This test was performed at variable amplitudes and a constant frequency. Amplitude sweep analysis can help in determining the limit of Linear Viscoelastic (LVE) range which indicates that below this limiting value, G' and G" curves remain on a constant plateau, meaning that the structure of the sample shows stability under the given experimental conditions. Yield point determination is the critical stress where material just starts to flow or determines the essential force for applying formulation. Flow point which is the minimum stress to make the material flow where viscous modulus (G") overtakes elastic/storage modulus (G'). The optimized formulation and FD gel were analyzed in shear strain range from 0.01 to 100% at a constant frequency of 10 rad/sec to evaluate G' and G" their behavior at 25^{o}C.

4.2.6.2.2 Frequency sweep test

The formulations were measured in angular frequency range of 0.1 to 100 rad/s to determine the time-dependent viscoelastic behavior of the samples at a constant strain of 0.5% which was taken from the amplitude sweep test within the LVE range. Parameters that can be evaluated by frequency sweep are G', G" and complex viscosity. In such analysis, the high-frequency region indicates the short-term behavior of the materials, and the lower frequency region indicates the long-term behavior of the materials. This experiment can help to simulate the experimental condition of the dispersion stability/ phase separation or relaxation phenomenon happening in materials.

4.2.6.3 Spreadability

The LCNP gel and FD gel's spreadability was determined by weighing 50 mg of gel onto the glass slide. Another glass slide with a weight of 50g was placed over it. After 2 min, the weight was removed, and the diameter of the placed gel was measured. The spreadability was calculated using below mentioned formula [16].

Spread ability factor = $\frac{Area\ covered\ by\ sample\ (cm2)}{Weight\ of\ samlpe\ (g)}$

4.2.7 Compatibility studies

4.2.7.1 Fourier transform infrared spectroscopy

Fourier transform infrared spectroscopy (FTIR) of lyophilized TF-LCNP, pure drug, and the physical mixture was recorded using Attenuated total reflection (ATR) - FTIR (BRUKER, USA). The spectra were recorded to investigate the interaction among the excipients and the final formulation. The spectrum was recorded at wavelengths from 4000 to 200 cm^{-1} with a resolution of 1 cm^{-1} for 25 scans.

4.2.7.2 Differential scanning calorimetry

Differential scanning calorimetry (DSC) analysis of lyophilized TF-LCNP, pure drug, and physical mixture were performed using DSC-60 (Shimadzu, Japan). The crimped empty aluminum crucible was taken as reference, and the other crucible was loaded with the mentioned excipients and formulation (approximately 3 to 5 mg). The reference and the other formulation crucible were exposed to 30-300^{0}C with 10^{0}C/min heating rate. The heating rate was maintained by heat flux DSC-60 (TA-60 WS Shimadzu corp., Japan), and the cooling was done by liquid nitrogen. The DSC thermograms were recorded using Lab Solutions TA Software.

4.2.8 Ex vivo skin permeation studies

The ex vivo TF permeation through the full thickness goat skin was performed for 24 h using a vertical Franz diffusion cell. The goat ear skin was collected from the slaughterhouse. The skin was processed neatly by removing the subcutaneous fat, and hair, and washed thrice using phosphate buffer saline. The processed skin was mounted onto the vertical Franz diffusion cell with a solvent system constituted of pH 7.4 phosphate buffer saline (PBS) in the receptor compartment. The assembly was equilibrated for 2h for the hydration of the skin. After this, the optimized TF-LCNP gel formulation (300 mg) and the cream (300 mg) were applied to the donor chamber. The whole assembly was maintained at 32 ± 0.5^{0}C at 80 rpm on a magnetic stirrer. The samples were collected at predetermined time intervals (1, 2, 4, 6, 8, 12, and 24 h) and replaced with the same receptor medium [17,18]. The collected samples were filtered through a 0.45 µ syringe filter prior to HPLC analysis. The filtered samples were analyzed at 285 by the validated HPLC method. The obtained results were analyzed, and the graph was plotted by taking time on the x-axis and % cumulative TF permeated on the y-axis. The lag time and the steady-state flux were calculated. The slope of the linear portion of the graph gives the permeation flux (µg/cm/h; units ‘J’).

4.2.8.1 Skin retention study

After completing 24h skin permeation study, the skin was detached from the assembly. The skin surface stratum corneum side was wiped with a cotton swab to remove the applied gel. The collected skin was allowed to dry for 6 h. The tape stripping technique was used to determine the amount of drug retained in the stratum corneum and viable parts of skin layers. Initial two tapes were discarded to remove the traces of unabsorbed TF. Then 13 tape strips were collected to separate the stratum corneum and then the remaining skin was chopped into pieces. The collected 13 tapes and skin samples were collected into the vials [17,18]. To extract the TF, methanol was added to these vials. The vials were kept aside for 6 h and subjected to sonication for 2 h for complete extraction of TF. All the samples were analyzed using the validated HPLC method.

4.2.8.2 Dermal distribution studies of dye -loaded LCNP (or) Mechanistic understanding of skin distribution

The distribution of coumarin-6-loaded LCNP into the skin layers was visualized using fluorescent optical microscopy (ZEISS). The coumarin-6-loaded LCNP was prepared as described in section 3.1.2. As a control, the coumarin dispersion in water was prepared (0.05% w/v). The coumarin-6-loaded LCNP and control were applied to the dorsal skin surface skin and placed on a Franz diffusion apparatus. The whole assembly was placed onto the magnetic stirrer at 37 ± 0.5^0C at 80 RPM. During the study, at a treatment period of 4h and 24h the whole skin was removed from the assembly and washed twice with pH 7.4 PBS before wiping with the cotton swab. Then the skin was placed onto the freezing microtome and sectioned into a size of 10 µ. The sectioned skin was visualized under a fluorescence microscope [19].

4.2.8.3 Dermal pharmacokinetic assessment of TF- LCNP

The dermal pharmacokinetic assessment study is necessary when you target the drug to the regional site. In Rheumatoid arthritis condition, inflammation occurs at the joint site and most of the immune cells are activated in the dermis region. Thus, targeting the drug specifically to the joint site provides significant improvement in the inflammatory condition. Ex vivo dermal pharmacokinetics studies were performed on goat skin. The study was performed as discussed in the ex vivo permeation study (section 3.6.5). The TF-LCNP gel and cream were applied (approximately 300 mg) on the stratum corneum side. At predetermined time intervals (1, 2, 4, 6, 8, 12, and 24 h), whole skin was collected, and the

epidermis and dermis layers were separated. The skin samples analysis was performed using a validated HPLC method. The dermal pharmacokinetic parameters such as time of maximum concentration (Tmax), Maximum concentration of drug achieved in the skin layer (Cmax), Area under the curve $(AUC)_{0-t,}$ and $AUC_{0-\alpha}$ were evaluated [20–22]. The obtained results were evaluated using the non-compartment model to calculate Tmax and Cmax. To calculate $AUC_{0-t,}$ and $AUC_{0-\alpha}$, linear trapezoidal rule was employed.

4.2.9 Stability studies

The developed TF-LCNP formulation and TF-LCNP gel were examined for 45 days at 4°C and 25 ± 0.5 °C. The stability of the TF-LCNP formulation was assessed by their mean particle size, PDI and entrapment efficiency. The stability of the TF-LCNP gel was assessed by assay and viscosity as discussed under section 4.2.6.2. Table 7 presents the stability data of TF-LCNP and TF-LCNP gel at 4 °C and 25 ± 0.5 °C.

4.2.10 Scale-up studies

The developed TF-LCNP formulation was scaled up to 2.5 times the initial volume of the batch. Initially, the process parameters' including probe size, were optimized by maintaining the TF amount: lipid mix (GMO and myristol): surfactant ratio constant. The batch was further characterized for entrapment efficiency, particle size, and PDI. The scale up formulation was characterized for particle size, PDI, and entrapment efficiency.

4.2.11 Statistical data analysis and interpretation

All the experiments were performed in triplicate. The data was presented as standard deviation (SD) ± mean.

4.3 Results and discussion

4.3.1 Solubility of tofacitinib in different liquid oils and Screening of compatibility of liquid oil with GMO

The drug should have the highest solubility in GMO and liquid oil to accomplish the highest entrapment efficiency. The solubility data of TF in various liquid oils was presented in Figure 4.1. TF exhibited highest solubility in oleic acid and myristol. Further, the compatibility of the selected oleic acid and myristol with GMO was determined by phase separation test. The GMO and liquid oil (oleic acid and myristol) 60:40 and 80:20 ratio exhibited excellent miscibility without phase separation.

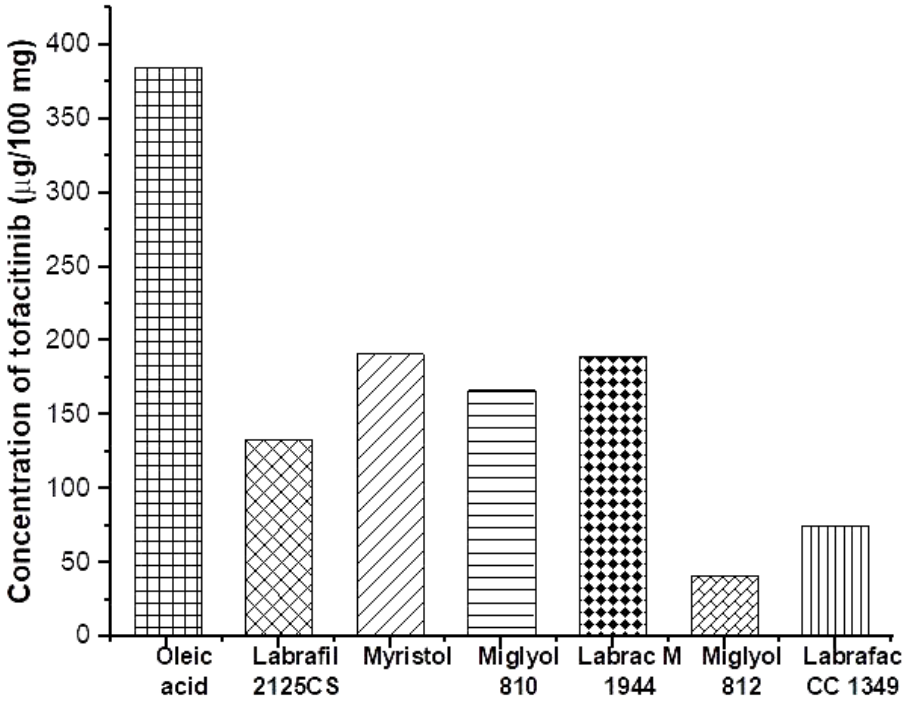

Figure 4.1. Solubility of TF in different liquid oils

4.3.2 Quality by design approach for LCNP development

4.3.2.1 Quality target product profile and Critical quality attributes

QTPP plays an essential role to achieve the safety and efficacy of the final product. The quality target product profile (QTPP) for liquid crystal nanoparticles of TF are postulated in Table 4.1 with their justification. The second most important step is CQAs which are derived from the QTPP which influences the final product quality. Thus, the critical quality attributes (CQAs) for liquid crystal nanoparticles of TF are discussed in Table 4.2.

Table 4.1. Quality target product profile (QTPP) postulated for liquid crystal nanoparticles of TF

QTPP Element	**Target**	**Justification**
Site of application	Topical	Topical application of designed formulations allows the dermal penetration of TF into the deeper regions of the skin, such as viable epidermis and dermis.
Route of administration	Topical	Avoids hepatic metabolism and reduce systemic side effects of TF. Application of lower doses is sufficient to achieve the therapeutic efficacy. High patient compliance.

Novel drug delivery system	LCNP and modified LCNP with added liquid oil and other penetration enhancers	LCNP and modified LCNP helps in improving drug loading, entrapment efficiency, and nano size enhances permeation across skin.
Dosage form and strength	LCNP loaded gel-based formulation with strength of 0.2% or 0.5% w/w	Convenient appliance with promising rheological performance. Adheres to the skin surface and partitioning of TF. As per literature and preclinical investigations, 0.2% w/w strength is effective to achieve the Cmax on topical application.
Release profile	Sustained release	Reduction of the number of applications permit improved patient compliance.
Stability	Six months (at the refrigeration conditions)	To maintain the therapeutic effect of the LCNP, it is essential to maintain the physical, chemical and biological stability of the product under short-term/long-term storage conditions.

Table 4.2. Critical quality attributes (CQAs) for liquid crystal nanoparticles of TF and its justifications

Product Quality attributes	**Target**	**Justification**	**Is this CQA ?**
Physical attributes	Smooth & translucent gel without unpleasant Odor	The physical attributes (color, appearance, and odor) are not considered critical. However, satisfactory physical attributes enhance the patient compliance but it is not directly associated to safety and efficacy	No
TF solubility in nanocarriers system i.e. drug loading	Up to 40%	Effect on drug release, skin permeation, and therapeutic effect	Yes
Particle size	Nano size i.e., 100 to 300 nm	Particle size is considered as critical parameter as it influences the skin permeation, physical stability and biodistribution of TF LCNP (therapeutic efficacy)	Yes
Zeta potential	-20 to +20 mv	Affect the physical stability and, skin permeation	No
Entrapment efficiency	50 – 100%	----	Yes

Permeation flux		Permeation flux represents average amount of drug released per hour from the LCNP	Yes
Viscosity	Dispersion viscosity 100 to 500 mPas	Affects the drug release	Yes
Skin penetration	To achieve minimum effective concentration in desired time	Affects the efficacy	Yes

4.3.2.2 Quality risk management

Ishikawa fish bone diagram of TF- LCNP describes the cause-effect correlation among the risk factors. It presents the critical material attributes and process parameters that affects the final product quality (Figure 4.2). In addition, the parameters mentioned in this diagram assist us to identify the failure modes by which the product quality might get affected. Thus, the REM for qualitative risk assessment of CMAs and CPPs of topical LCNP was presented in Table 4.3.

Table 4.3. REM for Qualitative risk assessment of CMAs and CPPs of Topical LCNP

CQAs		**Risk estimation matrix for CMAs and CPPs**							
	Amount of lipid	**Type of liquid oil**	**Amount of liquid oil**	**Surfactant concentration**	**Temperature**	**Stirring speed**	**Stirring time**	**Probe sonication time**	**Probe sonication amplitude**
Particle size	High	High	High	High	Medium	Medium	Medium	High	Low
Poly dispersity index (PDI)	High	Medium	High	High	High	Medium	Medium	High	Medium
Entrapment Efficiency (%)	High	High	High	High	Medium	High	Low	High	Medium
In vitro drug release (%)	Medium	High	Medium	High	Low	Medium	low	Low	Low

The REM suggested that the factors such as amount of glyceryl monooleate, amount of liquid oil, and surfactant concentration were found to be at high risk; and the probe sonication time, type of liquid oil and temperature were found to be medium risk. The RPN to the factors was allotted based on the literature survey and our previous laboratory research experience on LCNP. The modes of failure were prioritized with RPN score and determined the seriousness of their consequences. The FMEA analysis with computed RPN scores explains the reasonable effects on the CQAs of topical TF- LCNP. The high-risk factors and low risk parameters were segregated by giving a cut off value to the RPN values (Table 4.4). A cut off of 200 or above was considered for the high risk. The factors such as amount of lipid, type of liquid oil, amount of liquid oil, surfactant concentration, temperature, stirring speed, and probe sonication time possessed the high RPN score. The above said factors with high RPN score are subjected to factor screening design i.e., eight run, two level Taguchi OA design.

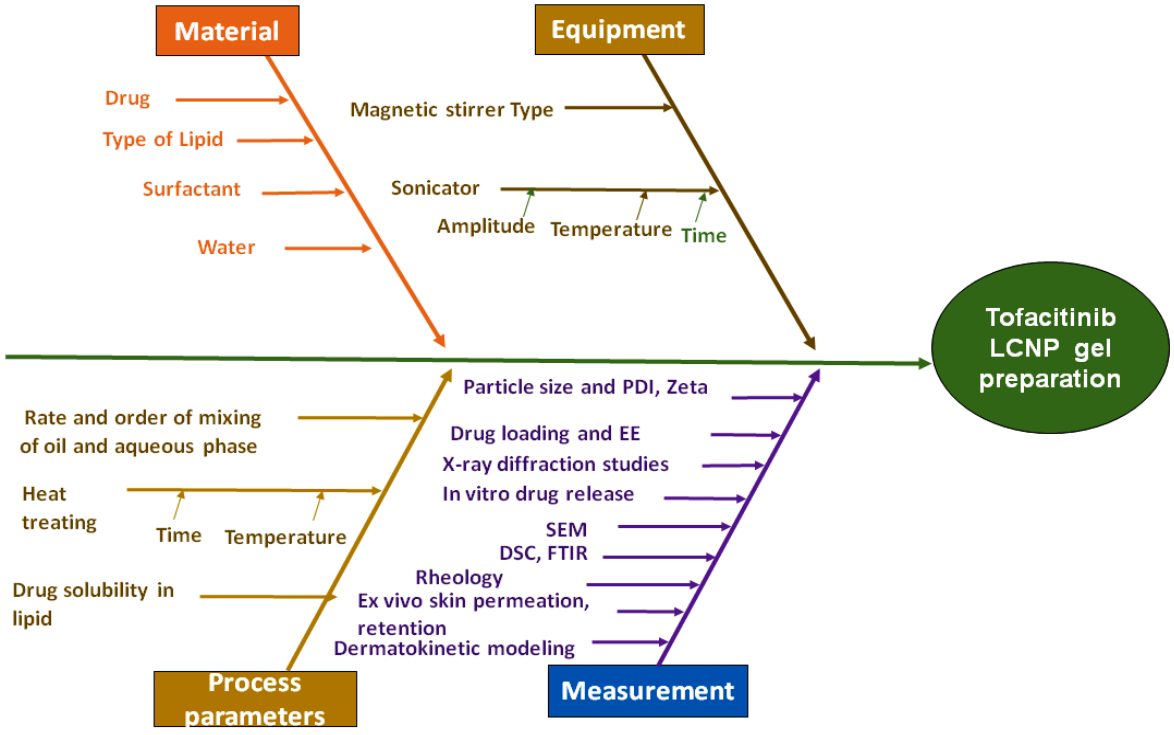

Figure 4.2. Ishikawa fish bone diagram for TF loaded liquid crystalline nanoparticles gel

Table 4.4. Failure mode and effect analysis

Failure modes	Severity	Occurrence	Detectability	RPN score
Amount of lipid	8	7	7	392
Type of liquid oil	7	7	6	294
Amount of liquid oil	7	6	6	252
Surfactant concentration	7	7	7	343
Temperature	8	6	7	336
Stirring speed	6	6	7	252
Stirring time	5	4	4	80
Probe sonication time	7	7	8	392
Probe sonication amplitude	2	2	1	4

4.3.2.3 Factor screening studies

Taguchi design or orthogonal arrays have been widely used to establish effects between the formulation variables and selected CQAs. Taguchi OA design matrix depicting the layout of various experimental runs for factor screening of topical delivery of TF-loaded liquid crystals loaded gel is presented in Table 4.5. This design initially helps in selecting the significant CMAs and process parameters from the insignificant ones. Screening design trials as per seven factors, eight run, two level Taguchi OA design are shown in Table 4.6. The Pareto charts and half-normal plots for screening of influential MAs and PPs as per Taguchi design using selected CQAs are presented in Figure 4.3 and 4.4.

Table 4.5. Taguchi OA design matrix depicting the layout of various experimental runs for factor screening of topical delivery of TF-loaded liquid crystals loaded gel

Independent variables	**Type**	**Levels**		**Critical quality attributes**
		Low (− 1)	High (+ 1)	
A: Amount of Glyceryl mono oleate (mg)	Numeric	150	200	Mean particle size (nm) PDI Entrapment Efficiency (%) In vitro drug release (%)
B: Amount of liquid oil (mg)	Numeric	50	100	
C: Surfactant concentration (%)	Numeric	0.5	1.0	
D: Probe sonication amplitude (%)	Numeric	20	25	
E: Probe sonication time (Sec)	Numeric	150	300	
F: Temperature (^{0}C)	Numeric	50	70	
G: Type of liquid oil	Categorical	Myristol	Oleic acid	

Table 4.6. Screening design trials as per seven factors, eight run, two level Taguchi OA design

	Independent variables with specified code						
RUN	**A (mg)**	**B(mg)**	**C (%)**	**D (%)**	**E (sec)**	**F (^{0}C)**	**G ***
1	-1(150)	-1(50)	-1 (0.5)	1(25)	1(300)	1(70)	1
2	1(200)	-1(50)	1(1)	-1(20)	1(300)	-1(50)	1
3	-1(150)	1(100)	1(1)	-1(20)	-1(150)	1(70)	1
4	1(200)	1(100)	-1(0.5)	1(25)	-1(150)	-1(50)	1
5	-1(150)	-1(50)	-1(0.5)	-1(20)	-1(150)	-1(50)	-1
6	1(200)	1(100)	-1(0.5)	-1(20)	1(300)	1(70)	-1
7	1(200)	-1(50)	1(1)	1(25)	-1(150)	1(70)	-1
8	-1(150)	1(100)	1(1)	1(25)	1(300)	-1(50)	-1

***Represents the categorical i.e. -1 (myristol), 1 (oleic acid)**

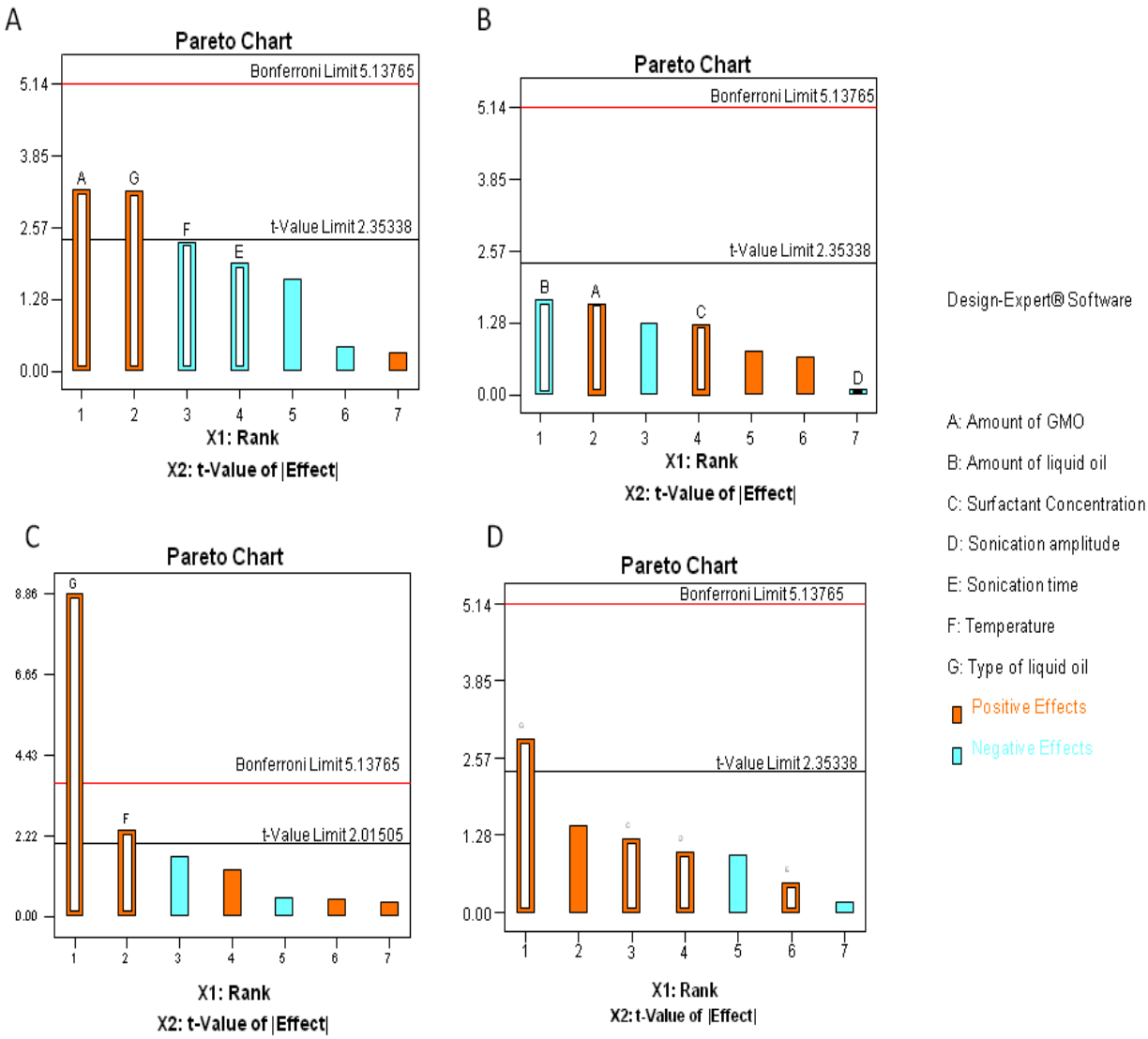

Figure 4.3. Pareto charts for the selected CQAs obtained from Taguchi orthogonal design presenting the (A) Particle size (B) Poly dispersity index (C) Entrapment efficiency and (D) zeta potential

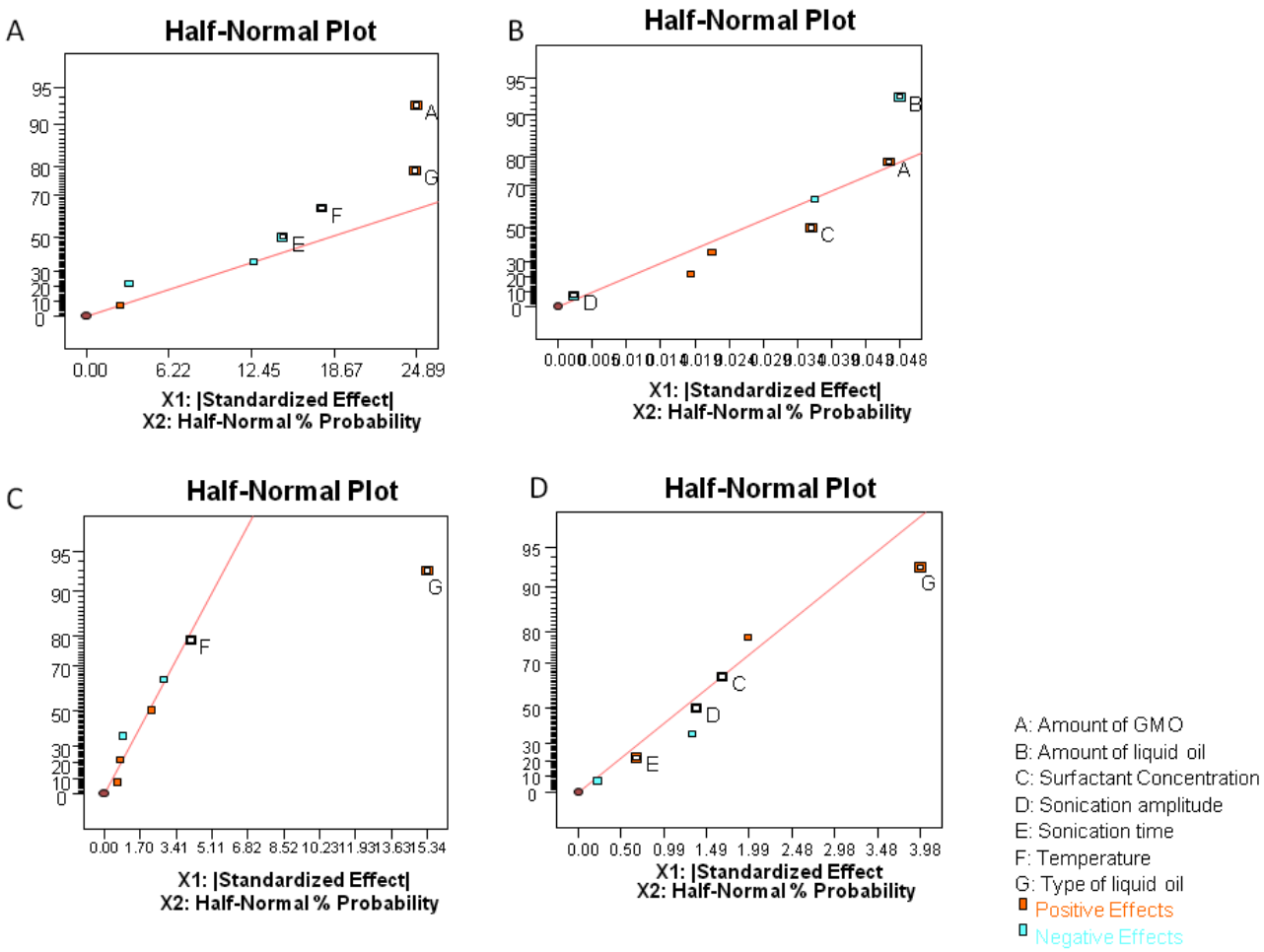

Figure 4.4. Half normal plots obtained from Taguchi orthogonal design (A) Particle size (B) Poly dispersity index (C) Entrapment efficiency and (D) zeta potential

In the Pareto charts, yellow and blue boxes represent the positive and negative effects of the MAs and PPs on the CQAs. The red and black line represents the Bonferroni limit and standard t-value limit respectively. The material and process parameters having significant effect on CQAs crossed the standard t-limit value [23]. The material attributes such as amount of GMO, amount of liquid oil was found to exceed standard t-value limit for particle size. The parameters like type of liquid oil and temperature were found to exceed the Bonferroni limit and standard t-value limit for entrapment efficiency. For zeta potential, type of liquid oil crossed the t-value limit whereas none of the material and process parameter showed significant effect for PDI [24]. The surfactant concentration, probe sonication time, and probe sonication amplitude were considered to be constant. But the qualitative analysis suggests that surfactant concentration and probe sonication time can show significant effect

based on their RPN score. In our previous trials, we found that the surfactant concentration and probe sonication time can show significant effect on the particle size and PDI. As we know the Taguchi design does not include the interaction effects [25], so while selecting the formulation variables for BBD we have considered our previous experience. Hence, the temperature was kept constant and surfactant concentration and probe sonication time were varied. The parameters such as amount of GMO, amount of liquid oil, surfactant concentration, and probe sonication time needed to be further optimized using the BBD.

Changes in the ratio of GMO to liquid oil were made along with the changes in the type of liquid oil (oleic acid and myristol). It was observed that myristol influenced the entrapment efficiency, with increased proportion of myristol the entrapment efficiency increased. In contrast, increase in proportion of oleic acid did not influence entrapment efficiency. It was observed that GMO and myristol in the ratio of 80: 20 demonstrated better controlled release. Thus, GMO and myristol (80:20) were selected as the amount of lipid for further optimization by BBD.

4.3.2.4 Optimization by Box–Behnken design

BBD is chosen for optimization of LCNP as it gives fewer experimental runs over central-composite design, factorial design, D-optimal design and mixture design. Moreover, it has simpler design implementation and interpretation. The screened MAs and PPs such as amount of lipid (GMO and myristol in 80: 20), surfactant concentration, and probe sonication time were further optimized by employing BBD at three levels (-1, 0, +1). The assigned low and high levels to screened CMAs and CPPs were presented in Table 4.7. A Total 17 runs with three central points were generated. The suggested experimental batches by BBD were tabulated in Table 4.8. The value of three responses was fitted to different rate equations, like first order, second order and quadratic model. The best-fitted model was selected based on the R^2, SD and % CV values.

Table 4.7. Selected low and high levels of independent variables (CMAs and CPPs) for further optimization using Box-Behnken design

Selected CMAs and CPPs	Goal	Lower Limit (-1)	Upper Limit (+1)
A: Amount of lipid (mg)	In range	150	250
B: Surfactant concentration (%)	In range	0.5	1
C: Probe sonication time (minutes)	In range	2	6

Table 4.8. Suggested experimental batches by Box-Behnken design with results

Batch	Amount of lipid (mg)	Surfactant (%)	Probe sonication time (min)	Entrapment efficiency (%)	Particle size	PDI
1	250	0.75	2	40.62 ±7.09	112.1±7.85	0.242
2	200	0.5	2	54.47 ±1.10	123.2±6.37	0.066
3	250	0.75	6	61.3 ±2.24	98.87± 11.11	0.24
4	200	0.75	4	59.7 ±6.38	82.16± 2.54	0.101
5	200	0.75	4	59.6 ±1.26	81.01±4.39	0.083
6	200	0.75	4	57.3 ±6.40	80.42± 2.77	0.08
7	250	0.5	4	50.2 ±11.73	115.2±2.44	0.085
8	200	0.75	4	54 ±1.37	86.39± 1.86	0.13
9	200	0.75	4	52.7 ±7.46	78.75±3.32	0.108
10	150	0.75	2	50.03 ±1.92	85.89± 2.88	0.151
11	200	0.5	6	45.52 ±7.87	97.1± 1.76	0.136
12	250	1	4	70.5 ±7.64	79.34± 2.55	0.101
13	200	1	2	55.84±3.12	84.78± 3.36	0.176
14	200	1	6	68 ±1.21	63.65± 2.04	0.96
15	150	1	6	62 ±0.71	63.7± 1.53	0.16
16	150	1	4	55 ± 4.47	62.1 ± 2.49	0.178
17	150	0.5	4	39 ± 0.66	83.4 ± 2.05	0.072

Table 4.9 shows the coded equations, comparative values of R^2 and adjusted R^2. The best fit model was found to be a quadratic model. In the research study, the obtained second order polynomials used for particle size has highest regression (0.9768) compared to entrapment efficiency (0.8766) and PDI (0.7624). This signifies that the response variations can be explained by response surface models as a function of critical process parameters. The values greater than 0.1000 indicate the model terms are insignificant. The lack of fit in all the three responses showed insignificant for the final model. Therefore, the obtained results provide good fitness to the response surface methodology to the amount of lipid, surfactant concentration and probe sonication effect. The coded equations of responses viz. entrapment

efficiency, particle size and PDI are presented in Table 4.9. The obtained equations (Table 4.9) for responses demonstrated that the amount of lipid (GMO and myristol ratio) has a positive effect on all the three responses. It was observed that as the amount of lipid ratio increased, the particle size of LCNP increased because the number of surfactant molecules per lipid mixture is reduced [26].

The probe sonication time exhibited a positive effect on response of entrapment efficiency, and negative effect on the size and PDI [27]. The surfactant concentration showed positive effect on response of entrapment efficiency and PDI, but negative effect on the size. The coefficient with more than one factor represents interaction between the chosen variables or quadratic relationship. As the variables are varied at three levels a different degree of response could be expected which can be a nonlinear relationship between the independent variables and responses. The obtained equations demonstrate that all the three responses (entrapment efficiency, particle size and PDI) were affected by the three factors. The interaction between the amount of lipid and probe sonication; surfactant concentration and probe sonication were favorable for entrapment efficiency, size, and PDI as they are showing a positive co efficient (Table 4.9). The interaction effect between the amount of lipid and surfactant concentration has showed a negative coefficient means antagonistic effect for all the three responses. The A^2 and B^2 in equations present quadratic effect in all the three independent variables on the responses. Among the two responses, particle size exhibits highest negative quadratic effect by probe sonication time (co-efficient value of 8.7). The positive quadratic effect was showed by surfactant concentration on entrapment efficiency and particle size (co efficient value of 2.85 and 2.9).

Table 4.9. Estimated coded model equations along with regression coefficients for box Behnken design effects against the CQAs

CQA s	Coded Equation	R^2	AdjustedR^2
Entrapment Efficiency	56.22298 + 4.249902 A + 7.960028 B +2.411348 C – 0.01756 AB + 6.529805 AC + 6.580056 BC – 4.85328 A^2 + 2.85158 B^2 – 2.78078 C^2	0.8766	0.718
Size	81.53 + 12.8374 A – 15.8625 B – 9.36615 C – 4.17256 AB + 0.309805 AC + 1.775056 BC + 1.54922 A^2 + 2.19408 B^2 – 8.72172 C^2	0.9768	0.9470
PDI	0.169414 + 0.13242 A + 0.030437 B – 0.03162 C – 0.05312 AB + 0.042983 AC + 0.004373 BC	0.7624	0.6199

The regression co- efficient of the fitted quadratic equation was evaluated by ANOVA. The ANOVA data in Table 4.10 presents ANOVA for regression coefficients for Box Behnken design effects (Linear, Quadratic, and Interaction) against the CQAs i.e., dependent variables to establish the best fitted quadratic equation. The variables values with high F-value and low P-value exhibits the most significant effect on the responses. The linear term value signifies that surfactant concentration exhibits highest significant effect on the entrapment efficiency and particle size of LCNP. The quadratic term of amount of lipid exhibits a significant effect on the particle size. The interaction of the amount of lipid and surfactant concentration has showed a significant effect on the PDI while all the other terms have insignificant effect. The interaction of effect of amount of lipid and probe sonication time has shown a significant effect on particle size [28].

Table 4.10. ANOVA for regression coefficients for Box Behnken design effects (linear, quadratic, and interaction) against the CQAs i.e., dependent variables to establish the best fitted quadratic equation

Effect	Variable	Entrapment efficiency		Particle size		PDI	
		F- value	P- value	F- value	P- value	F- value	P- value
Linear effect	A	6.403986	0.0392	72.73267	< 0.0001	1.548598	0.2417
	B	25.75436	0.0014	127.3052	< 0.0001	9.075136	0.0131
	C	2.061636	0.1942	38.71664	0.0004	8.828506	0.0140
Interaction effect	AB	6.48E-05	0.9938	4.554125	0.0702	14.47699	0.0035
	BC	6.878075	0.0343	0.019272	0.8935	7.713651	0.0195
	AC	9.098652	0.0195	0.824185	0.3941	0.098109	0.7605
Quadratic term	A^2	4.561895	0.0701	0.578607	0.4717	-	-
	B^2	1.380178	0.2785	1.017072	0.3468	-	-
	C^2	1.497642	0.2606	18.33841	0.0036	-	-

4.3.2.5 Response surface analysis

The best fit quadratic model provided response surface plots for entrapment efficiency and particle size. Figure 4.5 (a-c) presents the 3D response surface plots for selected CQAs of topical LCNP. These plots presented the individual and interaction effects of variables on the selected responses. 2D-contour designs for particle size are portrayed in Figure 4.5(a). The curvilinear shape of response surface plot characterizing a nonlinear trend means increase in size with increasing concentration of GMO and myristol by keeping the Lutrol® constant. This can be attributed to increase in the viscosity of the dispersion medium. As the Lutrol® concentration and probe sonication time are increased with the given GMO, the particle size starts decreasing. Decrease in size of the LCNP is due to the reduction of the surface tension of the nanoparticles.

3D-response surface plots and 2D-contour plots for % entrapment efficiency are portrayed in Figure 4.5(c). Both low and high levels of GMO and myristol showed increase in the drug entrapment. The increase in TF entrapment efficiency was observed with gradual increase in surfactant concentration at low lipid amount [26,28]. The interaction effect can be clearly

seen among the selected variables with entrapment efficiency as the response variable. The high level of amount of lipid and Lutrol® showed high entrapment efficiency. Similarly, the high and medium level lipid and high levels of Lutrol® and sonication time also showed significantly high entrapment of TF. The high entrapment efficiency can be attributed to the strong hydrophobic interactions of GMO and myristol with the TF (Log P 1.15).

A

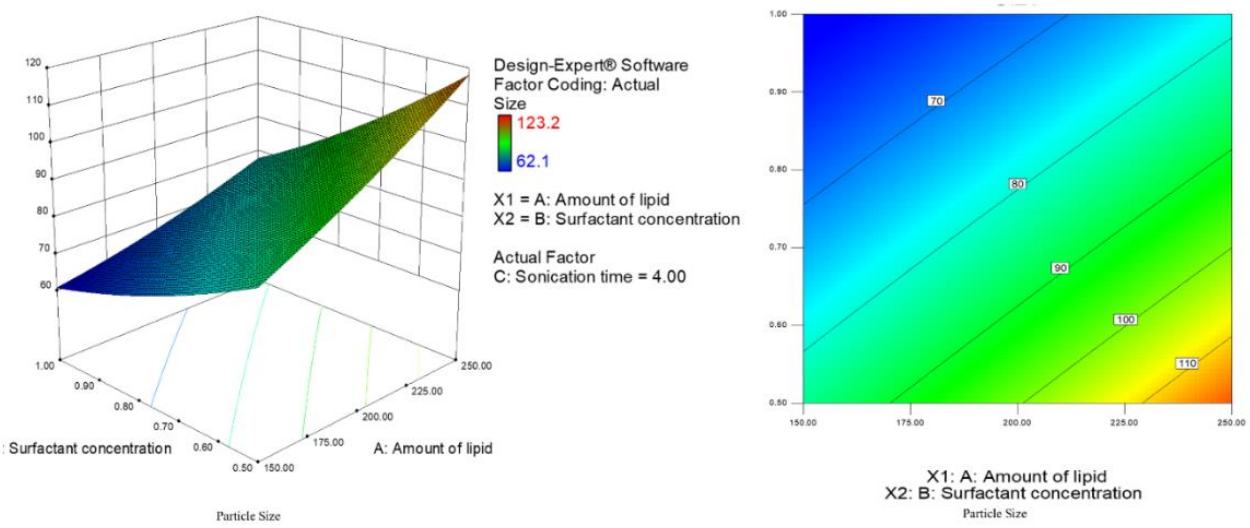

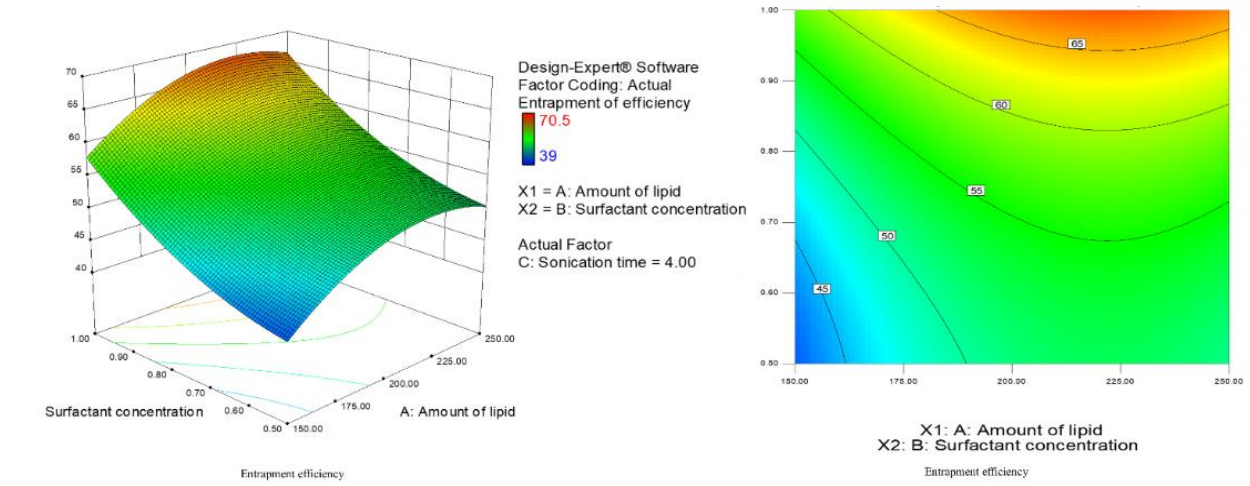

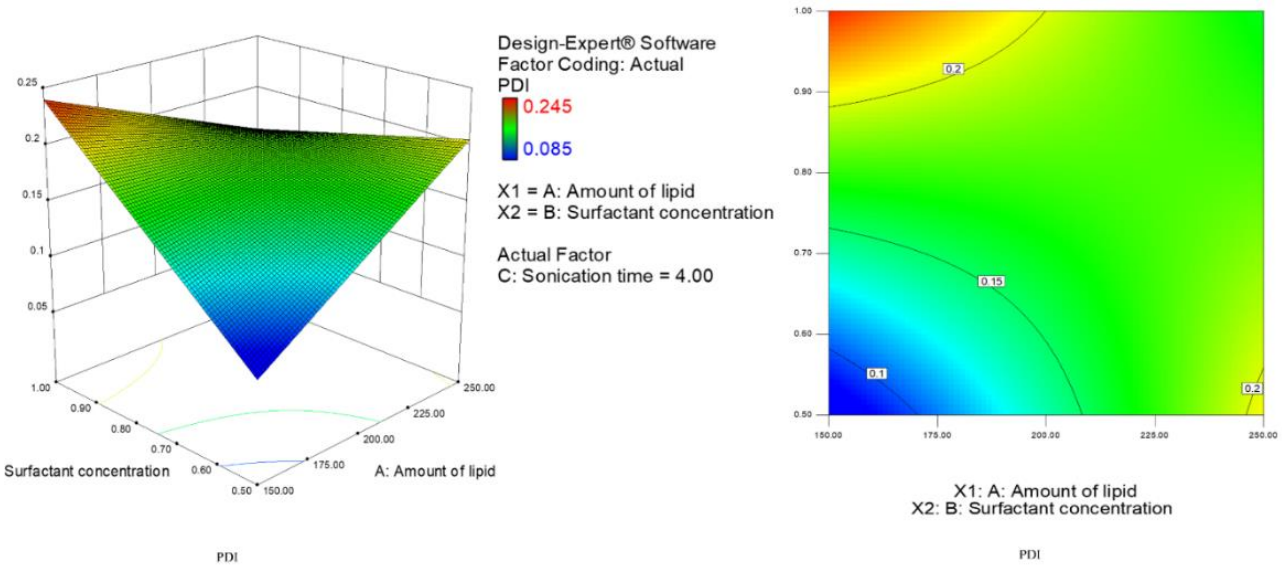

Figure 4.5. 3D Response surface plots and Contour plots for selected CQAs of topical TF-LCNP i.e. (A) Particle size (Response 1) (B) Poly dispersity index (Response 2) (C) Entrapment efficiency (Response 3)

4.3.3 Characterization of TF-LCNP

4.3.3.1 Size, polydispersity index and zeta potential measurements

The obtained results are presented in Table 4.11. The optimized TF loaded LCNP exhibited a ultra-fine particle size (< 100 nm) and PDI (< 0.15). The obtained results confirm that the developed LCNP system cascades in narrow PDI and affirms homogeneous nanoparticles [29]. The zeta potential value of the developed LCNP was found to be -25 mV.

Table 4.11. Results of optimized batch composition

Responses	**Predicted results**	**Actual results**	**% Relative**
Particle size (nm)	68.33 ± 4.04	74.82 ± 4.26	8.67
PDI	0.168 ± 0.033	0.124 ± 0.024	- 35.48
Entrapment Efficiency (%)	72.41 ± 4.51	68.29 ± 5.24	- 6.03

The particle charge of the LCNP plays an important role in skin permeation. It was reported that the negatively charged particles can create repulsive forces with the skin and could permeate through the channels of skin easily [30]. The obtained zeta potential value confirmed that the developed LCNP are stable, without any aggregation. It is presumed that Lutrol® provided the stearic hindrance by adsorption of hydrophobic chain on to the surface

of the liquid crystals and the hydrophilic ethylene oxide chain into the aqueous phase, thereby preventing the aggregation of LCNP [31].

4.3.3.2 Drug entrapment efficiency

The amount of drug in 1mL dispersion was found to be 499.08 ± 1.24 µg/mL. The drug entrapment of developed TF-LCNP formulation was found to be 68.29 ± 5.24 %. The acquired entrapment efficiency results confirmed that the high solubility of TF in the selected lipid system. The obtained results and structural features of GMO also confirm high affinity towards the liquid lipid.

4.3.3.3 Field emission scanning electron microscopy and Transmission electron microscopy

SEM and TEM are performed to appraise the surface morphology and architecture of the LCNP. The SEM and TEM images of TF-LCNP are depicted in Fig. 4.6. It can be observed from the images that the particles are uniform in shape with smooth surface. The particle size range obtained was 41.85 nm to 80.62 nm, as shown by dynamic light scattering technique without aggregations. The TEM Data (4.6C) confirms the hexagonal structure of the developed TF-LCNP.

A B

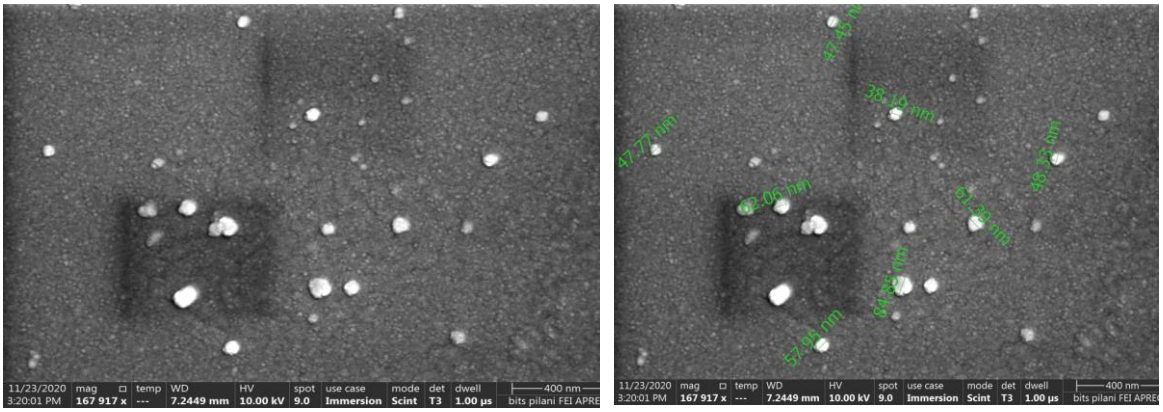

C

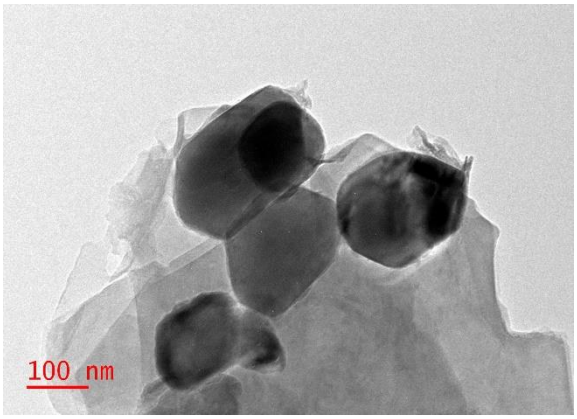

Figure 4.6. (A & B) Field Emission Scanning Electron Microscopy images of TF-LCNP (10 kV at a agnification range of 1000x – 170000x); (C) Transmission electron microscopy images of TF-LCNP

4.3.3.4 Polarized light microscopy

All the transparent crystal structures apart from those of the cubic system which are usually optically isotropic display the phenomenon of double refraction. The re-dissolved TF-LCNP showed a dark field under the cross-polarizing microscope (Figure 4.7). The Figure 4.7 affirmed that the LCNP are crystalline nature [32].

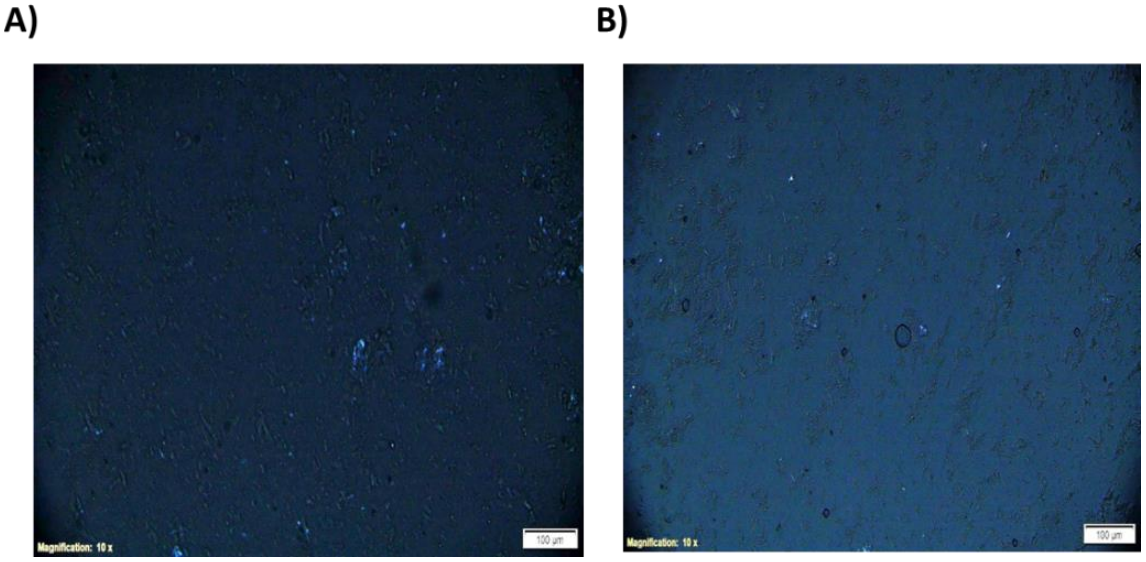

Figure 4.7. Cross-polarizing microscope images of TF-LCNP

4.3.3.5 Powder X-ray diffraction

Figure 4.8 presents the Powder X-ray diffraction **(**PXRD) for TF (pure drug), physical mixture and TF-LCNP. The PXRD spectra of TF exhibited characteristic peak of 100 % relative intensity at 2θ position of 32.154. Also, other important peaks corresponding to 66.57, 46.68, 41.39, 40.29, 40.19, 36.83, 35.22, 33.94, 31.27, 13.94, 11.25, 8.09, 7.57, and 6.5% relative intensity were observed at 2θ values of 19.125, 33.870, 14.372, 23.182, 28.965, 20.086, 16.977, 21.325, 38.652, 23.915, 26.554, 6.510, 20.347, and 11.158, respectively, indicating its crystalline nature. The crystalline nature of TF was also supported by the DSC data (Fig. 2S). In case of TF-LCNP, there were no sharp diffraction peaks; especially the peaks of TF were not apparent which indicates the non-crystalline nature of TF-LCNP. The TF-LCNP presents two sharp peaks indicating the diffuse four spot wide

angle patterns, and the TF peaks were masked. The obtained pattern may be due to the uniform liquid-like arrangement in LCNP layers and bicontinuous form of cubosomes [33]. It was evident from the XRD finding that the TF was converted into the amorphous form inside the LCNP (Figure 4.8).

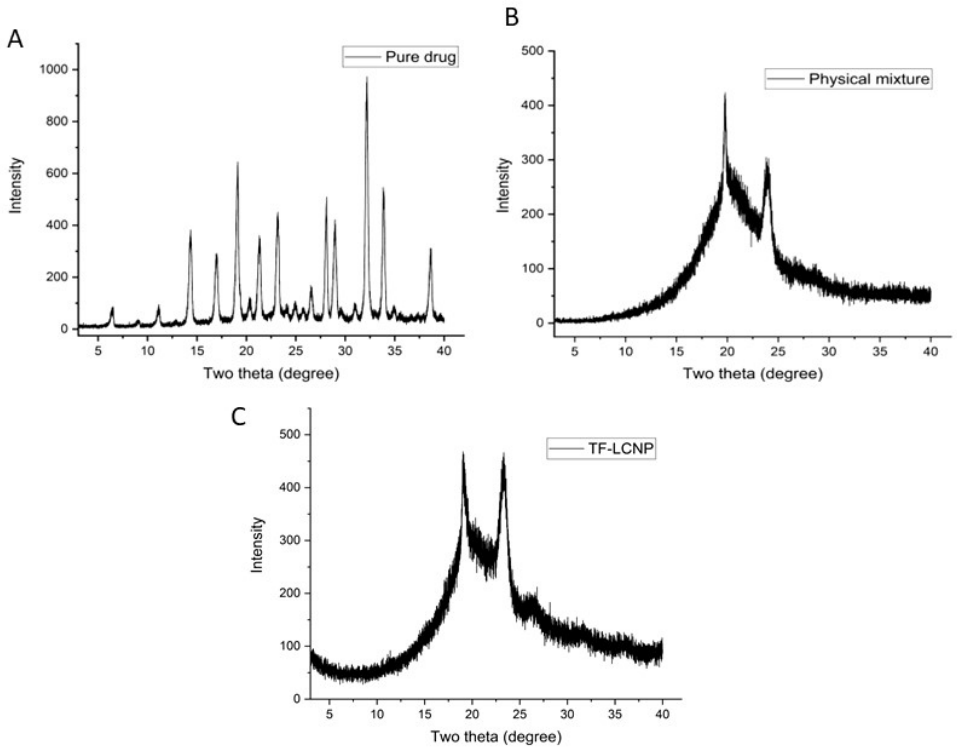

Figure 4.8: Powder X-ray diffraction (PXRD) under (10× magnification) (A) TF (pure drug) (B) physical mixture and (C) TF-LCNP

4.3.3.6 In vitro drug release

The drug release patterns of developed TF-LCNP and free drug data are depicted in Figure 4.9. The free drug showed 100 % TF release in 2 h while the developed TF-LCNP showed ~35% release in initial 30 mins, 35-50 % in 1 hour, and then sustained release upto 90% till the 16 h. This initial fast release in case of TF-LCNP due to the free drug and the surface bound drug on LCNP. The surface bound drug on LCNP was due to the rapid cooling of lipids from higher temperature to room temperature during the preparation of LCNP [34]. The sustained release of TF from LCNP was obtained due to the unique structural features of the LCNP i.e. aqueous and lipid channels. The observed sustained drug release pattern

can be attributed to TF dissolved in liquid lipid, and also the strong interaction of GMO with myristol.

The possible release mechanism was investigated using DD solver by curve-fitting method. The release kinetics including correlation coefficient data, AIC, MSC data are tabulated in Table 4.12. When comparing the models, the model with highest correlation coefficient value, lowest AIC, and MSC values greater than 2 are considered as best fit model. This confirmed that the TF-loaded LCNP followed Koresmeyer peppas model with n value of 0.197. The obtained n value indicated that TF followed quasi-Fickian diffusion from non-swellable matrix diffusion meaning usual molecular diffusion of the TF due to a chemical potential gradient.

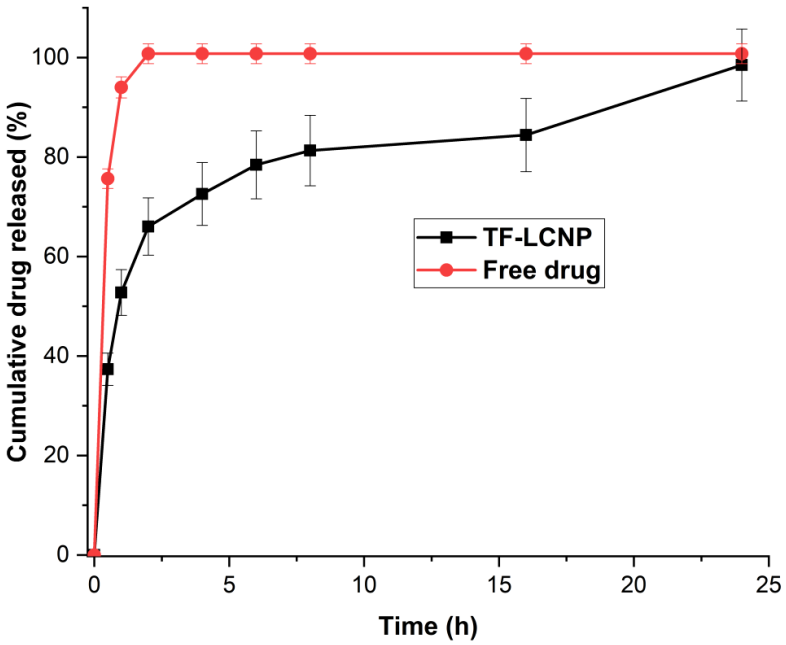

Figure 4.9: The drug release patterns of optimized TF-LCNP and free drug

Table 4.12. Possible release mechanism of TF loaded LCNP and free drug by curve-fitting method

	TF –LCNP				**Free drug**			
Kinetics model	**R^2**	**K**	**AIC**	**MSC**	**R^2**	**K**	**AIC**	**MSC**
Zero order	0.6753	6.008	90.219	- 1.73	0.4078	6.481	96.28	-3.40
First order	0.9322	0.789	96.283	1.56	0.9995	2.828	14.96	5.63
Hixson--Crowell	0.8985	0.064	76.214	-0.435	0.6187	0.070	89.54	-2.65
Higuchi	0.8845	25.364	76.245	-0.435	0.6150	31.22	88.85	-2.57
Koresmeyer peppas	**0.9876**	**52.747**	**50.507**	**2.42**	**0.9931**	**89.6**	**17.5**	**3.1**
	n value : 0.196 T50 : 0.762 T80 : 8.348				n value : 0.197 T50 : 0.052 T80 : 0.562			

4.3.4 Characterization of TF-LCNP Gel

4.3.4.1 pH and appearance

Since the TF-LCNP gel was a topical formulation to be applied to the skin, pH measurement was needed to promise the innocuous nature of the formulation. The pH of optimized TF-LCNP gel was found to be 5.8 ± 0.4. The pH was within the accepted pH range of human skin (4.5–6.4). Thus, the optimized formulation was considered to be acceptable to avoid the risk of skin irritation upon application. The prepared TF-LCNP gel formulations were viscous in nature with smooth texture and homogenous in appearance.

4.3.4.2 Rheological behavior

Amplitude sweeps test was performed to describe the deformation behavior of TF-LCNP gel and FD gel in the non-destructive deformation range and at determining the upper limit of this range. Figure 4.10 (B & E) represents the results of amplitude sweeps test of TF-LCNP gel and FD gel (0.75%). Herein, Figure 4.10 is presented with shear stress plotted on the x-axis, and storage modulus G' and loss modulus G" plotted on the y-axis. The LVE region (limits of the linear viscoelastic region) was first determined, as it demonstrates the range in which the analysis could be conceded out without destroying the structure of the

formulations. The linearity limit values in terms of the strain (γL) for TF-LCNP gel and FD gel were 0.878 % and 0.0288 %. Furthermore, G' and G" values in the LVE region are also evaluated. G' and G" correspond to the gel strength and deformation energy during shearing, indicating the formulation's viscoelastic nature. In both the TF-LCNP gel and FD gel, the G' > G" in the LVE region, proffering a gel-like structure to the sample. This is because initially, the individual microcracks are small, and upon increasing stress continuously, the microcracks spread onto the whole sample (three-dimensional network). Thus, the material starts to flow (G' = G"). After determining the LVE region, the frequency sweep test was performed to determine the flow behavior and inner structure of SEPINEO®P600 polymer and stability of dispersions on long-term storage. Figure 4.10 (C & F) represents the results of frequency sweeps test results of TF-LCNP- gel and FD gel (3.5 %). Figure 4.10 is presented with angular frequency plotted on the x-axis and storage modulus G' and loss modulus G" plotted on the y-axis. It was confirmed that for TF-LCNP-gel and FD gel the obtained G' and G" are within the LVE region; thus, the sample has showed no change during the test period.

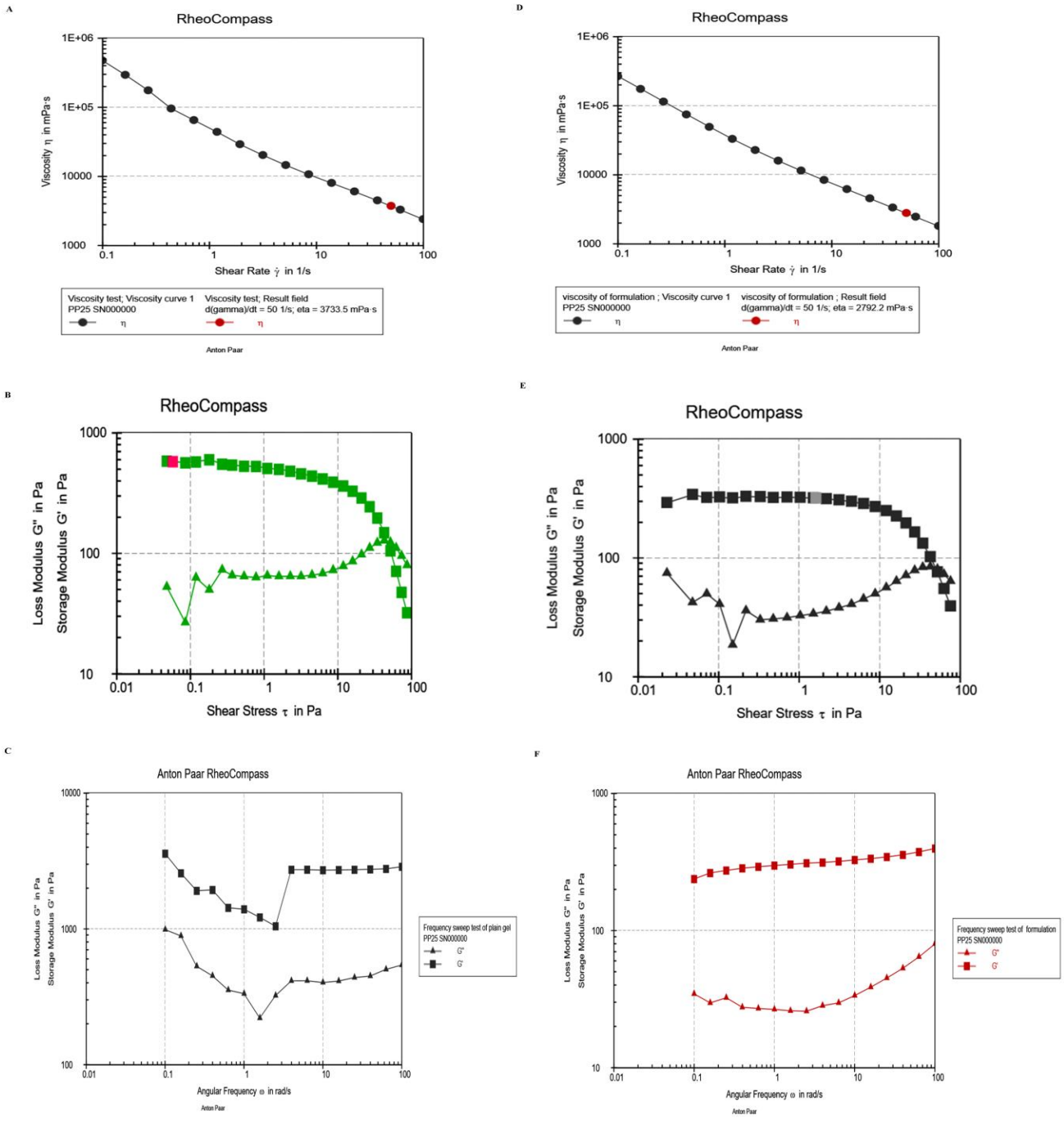

Figure 4.10: Rheology patterns (A) & (D) viscosity of TF-LCNP gel and FD gel; (B) & (E) Amplitude sweep test of TF-LCNP gel and FD gel (C) & (F)Frequency sweep test of TF-LCNP gel and FD gel.

4.3.5 Compatibility studies

4.3.5.1 Fourier transform infrared spectroscopy

The FTIR - ATR spectra of TF, physical mixture of all components of LCNP formulation and optimized TF-LCNP formulation were studied to understand the interaction among the chosen drug and excipients (Figure 4.11). The FTIR characteristic peaks of TF were observed in the region of 734.54 cm-1 (C-H bending of aromatic), 1334 cm-1 (C-N stretch), 1470 cm-1 (C-H bending of aliphatic), 1567. 29 cm-1 (C == C stretch), 1687.44 cm-1 (C = O stretching of ketone), 2273 cm-1 (C ≡N), 2918.51 cm-1 (C-H stretch), 3258 cm-1 (N-H stretch). The FTIR spectrum of optimized TF-LCNP shows intact characteristic peaks of drug with less intensity. The less intensity might be due to the entrapment of TF in the LCNP formulation.

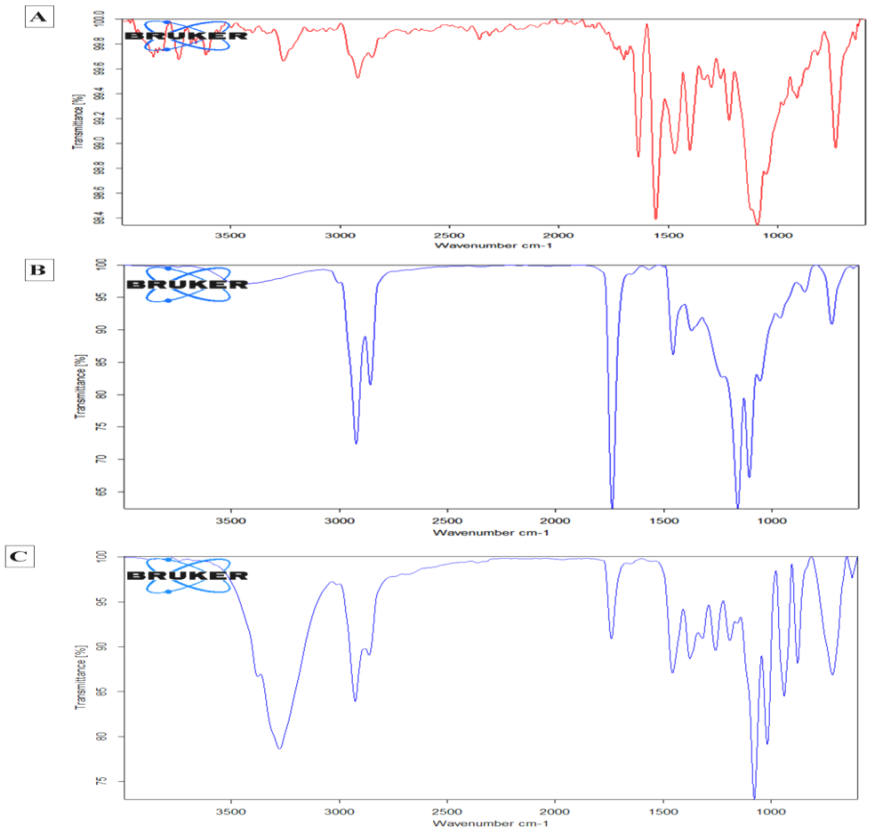

Figure 4.11. FTIR spectrum (A) Pure drug (TF); (B) Physical mixture (C) TF-LCNPs

4.3.5.2 Differential scanning calorimetry

Differential scanning calorimetry is primarily used to study the interaction among the drug and formulation excipients, and also used to verify the thermodynamics of phase transitions and conformational changes [35]. Figure 4.12 presents the DSC spectra of TF, physical mixture and optimized TF-LCNP. TF (pure drug) exhibited a sharp endothermic peak at 154.5^0 C represents the melting point and crystalline nature. In case of the physical mixture, the disappearance of TF peak was observed; indicating the complete solubilization of TF in the lipid matrix. The physical mixture presents the characteristic peak at 56^0C (Lutrol R). The same peak was also observed in the optimized LCNP, confirming that there is no interaction among the TF and chosen excipients.

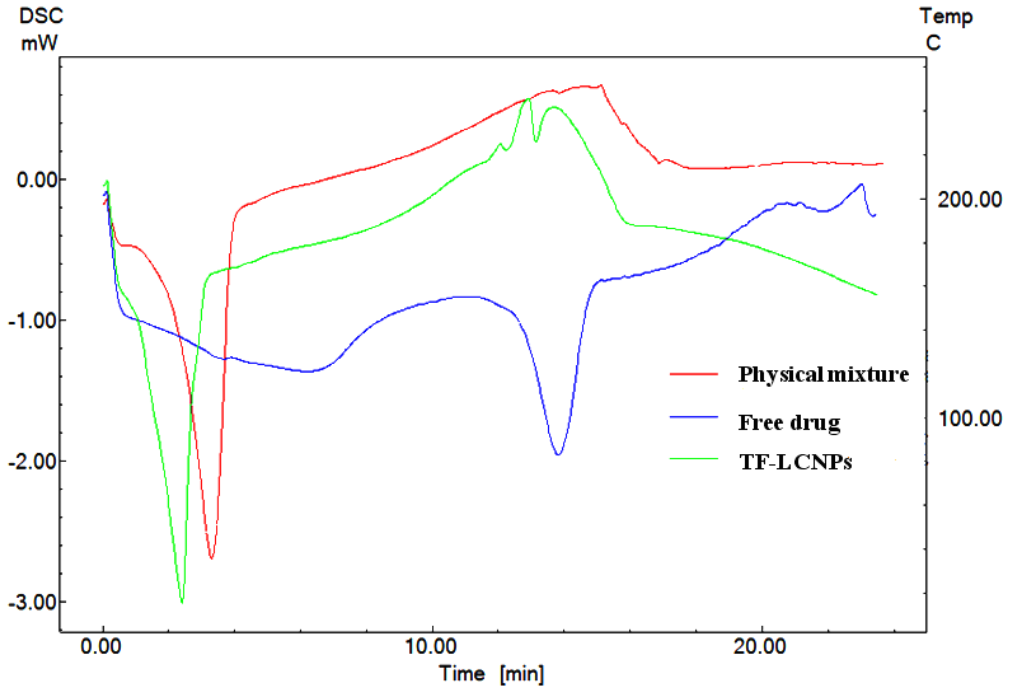

Figure 4.12. Differential scanning thermograms of Physical mixture, Free drug and TF-LCNP

4.3.6 Ex vivo skin studies

4.3.6.1 Ex vivo skin permeation studies

The ex vivo permeation profile of TF from TF-LCNP SEPINEO gel and free drug loaded formulations (FD gel) through goat skin model are presented in Figure 4.13. The amount of TF permeated through from LCNP SEPINEO gel and FD gel after 24 h was found to be 63.81 ± 4.32 and 38.5 ± 2.78 µg/cm^2 respectively. Percutaneous absorption is an important

step in transdermal delivery. The flux values of LCNP loaded SEPINEO gel and FD gel after were found to be 2.643 ± 0.542 µg/cm^2/h and 1.607 ± 0.184 µg/cm^2/h, respectively. The Kp value of LCNP gel formulation and FD gel were found to be 1.76 ×10 $^{-2}$ and 0.11 ×10^{-2} cm/h, respectively. The TF-LCNP gels permeability was highest with significant increment ($P < 0.001$) after 6 h compared to FD gel. The reason might be the permeation effect of GMO and myristol. Moreover, from the graph it can be observed that TF-LCNP gels has not shown any lag time in TF penetration through the skin. This indicates that glycerol monoester of oleic acid and myristol temporarily reduce skin resistance thereby enhancing the drug passage. Additionally, Lutrol® enhances the penetration by increasing the thermodynamic effect of TF and by emulsifying the sebum. The internal bicontinuous cubic phases and the structural similarity of GMO and myristol with the skin lipids favor LCNP permeation through the inter-corneocyte gaps. The penetration mechanism of TF-LCNP gels through skin layers was investigated by curve fitting mechanism. The Koresmeyer- peppas model has shown n-value of 1.687. This would indicate the drug transport mechanism associated with the stresses and state-transition in SEPINEO P600 polymer, which is the Case-II relaxational release. The penetration of TF-LCNP into various layers of skin: diffusion into the upper dermis and then releases the TF into the synovial tissue in sustained manner.

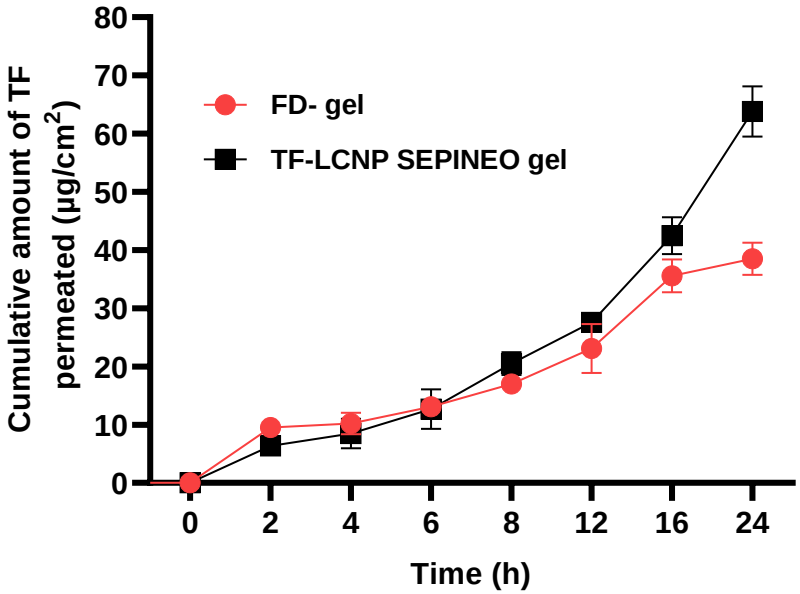

Figure 4.13. Ex vivo skin permeation profile of TF from LCNP gel (Data represented as mean ± SD, n = 3).

4.3.6.2 Skin retention study

Before starting this experiment, the extraction efficiency of TF from skin tissue of goat was estimated by validated HPLC method. The % recovery of TF from skin tissue was found to be 98.85 ± 1.59 %. The accumulation of TF in stratum corneum and viable skin layers of goat ear after application of TF-LCNP SEPINEO gel and FD gel, for 24 h was studied. After 24 h of study, the amount of TF in the epidermis and dermis with TF-LCNP SEPINEO gel, and FD gel was found to be 14.91 ± 2.89 µg, 19.92 ± 1.62 µg and 8.37 ± 0.50 µg, 7.79 ± 3.46 µg respectively (Figure 4.14). As compared to the FD gel, TF-LCNP SEPINEO gels showed 1.78 times and 2.25 times higher retention in the stratum corneum and viable parts of dermis layers, respectively. The higher retention of the TF in the epidermis and dermis layers was due to the small size of LCNP (less than 80 nm). The reported study confirmed that the particles with diameter of 70 nm or below have shown maximum deposition in both epidermal and dermal layer [36]. Moreover, the low particle size favors LCNP accumulation at the inflamed site due to enhanced permeation effect. The skin retention study and the presence of high concentration of TF in the receptor compartment confirmed that the high amount of TF would be available at the site of action.

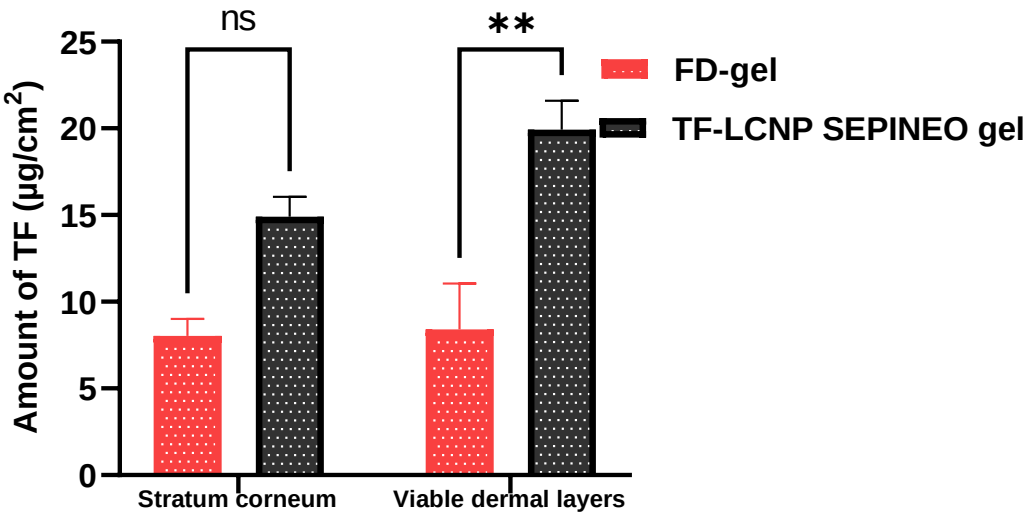

Figure 4.14. The amount of TF in stratum corneum and viable parts of skin (Data represented as mean ± SD, n = 3) (****P<0.0001)

4.3.7 Mechanistic understanding of skin distribution

To determine the drug distribution in different layers of the skin coumarin-6 was loaded into the optimized LCNP formulation. The reason for selecting coumarin 6 is it is poorly permeable compound into the skin and also has the nearby log P to TF. The results presented that coumarin 6 as aqueous dispersion exhibits low permeation into the skin layers and less green fluorescence (superficial layers of skin). The coumarin 6-loaded LCNP show high intensity on the dermis layers at 12 h study (Figure 4.15). The high intensity of dye at 12 h confirmed that the optimized LCNP composition could cross the stratum corneum and epidermis region.

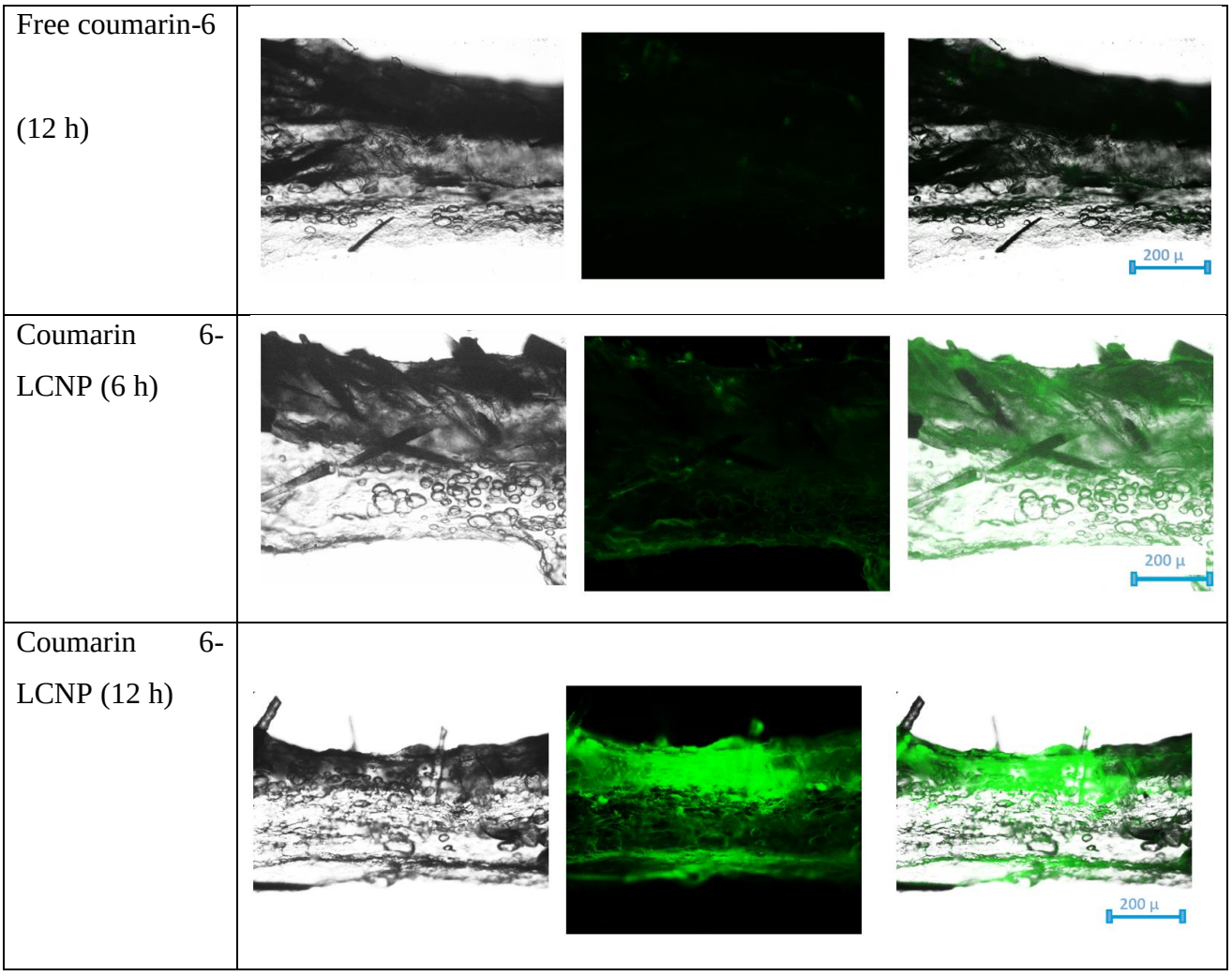

Figure 4.15. Mechanistic understanding of the TF distribution in different layers of the skin at 6 h and 12 h (A) free coumarin and (B) coumarin-6 loaded optimized LCNPs formulation

4.3.8 Dermal pharmacokinetics of TF-LCNP on Topical application

Figure 4.16 represents the variation of TF distribution in epidermis and dermis of the goat ear skin after single application of FD gel and TF-LCNP SEPINEO gel. Thus, the data were additionally processed using dermal pharmacokinetics modeling to get the maximum insight. The amount of TF in the skin layers from TF-LCNP SEPINEO gel was found to be significantly higher than TF from the FD gel. The numeric values of various dermal pharmacokinetic parameters (AUC total $_{(0\text{-}24h)}$, AUC $_{0\text{-}\infty}$, Cmax Skin, Tmax Skin, and Cl) are presented in Table 4.13. The Cmax value was significantly higher in epidermis and dermis in case of TF-LCNP SEPINEO gel, i.e., 39.38 ± 4.63 μg/cm^2 (nearly 4 times), 31.23 ± 3.42 μg/cm^2 (more than 3 times) compared with the FD gel 10.08 ± 2.81 μg/cm^2 and 10.11 ± 1.81 μg/cm^{2,} respectively. The Cmax for TF-LCNP is found to be nearly 4 times for epidermis and little more than 3 times in dermis compared to data for FD gel The LCNP showed equilibrium steady state in epidermis and dermis from 5-8 h and after then it was decreased, as maximum TF was permeated across the skin. This might be due to the unremitting transport of TF from LCNP all the way through skin layers. It was significant that TF's permeation and elimination rates via developed lipidic system with GMO and myristol were nearly equal like LCNP. The obtained data interpret that the developed LCNP has improved the TF permeation through the skin compared to gel. Possible permeation of TF was observed to some extent in case of FD gel as the gel is 3-in-1 polymer which is an Acrylamide/Sodium Acryloyl di methyl Taurate Copolymer/Isohexadecane and Polysorbate 80. The extended permeation, equilibration of TF through skin layers via LCNP formulation might be due to the interaction of GMO and myristol with the skin lipids. This promotes synergism, and facilitation and interaction of TF. So, it was validated that TF transport to the skin layers via lipidic system was efficiently ascertaining adequate TF supply to arthritis site. Similarly, $AUC_{\mathbf{(0\text{-}24h),\ 0\text{-}\ inf}}$ values for both epidermis and dermis were also found to be higher for FD-LCNP compared to FD gel.

A

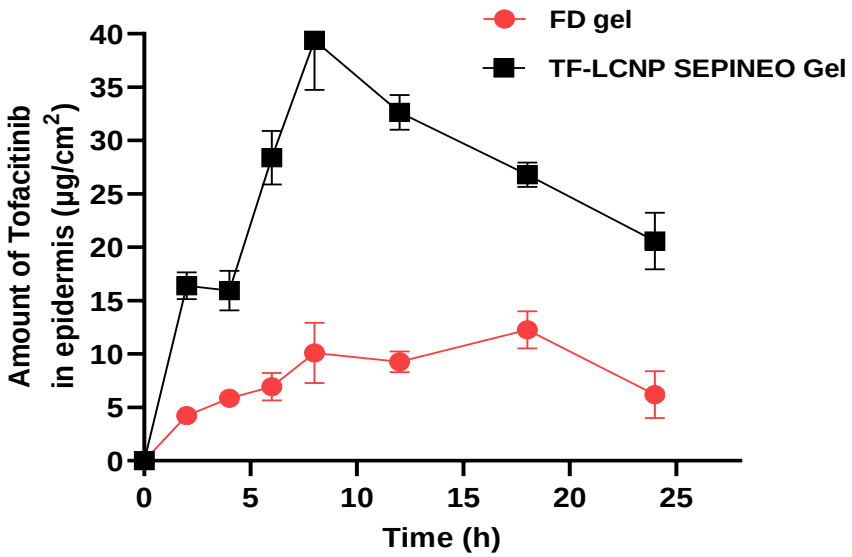

B

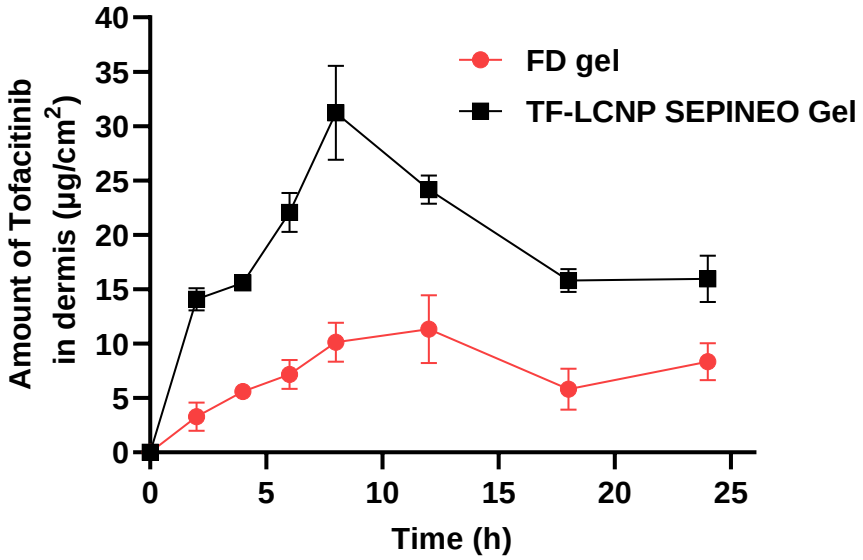

Figure 4.16. Dermal pharmacokinetics of TF-LCNP for topical application i.e., amount of TF in epidermis and dermis at various time points (Data represented as mean ± SD, n = 3).

Table 4.13. Various dermatokinetics parameters (mean ± SD) of topical application of TF formulations (FD gel and TF-LCNP SEPINEO gel and) in epidermis and dermis (n = 5)

Parameters	**Units**	**FD gel**		**TF-LCNP SEPINEO Gel**	
		Epidermis	**Dermis**	**Epidermis**	**Dermis**
AUC total (0-24h)	**µg/cm²*h**	246.79 ± 9.33	224.73 ± 56.39	637.313 ± 45.22	460.594 ± 34.55
AUC 0- inf	**µg/cm²*h**	320.10 ± 10.96	588.43 ± 88.03	1174.468 ±12.96	821.578 ±13.76
C_{max} Skin	**µg/cm²**	13.68 ± 0.54	11.34± 3.01	43.388 ±1.22	31.232 ± 2.4
T_{max} Skin	**h**	12	12	8	8
Cl	**µg/h**	0.46 ± 0.016	0.26 ±0.166	0.1277 ± 0.012	0.1825 ± 0.017

4.3.9 Stability Studies

The developed TF- LCNP was evaluated for storage stability up to 45 days at 4^0C and 25^0C. The stability data of TF- LCNP is represented in Table 4.14. The % deviation data of particle size and PDI (Table 4.14) demonstrated the stability of TF-LCNP without aggregation. Similarly, the assay and viscosity data of TF-LCNP gel has not showed any significant changes compared to the initial data. This confirmed the stability of TF-LCNP in the finished dosage form as a gel. The stability of the TF-LCNP may be due to the presence of the tri-block copolymer in Lutrol® F 127 which can contribute the stearic stabilization of developed TF-LCNP system.

Table 4.14. Stability data of TF-LCNP after 45 days at different storage conditions

Formulation	**TF-LCNP**			**TF-LCNP Gel**
Storage conditions	**2-8^{0}C**			
	Particle size	**PDI**	**EE**	**Assay**
1st day				
20 days	79.18 ± 0.593	0.165 ± 0.024	64.714± 5.027	101.45 ± 2.85
45 days	83.29 ± 1.46	0.180 ± 0.009	62.846± 1.7139	99.85 ± 1.67
	25 ± 2^{0}C			
20 days	80.02 ± 2.45	0.204 ± 0.054	64.532 ± 5.1022	98.98 ± 1.44
45 days	90.36 ± 1.87	0.290 ± 0.120	62.622 ± 2.4652	99.60 ± 1.67

4.3.10 Scale up studies

The particle size, PDI and entrapment efficiency of 25 g batch of TF-LCNP was presented in Table 15. In comparison with the initial 10 g data of TF-LCNP formulation (Table 11), the scale up batch showed equivalent result with respect to particle size and PDI and entrapment efficiency. During nanoparticles scale up, mass transfer and momentum changes occurs drastically. However, in our study during the formulation development, the processing steps were less and use of organic solvent was avoided. Thus, the formulation characteristics were not altered even after scaled up to 2.5-fold.

4.4 Conclusion

The selection of CMAs plays a crucial role in development of the drug carrier system for topical drug delivery. Thorough literature study revealed that the liquid crystalline nanoparticles prepared using GMO have proven their potential in delivering the drugs to the skin layers. In the present study, we made an attempt to design liquid crystalline nanoparticles using liquid oil along with GMO. To achieve the proposed objective, systematic QbD principles were implemented. The initial screening using the Taguchi L8 OA determined the impact of different liquid oils on the particle size, PDI, entrapment efficiency and in vitro drug release. The in vitro release study has not showed any significant difference on using the different concentrations of oleic acid along with the GMO; whereas myristol exhibited a significant difference on particle size on changing the concentration. Thus, myristol was chosen along with the GMO, and for the further optimization BBD was implemented. The BBD implemented the effect of chosen independent variables including amount of lipid mix (GMO: myristol), amount of surfactant and probe sonication time on the chosen dependent variables such as particle size, PDI and entrapment efficiency. The systematically designed TF-LCNP depicted all the desired physicochemical attributes for topical delivery. The optimized TF-LCNP formulation was further incorporated into SEPINEO™ P 600 gel, evaluated and compared with FD gel for in vitro skin studies. Overall, the developed LCNP demonstrated uniform nano-size range with good entrapment efficiency and stability. In the ex vivo studies, Cmax found to be increased for both epidermis (nearly 4 times) and dermis (more than 3 times) and the $AUC_{total\ (0\text{-}24h)}$ of TF-LCNP were found to be increased, 2.5 times in epidermal and doubled in dermal layers compared to FD gel. The obtained findings suggest that the designed TF- LCNP are efficient

in carrying the drug to the inflamed dermis layers which is indicative of the increased efficacy of TF.

References

1. CHMP. Committee for Medicinal Products for Human Use (CHMP) Assessment report [Internet]. Available from: www.ema.europa.eu/contact.

2. Hagen M, Baker M. Skin penetration and tissue permeation after topical administration of diclofenac. *Curr Med Res Opin.* 33(9), 1623-1634 (2017).

3. Schwartz DM, Kanno Y, Villarino A, Ward M, Gadina M, O'Shea JJ. JAK inhibition as a therapeutic strategy for immune and inflammatory diseases. *Nat. Rev. Drug Discov.*16(12), 843–862 (2017).

4. Barbosa AI, Torres T, Lima SAC, Reis S. Hydrogels: A Promising Vehicle for the Topical Management of Atopic Dermatitis. *Adv. Ther.* 4(7), 2100028 (2021).

5. Waghule T, Gorantla S, Rapalli VK, *et al.* Emerging Trends in Topical Delivery of Curcumin Through Lipid Nanocarriers: Effectiveness in Skin Disorders. *AAPS PharmSciTech.* 21(7), 1-12 (2020).

6. Rapalli VK, Waghule T, Hans N, *et al.* Insights of lyotropic liquid crystals in topical drug delivery for targeting various skin disorders. *J. Mol. Liq.* 315, 113771 (2020).

7. Shoaib A, Mangla B, Javed S, Sultan MH, Alqahtani SS, Shakeel F. Vicissitudes of liquid crystals for solubility enhancement of poorly soluble drugs. *J. Mol. Liq.* 321, 114924 (2021).

8. Lim DG, Jeong WW, Kim NA, *et al.* Effect of the glyceryl monooleate-based lyotropic phases on skin permeation using invitro diffusion and skin imaging. *Asian J. Pharm. Sci.* 9(6), 324–329 (2014).

9. Milak S, Zimmer A. Glycerol monooleate liquid crystalline phases used in drug delivery systems. *Int. J. Pharm.*478(2), 569–587 (2015).

10. Guo C, Wang J, Cao F, Lee RJ, Zhai G. Lyotropic liquid crystal systems in drug delivery. *Drug Discov. Today.* 15(23–24), 1032–1040 (2010).

11. Gupta R, Dwadasi BS, Rai B, Mitragotri S. Effect of Chemical Permeation Enhancers

on Skin Permeability: In silico screening using Molecular Dynamics simulations. *Sci. Rep*. 9(1), 1–11 (2019).

12. Rapalli VK, Banerjee S, Khan S, *et al.* QbD-driven formulation development and evaluation of topical hydrogel containing ketoconazole loaded cubosomes. *Mater. Sci. Eng. C.* 119, 111548 (2020).

13. Rapalli VK, Banerjee S, Khan S, *et al.* QbD-driven formulation development and evaluation of topical hydrogel containing ketoconazole loaded cubosomes. *Mater. Sci. Eng. C.* 119,11548 (2021).

14. Rapalli VK, Khosa A, Singhvi G, Girdhar V, Jain R, Dubey SK. Application of QbD Principles in Nanocarrier-Based Drug Delivery Systems. In: *Pharmaceutical Quality by Design*, Elsevier, 255–296 (2019).

15. Bao W, Tian F, Lyu C, *et al.* Experimental and theoretical explorations of nanocarriers' multistep delivery performance for rational design and anticancer prediction. *Sci. Adv*. 7(6), 2458 (2021).

16. Mahmood A, Rapalli VK, Gorantla S, Waghule T, Singhvi G. Dermatokinetic assessment of luliconazole-loaded nanostructured lipid carriers (NLCs) for topical delivery: QbD-driven design, optimization, and in vitro and ex vivo evaluations. *Drug Deliv. Transl. Res.* 12(5), 1118-1135 (2021).

17. Rapalli VK, Kaul V, Waghule T, *et al.* Curcumin loaded nanostructured lipid carriers for enhanced skin retained topical delivery: optimization, scale-up, in-vitro characterization and assessment of ex-vivo skin deposition. *Eur. J. Pharm. Sci.* 152,105438 (2020).

18. Waghule T, Patil S, Rapalli VK, *et al.* Improved skin-permeated diclofenac-loaded lyotropic liquid crystal nanoparticles: QbD-driven industrial feasible process and assessment of skin deposition. *Liq. Cryst.*48(7), 991-1009 (2020).

19. Garg NK, Tyagi RK, Singh B, *et al.* Nanostructured lipid carrier mediates effective delivery of methotrexate to induce apoptosis of rheumatoid arthritis via NF-κB and FOXO1. *Int. J. Pharm.* 499(1–2), 301–320 (2016).

20. Rapalli VK, Sharma S, Roy A, Alexander A, Singhvi G. Solid lipid nanocarriers

embedded hydrogel for topical delivery of apremilast: In-vitro, ex-vivo, dermatopharmacokinetic and anti-psoriatic evaluation. *J. Drug Deliv. Sci. Technol.* 63, 102442 (2021).

21. Rapalli VK, Singhvi G. Dermato-pharmacokinetic: assessment tools for topically applied dosage forms. *Expert Opin. Drug Deliv.* 18(4), 423-426 (2020).

22. Sharma G, Saini MK, Thakur K, *et al.* Aceclofenac cocrystal nanoliposomes for rheumatoid arthritis with better dermatokinetic attributes: A preclinical study. *Nanomedicine*. 12(6), 615–638 (2017).

23. Chang JS, Huang Y Bin, Hou S Sen, Wang RJ, Wu PC, Tsai YH. Formulation optimization of meloxicam sodium gel using response surface methodology. *Int. J. Pharm.* 338(1–2), 48–54 (2007).

24. Singh B, Dahiya M, Saharan V, Ahuja N. Optimizing drug delivery systems using systematic "design of experiments." Part II: Retrospect and prospects. *Crit. Rev. Ther. Drug Carrier Syst.* 22(3), 215–293 (2005).

25. Negi P, Singh B, Sharma G, Beg S, Raza K, Katare OP. Phospholipid microemulsion-based hydrogel for enhanced topical delivery of lidocaine and prilocaine: QbD-based development and evaluation. *Drug Deliv.* 23(3), 951–967 (2016).

26. Achouri D, Hornebecq V, Piccerelle P, Andrieu V, Sergent M. Self-assembled liquid crystalline nanoparticles as an ophthalmic drug delivery system. Part I: Influence of process parameters on their preparation studied by experimental design. *Drug Dev. Ind. Pharm.* 41(1), 109–115 (2015).

27. Karaman S, Yilmaz MT, Ertugay MF, Baslar M, Kayacier A. Effect of ultrasound treatment on steady and dynamic shear properties of glucomannan based salep dispersions: Optimization of amplitude level, sonication time and temperature using response surface methodology. *Ultrason. Sonochem.* 19(4), 928–938 (2012).

28. Verma P, Ahuja M. Cubic liquid crystalline nanoparticles: optimization and evaluation for ocular delivery of tropicamide. *Drug Deliv.* 23(8), 3043–3054 (2016).

29. Mitri K, Shegokar R, Gohla S, Anselmi C, Müller RH. Lipid nanocarriers for dermal delivery of lutein: Preparation, characterization, stability and performance. *Int. J.*

Pharm. 414(2), 267–275 (2011).

30. Kohli AK, Alpar HO. Potential use of nanoparticles for transcutaneous vaccine delivery: Effect of particle size and charge. *Int. J. Pharm.* 275(1–2), 13–17 (2004).

31. Lancelot A, Sierra T, Serrano JL. Nanostructured liquid-crystalline particles for drug delivery. *Expert Opin. Drug Deliv.*11(4), 547–564 (2014).

32. Elnaggar YSR, Etman SM, Abdelmonsif DA, Abdallah OY. Novel piperine-loaded Tween-integrated monoolein cubosomes as brain-targeted oral nanomedicine in Alzheimer's disease: Pharmaceutical, biological, and toxicological studies. *Int. J. Nanomedicine.* 10, 5459–5473 (2015).

33. Barauskas J, Johnsson M, Joabsson F, Tiberg F. Cubic phase nanoparticles (cubosome): Principles for controlling size, structure, and stability. *Langmuir*. 21(6), 2569–2577 (2005).

34. Zeng N, Gao X, Hu Q, *et al.* Lipid-based liquid crystalline nanoparticles as oral drug delivery vehicles for poorly water-soluble drugs: Cellular interaction and in vivo absorption. *Int. J. Nanomedicine*. 7, 3703–3718 (2012).

35. Chiu M, Prenner E. Differential scanning calorimetry: An invaluable tool for a detailed thermodynamic characterization of macromolecules and their interactions In: *Journal of Pharmacy and Bioallied Sciences*, Wolters Kluwer - Medknow Publications, 39–59 (2011).

36. Danaei M, Dehghankhold M, Ataei S, *et al.* Impact of Particle Size and Polydispersity Index on the Clinical Applications of Lipidic Nanocarrier Systems. *Pharmaceutics*. 10(2), 57 (2018).

5 Introduction

The topical treatment of pain needs an improved concentration of TF in the synovial region and skin layers instead in the plasma. Topically applied drugs may have a depot effect in skin layers and exhibit sustained release of the drug into the surrounding tissues [1,2]. But the major challenge in the topical application of any drug, including TF, is penetration through the stratum corneum and permeation into the deeper layers of the inflamed joint [2,3].

To overcome these issues in recent days, few attempts have been made for the topical administration of TF and other drugs, including liquid crystal nanoparticles, proposomes, and microneedles to treat various skin disorders [4–6]. Lipid-based topical vesicular drug delivery gained importance because of rapid penetration through the epidermis of the skin with low toxicity [7]. Vesicular drug delivery systems can easily permeate through the skin, but the percutaneous permeability depends on the elasticity of vesicles [8]. The modified liposomes with ethanol and propylene glycol have shown more skin permeability compared to the conventional liposomal formulations. The use of propylene glycol in place of ethanol acts as an edge activator on liposomes, and these are named 'proglycosomes'. These proglycosomes have shown excellent encapsulation efficiency [5,9]. However, the proglycosomes have shown excellent permeation properties through the skin but lack the ability to target the inflammatory site i.e., site-specific drug delivery.

In RA disease conditions, the inflamed skin layers and synovial fluid shows the presence of CD44 (cluster of differentiation) on the surface of activated macrophages [10]. The CD44 is a glycoprotein involved in cell division, migration, adhesion, and signaling. CD44 consists of binding sites for hyaluronic acid (HA) and chondroitin sulphate (CS) where HA binds to the N-terminal of the CD44 and CS binds to the variant stem fibrin region. The HA and CS act as the natural ligand for the CD44 [11]. So, CD44 can serve as a novel active targeting site for RA treatment through topical administration. In addition, HA helps in cartilage and bone growth by promoting the growth of new cells and tissues and also known to reduce the inflammation at the joint site [12]. Similarly, CS is distributed in cartilage around the joint and ligament. The available literature suggests that, the HA and CS coated tofacitinib loaded proglycosomes could be a one of the potential approaches to achieve active and site-specific targeting.

Thus, the current research work aimed on the development of HA coated and CS coated TF-loaded proglycosomes as a novel nano-topical drug delivery systems for targeting CD44 in the inflamed skin layers as a vehicle for TF.

5.1 Materials and methods

Soya phosphatidyl choline with 70 % phosphatidyl choline (LIPOID S 75) was received as a generous gift from Lipoid GmbH, Germany. Cholesterol was procured from Hi media. Stearyl amine was procured from Sigma Aldrich. Propylene glycol USP grade was procured from JT bakers. HA was obtained from Tokyo Chemical Industry Co. Ltd. All the organic solvents used during this work were of analytical grade.

5.2 Method of preparation of Proglycosomes

Two preparation techniques were studied and utilized to achieve positively charged nano-size proglycosomes with good entrapment efficiency. The techniques are the direct mixing method and the Thin film hydration (TFH) method [5,13].

Initially, proglycosomes were prepared by direct mixing method followed by probe sonication. In brief, the batch quantity of propylene glycol (25%) containing tofacitinib (5 mg), soy phosphatidylcholine, and cholesterol (1:1 ratio) were melted at 55 ± 2°C. Batch quantity of aqueous phase i.e., Milli Q water was added into the melted mixture and stirring was continued for 15 min. Then the dispersion was subjected to probe sonication for size reduction. Further, stearyl amine was added to the drug-loaded Proglycosomes in different amounts to obtain positively charged Proglycosomes. The effect of pre-added and/or post-added stearyl amine on mean vesicle size, polydispersity index, and zeta potential was studied.

In the second method, proglycosomes were prepared by the TFH method. In Brief, the batch quantity of soy phosphatidylcholine, cholesterol, stearyl amine were dissolved in a 15.0 ml mixture of chloroform and methanol (4:1 v/v) in a round-bottomed flask. The formulation variable phospholipid to cholesterol ratio was optimized to achieve desired proglycosomes. Then, the solvent was evaporated using buchi® Rotavapor® R-210 jacketed evaporator (29/32 joint, 240V) to remove the traces of organic solvent and to form a thin lipid film. The obtained thin lipid film was hydrated using respective propylene glycol solution at 40^0C for 30 min at 90 rpm. The resultant dispersion was probe sonicated at 20 % amplitude for 2 min 30 sec for size reduction (Figure 5.1a) [13].

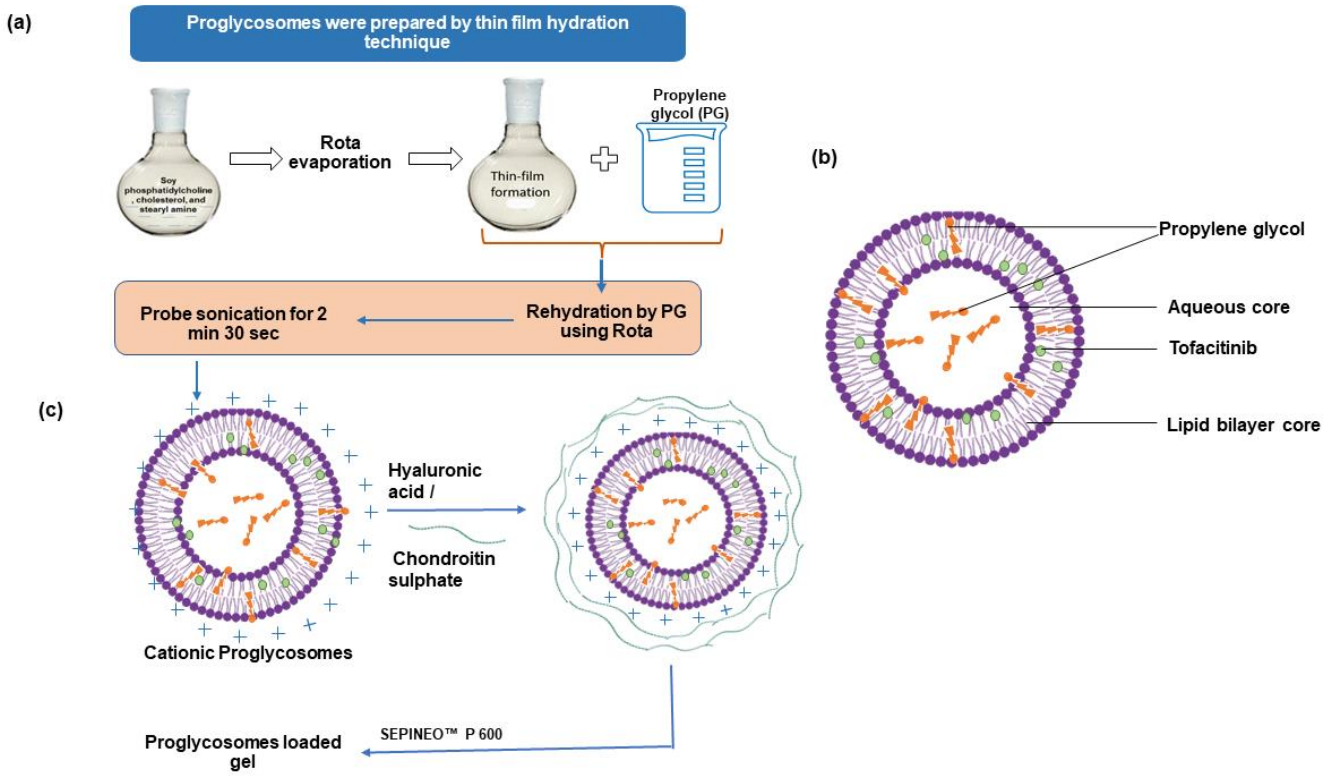

Figure 5.1. Schematic representation of (A) Tofacitinib loading into the proglycosomes prepared by thin film hydration method, (B) Structure of proglycosomes, (C) self-assembly by electrostatic interaction of chondroitin sulphate onto cationic proglycosomes

5.2.1 Optimization of formulation variables of proglycosomes

The formulation variables such as soy phosphatidylcholine to cholesterol ratio and percentage of propylene glycol (25% and 35%) were optimized to obtain the proglycosomes of required quality attributes. Table 1 presents the formulation variables compositions. The quality attribute parameters included vesicle size, PDI, zeta potential, and entrapment efficiency.

5.2.2 Deposition of hyaluronic acid onto the surface of proglycosomes

The cationic proglycosomes were coated by anionic polysaccharide i.e., HA with medium molecular weight. The concentration of HA was optimized for achieving the best possible physicochemical parameters. Varied concentrations of HA (0.02 % to 0.2 % w/v) were prepared in water. Then, 1 mL of optimized proglycosomes dispersion was added drop by drop to 1 mL of varied concentrations of HA solution under constant stirring at 800 rpm for 15 min using a magnetic stirrer (Tarson) (Figure 5.1b).

5.2.3 Deposition of chondroitin sulphate onto the surface of proglycosomes

The obtained proglycosomes were coated by CS mediated by ionic interactions. The optimization studies were carried out to acquire desired particle size and PDI. Initially, the different volumes and concentrations of CS solutions (0.01 to 0.05%) were prepared and into this, the proglycosomes formulation was added under constant stirring at 800 rpm for 15 min. Then the cs coated proglycosomes dispersion was centrifuged at 3000 rpm for 30 min to separate the uncoated CS (Figure 5.1b).

5.3 Characterization of Tofacitinib loaded proglycosomes, hyaluronic acid and chondroitin sulphate coated tofacitinib loaded Proglycosomes

5.3.1 Size, Poly dispersibility index, and Zeta potential

The prepared Normal proglycosomes (N-TF-PG), hyaluronic acid coated proglycosomes (HA-TF-PG) and chondroitin sulphate coated proglycosomes (CS-TF-PG) were characterized for Size, Polydispersity index, and Zeta potential using dynamic light scattering i.e., Zetasizer Nano ZS (Malvern Instruments, Malvern, UK). Prior to analysis, all the samples were diluted 15-fold with Milli Q water. For particle size measurement, 1 mL of diluted sample was taken into Zetasizer nano ZS 90. Whereas for Zeta potential measurement, the diluted sample was taken to DTS1060 capillary cell. All the measurements were conducted at 25°C in triplicate.

5.3.2 Entrapment efficiency

The total amount of TF in N-TF-PG, HA-TF-PG and CS-TF-PG was determined individually.

The prepared N-TF-PG, HA-TF-PG and CS-TF-PG were centrifuged at 4 °C at 3000 rpm for 30 min to separate free drug on surface and uncoated hyaluronic acid. The lysis of prepared N-TF-PG, HA-TF-PG and CS-TF-PG were performed by adding methanol and centrifuged at 15000 rpm for 20 min.

The supernatant containing N-TF-PG, HA-TF-PG and CS-TF-PG were collected. The obtained samples were filtered using a 0.22 μm nylon syringe filter and analyzed for the amount of entrapped TF using HPLC at 285 nm [14,15]. The entrapment efficiency was calculated using the below mentioned formula:

$$\% \text{ Entrapment efficiency} = \frac{\textbf{Amount of drug entrapped}}{\textbf{Total amount of drug present}} \boldsymbol{x\ 100}$$

5.3.3 Nuclear Magnetic Resonance spectroscopy

^{1}HNMR (500 H2, Bruker, Germany) spectroscopy analysis was performed to confirm the electrostatic binding of HA and CS molecules to the Proglycosomes. The procedure in briefly, HA (Approximately 5 mg), and optimized HA-TF-PG were dissolved in D_2O and d-DMSO, respectively. Similarly, CS (Approximately 5 mg), and optimized CS-TF-PG were dissolved in D_2O and d-DMSO, respectively. The obtained samples were analyzed by a ^{1}HNMR spectrometer.

5.3.4 Attenuated total reflection-Fourier transform infrared spectroscopy

Attenuated total reflection-Fourier transform infrared spectroscopy (ATR-FTIR) analysis was performed to confirm the formation of electrostatic interaction of HA molecules and CS onto the surface of proglycosomes. ATR - FTIR (BRUKER, USA) was used for recording the FTIR spectra of Pure drug, Physical mixture, HA, CS, HA-TF-PG and CS-TF-PG. The samples were obtained at 25 scans/min at a resolution of 1 cm^{-1} in between 4000 and 200 cm^{-1}.

5.3.5 Surface morphology analysis

The surface morphology of prepared N-TF-PG, HA-TF-PG and CS-TF-PG were assessed by performing a Field emission scanning electron microscope (FESEM; apreo switch XT micro-scope, USA) and TEM (FEI Tecnai – Netherlands; Model: G2 F30 S-Twin). The N-TF-PG, HA-TF-PG and CS-TF-PG formulations were spread on the coverslip and subjected to drying under vacuum. The dried coverslips were sputter-coated with gold for 60 sec using a gold sputter module (Quorum, UK). The prepared samples were examined under FESEM at a magnification range of 10000x – 100,000 xs using T1 and T2 detectors [16].

The sample preparation of N-TF-PG and HA-TF-PG for TEM analysis involved initial staining with the uranium acetate and then placing them on copper grid. Further, the dried sample were analysed using TEM at 100 kV [17].

5.3.6 In vitro release of TF from drug solution, N-TF-PG, HA-TF-PG and CS-TF-PG

In vitro release studies from drug solution, N-TF-PG, HA-TF-PG and CS-TF-PG were determined by dialysis bag method (Hi media) with molecular weight cut-off 12000 to 14000 Da. The release

media consisted of phosphate buffer saline pH 7.4 and 0.15% w/v sodium lauryl sulphate [18]. Then 1 mL of N-TF-PG, HA-TF-PG and CS-TF-PG formulations equivalent to 5 mg of TF were taken into the dialysis bag and placed into the above-mentioned release media. The whole assembly was kept on a magnetic stirrer maintained at 32 ± 0.5°C and operated at 100 rpm. At predetermined time intervals i.e., 30 min, 1, 2, 3, 4, 6, and 7 h an aliquot of 0.5 mL of sample was withdrawn and replaced with an equal volume of fresh release media maintained at 32 ± 0.5°C. The collected samples were then filtered through a 0.45 µ filter and the amount of drug release at respective time points was analyzed by validated HPLC method at 285 nm [15]. The obtained in vitro release data were fitted into the DD solver excel add-in to obtain the kinetic model's information (zero-order, first-order, Higuchi, Hixon−Crowell, and Korsmeyer−Peppas). The correlation coefficient values, AIC, and MSC values were obtained for various dissolution models of TF-loaded nanoformulations. The best fit model was selected based on the obtained values.

5.3.7 Preparation of N-TF-PG, HA-TF-PG and CS-TF-PG gel

The gelling agent was added into the optimized N-TF-PG, HA-TF-PG and CS-TF-PG to enhance the topical applicability and stability of the system. The gelling system of optimized N-TF-PG HA-TF-PG and CS-TF-PG were prepared using different concentrations of SEPINEO™ P 600 ranging from 0.5 and 1.5 % w/w. SEPINEO™ P 600 is a 3-in-1 polymer which is an Acrylamide/Sodium Acryloyl di methyl Taurate Copolymer/Isohexadecane and Polysorbate 80 [19]. It is used as a thickening agent polymer for topical application without any neutralization step and shows good compatibility with propylene glycol [19]. Thus, this helps to protect the surface coated HA and CS from degradation.

5.4 Evaluation of N-TF-PG, HA-TF-PG and CS-TF-PG gel

5.4.1 Physical examination and pH

The prepared N-TF-PG, HA-TF-PG and CS-TF-PG gels were characterized for smoothness, homogeneity, and lucidity on visual examination. The pH of gels was determined using a digital pH meter (Model MK–VI, Kolkata, India) [2].

5.4.2 Drug content

N-TF-PG, HA-TF-PG and CS-TF-PG gels (500 mg) were dissolved in 5 mL of methanol and placed it on a bath sonicator for 15 min to completely solubilize the drug. Then the obtained sample

was filtered through a 0.45 µ membrane filter and analyzed by the validated HPLC method. The experiment was performed in triplicate [18,20].

5.4.3 Viscosity and Rheological measurement of N-TF-PG and HA-TF-PG gel

The viscosity of optimized N-TF-PG, HA-TF-PG and CS-TF-PG gels was evaluated using Modular Compact Rheometer (MCR 92, Anton Paar GmbH, Austria). The measurement was carried out by utilizing Peltier temperature device (P-PTD 200) and Parallel plate (PP25) at 25 ± 2°C.

Viscosity measurements were carried out as a function of increasing the concentration of SEPINEO™ P 600 for a range 0.5 – 3.5 % with increasing shear rate. After viscosity evaluation, among different concentrations one concentration was chosen for further characterization of flow behavior. The determination of flow behavior of gels under stress is extremely useful as a quality control tool, as it aids in the maintenance of product quality and the reduction of batch-to-batch inconsistency. The minimum stress that must be applied before the material truly begins to flow is known as yield stress. Amplitude test (mechanical stability) and frequency sweep test (time dependent visco elastic behavior) were carried out to determine the flow behavior of gels. The amplitude test of plain gel, optimized N-TF-PG, HA-TF-PG and CS-TF-gels gel preparations were evaluated at a shear strain ranging from 0.01 to 100% at constant frequency 10 rad/sec. The frequency sweep test of plain gel, optimized N-TF-PG, HA-TF-PG and CS-TF-PG gel preparations were evaluated at angular frequency range of 0.1 to 100 rad/s at 0.5% constant strain [21,22].

5.4.4 Spreadability

The developed N-TF-PG, HA-TF-PG, CS-TF-PG and plain gel's spreadability was determined by reported Parallel plate method [23,24]. A weighted amount of gel i.e., 50 mg was placed between two glass plates (10 X 10 cm). A weight of 50 g was placed on the upper glass slide for 2 min to spread uniformly. After that, the weight was removed and the increase in diameter of the placed gels was measured. The following equation was used to calculate the spreadability.

$$S = \frac{A}{W}$$

Here, S is spreadability factor, A is area covered by the placed gel (mm^2), W is weight of the sample (g).

5.5 *Ex vivo* studies

5.5.1 Skin permeation study

Permeation study of TF loaded sepineo gel (FD-gel), optimized N-TF-PG, HA-TF-PG and CS-TF-PG were carried out using goat ear skin obtained from slaughterhouse of Pilani, India. The subcutaneous tissue was separated from the collected skin and the hair on dorsal skin surface was removed using hair clipper. Further the skin was washed thrice with phosphate buffer saline. The processed skin was placed on the Franz diffusion cell (diameter of 1.33 cm^2) that is dorsal side facing the donor compartment and the ventral side facing the receptor compartment. A volume of 18 mL of phosphate buffer saline was placed on the receptor compartment and a weighed quantity of 300 mg each of FD-gel, N-TF-PG gel, HA-TF-PG gel and CS-TF-PG gel were applied on donor compartment. The Franz diffusion setups were placed on the magnetic stirrer at 80 rpm at 32 ± 0.5°C. Then, an aliquot of 1 mL of sample was withdrawn at predetermined time intervals i.e., 1, 2, 4, 6, 8, 12, 16, 24, 36 h and replaced with equal volume of fresh PBS maintained at 32 ± 0.5°C. The amount of drug present in the receptor compartment at time points was determined using validated HPLC method at 285 nm [15,25]. The acquired data was examined, and a graph was plotted between time (X-axis) and % cumulative TF permeated (Y-axis). The permeation flow (mg/cm/h; units 'J') is determined by the slope of the linear portion of the graph.

5.5.2 Skin deposition by tape stripping technique

The skin was taken out from the assembly after completing skin permeation study. A cotton swab was wiped across the skin's surface on the donor compartment side to remove the applied FD-gel, N-TF-PG gel, HA-TF-PG gel and CS-TF-PG gel. The cotton swab was dipped into methanol and the amount of unabsorbed drug was determined. The collected skin was dried for 2 h and then tape stripping technique was employed to separate the stratum corneum. A total of 13 strips and left-over skin i.e., viable skin was collected into the vial containing methanol to quantify the amount of TF in stratum corneum and viable skin layers. The tape strip samples, and skin samples were analyzed using the validated HPLC method [20,26].

5.5.3 Dermal distribution studies of dye loaded N-TF-PG, HA-TF-PG and CS-TF-PG

Coumarin -6 was selected as the fluorescent dye, as its log P (1.12) matches with that of TF. The dye loaded N-TF-PG, HA-TF-PG and CS-TF-PG were prepared as per ex vivo studies. The free

coumarin dispersion equivalent to formulation (0.05 %) was prepared. The skin was processed as discussed under section 3.1.5 and mounted onto the Franz diffusion cell. The prepared dye loaded formulations (0.5 mL) and free dispersion was mounted on the surface of the donor compartment. The whole assembly was kept on magnetic stirrer at 80 rpm at 32 ± 0.5°C. The skin was collected and washed with buffer to remove the absorbed coumarin at 1 h, 6 h, and 24 h. The skin was placed onto the freezing microtome and sectioned into a 10 µ size. Then the skin was examined under ZEISS fluorescent optical microscope for the distribution of coumarin-6 in skin layers [24,26].

5.5.4 Dermatokinetics of N-TF-PG, HA-TF-PG and CS-TF-PG

The excised goat ear skin was used for the dermatokinetics modeling studies. The skin tissue was processed as discussed in Section 2.9. A weighed amount of 300 mg of FD-gel, N-TF-PG and HA-TF-PG, and CS-TF-PG, gel was applied on the dorsal side of skin. At predetermined sample times (2, 4, 6, 8, 12, 16, 24, 32 h), whole skin was removed from the Franz cell. The collected skin samples were rinsed three times with phosphate buffer saline (PBS, pH 7.4) to remove adhering formulation and separated the epidermal and dermal layers. Both parts were cut into small pieces separately using a scalpel blade and macerated in 5 mL of methanol for complete tofacitinib extraction. The samples were filtered through 0.45 µ membrane filter and the obtained filtrates were analyzed using validated HPLC method. Then the dermal pharmacokinetics data C_{Skin} (TF concentration in the skin at time t,) C_{max} (Maximum concentration of TF achieved in the skin layer), AUC_{0-t} and $AUC_{0-\infty}$ were determined. The non-compartmental pharmacokinetic model was used to calculate T_{max} and C_{max} from the acquired values. The linear trapezoidal rule was used to determine AUC_{0-t} and $AUC_{0-\infty}$ [4,27].

5.6 Assessment of stability of N-TF-PG, HA-TF-PG and CS-TF-PG gel

The physicochemical stability of N-TF-PG, HA-TF-PG and CS-TF-PG gel was evaluated at 20 and 45 days of storage at 2–8 °C, and 25 °C at 60 % relative humidity. The changes in gel's viscosity, spreadability and assay were observed.

5.7 Statistical data analysis

All the experiments were performed in triplicate. The statistical analysis of in vitro, *ex vivo* and *in vivo* results was performed using GraphPad Prism 8.0 (Systat Software Inc.). Two-way ANOVA was used to compare the mean of the two groups, and a results Statistical significance was considered at $p < 0.05$.

5.8 Results and discussion

5.8.1 Preparation and optimization of proglycosomes and its characterization

Proglycosomes were prepared by two different techniques i.e., mixing method and TFH method. The N-TF-PG prepared by mixing method showed average particle size of 105.9 ± 4.45 nm (PDI: 0.276 ± 0.045) with nearly neutral charge -3.36 mV). Upon addition of TF to the proglycosomes there was a change in the zeta potential to -8.52 mV and the tofacitinib entrapment efficiency was found to be 68.4 ± 3.85 %.

Further, cationic Proglycosomes were prepared by direct mixing method with addition of stearyl amine either pre added and post added (0.05%, 0.1%, and 0.2%). Initially, different amounts of stearyl amine i.e., 1 mg, 2 mg, 3 mg, 4 mg, 6 mg, 8 mg, and 10 mg to 25 % propylene glycol (PG) solution in water. It was observed that addition of 1 mg and 2 mg the solution was clear whereas upon increasing the concentration turbid appearance was observed. Thus, formulation batches with pre added stearyl amine with 1 mg and 2 mg were prepared. It was observed that pre-added stearyl amine did not affect the zeta potential of developed N-TF-PG. However, the post added stearyl amine solution at concentration of 0.05 %, 0.1 % and 0.2 % showed increase in zeta potential (25.5, 29.4 and 33.4), vesicle size and PDI i.e., 294.5 ± 7.62 (PDI:0.593), 345 ± 18.24 (PDI:0.564) and 848.1 ± 12.54 (0.683) respectively.

The cationic N-TF-PG prepared by THF method showed significant effect upon varying the phospholipid to cholesterol ratio. Figure 5.2a and 5.2b represents the effect of soy phospholipid to cholesterol ratio on particle size, poly dispersity index, zeta potential and entrapment efficiency of tofacitinib loaded proglycosomes. It was observed that with the increase in cholesterol concentration, there was a significant increase in particle size and PDI, with concurrent decrease in the encapsulation efficiency. This could be due to filling of the spaces between the phospholipid molecules with the cholesterol, which resulted in rigid vesicular structures. Additionally, the decrease in entrapment efficiency could be due to an increase competence of cholesterol level with

tofacitinib. This contributed to leaching of tofacitinib due to the disruption of membrane vesicles. However, it was also noted that any increase in the concentration of phospholipid greater than cholesterol led to increased particle size, PDI, and zeta potential. Also, the change in the propylene glycol concentration also showed a significant increase in the particle size and slight decrease in entrapment efficiency. The added PG occupies the aqueous core and increases the vesicle size due to swelling of vesicles. The Table 5.1 presents the effect of propylene glycol concentration on particle size, PDI, zeta and entrapment efficiency. The optimized cationic proglycosomes were obtained with soy phosphatidyl choline (SPC) and cholesterol (1:1 ratio), 25 % PG and 1.2 mg stearyl amine. They showed lower particle size (100.17 ± 2.57 nm), PDI (0.286 ± 0.063), zeta potential (~ 38.5 ± 2.68 mV) and good entrapment efficiency (84.03 ± 1.60 %).

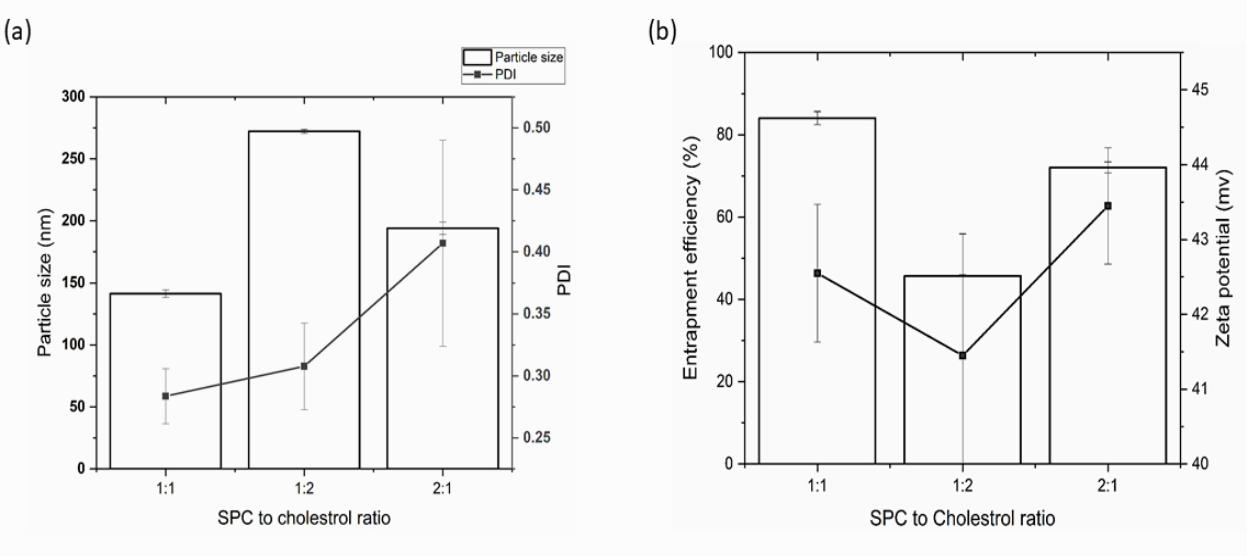

Figure 5.2. Effect of phospholipid to cholesterol ratio on (a) particle size and PDI, (b) entrapment efficiency and zeta potential of proglycosomes

Table 5.1. Effect of propylene glycol on particle size and PDI of N-TF-PG

Parameter	Size	PDI	Zeta potential	Entrapment efficiency
N-TF-PG (25 %)	100.17 ± 2.57	0.286 ± 0.063	38.5 ± 2.68	84.03 ± 1.60
N-TF-PG (35 %)	262.63 ± 11.36	0.319 ± 0.043	32.7 ± 1.22	77. 70 ± 2.36

5.8.2 Optimization of hyaluronic acid coated tofacitinib loaded proglycosomes and characterization

Non-covalent technique was used to deposit HA and CS onto prepared cationic nanocarrier systems. Non-covalent techniques was based on the direct deposition of HA and CS onto a surface through surface interactions such as electrostatics, hydrophobic interactions, and hydrogen bonds [28,29]. The uncoated proglycosomes were prepared by SPC (zwitterionic), stearyl amine (cationic) and cholesterol (neutral charge). The cationic charge was induced on the surface of the proglycosomes by stearyl amine. The cationic proglycosomes containing amine group interact with the negatively charged HA and CS with carboxyl group *via* ionic interactions [30].

Further, the concentration of HA used to coat the cationic proglycosomes (N-TF-PG) was optimized from the range of 0.025 to 0.2 % w/v to the total preparation. Figure 5.3a presents the effect of strength of HA solution on the particle size and zeta potential of the Tofacitinib loaded cationic proglycosomes. The charge reversal from positive to negative were used to determine the suitable strength of HA solution. Addition of lower concentration (0.25%) of HA solution to N-TF-PG showed less charge reversals (~ -13.3), high particle size, PDI and precipitation. This could be due to inadequate coating, which causes unwanted interactions between partially coated HA-TF-PG and aggregation. Upon increasing the concentration of HA solution at 0.1% showed increased strength of interaction with uniform particle size (249.5 ± 3.32), PDI (0.224 ± 0.035) with complete charge reversal to anionic (~ -25.5) (Figure. 5.3c and 5.3e). Further increasing the concentration of HA solution to 0.2% lead to the formation of precipitate with slight increase in particle size. Thus 0.1% HA solution was considered as optimal concentration. The % entrapment efficiency of HA-TF-PG was found to be 80.25 ± 4.22 %. The optimum critical quality attributes of HA-TF-PG are shown in Table 5.2.

Also, suitable amount of chondroitin sulphate needs to be added to obtain satisfactory CS coated proglycosomes. They showed lower Particle size (100.17 ± 2.57 nm), PDI (0.286 ± 0.063), zeta potential ~ 38. The concentration of chondroitin sulfate used to coat the cationic proglycosomes was optimized from the range of 0.01 % to 0.05 % w/v to the total preparation. The 0.01 %, and 0.05% concentration of CS solution showed precipitate this could be due to the charge imbalances. Figure 5.3b presents the effect of the strength of CS solution on the vesicle size and zeta potential of the TOF-loaded cationic PG. The 0.03 % CS-coated PG showed a uniform peak and good PDI with zeta potential of ~ −30.2 mV. The optimized CS-TOF-PG formulation resulted in a vesicle size of 181.13 ± 7.21 nm and a PDI of 0.188 ± 0.04 with a zeta potential of −30.2 ± 1.82 mV (Figure 5.3d&5.3f).

Table 5.2. Results of optimized parameters of HA and CS coated Proglycosomes

Parameter	Size	PDI	Zeta potential	Entrapment efficiency
HA-TF-PG	248.85 ± 3.32	0.279 ± 0.153	-25. 35 ± 2.89	83.88 ± 2.62
CS-TF-PG	181.13 ± 7.21	0.188 ± 0.04	−30.2 ± 1.82	78.85 ± 3.65 %

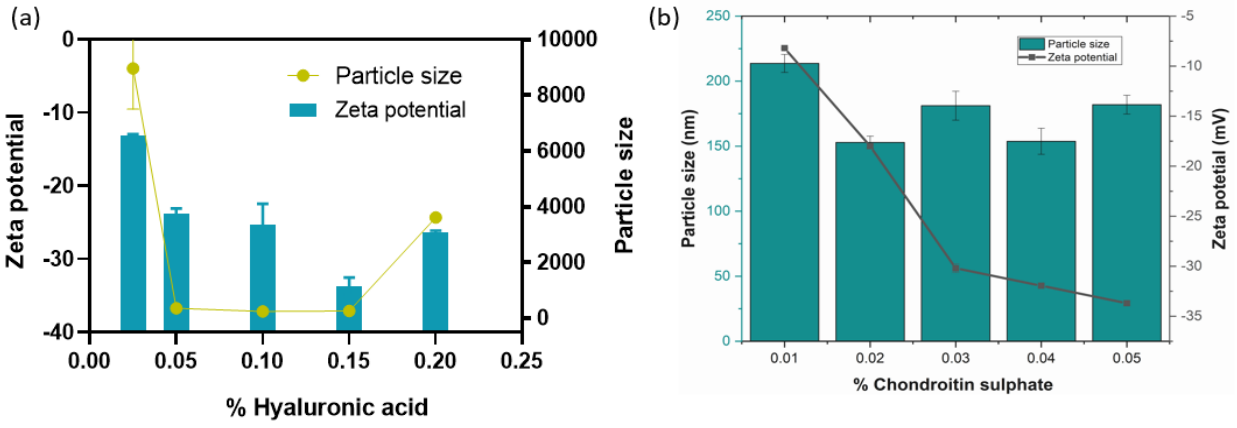

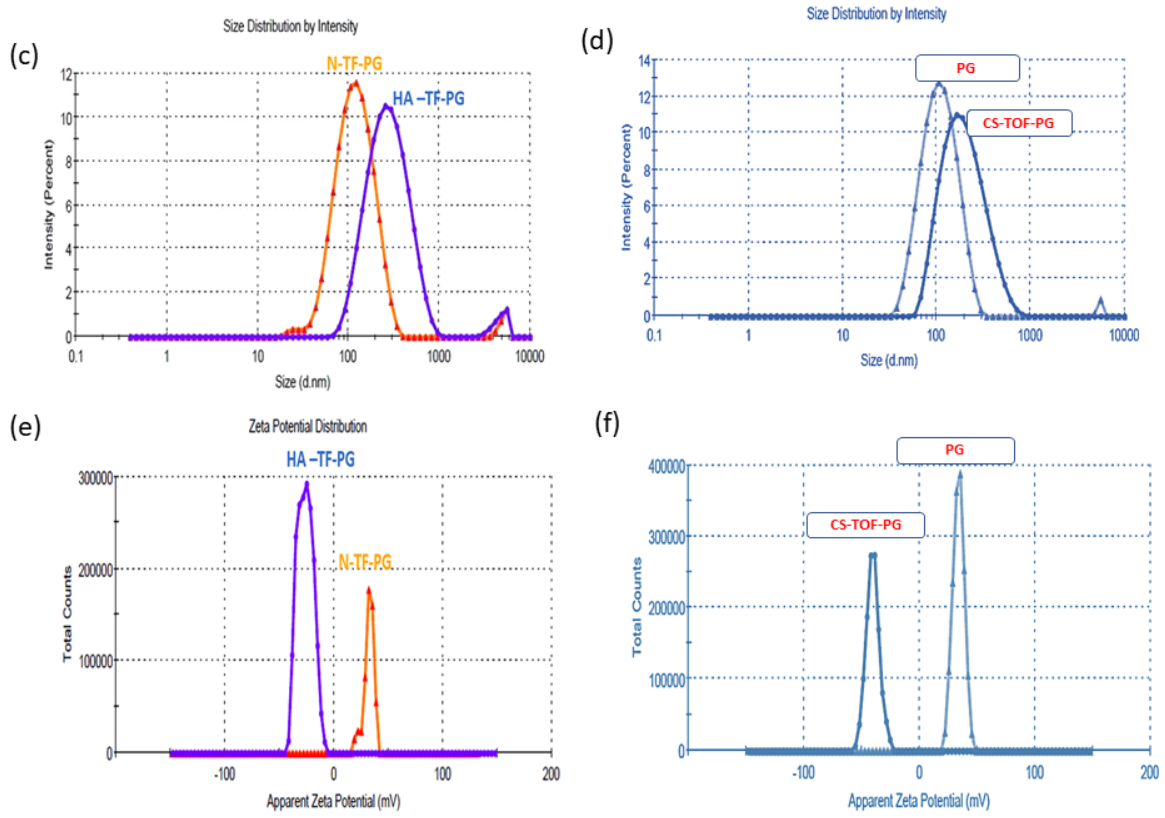

Figure 5.3. (a&b) The effect of hyaluronic acid and chondroitin sulphate on particle and zeta potential, (c&d) Particle size image of proglycosomes (N-TF-PG), HA-TF-PG and CS-TF-PG, (e&f) Zeta potential image of N-TF-PG, HA-TF-PG and CS-TOF-PG using Malvern zeta sizer.

5.8.3 Characterization of electrostatic interaction between cationic proglycosomes (N-TF-PG) and hyaluronic acid / chondroitin sulphate

5.8.3.1 Attenuated total reflection-Fourier transform infrared spectroscopy

The ATR-FTIR spectra for HA, CS, physical mixture, HA-TF-PG and CS-TF-PG are presented in Figure 5.4. The spectra were recorded to understand the formation of electro static interaction and to confirm deposition of HA on the surface of proglycosomes and CS on the surface of proglycosomes by amide bond.

The FTIR characteristic peaks of HA presents strong characteristic peak at 1731 cm^{-1} and its weak overtone band at 3320 cm^{-1} which corresponds to carbonyl group. The FTIR spectra of physical mixture shows 2800 cm^{-1} peak represents the amine group. Whereas in HA-TF-PG spectra the

amine peak disappears and the appearance of strong broad sharp peak at 3297 cm^{-1} corresponds to the formation of amide and also electro static interactions (Figure 5.4a).

FTIR spectra obtained from chondroitin sulphate and tofacitinib-loaded CS-coated proglycosomes are presented in Figure 5.4b. FT-IR spectra of CS showed absorption peaks at 1608.97 cm^{-1} for carbonyl carbon and 1219 cm^{-1} for the negatively charged OSO^{3-} group. The Physical mixture shows the amine group peak at 2916.15 cm-1. In the CS-TOF-PG formulation, the appearance of an amide bond can appear as a strong broad sharp peak at 3297.79 cm^{-1}.

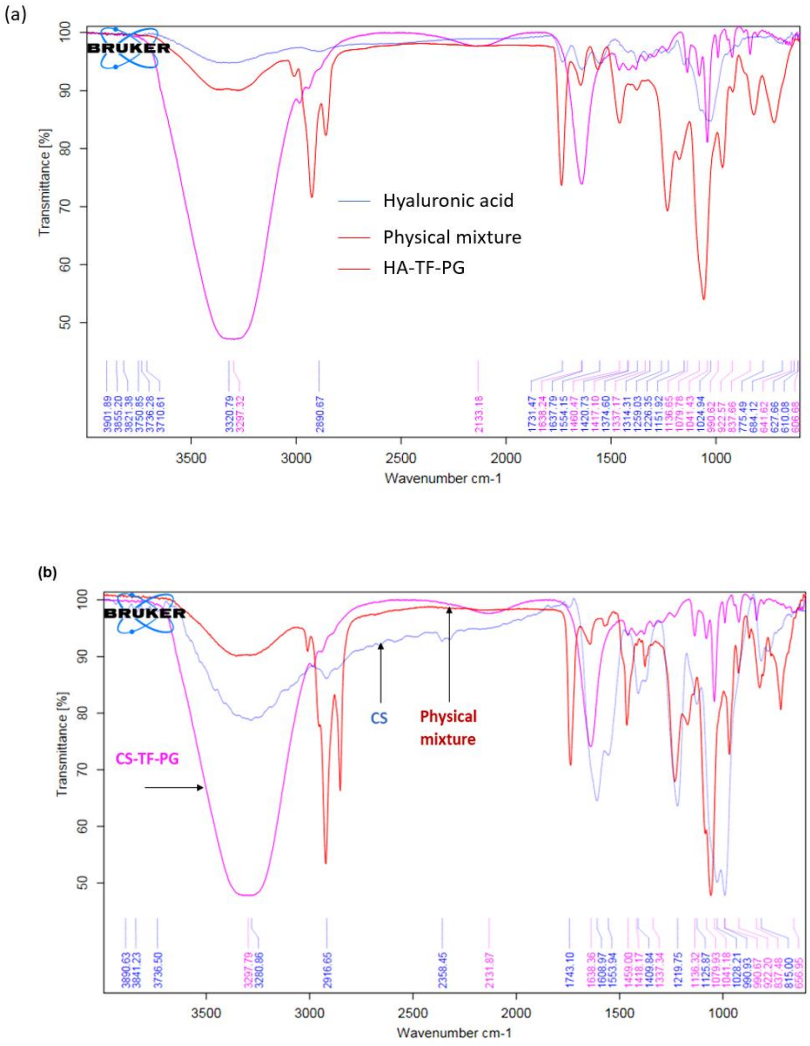

Figure 5.4. (a) FTIR spectrum of pure hyaluronic acid (blue color), Physical mixture along with drug (red color), optimized HA-TF-PG (magenta color); (b) FTIR spectrum of pure chondroitin

sulphate (blue color), Physical mixture along with drug (red color), optimized CS-TF-PG (magenta color).

5.8.3.2 Nuclear Magnetic Resonance spectroscopy

The Figure 5.5a and 5.5b represents the ^{1}HNMR spectra of HA, HA-TF-PG and CS, CS-TF-PG respectively. The signal assignment at δ 1.92 ppm, δ 3.2 – 4.0 ppm and δ 4.4 ppm of ^{1}HNMR spectrum of HA was attributed to the acetyl group proton, glucosidic proton and anomeric proton respectively. The peaks at 2.5 ppm, 3.2-3.3 ppm of ^{1}HNMR spectrum HA-TF-PG indicates the phospholipid acyl chains in the Proglycosomes. Also, ^{1}HNMR spectrum of optimized HA-TF-PG confirms the electros static interaction by showing doublet peak at δ 0.99 ppm and broad peak at δ 5 ppm.

The ^{1}H-NMR results were analyzed to confirm the binding of CS onto the surface of the proglycosomes. The CS spectra illustrated that signals were observed at 1.94 ppm (acetyl group), 3.2 ppm (glucosidic bonds), and 4.4 ppm (anomeric proton). The CS-TOF-PG spectra illustrated the signal at 0.98 ppm and 4.98 ppm confirms the electrostatic interaction between the CS and proglycosomes.

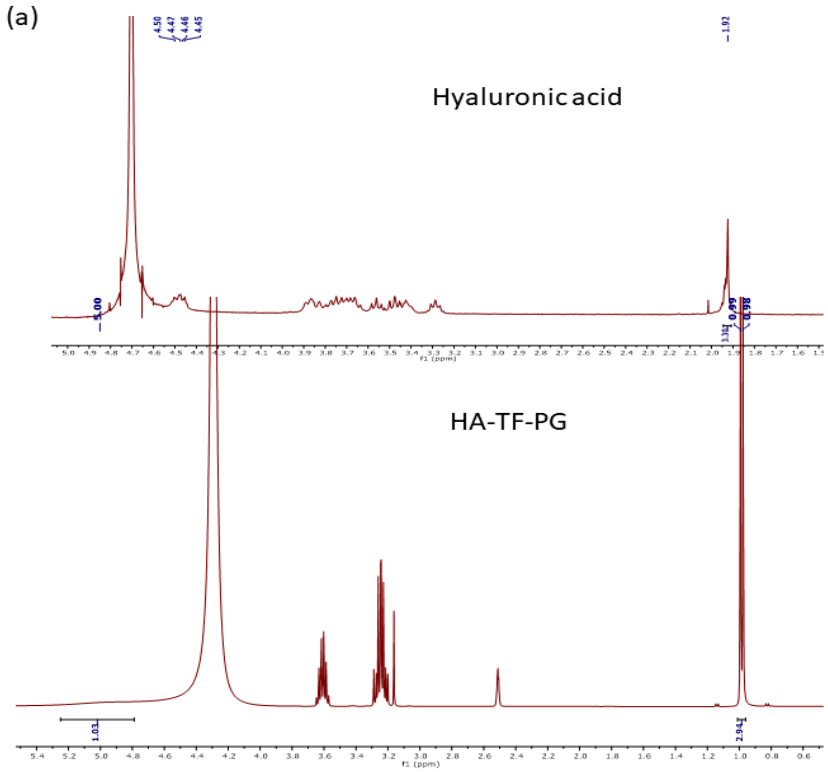

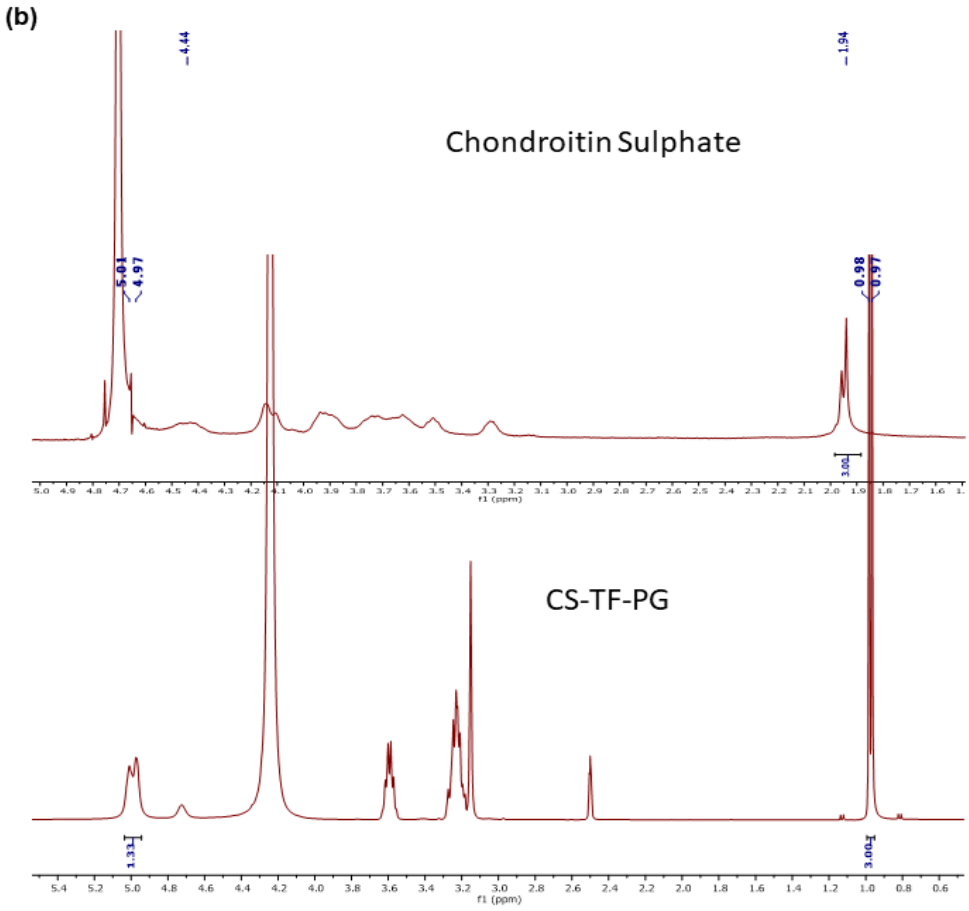

Figure 5.5. (a) Proton Nuclear magnetic resonance of pure hyaluronic acid, and HA-TF-PG, (b) Proton Nuclear magnetic resonance of pure chondroitin sulphate and CS-TF-PG.

5.8.4 Physicochemical characterization of prepared N-TF-PG, HA-TF-PG and CS-TF-PG

5.8.4.1 Surface morphology analysis

FESEM and TEM used to investigate the morphological characteristic of N-TF-PG, HA-TF-PG and CS-TF-PG. The SEM images of Figure 5.6a, 5.6b and 5.6c represents that N-TF-PG, HA-TF-PG and CS-TF-PG were spherical in shape without fusion. Also, the vesicle size of both the formulations were well correlated with the measured values of particle size analyzer. In case of N-TF-PG image, there is no matrix around proglycosomes, whereas the HA-TF-PG and CS-TF-PG images showed a dense hydrophilic matrix around the proglycosomes. This also confirms the deposition of HA on the surface of proglycosomes (Figure 5.6d, 5.6e, and 5.6f).

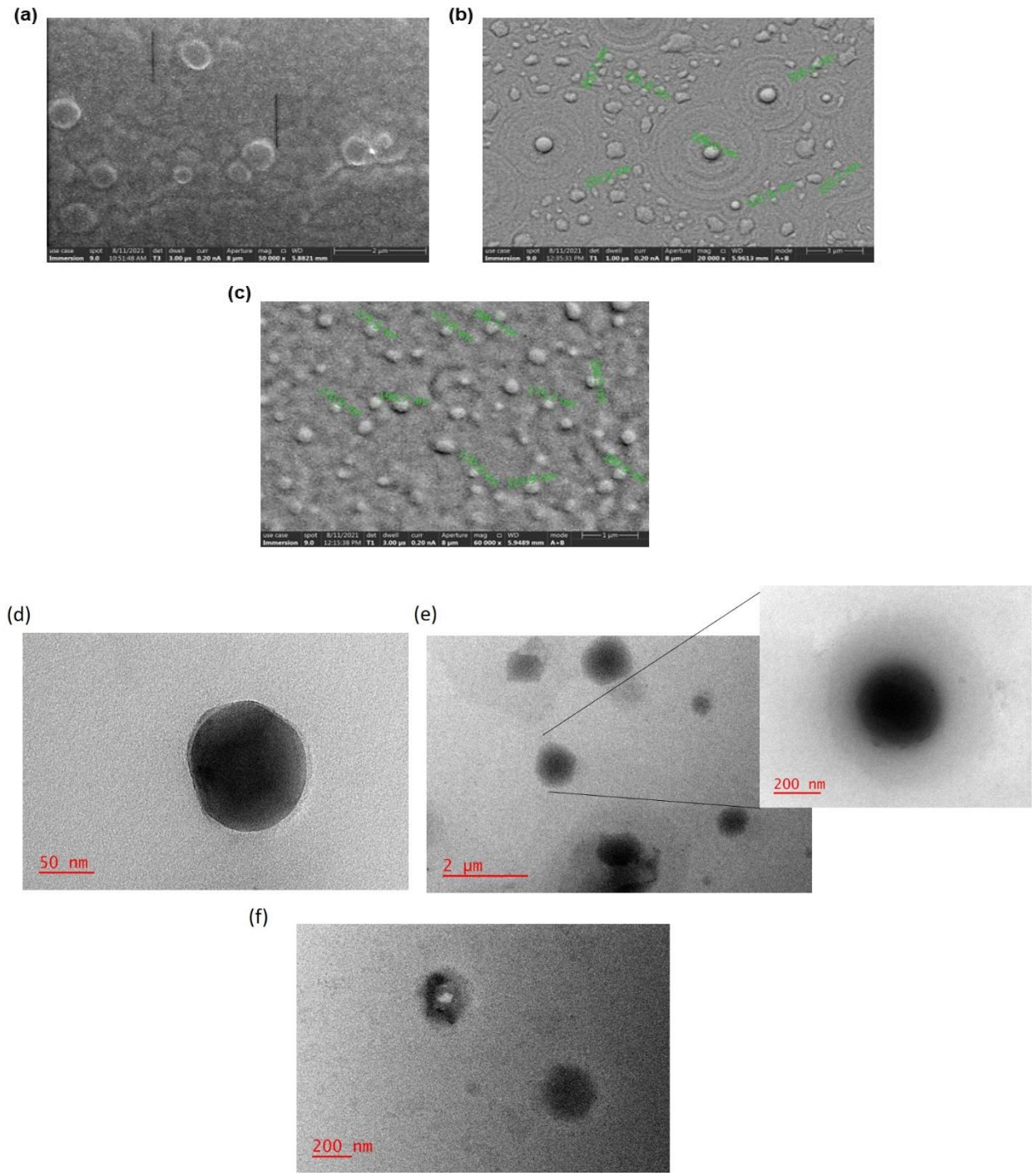

Figure 5.6. Nanovesicle size image of (a) N-TF-PG (b) HA-TF-PG (c) CS-TF-PG dispersion from SEM analysis; TEM images of (d) N-TF-PG (e) HA-TF-PG (f) CS-TF-PG dispersion

5.8.5 In vitro drug release study

The diffusion of TF across dialysis membrane from Free drug solution, N-TF-PG, HA-TF-PG and CS-TF-PG are shown in Figure 5.7. The N-TF-PG, HA-TF-PG and CS-TF-PG demonstrated 38 % 48 % and 40 % drug release in 2 h respectively. The burst release in initial 2 h could be due to the surface bound drug on the proglycosomes. The release of TF from N-TF-PG, HA-TF-PG and CS-TF-PG was released for up to 7 h, whereas free drug solution diffused completely (100%) across membrane within 2 h The extended release of TF from N-TF-PG, HA-TF-PG and CS-TF-PG could be because of phospholipid membrane in case of N-TF-PG, while HA-TF-PG and CS-TF-PG exhibited double-barrier effect offered by HA coating and phospholipid membrane. The possible release kinetics data, correlation coefficients, Akaie information criterion (AIC), and Model selection criteria (MSC) values of TF loaded Proglycosomes, and drug solution are presented in Table 5.3. When comparing the models, the one with the highest correlation coefficient, lowest AIC, and MSC larger than 2 is deemed the best fit. The above mentioned best fit values of N-TF-PG (R^2: 0.9981, AIC: 17.96, MSC: 5.864), HA-TF-PG (R^2: 0.9982, AIC: 21.63, MSC: 5.05) and CS-TF-PG (R^2: 0.9734, AIC: 35.59, MSC: 3.05) values demonstrated that these followed Korsemeyer peppas model. The n values were found to be 0.528 and 0.420 these suggests that the TF followed quasi Fickian diffusion transport mechanism and non swellable matrix-diffusion release mechanism.

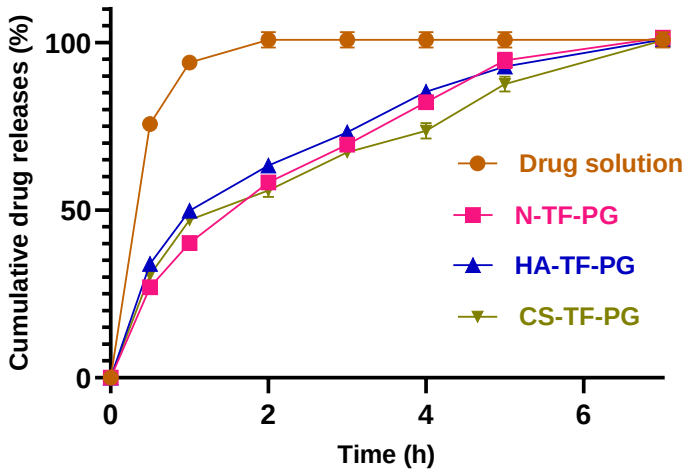

Figure.5.7. In vitro release profile of TF from drug solution, HA-TF-PG, and CS-TF-PG (The results are presented as mean ± standard deviation).

Table 5.3. Possible release mechanism of TF loaded Proglycosomes and free drug by curve-fitting method

	Free drug				**N-TF-PG**				**CS-TF-PG**				**HA-TF-PG**			
Kinetics model	R^2	**K**	**AIC**	**MSC**	**R^2**	**K**	**AIC**	**MSC**	**R^2**	**K**	**AIC**	**MSC**	**R^2**	**K**	**AIC**	**MSC**
Zero order	0.4078	6.481	96.28	-3.40	0.6770	19.61	53.1	0.844	0.4478	18.763	54.829	0.3081	0.9824	19.985	57.11	-0.01
First order	0.9995	2.828	14.96	5.63	0.9638	0.472	37.78	3.034	0.8724	0.444	44.574	1.7732	0.9784	0.554	40.89	2.31
Hixson--Crowell	0.6187	0.070	89.54	-2.65	0.9537	0.124	39.51	2.786	0.8118	0.115	47.29	1.3848	0.9816	0.143	45.478	1.65
Higuchi	0.6150	31.22	88.85	-2.57	0.9966	41.23	21.32	5.385	0.9684	39.715	34.796	3.170	0.9978	42.578	33.851	3.31
Koresmeyer peppas	0.9931	89.6	17.5	3.1	0.9981	39.715	17.96	5.864	0.9734	41.927	35.599	3.055	0.9982	47.351	21.635	5.05
	n value - 0.197 T50 – 0.052 T80 – 0.562				n value - 0.528 T50 – 1.547 T80 – 3.767				n value - 0.459 T50 – 1.467 T80 – 4.084				n value - 0.420 T50 – 1.139 T80 – 3.490			

5.8.6 Characterization of N-TF-PG, HA-TF-PG and CS-TF-PG gel

5.8.6.1 Physical examination, pH and Drug content

The prepared N-TF-PG, HA-TF-PG and CS-TF-PG gels were white in color with good homogeneity. The optimal pH of the prepared gels was found to be 5.5. Usually, the pH of the skin pH ranges from 4.5 to 6.4.

5.8.6.2 Rheology and Spreadability behavior of N-TF-PG, HA-TF-PG and CS-TF-PG gel

The gels' rheological behavior depends on the concentration of the polymer (SEPINEO P600). Sepineo concentrations ranged between the 0.5% to 5% (*w*/*w*) were evaluated. Viscometer measures viscosity as a function of shear stress or shear rate. Table 5.4 presents the rheological data and spreadability factor data of N-TF-PG loaded formulations of varied concentrations of (SEPINEO P600). In a rheometer, the stress is calculated from the torque. The torque values for 0.5, 1, 1.5, 2.0, 2.5 % of (SEPINEO P600) were found to be very low i.e., less and also the viscosity was found to be less than less than 4000 m. Pas. Whereas the torque values of 3.0 and 3.5 % were found to be good i.e., 34.2 and 37.5 with viscosity of 5296.3 and 5542 m. Pas respectively. Usually, the marketed gels viscosity values nearby or around 10000 m. Pas were found to be optimum. Also, the Spreadability factor (S) value was found to be decreased upon increasing the concentration of gelling polymer. The 'S' values of the N-TF-PG, HA-TF-PG and CS-TF-PG gels was observed to be 7441.42 ± 65.03 mm^2/g, 6290.75 ± 51.32 mm^2/g and 6178.24 ± 34.78 mm^2/g. The 'S' values of developed gels (3.5%) demonstrated that these gels can spreads evenly on the skin and supports excellent absorption. Thus, based on the viscosity and 'S' values, 3.5 % of N-TF-PG loaded SEPINEO P600 was considered to be optimum concentration.

The free drug loaded gel (FD-gel), optimized N-TF-PG, HA-TF-PG and CS-TF-PG loaded gels (3.5%) were evaluated for its rheological behavior. The shear rate (1/s) Vs viscosity plots of plain gel, N-TF-PG, HA-TF-PG and CS-TF-PG gels were presented in Figure 5.8. There is a steep decrease in viscosity was observed upon increasing the shear rate which confirms the non-Newtonian and pseudoplastic behavior of gel [4]. Figure 5.8 presents shear strain (%) Vs storage modulus G' (units – Pa; elastic portion) and loss modulus G" (units – Pa; viscous portion). The values of G' > G" in plain gel, N-TF-PG, HA-TF-PG and CS-TF-PG gels which confirms the gel like Viscoelastic solids behavior due to the links inside the material [21,31]. Figure 5.8 presents

the frequency sweep test graph i.e., angular frequency (units - rad/s; X-axis) Vs G' and G" (Pa; Y-axis). This graph helps to understand the developed gels structural behavior. In this the G′>G″ this confirms high degree of crosslinking which indicative of the good structural strength of developed gels.

Table 5.4. Viscosity of different concentrations of SEPINO P600 gel

Surface modified nanocarrier loaded SEPINO gel (%)	**T0 (Tau zero)**	**Viscosity (m. Pas)**
0.5 %	-	16.963
1.0 %	1.1697	478.76
1.5 %	2.1317	720.22
2.0 %	25.731	2587
2.5 %	11.266	3748.7
3.0 %	34.2	5296.3
3.5 %	37.57	5542

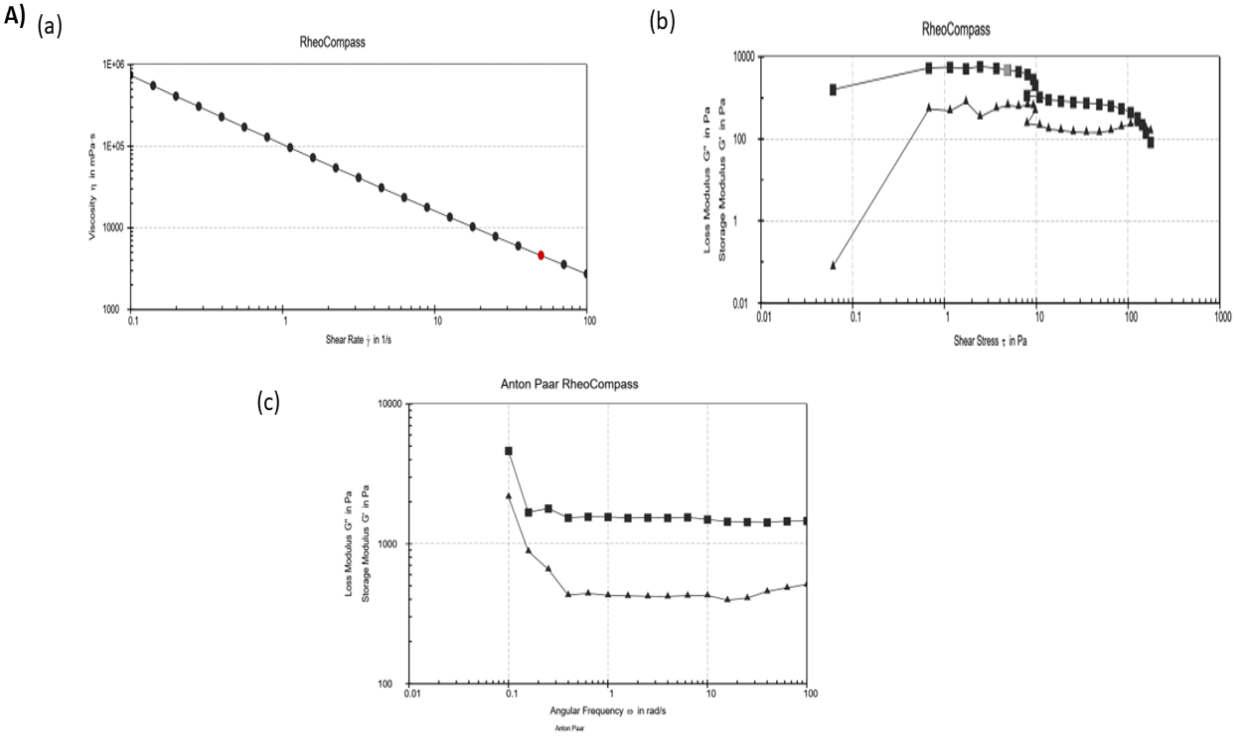

B) (a)

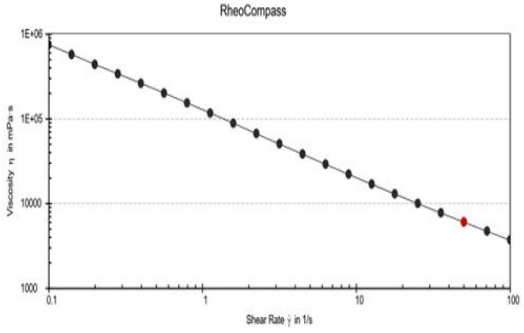
RheoCompass
Viscosity η in mPa s
Shear Rate γ̇ in 1/s

(b)

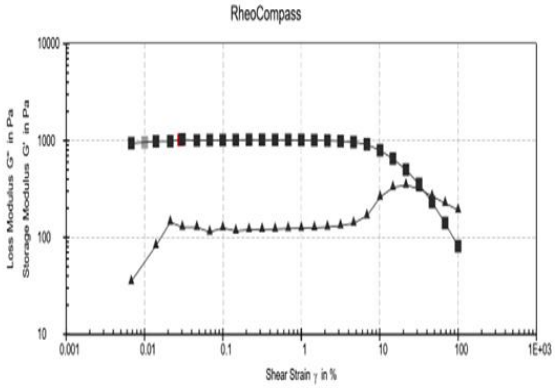
RheoCompass
Loss Modulus G'' in Pa
Storage Modulus G' in Pa
Shear Strain γ in %

(c)

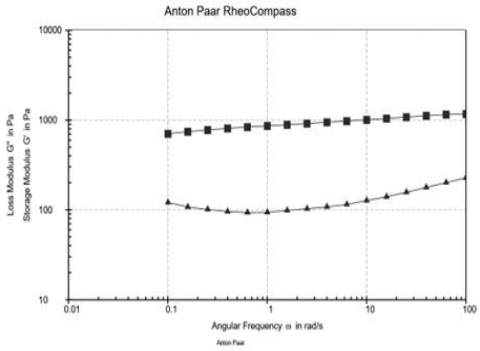
Anton Paar RheoCompass
Loss Modulus G'' in Pa
Storage Modulus G' in Pa
Angular Frequency ω in rad/s

C) (a)

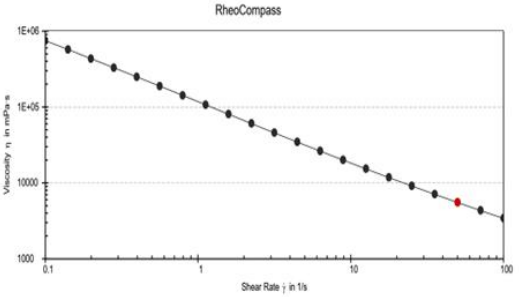
RheoCompass
Viscosity η in mPa s
Shear Rate γ̇ in 1/s

(b)

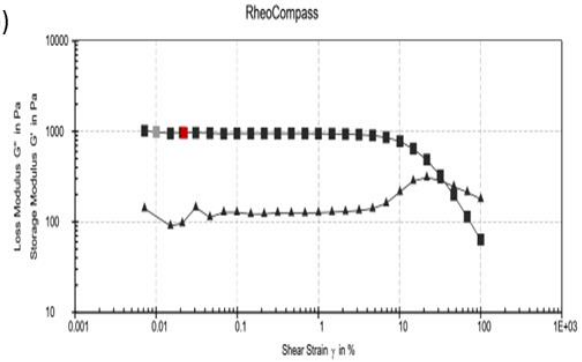
RheoCompass
Loss Modulus G'' in Pa
Storage Modulus G' in Pa
Shear Strain γ in %

(c)

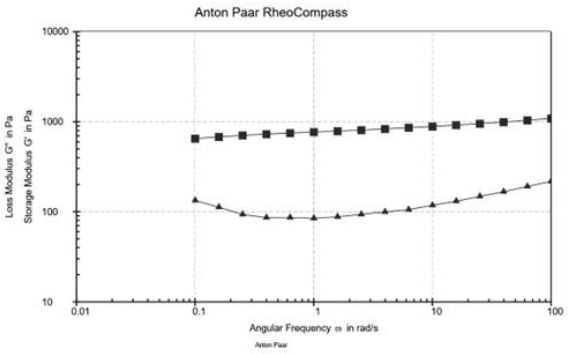
Anton Paar RheoCompass
Loss Modulus G'' in Pa
Storage Modulus G' in Pa
Angular Frequency ω in rad/s

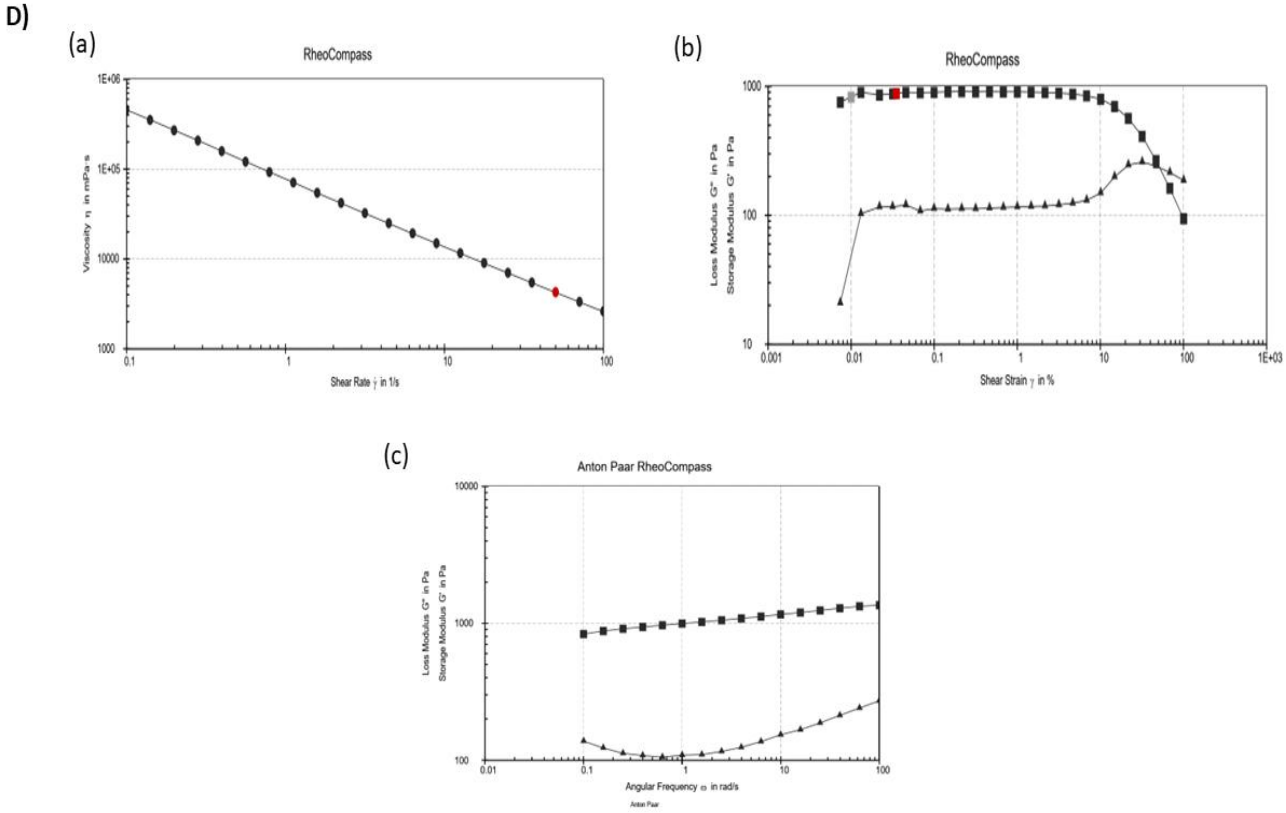

Figure 5.8. Rheology data (A) (a) viscosity of FD gel (b) Amplitude sweep test of FD gel (c) Frequency sweep test of FD gel; (B) Rheology data (a) viscosity of N-TF-PG gel (b) Amplitude sweep test of N-TF-PG gel (c) Frequency sweep test of N-TF-PG gel; (C) Rheology data (a) viscosity of HA-TF-PG gel (b) Amplitude sweep test of HA-TF-PG gel (c) Frequency sweep test of HA-TF-PG gel; (D) Rheology data (a) viscosity of CS-TF-PG gel (b) Amplitude sweep test of CS-TF-PG gel (c) Frequency sweep test of CS-TF-PG gel.

5.8.7 *Ex vivo* studies

The activity of TF is elicited at specific site on topical application. T cells and B cells are pharmacological targets that are found in the dermal layer. Thus, the developed HA-TF-PG and CS-TF-PG gel formulations were consequently studied for TF permeation through skin, retention on skin layers and dermal pharmacokinetics, compared with equivalent strength of N-TF-PG gel.

5.8.7.1 Skin permeation and deposition study

The permeation profile of TF from plain gel, N-TF-PG gel, HA-TF-PG gel and CS-TF-PG gel formulations across skin was illustrated in Figure 5.9. The Kp values of TF from plain gel, N-TF-

PG gel, HA-TF-PG gel and CS-TF-PG gel were found to be 3.708 * 10-2 cm/h, 6.512 * 10-2, 3.238 * 10-2 cm/h and 3.562 * 10-2 cm/h respectively. The cumulative amount of TF permeated across skin was found to be 42.57 ± 9.06 µg/cm2, 68.68 ± 12.27, 60.77 ± 5.73 and 58.95 ± 4.71 µg/cm2 for plain gel, N-TF-PG gel, HA-TF-PG gel and CS-TF-PG gel respectively. The penetration enhancement indicated by the N-TF-PG gel is attributed to small particle size (nearly 100 nm), and positive charge.[3] The flux of TF from plain gel, N-TF-PG gel, HA-TF-PG gel and CS-TF-PG gel were found to be 5.295 ± 0.753, 9.333 µg/cm2/h ± 1.229 µg/cm2/h, 4.792 ± 0.389 µg/cm2/h, and 5.12 ± 1.373 µg/cm2/h respectively. It was found that N-TF-PG gel exhibited 1.76-fold high flux compared to HA-TF-PG gel. The increase in flux may be attributed to the synergistic effect of the propylene glycol and the phospholipids used in the formulation. It was reported that nanocarriers with a positively charged surface can interact with negatively charged skin by ionic interaction and allowing TF to penetrate deeper into the skin [32].

Interestingly, it was observed that the amount of TF permeated through the skin from N-TF-PG and HA-TF -PG at 8 h was found to be similar upon considering the standard deviation i.e., nearly 35 µg/cm^2. Notably, the amount of TF present in the stratum corneum was found to be 1.92-fold and 2.3 folds higher with HA-TF -PG gel compared with N-TF-PG gel and FD-gel respectively. Also, compared to FD-gel the quantity of TF present in dermal layers with N-TF-PG gel, HA-TF -PG and CS-TF -PG gels were found to be 2.56-fold, 3.15-fold and 3.39-fold high. Figure 5.9 presents the amount of TF in the stratum corneum and viable dermal layers on application of plain gel, N-TF-PG gel, HA-TF -PG gel and CS-TF -PG gel. This could be due to water retaining ability of HA that is hyaluronan is anionic due to the presence of the carboxylate group attracts water molecules *via* hydrogen bonding. With this the HA on the surface of the HA-TF-PG expands and loosens the brick like thick cells in stratum corneum which increases the skin hydration and improves the permeation and accumulation in skin [33,34].

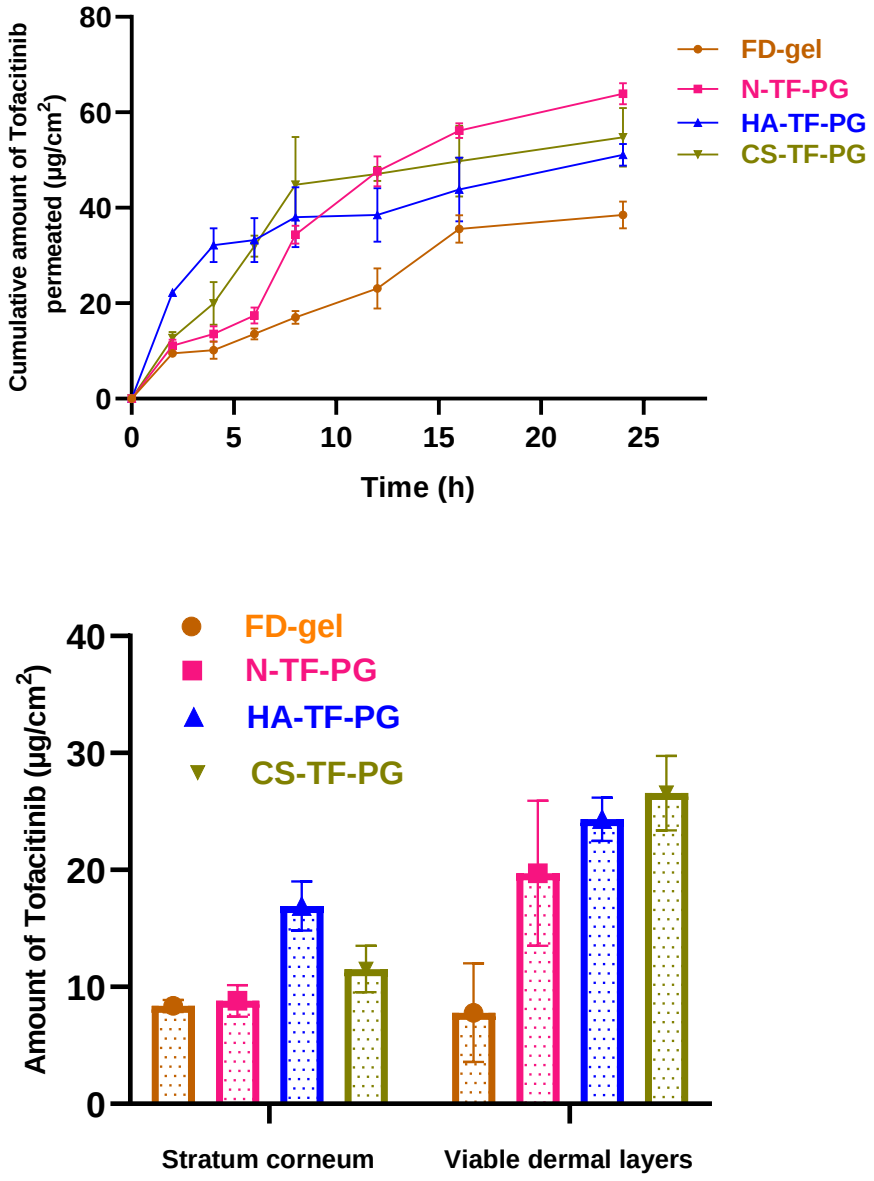

Figure 5.9. Ex vivo skin permeation and retention profile of TF from FD gel, N-TF-PG, HA-TF-PG and CS-TF-PG gel.

5.8.7.2 Dermal distribution studies of dye loaded N-TF-PG, HA-TF-PG and CS-TF-PG

Fluorescence microscopic analysis study was performed to observe the penetration potential of developed N-TF-PG, HA-TF-PG and CS-TF-PG. Thus coumarin-6 was loaded into the developed formulations to assess the permeation efficiency. The reason for selection of coumarin -6 is that it is having the nearby log P as that of TF. The skin was examined at 4 h after 12 h application of

coumarin-6 from free coumarin dispersion, N-TF-PG, HA-TF-PG and CS-TF-PG. Figure 5.10 shows the understanding the distribution of Tofacitinib in the skin layers using coumarin dye i.e., free drug, Coumarin -6 loaded optimized N-TF-PG, coumarin-6 loaded optimized HA-TF-PG and coumarin-6 loaded optimized CS-TF-PG. According to the obtained findings, coumarin 6 as an aqueous dispersion has poor penetration into the skin layers and low green fluorescence signal. Whereas the N-TF-PG, HA-TF-PG, and CS-TF-PG at 12 h study showed high fluorescence signal in dermal region. This confirmed that the N-TF-PG, HA-TF-PG and CS-TF-PG formulations can cross the stratum corneum and reside in dermal region.

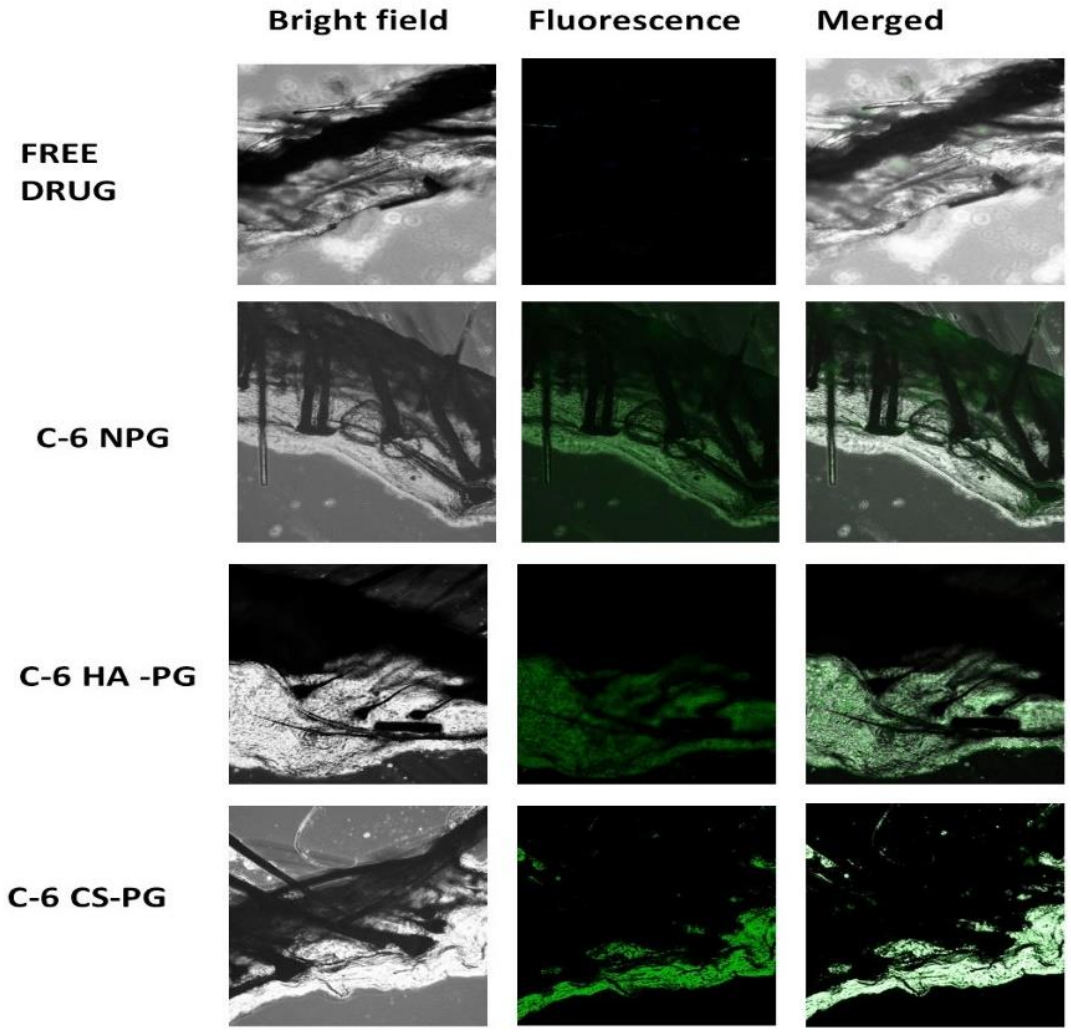

Figure 5.10. Understanding the distribution of Tofacitinib in the skin layers using coumarin dye i.e., Free coumarin, Coumarin -6 loaded optimized N-TF-PG, coumarin -6 loaded optimized HA-TF-PG and coumarin -6 loaded optimized CS-TF-PG.

5.8.7.3 Dermatokinetics of N-TF-PG gel, HA-TF-PG gel and CS-TF-PG gel

The assessment of topical bioavailability implicates the estimation of drug in target site itself. In RA, majority of immune cells are activated in the dermis region nearby inflammation site. Thus, we have performed dermal pharmacokinetic to determine the amount of TF in the regional site with respect to time. Figure 5.11 presents the distribution of TF in epidermal and dermal layers after single application of FD-gel, N-TF-PG gel, HA-TF-PG gel and CS-TF-PG gel. The results demonstrated that CS-TF-PG, HA-TF-PG and N-TF-PG gel delivered TF to the dermis layer significantly high ($p < 0.05$) compared to the FD-gel. Table 5.5 compiled the numeric values of $AUC_{0–32\ h}$, maximum concentration of TF in skin ($C_{Skin\ max)}$, time to reach maximum level in skin and skin elimination and clearance. The total amount of TF accumulated ($AUC_{(0\text{-}28h)}$) in dermal layers was significantly higher with N-TF-PG gel (403.323 ± 22.346 μg/cm^2*h), HA-TF-PG (471.166 ± 43.83 μg/cm^2*h) gel and CS-TOF-PG gel (489.03 ± 13.96 μg/cm^2*h) in comparison to plain gel (224.728 ± 56.39 μg/cm^2*h). The C_{max} value of TF in dermal layer was also significantly higher with HA-TF-PG gel application (23.480 ± 3.23 μg/cm^2), CS-TF-PG gel application (23.47 + 2.87 μg/cm^2) and N-TF-PG gel (18.179 ± 1.451 μg/cm^2) compared with plain gel (11.338 ± 3.01 μg/cm^2). It was reported that the vesicular carriers can exhibit high permeation profile that the phospholipid molecules and propylene glycol improve molecular transport over the skin by changing lipid tight packing.[35] Whereas the conducted dermal kinetics study gave an accord that the developed proglycosomes could not only increase the permeation of TF can also localize the drug in the skin layers. Additionally, the HA and CS coating and the SEPINEO™ P 600 containing Acrylamide/Sodium Acryloyl dimethyl Taurate Copolymer could have helped to form depot for TF molecules.

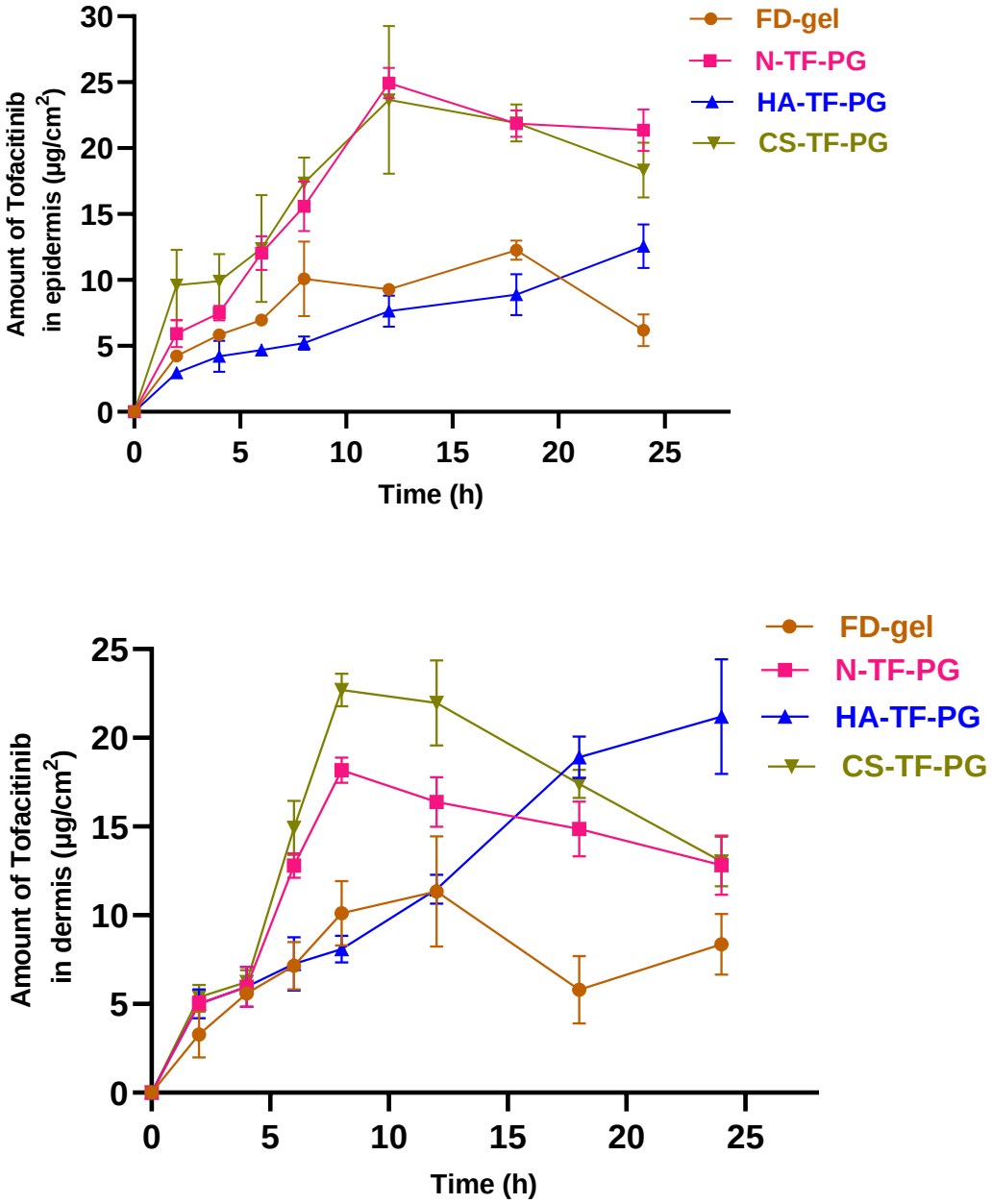

Figure 5.11. Dermatokinetics profile of TF from FD-gel, N-TF-PG, HA-TF-PG and CS-TOF-PG gel in epidermal and dermal layers (Data represented as mean ± SD, n = 3).

Table 5.5. Dermatokinetics parameters (mean ± SD) of topical application of TF Proglycosomes formulations in epidermis and dermis (n = 5)

Parameters	**Units**	**FD-gel**		**N-TF-PG**		**HA-TF-PG**		**CS-TF-PG**	
		Epidermis	**Dermis**	**Epidermis**	**Dermis**	**Epidermis**	**Dermis**	**Epidermis**	**Dermis**
$AUC_{total\ (0\text{-}24h)}$	$\mu g/cm^2*h$	246.79 ± 9.33	224.73 ± 56.39	576.94 ± 34.98	403.32 ± 22.35	276.71 ± 30.79	471.166 ± 43.83	553.24 ± 14.79	489.03 ± 13.96
$AUC_{0\text{-}inf}$	$\mu g/cm^2*h$	320.10 ± 10.96	588.43 ± 88.03	2064.19 ± 725.94	1954.78 ± 386. 91	NA	NA	NA	NA
C_{max} Skin	$\mu g/cm^2$	13.68 ± 0.54	11.34± 3.01	24.95 ± 2.32	18.18 ± 1.45	14.34 ± 1.59	23.480 ± 3.23	22.61 ± 1.88	23.48 ± 2.87
T_{max} Skin	h	12	12	12	8	24	24	12	12
Cl	µg/h	0.46 ± 0.016	0.26 ±0.166	0.08 ± 0.027	0.10 ± 0.073	NA	NA	NA	NA

5.8.8 Assessment of stability of N-TF-PG, HA-TF-PG and CS-TF-PG gel

The developed N-TF-PG gel, HA-TF-PG gel and CS-TF-PG gel were evaluated for storage stability for up to 90 days at 4 °C, and 25°C. The amount of TF in the N-TF-PG, HA-TF-PG gel and CS-TF-PG gel did not change considerably upon storage for 90 days (Table 5.6). Also, the viscosity and spreadability data also have not shown a significant difference at (2–8°C) and room temperatures. This confirmed the physical and rheological stability of HA-TF-PG and CS-TF-PG in the finished dosage form as a gel.

Table 5.6. Stability data of N-TF-PG and HA-TF-PG at different storage conditions

Formulation	**N-TF-PG Gel**			**HA-TF-PG Gel**			**CS-TF-PG Gel**		
	4^0C								
Parameters	**Assay (%)**	**Viscosity (m Pas)**	**Spreadability (mm^2/g)**	**Assay (%)**	**Viscosity (m Pas)**	**Spreadability (mm^2/g)**	**Assay (%)**	**Viscosity (m Pas)**	**Spreadability (mm^2/g)**
Initial	100.11 ± 0.14	5233.2	7441.42± 65.3	100.972 ± 0.167	5547.5	6290.75 ± 51.3	99.99 ± 0.41	5525.6	6178.24 ± 34.78
1 month	100.150± 0.18	5356.2	6903 ± 68.3	101.15 ± 0.150	5482.8	7098 ± 39.1	99.47 ± 0. 47	5422.2	6903.08 ± 33.44
3 months	100.021 ± 0.33	5233.2	6332 ± 32	100.936 ± 0.229	5356.5	6903 ± 33.4	98.82 ± 0.15	5549	6519.66 ± 56.69
	25 ± 2^0C								
1 month	101.15 ± 0.149	5345.2	7098 ± 59.1	100.23 ± 0.285	5547.5	6903 ± 33.4	98.64 ± 0. 12	5258.3	6332.05 ± 65.46
3 months	101.0 ± 0.236	5463	6710 ± 88.7	100.03 ± 0.419	5356.0	7297 ± 34.8	97.74 ± 0. 16	5108.4	6903.08 ± 68.30

5.9 Conclusion

In this work, the hydrophilic HA and CS has been successfully incorporated onto the surface of the proglycosomes for the study of site-specific delivery of TF via CD44 receptors in the RA region. The coating is mediated by electrostatic interaction between the negatively charged HA and CS and positively charged proglycosomes respectively. HA-TF-PG and CS-TF-PG were successfully prepared by the TFH technique and the formulation and process variables were optimized to obtain desired vesicle size, PDI, and entrapment efficiency. The surface coating was confirmed by zeta potential data that complete charge reversal and formation of the amide bond were confirmed by NMR data. The ex vivo permeation and dermatokinetics data in phosphate buffer saline (pH 7.4) suggested that HA coating was found to be effective in retaining proglycosomes in skin layers. The total amount of TF permeated and accumulated ($AUC_{(0\text{-}28h)}$) in dermal layers as well as Cmax in these two layers were found to be significantly higher with HA-TF-PG gel and CS-TF-PG gel in comparison to plain gel ($P<0.001$).

References

1. Ruela ALM, Perissinato AG, Lino ME de S, Mudrik PS, Pereira GR. Evaluation of skin absorption of drugs from topical and transdermal formulations. *Brazilian J. Pharm. Sci.* 52(3), 527–544 (2016).

2. Waghule T, Patil S, Rapalli VK, *et al.* Improved skin-permeated diclofenac-loaded lyotropic liquid crystal nanoparticles: QbD-driven industrial feasible process and assessment of skin deposition. *Liq. Cryst.* 48(7), 991-1009 (2020).

3. Hagen M, Baker M. Skin penetration and tissue permeation after topical administration of diclofenac. *Curr Med Res Opin.* 33(9),1623-34 (2017).

4. Gorantla S, Saha RN, Singhvi G. Exploring the affluent potential of glyceryl mono oleate – myristol liquid crystal nanoparticles mediated localized topical delivery of Tofacitinib: Study of systematic QbD, skin deposition and dermal pharmacokinetics assessment. *J. Mol. Liq.* 346, 117053 (2022).

5. Kathuria H, Nguyen DTP, Handral HK, Cai J, Cao T, Kang L. Proposome for transdermal delivery of tofacitinib. *Int. J. Pharm.* 585, 119558 (2020).

6. Cárcamo-Martínez Á, Mallon B, Anjani QK, *et al.* Enhancing intradermal delivery of

tofacitinib citrate: Comparison between powder-loaded hollow microneedle arrays and dissolving microneedle arrays. *Int. J. Pharm.* 593, 120152 (2021).

7. Chuang SY, Lin CH, Huang TH, Fang JY. Lipid-Based nanoparticles as a potential delivery approach in the treatment of rheumatoid arthritis. *Nanomaterials.* 8(1), 42-54 (2018).

8. Hussain A, Singh S, Sharma D, Webster TJ, Shafaat K, Faruk A. Elastic liposomes as novel carriers: Recent advances in drug delivery. *Int. J. Nanomedicine*. 12, 5087–5108 (2017).

9. Garg V, Suri R, Jain GK, Kohli K. Proglycosomes: A novel nano-vesicle for ocular delivery of tacrolimus. *Colloids Surfaces B Biointerfaces*. 157, 40–47 (2017).

10. Gorantla S, Gorantla G, Saha RN, Singhvi G. CD44 receptor-targeted novel drug delivery strategies for rheumatoid arthritis therapy. *Expert Opin. Drug Deliv.* 18(11), 1553–1557 (2021).

11. Teriete P, Banerji S, Noble M, *et al.* Structure of the regulatory hyaluronan binding domain in the inflammatory leukocyte homing receptor CD44. *Mol. Cell*. 13(4), 483–496 (2004).

12. Cadinoiu AN, Rata DM, Atanase LI. Biocompatible injectable polysaccharide materials for drug delivery. In: *Polysaccharide Carriers for Drug Delivery*, Elsevier, 127–154 (2019).

13. Jain S, Kumar D, Swarnakar NK, Thanki K. Polyelectrolyte stabilized multilayered liposomes for oral delivery of paclitaxel. *Biomaterials*. 33(28), 6758–6768 (2012).

14. Mahtab A, Rabbani SA, Neupane YR, *et al.* Facile functionalization of Teriflunomide-loaded nanoliposomes with Chondroitin sulphate for the treatment of Rheumatoid arthritis. *Carbohydr. Polym.* 250, 116926 (2020).

15. Gorantla S, Saha RN, Singhvi G. Design of experiment-driven stability-indicating RP-HPLC method for the determination of tofacitinib in nanoparticles and skin matrix. *Futur. J. Pharm. Sci.* 7(1), 1–12 (2021).

16. Jannu AK, Puppala ER, Gawali B, *et al.* Lithocholic acid-tryptophan conjugate (UniPR126) based mixed micelle as a nano carrier for specific delivery of niclosamide to prostate cancer via EphA2 receptor. *Int. J. Pharm.* 605, 120819

(2021).

17. Bao W, Tian F, Lyu C, *et al.* Experimental and theoretical explorations of nanocarriers' multistep delivery performance for rational design and anticancer prediction. *Sci. Adv*. 7(6), 24568 (2021).

18. Gorantla S, Saha RN, Singhvi G. Spectrophotometric method to quantify tofacitinib in lyotropic liquid crystalline nanoparticles and skin layers: Application in ex vivo dermal distribution studies. *Spectrochim. Acta - Part A Mol. Biomol. Spectrosc.* 255, 119719 (2021).

19. VERSATILE APPLICATIONS *All dosage forms- Specific pharmaceutical red drums FCU26 (DMF): 25 Kg SEPINEO TM P 600 A key polymer for topical pharmaceutical innovation.

20. Hertzog DL, McCafferty JF, Fang X, *et al.* Development and validation of a stability-indicating HPLC method for the simultaneous determination of Losartan potassium, hydrochlorothiazide, and their degradation products. *J pharm and biomed anal.* 30(3):747-760 (2002).

21. Mahmood A, Rapalli VK, Gorantla S, Waghule T, Singhvi G. Dermatokinetic assessment of luliconazole-loaded nanostructured lipid carriers (NLCs) for topical delivery: QbD-driven design, optimization, and in vitro and ex vivo evaluations. *Drug Deliv. Transl. Res.* 12(5), 1118- 1135 (2021).

22. Singhvi G, Krishna RV, Krishna K V., Dubey SK. Alginate: Drug Delivery and Application. In: *Alginates*, Apple Academic Press, 307–334 (2020).

23. Garg A, Aggarwal D, Garg S, Singla AK. Spreading of semisolid formulations: An update. *Pharmaceutical Technology North America.* 26(9), 84-90 (2002).

24. Rapalli VK, Sharma S, Roy A, Singhvi G. Design and dermatokinetic evaluation of Apremilast loaded nanostructured lipid carriers embedded gel for topical delivery: A potential approach for improved permeation and prolong skin deposition. *Colloids Surfaces B Biointerfaces*. 206, 111945 (2021).

25. Garg NK, Tyagi RK, Singh B, *et al.* Nanostructured lipid carrier mediates effective delivery of methotrexate to induce apoptosis of rheumatoid arthritis via NF-κB and FOXO1. *Int. J. Pharm.* 499(1–2), 301–320 (2016).

26. Jain S, Mistry MA, Swarnakar NK. Enhanced dermal delivery of acyclovir using solid lipid nanoparticles. *Drug Deliv. Transl. Res.*1(5), 395-406 (2011).

27. Rapalli VK, Singhvi G. Dermato-pharmacokinetic: assessment tools for topically applied dosage forms. *Exp opi drug deliv.* 18(4), 423–426 (2020).

28. Barbault-Foucher S, Gref R, Russo P, Guechot J, Bochot A. Design of poly-epsilon-caprolactone nanospheres coated with bioadhesive hyaluronic acid for ocular delivery. *J. Control. Release*. 83(3), 365–375 (2002).

29. Park JH, Cho HJ, Yoon HY, *et al.* Hyaluronic acid derivative-coated nanohybrid liposomes for cancer imaging and drug delivery. *J. Control. Release* 174(1), 98–108 (2014).

30. Xie J, Ji Y, Xue W, Ma D, Hu Y. Hyaluronic acid-containing ethosomes as a potential carrier for transdermal drug delivery. *Colloids Surf. B. Biointerfaces*. 172, 323–329 (2018).

31. Simta J, Kavita I, Milind B. Novel Long Retentive Posaconazole Ophthalmic Suspension. *Pharm sci tech.* 4(1), 1-8 (2020).

32. Gorantla S, Dabholkar N, Sharma S, Rapalli VK, Alexander A, Singhvi G. Chitosan-based microneedles as a potential platform for drug delivery through the skin: Trends and regulatory aspects. *Int. J. Biol. Macromol.* 184, 438–453 (2021).

33. Jeon S, Yoo CY, Park SN. Improved stability and skin permeability of sodium hyaluronate-chitosan multilayered liposomes by Layer-by-Layer electrostatic deposition for quercetin delivery. *Colloids Surfaces B Biointerfaces*. 129, 7–14 (2015).

34. Dabholkar N, Gorantla S, Waghule T, *et al.* Biodegradable microneedles fabricated with carbohydrates and proteins : Revolutionary approach for transdermal drug delivery. *Int. J. Biol. Macromol.* 170, 602–621 (2021).

35. Zhao YZ, Lu CT, Zhang Y, *et al.* Selection of high efficient transdermal lipid vesicle for curcumin skin delivery. *Int. J. Pharm.* 454(1), 302–309 (2013).

6 *In vivo* anti-arthritic efficacy studies in rats, on topical application of developed formulations and oral administration of pure tofacitinib solution

In order to investigate the safety and efficacy of localization and site-specific delivery, the formulations were tested in Complete Freund's Adjuvant (CFA) administered diseased RA model in Wister rats. The CFA-induced paw edema model is the most consistent chronic inflammation screening model and a highly predictive model of efficacy in human inflammatory disease. The administration of CFA to the rat activates the immune system by stimulating cellular mediators and certain immunoglobulins. This further lead to localized joint inflammation associated with synovial membrane thickening and irreversible cartilage damage [1]. The *in vivo* anti-arthritis efficacy studies were carried out in Wistar rats. The current study protocol was duly approved by the IAEC prior to the commencement of work (Protocol No. IAEC/RES/31/05). The animals have been housed in individually ventilated cages and fed with standard feed water and libitum (light and dark cycles of 12 h) for one week prior to the experiment.

6.1 Materials and methods

Complete Freund's Adjuvant (CAS.# 9007–81–2) was procured from Sigma Aldrich. All ELISA assay cytokine kits were acquired from KINESISDx, USA. Bead-based cytokine antibodies were acquired from BD Biosciences,USA. All primary antibodies and secondary antibodies were obtained from Cell Signaling Technologies, Danvers, MA, USA. All the organic solvents used during this work were of analytical grade.

6.1.1 Development of adjuvant induced RA rat model

The RA was induced in male Wistar rats by injecting 100 µL of CFA to the right hind paw sub-plantar region (All animal groups except the normal control). Figure 6.1 presents the schematic representation presenting the two treatment cohorts investigated in the *in vivo* efficacy studies of TF.

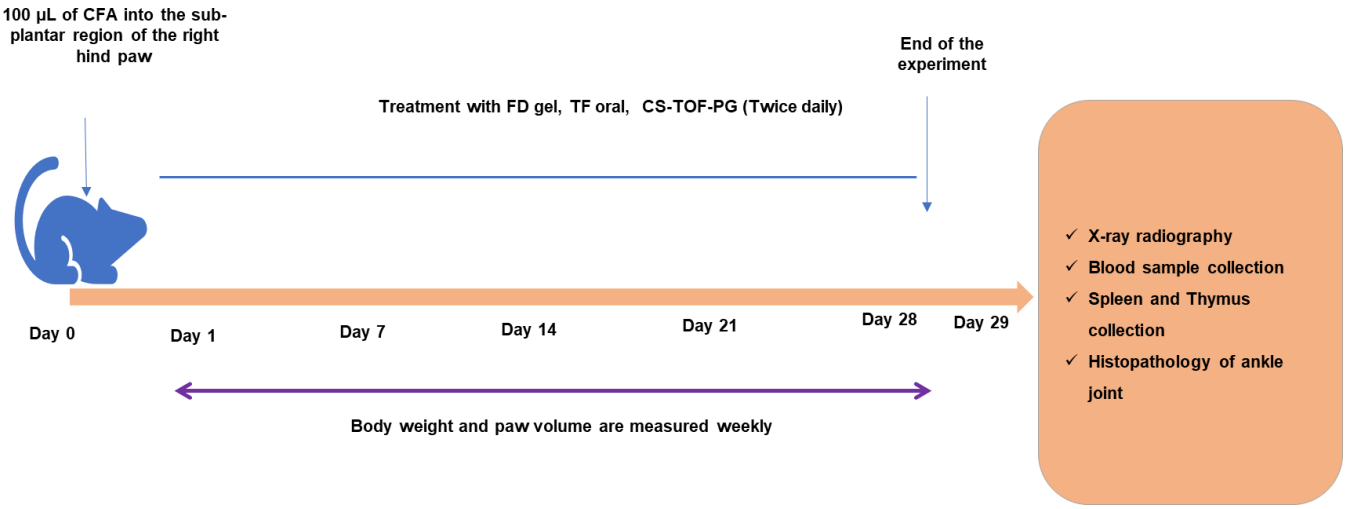

Figure.6.1. Schematic representation of the two treatment cohorts investigated in the *in vivo* efficacy studies of TF

The amount of TF administered orally was 0.1 mg/kg and topical application of CS-TF-PG gel and FD gel to the CFA rats (500 mg gel applied). Hereafter the treatment blood collection, spleen and thymus index, x-ray, and histopathology analysis were performed.

6.1.2 *In vivo* systemic absorption and skin retention study

Freund's complete adjuvant (FCA) induced arthritis rats were divided into 5 groups with six animals in each group. Among these one group was used as normal control and 4 groups were treated with formulations FD-gel, developed N-TF-PG gel, HA-TF-PG gel and CS-TF-PG gel. At predetermined time points (1, 2, 4, and 6 h) the blood was collected from the retro orbital region. The blood sample was collected in to the ethylenediaminetetraacetic acid (EDTA) coated Eppendorf and centrifuged at 3000 rpm at 4 °C. Then at 6 h time point the skin sample was collected. The TF was extracted from each plasma and skin samples and were analyzed by validated bio-analytical and analytical methods respectively.

6.1.3 Treatment method

All the developed formulation were evaluated for the *in vivo* efficacy on topical application in treatment of RA induced animal model and compared with the oral solution. The complete treatment details are presented in Table 6.1 and 6.2.

Formulation I: *In vivo* efficacy evaluation of the optimized tofacitinib loaded liquid crystal nanoparticles (TF-LCNP) in the RA induced animal model

Table 6.1. The treatment details of performed *in vivo* efficacy study of Liquid crystal nanoparticles

Group	**Treatment**
Group -I	Normal control (NC; With no immunization)
Group -II	Disease control group (DC; Freund's complete adjuvant injected animals)
Group-III	DC treated with pure drug loaded gel (FD-gel)
Group - IV	DC treated with TF-LCNP gel
Group - V	DC treated with Oral administration of TF (TF -oral)

(in earlier page mentioned 4 groups are taken but here 5 groups are listed)

Formulation II: *In vivo* efficacy evaluation of the optimized hyaluronic acid and chondroitin sulphate coated tofacitinib loaded proglycosomes in the RA induced animal model

Table 6.2. The treatment details of performed *in vivo* efficacy study of TF loaded proglycosomes

	Set -II
Group -I	Normal control (NC; With no immunization)
Group -II	Disease control group (DC; Freund's complete adjuvant injected animals)
Group-III	DC treated with pure drug loaded gel (FD-gel)
Group - IV	DC treated with N-TF-PG gel
Group - V	DC treated with HA-TF-PG gel
Group -VI	DC treated with CS-TF-PG gel
Group - VII	DC treated with oral administration of TF (TF -oral)

The FD-gel, TF-LCNP gel, N-TF-PG gel, HA-TF-PG gel and CS-TF-PG gel were topically applied to the ankle joint for 28 days consistently (500 mg gel applied).

6.1.4 Methodology

6.1.4.1 Validation parameters for the clinical assessment of RA

The clinical assessment of RA was performed based on the data of body weight, paw volume, arthritis score and joint stiffness. Starting on the day after inoculation of CFA, body weight was

assessed every week throughout the study and expressed as a percent increase in body weight. During the study, each animal's hind paw volumes were assessed using a Plethysmometer on 7^{th}, 14^{th}, 21^{st}, and 28^{th} days. The difference in paw volumes between the treatment groups and control groups was measured. Based on the above data the severity of arthritis was confirmed and observed throughout the study period.

6.1.4.2 Spleen and thymus weight

The reported literature suggests that FCA-induced rats develop splenomegaly and lymphadenopathy. Thus, the effect of formulation-treated groups (FD-gel, TF-oral, TF-LCNP, N-TF-PG, HA-TF-PG and CS-TF-PG) were compared with diseased and normal groups by weighing the spleen and thymus.

6.1.4.3 X-ray radiography

Adjuvant induced arthritis is characterized by a number of clinical signs such as bone resorption, soft tissue edema, and joint deformity. Thus, radiographic study of the animals' hind paws was performed with an X-ray machine at the end of the experiment (Day 29). Rats were anesthetized with ketamine and xylazine and imprisoned to a radiographic box at a distance of roughly 50 cm from the X-ray source to examine bone deterioration in the paws prior to sacrifice.

6.1.4.4 Quantitative analysis of CD44 protein expression in skin tissue samples

In RA disease condition, the inflamed skin layers show the presence of CD44 on the surface of activated macrophages. Thus, the study was performed in all the above-mentioned groups in section 6.1.3. RA induced rat (DC) groups treated with the plain gel, TF-LCNP, N-TF-PG, HA-TF-PG and CS-TF-PG. The skin tissue was collected from the above-mentioned animal groups and TRIzol (TRI Reagent®solution) was added to extract the total RNA. The complementary DNA was synthesized using a Verso cDNA synthesis kit. The mixture of RNA sample, primer mix, and nuclease-free water was maintained at 70°C (5 minutes) and then flash cooled on ice. Primers of CD44 were acquired from Integrated DNA technologies. The relative gene expression's final reaction volume is found to be 10 µL and it was analyzed using RT-PCR applied biosystem, (Thermo Fisher Scientific, Singapore). The qRT-PCR reaction cycle conditions are 95^0C for 10 min; 40 cycles of 95^0C for 15 sec and 60^0C for 60 sec and performed using the Power Up TM SYBERTM Green Master Mix. The data were normalized using housekeeping gene i.e. GAPDH and analyzed using 2 - ΔΔCq method [2].

6.1.4.5 Cytokine's assessment using cytometric bead array (CBA) technique by flow cytometry

During RA condition, the macrophages and other immune cells produce pro-inflammatory cytokines such as TNF-α, IL-1, IL-6, PGE-2 and cytokine inhibitory factor IL-10. The inflammatory cytokines levels (TNF-α, IL-10, and IFN-Y) in the serum samples were analyzed by Attune NXT flow cytometer (Thermo Fisher Scientific) with BD™ Cytometric Bead Array (CBA) application. According to the manufacturer's protocol, the experiment was performed utilizing the commercially available BD^{TM} Cytometric Bead Array (CBA) inflammatory cytokines flex set customizable cytokines kit (BD biosciences, USA). 50 µL of capture bead reagent containing 1 µL of respective capture bead was added to the 50 µL of the sample. After that, gently combined and incubated for 1 h in the dark at room temperature. After 1 h of incubation, 50 µL of detection reagent with 1 µL of detection reagent cytokine bead were added and incubated for 1 h at room temperature in the dark. The pellet was then washed with 1 mL of wash buffer and centrifuged at 200 g for 5 min. Then the supernatant was collected, and 300 µL of wash buffer was added to the pellet and vortexed, followed by a flow cytometer analysis.

6.1.4.6 Cytokine's assessment using ELISA

The inflammatory cytokines levels (IL-1, IL-6, and PGE-2) in the serum samples were analyzed by commercially available Krishgen biosystems ELISA kits. The standard curve was plotted for the cytokines and serum samples were analyzed using coated plates as per manufacturers' recommendation. Procedure in brief was provided below.

The standards and samples were incubated in coated plates at 37°C for 2 h. After this washed with wash buffer and incubated for 1 h at 37°C with biotin labelled detection antibody. Followed by wash again and then incubated for 30 min at 37°C with streptavidin horseradish peroxidase. Then the samples were incubated for 30 min with TMB substrate. Then the reaction was stopped by adding stop solution and waited till the colour changed from blue to yellow, and the absorbance was measured at 450 nm using ELISA reader.

6.1.4.7 Evaluation of hematological parameters

Hematological parameters are primarily used to assess the RA disease activity before and after the treatment. Thus, estimation of hemoglobin, RBCs, and neutrophil count upon treatment with the developed TF-LCNP, N-TF-PG, HA-TF-PG and and CS-TF-PG provides the evidence for the therapeutic appraisal of TF loaded formulations in RA. The blood was collected into the EDTA

coated Eppendorf tube on 29th day. Further, the neutrophils, RBCs, and Hb were estimated using the Automated Haematology Analyzer [3].

6.1.4.8 Histopathological analysis of hind paw

On 29th day, after the x-ray radiography study the necropsy was done. During this time, the hind paws were dissected and processed for histology analysis. The specimens were preserved in a 10% neutral buffered formalin solution. After 48 h, decalcification of the specimen was performed using 10% formic acid and stored for another 21 days. After this, the sagittal slices of paws were obtained and further processed for paraffin embedding. For preparing the paraffin blocks, Thermo scientific embedding device was used. The prepared specimen embedded Parafilm blocks were sectioned into 5 mm thick using microtome (Thermo scientific) and stained with hematoxylin and eosin. Then, fluorescent optical microscopy (ZEISS) was used for imaging of the prepared sectioned hind paw specimen [4].

6.1.4.9 Statistical data analysis

All the experiments were performed in triplicate. The statistical analysis of in vitro, *ex vivo* and *in vivo* results was performed using GraphPad Prism 8.0 (Systat Software Inc.). Two-way ANOVA was used to compare the mean of the two groups, and a results Statistical significance was considered at $p < 0.05$.

6.2 Results and discussion

6.2.1 *In vivo* systemic absorption and skin retention study

In vivo systemic absorption of TF was quantified by analyzing the drug concentration in the plasma after topical application of TF plain gel, N-TF-PG, HA-TF-PG and CS-TF-PG gel to male wistar rats. After topical application of TF plain gel and N-TF-PG gel, detectable levels of TF were observed in the plasma at 6 h time point and the concentrations estimated were 65.77 ± 2.45 ng/mL and 42.23 ± 1.78 ng/mL respectively. Whereas, animals treated with HA-TF-PG and CS-TF-PG gel showed no detectable plasma levels of TF at the 6h. Thus at 6h, the animal skin was collected and the amount of drug in the skin was determined. The amount of TF in the skin with plain gel, N-TF-PG gel, HA-TF-PG gel and CS-TF-PG gel were found to be 1.89 ± 1.26 µg/cm^2, 4.52 ± 1.54 µg/cm^2, 5.35 ± 1.78 µg/cm^2 and 5.15 ± 1.20 µg/cm^2 respectively. It was observed that, compared to the Plain gel treated rat skin, the N-TF-PG, HA-TF-PG and treated rat group showed 2.3, 2.8, and 2.7 fold increments of TF in skin layers.

6.2.2 Formulation I: *In vivo* efficacy evaluation of the optimized tofacitinib loaded liquid crystal nanoparticles (TF-LCNP) in the RA induced animal model

6.2.2.1 Effect of TF loaded formulations on paw volumes and arthritic index

CFA administered rats showed increased right hind paw volumes, erythema, swelling, and deformity. Figure. 6.1b and 6.1c presents an increase in paw volumes and arthritic index of NC, DC and developed TF-LCNP gel treated group rats. It was observed that DC showed a significant increase in paw volume compared to NC. Also, the arthritic score was maximum in the DC group (3.9 ± 0.141) and lower ~~ed~~ in the FD-gel (3.1 ± 0.282), TF-LCNP gel (1.1 ± 0. 353), and TF-oral (3.2± 0. 282) treatment. It was observed that, a significant reduction in paw volume and arthritic score was observed with the TF-LCNP treated group ($p < 0.001$) compared to the DC (Figure 6.1a).

6.2.2.2 Effect of TF loaded formulations on rat's body weight of CFA induced inflammation

The body weights of rats treated with normal control (NC), diseases control (DC), FD-gel, and TF-LCNP gel are depicted in Figure 6.2d. The % change in body weights was recorded based on their day 1 bodyweight. It was observed that from day 3rd the DC showed a significant ($p < 0.001$) decrease in body weight compared to NC. The decrease in body weight is attributed to the change in the metabolism of lipid and proteins, hyperesthesia, skeletal muscle protein breakdown, and disease-associated stress. Whereas the TF-LCNP treated groups showed significant increase in body weights from day 7^{th} compared to the FD-gel and TF-oral. On day 28^{th} the statistical significance between the DC group vs FD-gel, TF-LCNP gel and TF-Oral treated groups were as $p < 0.05$, $p < 0.001$, and $p < 0.05$ respectively.

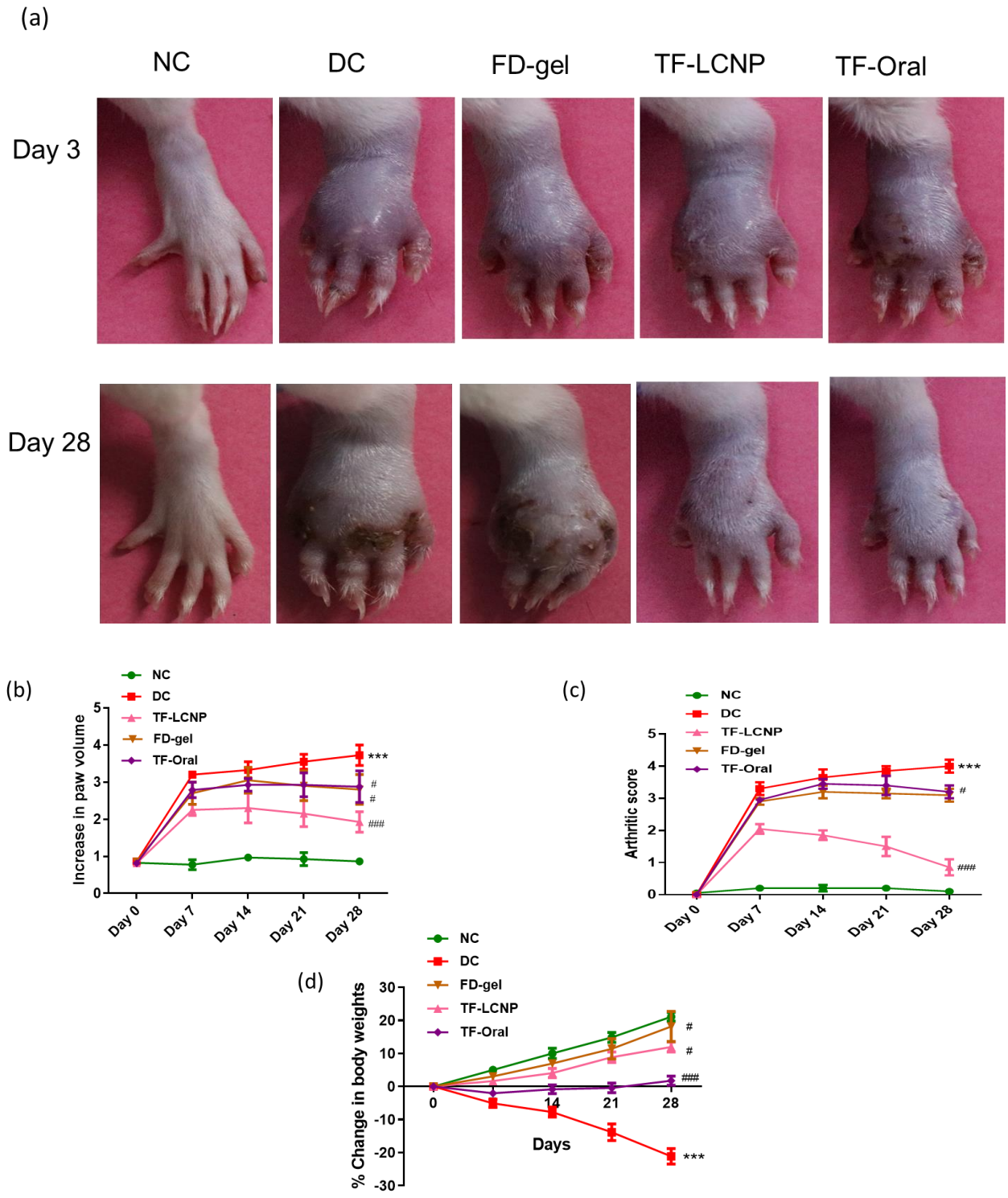

Figure.6.2. (a) Representative paw images of CFA rats before and after the treatment with FD-gel, TF-oral, and developed TF-LCNP gel (day 3 and day 28), (b,c,d) Effect of formulations on body weight, paw volumes, and arthritic score.

*All values were expressed as mean ± SEM (n = 6). Statistical significance was determined by two-way ANOVA followed by Bonferroni multiple comparison test. All the values were compared

with disease control group when #p < 0.05, ##p < 0.01, ###p < 0.001 on day 28; (NC- Normal control; DC-Disease control).

6.2.2.3 Effect of TF loaded formulations on lymphoid organ index

The reported literature support that, CFA-injected rats develop splenomegaly and generalized lymphadenopathy. Figure 6.3 (a&b) presents the spleen and thymus index of NC, DC, FD-gel, TF-LCNP gel, and TF-oral. DC group treated with TF-LCNP gel has significantly lowered the spleen and thymus index ($p < 0.001$, $p < 0.05$ and $p < 0.05$) compared to the, FD gel and TF-oral. These findings indicated the anti-arthritic potential of TF-LCNP, this might be due to the lymphocyte's inhibition and reduced immunological responses.

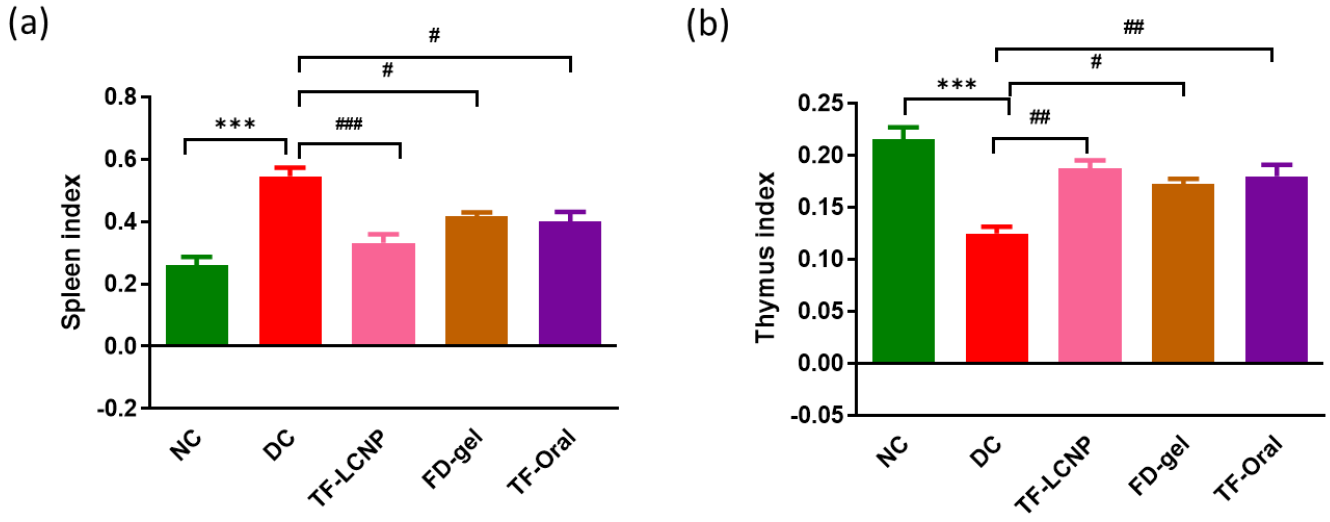

Figure.6.3. Effect of FD-gel, TF-oral, and TF-LCNP gel on (a) Spleen index (b) Thymus index

6.2.2.4 Radiographic analysis

The characteristic pathological features of the CFA model are bone erosion, joint space reduction, and periarticular soft tissue swelling. These symptoms were clearly observed in the DC group. Figure 6.4 presents the occurred pathological changes on CFA models on treatment with developed TF-LCNP gel. It was observed from Figure 6.4 that the NC group showed normal joint space without any swelling and deformity. A nearly similar picture results were obtained with TF-LCNP gel treated group. Compared to the plain gel treated and TF oral groups, the TF-LCNP gel treated groups showed reduced bone erosion, joint space reduction, and periarticular soft tissue swelling (TF-LCNP > FD gel ≥ TF oral). The above-mentioned interpretation was supported by the radiological score data. The effect of formulation on X-ray Radiography score was calculated and shown in Figure 6.4 the highest radiographic score was observed with the DC group and it was significantly reduced in the TF-LCNP treated group. The statistical significance by Bonferroni

multi comparison test value between the DC group vs FD-gel, TF-LCNP and TF-oral was #p < 0.05, ##p < 0.01, and non-significant respectively. The lowest radiographic score with TF-LCNP treated group confirms the effective delivery of TF to the inflammation site compared to oral administration.

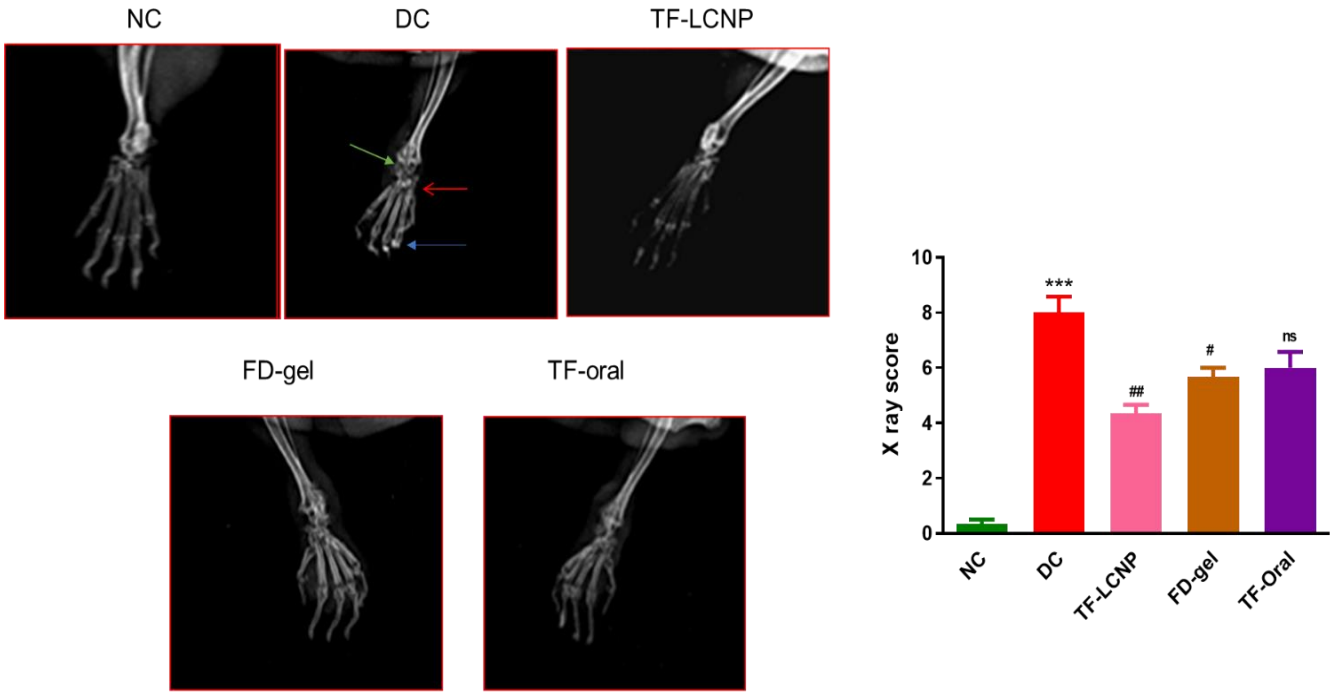

Figure 6.4. The radiographic images of NC, DC, and TF-LCNP gel treated groups. The DC showed the degeneration of digital ends (→), swelling of soft tissue (→), and reduction in joint space (→). The Effect of formulation on X-ray Radiography score. *All values were expressed as mean ± SEM (n = 3). Statistical significance was determined by one-way ANOVA followed by Banferroni multiple comparison test. All the values were compared with vehicle control group when *p < 0.05, **p < 0.01, ***p < 0.001.*

6.2.3 Quantitative analysis of CD44 protein expression in the CFA model

Figure 6.5. shows the levels of CD44 expression in the diseased model before and after treatment with FD-gel, TF-LCNP, and TF-oral formulations. It was observed that, the expression of CD44 protein in RA induced rat model was 5.40-fold higher than that in normal control (p < 0.001). The obtained data reflected that the developed TF-LCNP has lowered the CD44 levels compared to plain gel and TF-oral (p< 0.05). These findings were consistent with previous reports that levels of CD44 have been overexpressed in RA inflammatory sites which are in relation with severity of the inflammation [5,6]. The lower levels of CD44 upon treatment with developed formulations might be due to upon application of the TF-LCNP gel could be due to the efficiency of LCNP to permeate and retain in the dermal layers and releasing the TF in sustained manner. This could lead

to accumulation of TF at the RA inflammatory site and exerting pharmacological effects for a prolonged time.

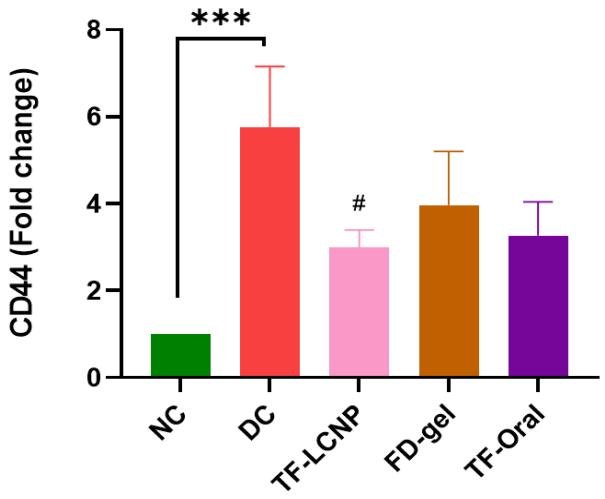

Figure 6.5. The mRNA expression levels of CD44 on FD-gel, TF-oral, and TF-LCNP gel treated groups

6.2.4 Cytokine's assessment

The widely accepted approach for understanding the diagnosis and prognosis of RA is the determination of cytokines levels in serum. Because in RA condition, the accumulation of pro-inflammatory cytokines TNF-α, IL-1, IL-6, and IFN-γ causes mobilization of leukocyte infiltration and edema. Further, these cytokines affect the COX-2 expression and increase the level of PEG2. The serum cytokine levels of TNF-α, IL-1, IL-6, IL-10, PGE-2, and IFN- in arthritis rats were compared with the NC. The cytokine levels of TNF-α, IL-1, IL-6, PGE-2, and IFN-γ were significantly reduced in DC group upon treatment with the TF-LCNP formulation when compared with the conventional TF-oral and plain gel. The levels of cytokines in NC, DC, and treated groups (with developed formulations, plain gel, TF-LCNP gel, and TF-oral) are presented in Figure 6.6. In addition, IL-10 is an anti-inflammatory cytokine that is involved in the regulation of the JAK-STAT signaling pathway in RA conditions. In this study, the immunized rats with CFA showed decreased levels of IL-10 compared to NC. A significant increase in IL-10 cytokines level was observed upon treatment with TF-LCNP gel compared to FD-gel and TF-oral. Here, Figure 6.6 the statistical significance was flagged as $^{###}P<0.001$, $^{##}P<0.01$, $^{#}P<0.05$.

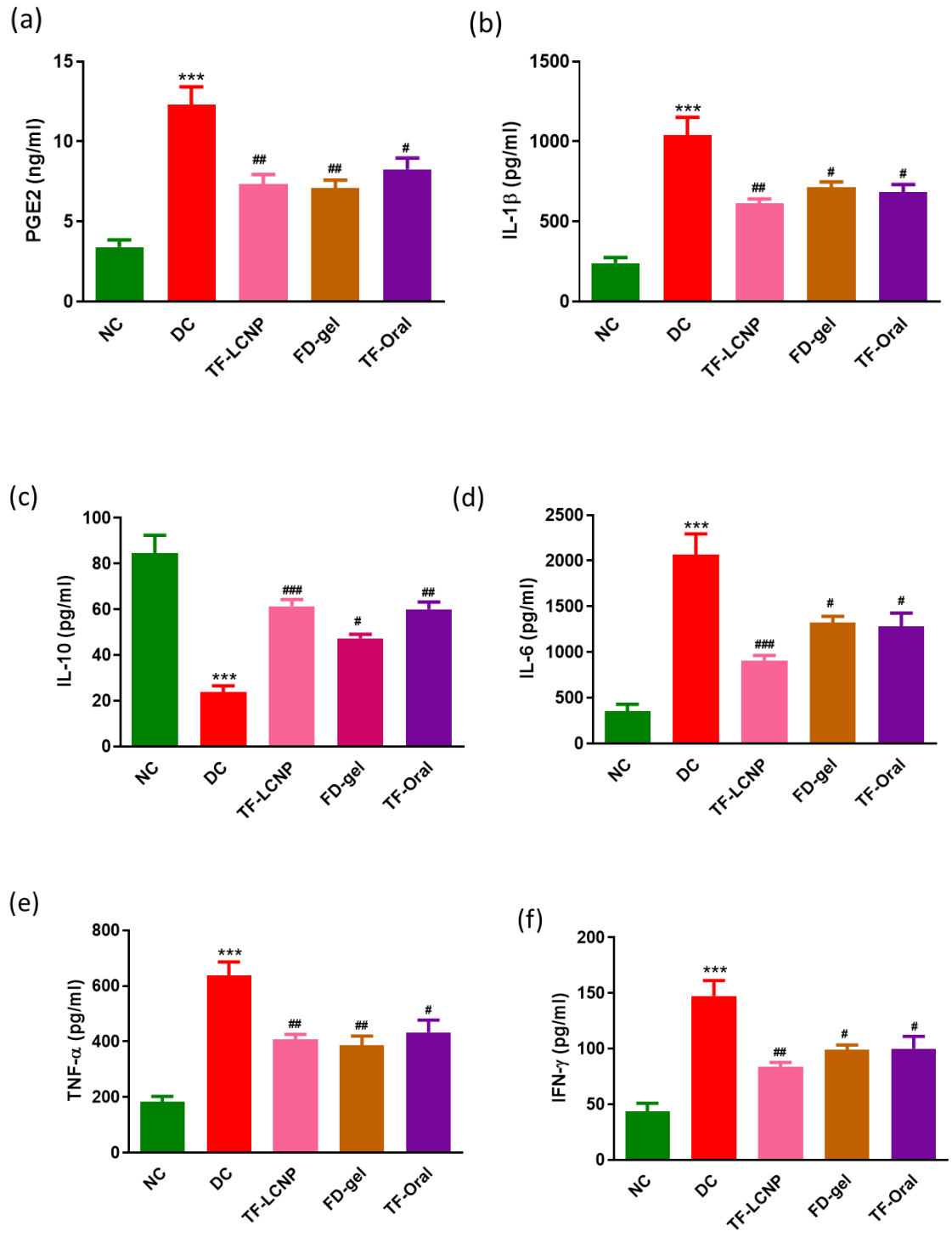

Figure 6.6. Effect of FD-gel, TF-oral and TF-LCNP gel on the levels of (a) PGE-2 (b) IL-1β (c) IL-10 (d) IL-6 (e) TNF- α (f) IFN-γ. All values were expressed as mean ± SEM (n = 3). *Statistical significance was determined by one-way ANOVA followed by Banferroni multiple comparison test.*

6.2.4.1 Evaluation of hematological parameters

The hematological parameters data (Figure 6.7) during day 29th for NC, DC, and formulation treated groups on topical application showed that there was no significant difference in neutrophil count in any of the treated groups. Whereas, it was observed that compared to plain gel treated CFA rats, the rats treated with TF-LCNP gel formulations has significantly higher RBCs ($^{\#}P<0.05$) and haemoglobin level ($^{\#\#}P<0.01$). These findings confirmed the indication of healthiness and decreased inflammatory condition in CFA rats.

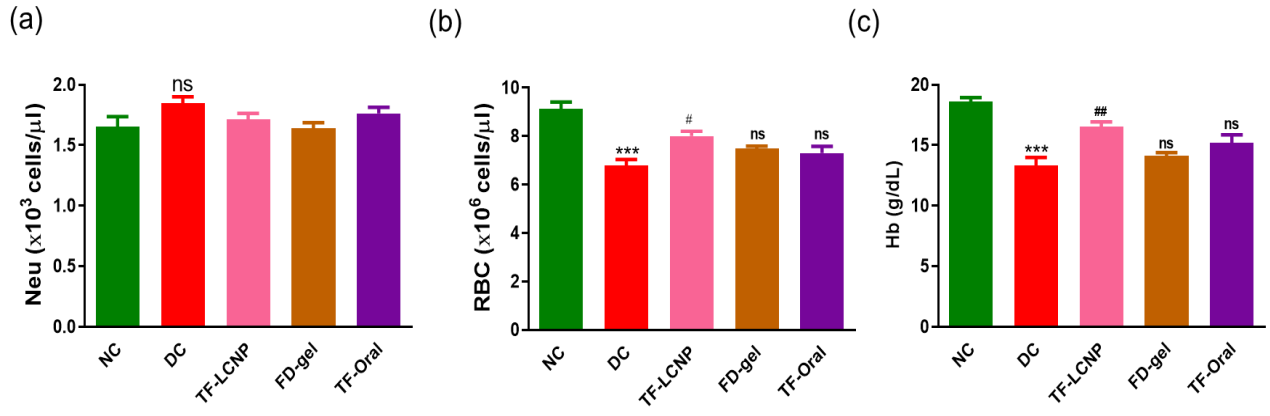

Figure 6.7. Effect of FD-gel, TF-oral, and TF-LCNP on (a) Neutrophil count (b) RBC (c) Hb count. *All values were expressed as mean ± SEM (n = 6). Statistical significance was determined by one-way ANOVA followed by Bonferroni multiple comparison test. All the values were compared with disease control group when #p < 0.05, ##p < 0.01, ###p < 0.001*

6.2.4.2 Histopathological observations of ankle joint

On the 29th day of study, the histological assessment of an arthritic paw was performed. The representative joint histopathology of the NC, DC, FD-gel treated, TF-LCNP, and TF-oral groups are presented in Figure 6.8. The NC group showed intact ankle joint without any abnormality. Whereas, the CFA-administered rat groups exhibited the hallmarks of RA i.e., higher number of infiltrating cells and pannus formation, degradation of bone, synovial thickening, and articular inflammation. Upon treatment with the developed formulations, we observed that the infiltrating cells count, pannus formation, synovial thickening were successfully reduced with TF-LCNP gel when compared to the FD-gel and TF-oral treated groups. In contrast, the TF-LCNP treated ankle joint showed a very low level of infiltrating cells, and reduced edema. These findings confirm that the TF-LCNP gel on topical application restored the joint space, lowered the joint tissue swelling and bone erosion to much extent.

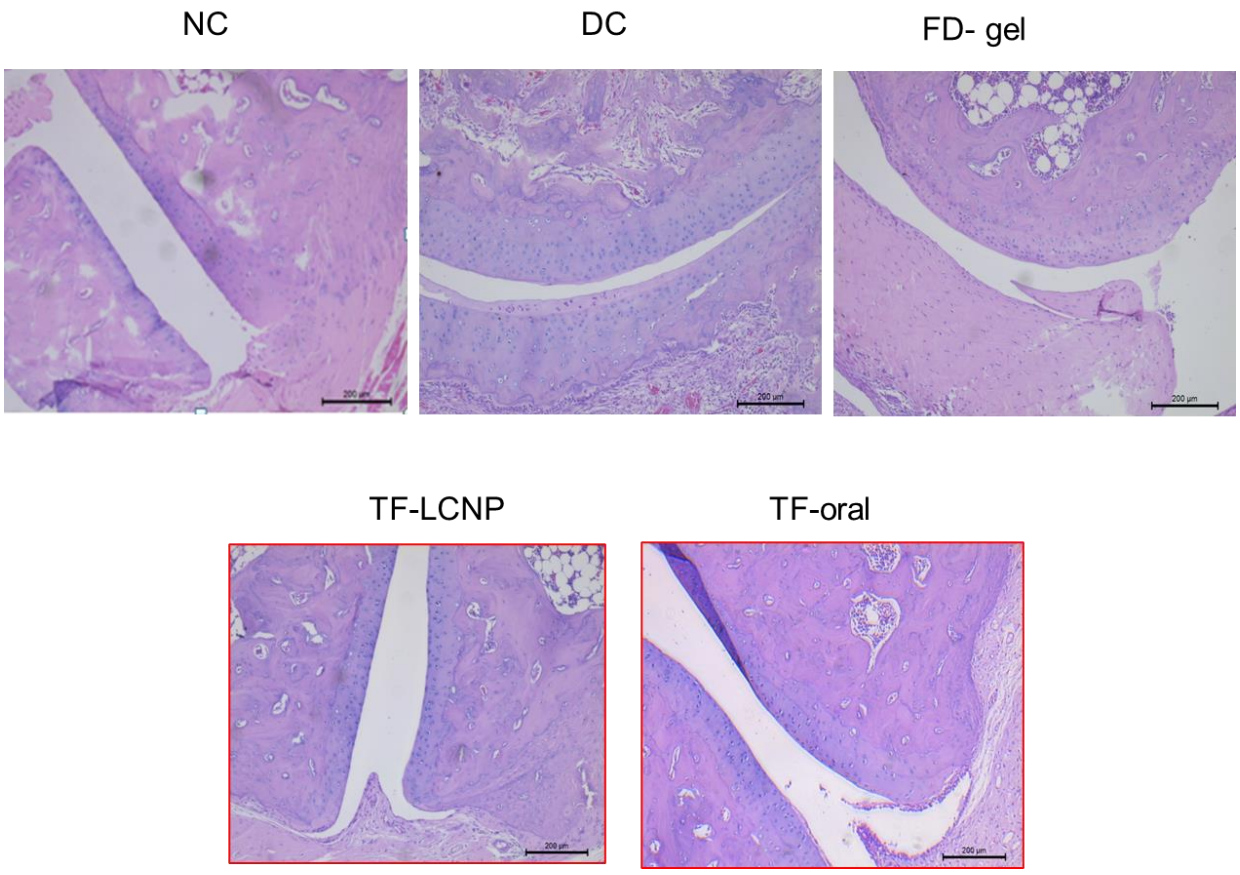

Figure 6.8. Histopathology sections of the NC, DC, FD-gel, TF-oral and TF-LCNP treated groups. Complete Freund's Adjuvant induced joint (DC) showing synovial hyperplasia, edema, inflammatory cell infiltrate (⟶), and narrowing of joint space (⟷). The reversal of these pathological changes induced by CFA upon treatment with N-TF-PG, and HA-TF-PG.

6.3 Formulation II: *In vivo* efficacy evaluation of the optimized hyaluronic acid and chondroitin sulphate coated tofacitinib loaded proglycosomes in the RA induced animal model

6.3.1 Physical parameters assessment

In the disease control model, based on the severity of inflammation the reduction in the body weight, swelling of paw volume, and increase in arthritic score values were observed. This could be due to the lipids and protein metabolism alteration, stress, less food intake and allodynia. Upon treatment with developed formulations the weight was significantly increased. The FCA immunized rat's representative images are presented in Figure 6.9a.

6.3.1.1 Paw volume and arthritis score

Further, to understand the RA severity, paw volume was measured and an arthritis score was calculated. Figure 6.9a presents the representative digital camera images of day 28th with and

without treatment of FD-gel, N-TF-PG gel, HA-TF-PG gel, CS-TF-PG gel formulations, and TF-oral. The disease model showed complete erythema and swelling of both toe and ankle and the complete reversal was observed with the formulation treated groups. The arthritic score was maximum in the DC group (4±0.28) and lowered significantly in the N-TF-PG gel (1.05 ±0.21), HA-TF-PG gel (0.8±0.14), CS-TF-PG gel (0.7±0.14), FD gel (3.15±0.14) and TF oral (3.1±0.42) on 21st day. The increase in paw volumes and arthritic index of NC, DC and developed formulation treated group rats on 3rd and 28th day are presented in Figure 6.9b and 6.9c. The paw volume and arthritis score were found to be significantly reduced with the HA-TF-PG gel (P<0.001), CS-TF-PG gel (P<0.001) whereas similar upon treatment with TF oral and FD gel.

6.3.1.2 Body weight

Compared to the healthy rats, the immunized diseased control group showed a significant ($p < 0.001$) decrease in body weight from day 3rd. Upon topical application of FD-gel, N-TF-PG gel, HA-TF-PG gel, CS-TF-PG gel and orally administered TF (TF dissolved in carboxy methyl cellulose; TF-oral), the body weights of rats increased significantly i.e., $^{\#}p < 0.05$, $^{\#\#}p < 0.01$, and $^{\#\#\#}p < 0.001$ respectively (Figure 6.9d). The order of weight gained upon treatment was HA-TF-PG> CS-TF-PG ≥ N-TF-PG> FD gel > TF oral.

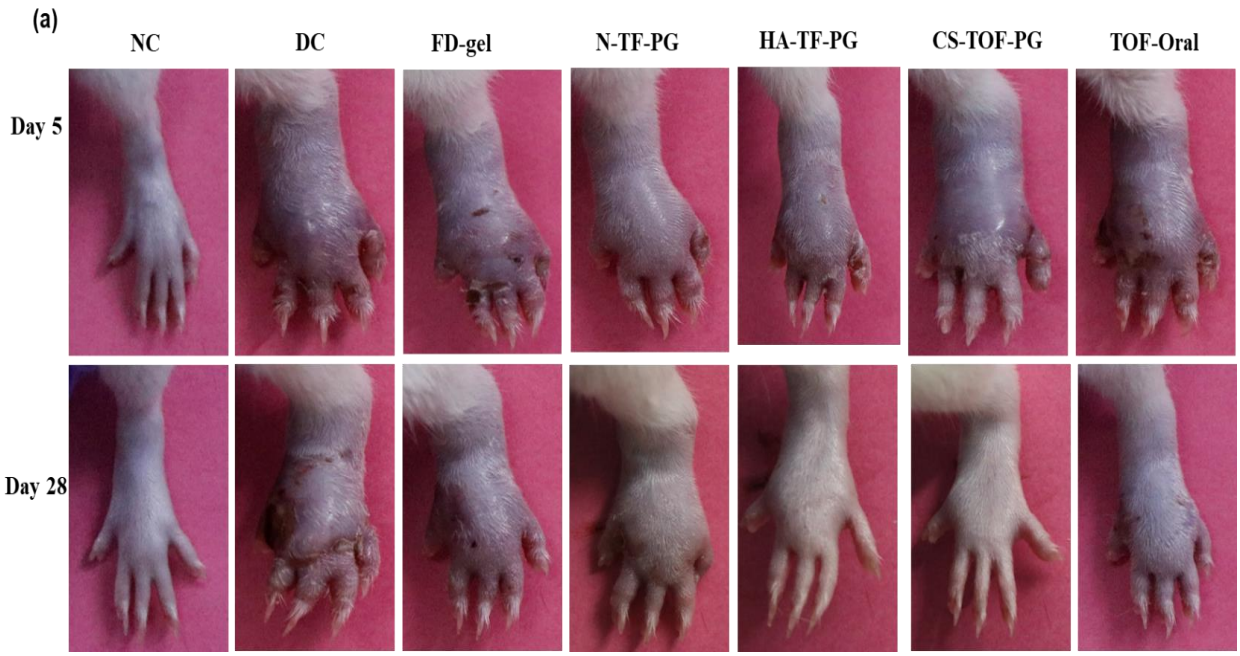

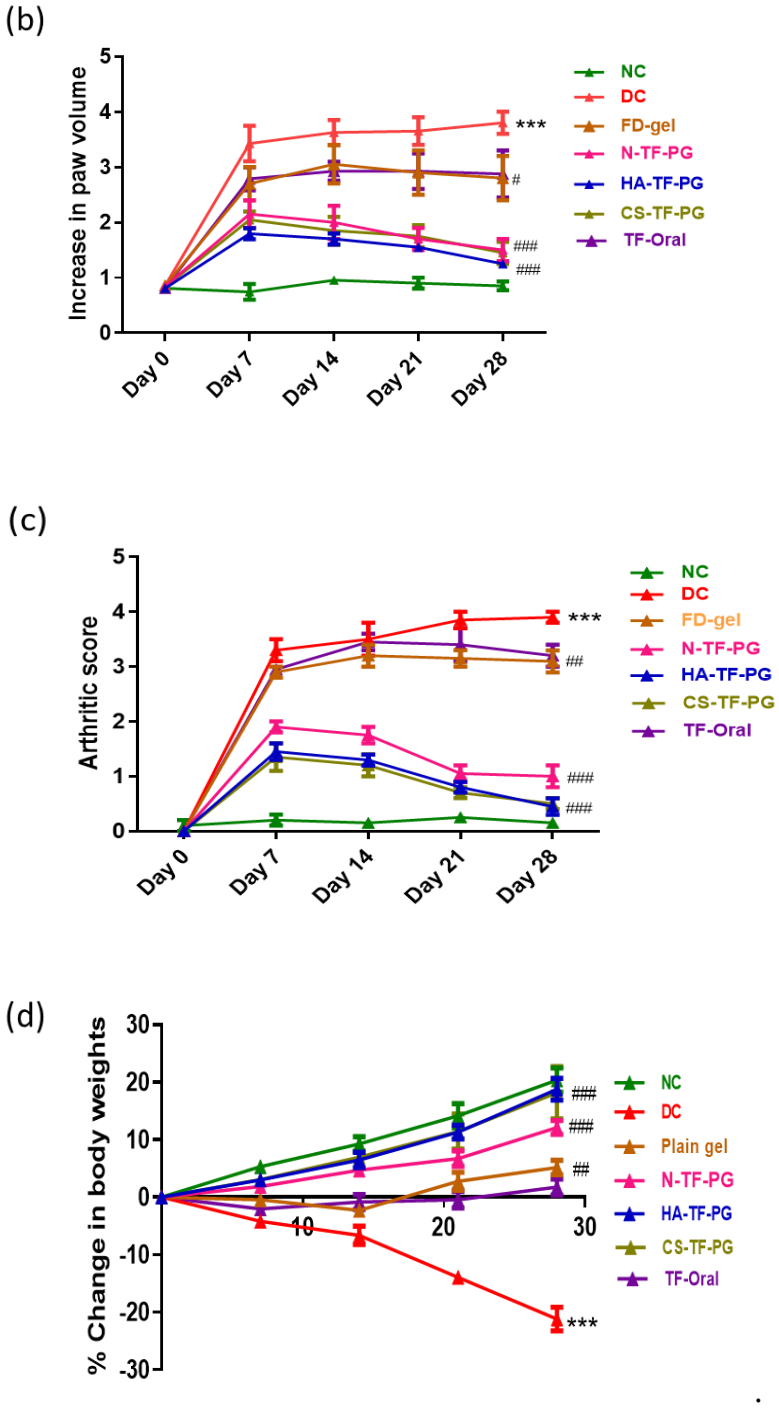

Figure 6.9. The effect of N-TF-PG, HA-TF-PG, and CS-TF-PG gel on topical application to treat arthritis inflammation and bone destruction, (A) representative digital photographs of the right hind limb of animals treated with various developed formulations in CFA rat (B) Measurement of paw volume (C) arthritis score

6.3.2 Spleen and thymus index

The increase in spleen and thymus index is related to splenomegaly and lymphadenopathy. Spleen and thymus index were increased in DC group upon treatment with HA-TF-PG gel, and CS-TF-PG gel it was normalized. Treatments of disease induced rats with HA-TF-PG gel and CS-TF-PG gel has significantly lowered ($p < 0.001$) spleen and thymus index compared to the DC group, (Figure 6.10a and 6.10b). Whereas, treatment with FD gel, and TF oral showed a slight reduction in spleen and thymus index.

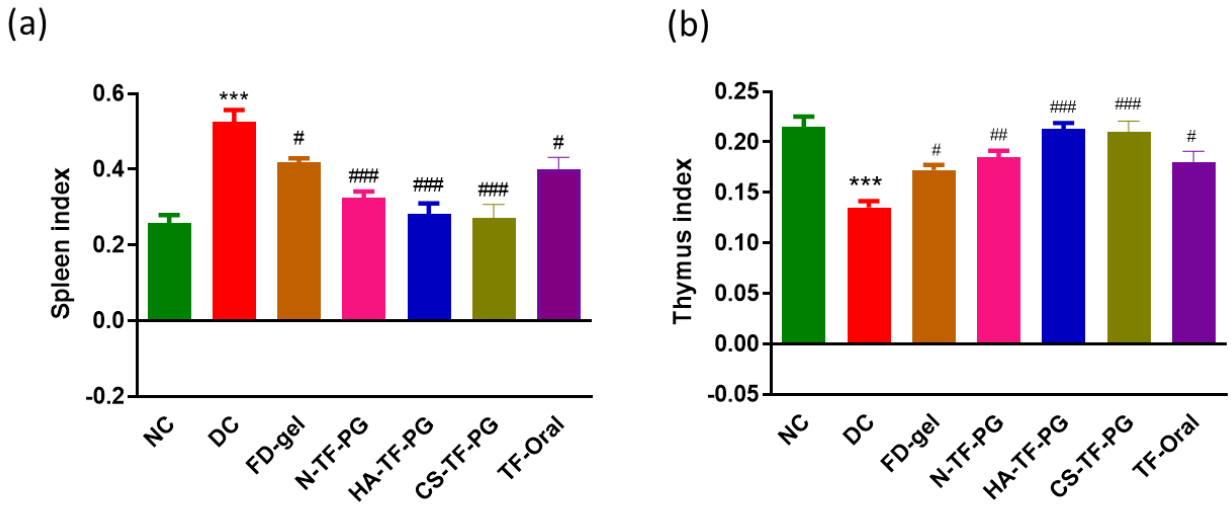

Figure 6.10. The effect of FD gel, TF oral, and CS-TF PG gel in CFA rat on topical, (a) Spleen index, (b) Thymus index, (n=6, # $p < 0.05$, # # $p < 0.01$ # # # $p < 0.001$ vs. disease control)

6.4 X-ray Radiographic study

The radiographs were taken after the treatment with N-TF-PG gel, HA-TF-PG gel CS-TF-PG, FD gel, and TF oral were compared with NC and DC for degeneration of digital ends, swelling of soft tissue and reduction in joint space (Figure 11A). The obtained radiographic score indicated that HA-TF-PG, and CS-TF-PG were more effective than the N-TF-PG gel, FD gel and TF oral. The highest radiographic score was observed with the DC group and it was significantly reduced by 75 %, 75%, 50 %, 35 % and 35 % with CS-TF-PG, HA-TF-PG gel, N-TF-PG gel, FD gel, and TF oral treated groups. The effect of formulation on X-ray radiography score was calculated and presented in Figure 11B.

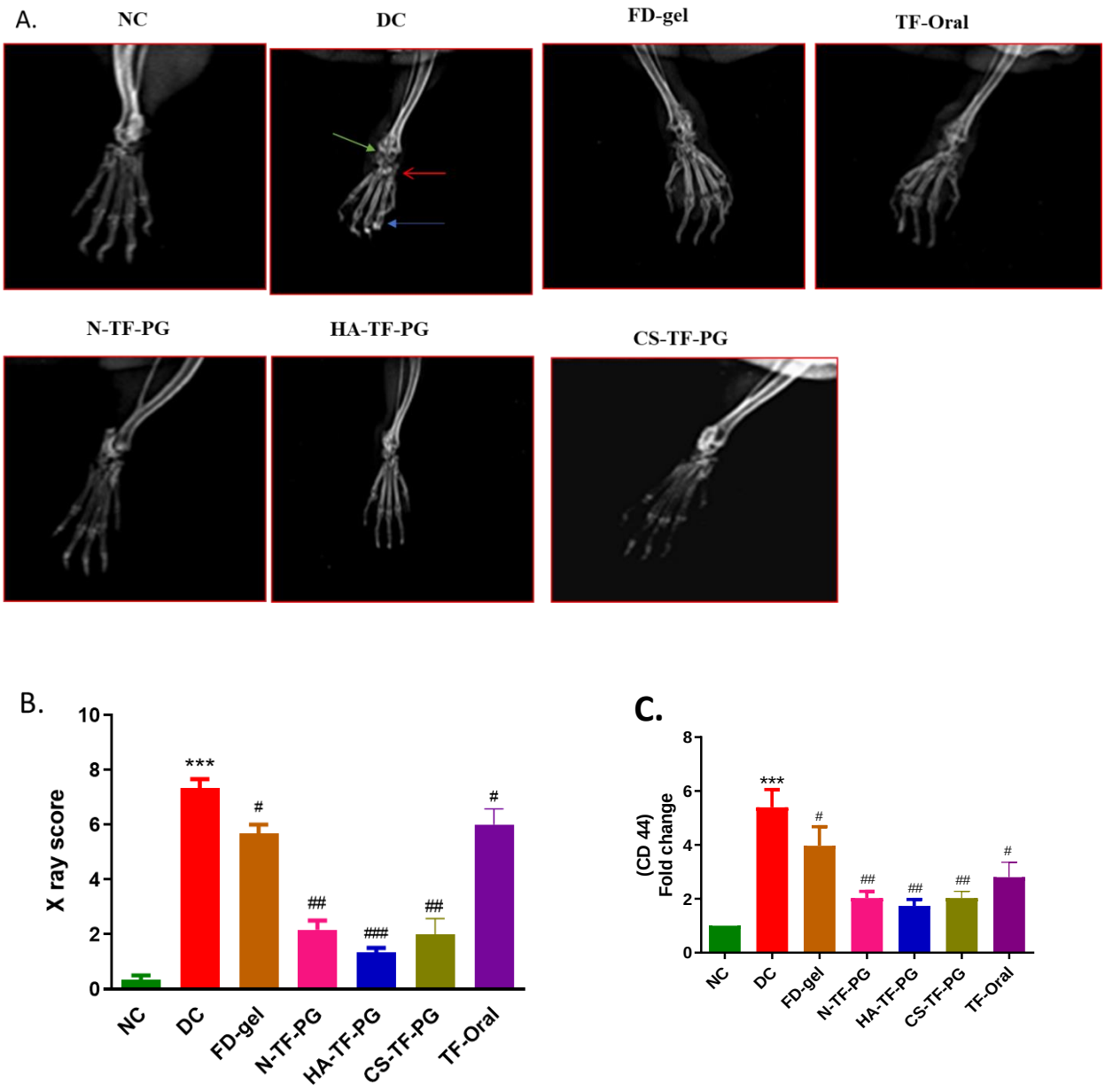

Figure.11. The effect of N-TF-PG, HA-TF-PG, CS-TF-PG gel on topical application to treat arthritis inflammation and bone destruction. The DC group showed the digital ends degeneration (⟵), soft tissue swelling (⟵) and reduction in joint space (⟵) (A) representative x- ray photographs of the right hind limb of animals treated with various FD gel, TF oral, and CS-TF PG gel in CFA rat (B) Measured x-ray score, (C) CD44 level, *(n = 6, #p < 0.05, ##p < 0.01, ###p < 0.001 when compared to the disease model*

6.5 Quantitative analysis of CD44 protein expression in the CFA model upon treatment with developed formulation

The expression of CD44 protein in the disease control was 5.7-fold higher than that in normal control ($p < 0.001$). Upon treatment with the developed formulations, the HA-TF-PG, CS-TF-PG has significantly lowered the CD44 levels compared to N-TF-PG gel, FD-gel and TF oral administration i.e., 1.95 and 1.4-fold respectively ($p< 0.001$). The levels of CD44 expression in the diseased model before and after treatment with developed gel formulations was showed in Figure 6.11C. The obtained data was supported by CD44 expression marker on macrophages, this was significantly reduced upon treatment with HA-TF-PG gel, CS-TF-PG gel compared to FD gel, TF oral and DC group. This could be due to the anchor of this CS to the surface of skin cells with high CD44 expression which lead to site specific accumulation of TF at the inflammatory site on topical application. The findings confirm that the HA and CS potentiates the anti-inflammatory activity of TF.

6.6 Cytokine assessment using cytometric bead array (CBA) technique by flow cytometry and ELISA

CFA immunization in rats triggers a variety of cytokines, such as increased pro inflammatory (PGE-2, IL-1, IL-6, TNF-α, and IFN- γ) and decreased anti-inflammatory (IL-10) cytokines. These aggravates the inflammatory response and ultimately leads to the leukocyte's infiltration mobilization, edema, cartilage destruction, and bone erosion [4]. The pro-inflammatory cytokines levels PGE-2, IL-1, IL-6, TNF-α, and IFN- γ were found to be significantly higher in DC i.e., 10.8 ng/mL, 888 pg/mL, 1900 pg/mL, 548 pg/mL, and 120 pg/mL respectively. The levels of cytokines before and after treatment with N-TF-PG, HA-TF-PG, CS-TF-PG, FD-gel and TF oral are illustrated in Figure 6.12. After the treatment with HA-TF-PG gel and CS-TF-PG gel, there was a remarkable decrease in the all the cytokines levels PGE-2 (4.1 ± 0.85 and 4.5 ± 0.61 ng/mL), IL-1(397.66 ± 66.66 and 410 ± 89.83 pg/mL), IL-6 (438.66 ± 140.98 and 450.33 ± 145.50 pg/mL), TNF-α (189.33 ± 70.43 and 257 ± 60.22 pg/mL), IL-10 (68.33 ± 10.06 and 74.66 ± 11.67 pg/mL), and IFN- γ (55.33 ± 11.67 and 62 ± 9.16 pg/mL) which were close to normal control. In addition, an anti-inflammatory cytokine (IL-10) is involved in the regulation of the JAK-STAT signaling pathway in RA conditions. Reduction of IL-10 ($P< 0.001$) has been observed in arthritis, upon treatment with HA-TF-PG and CS-TF-PG gel the level have been increased significantly ($P< 0.001$).

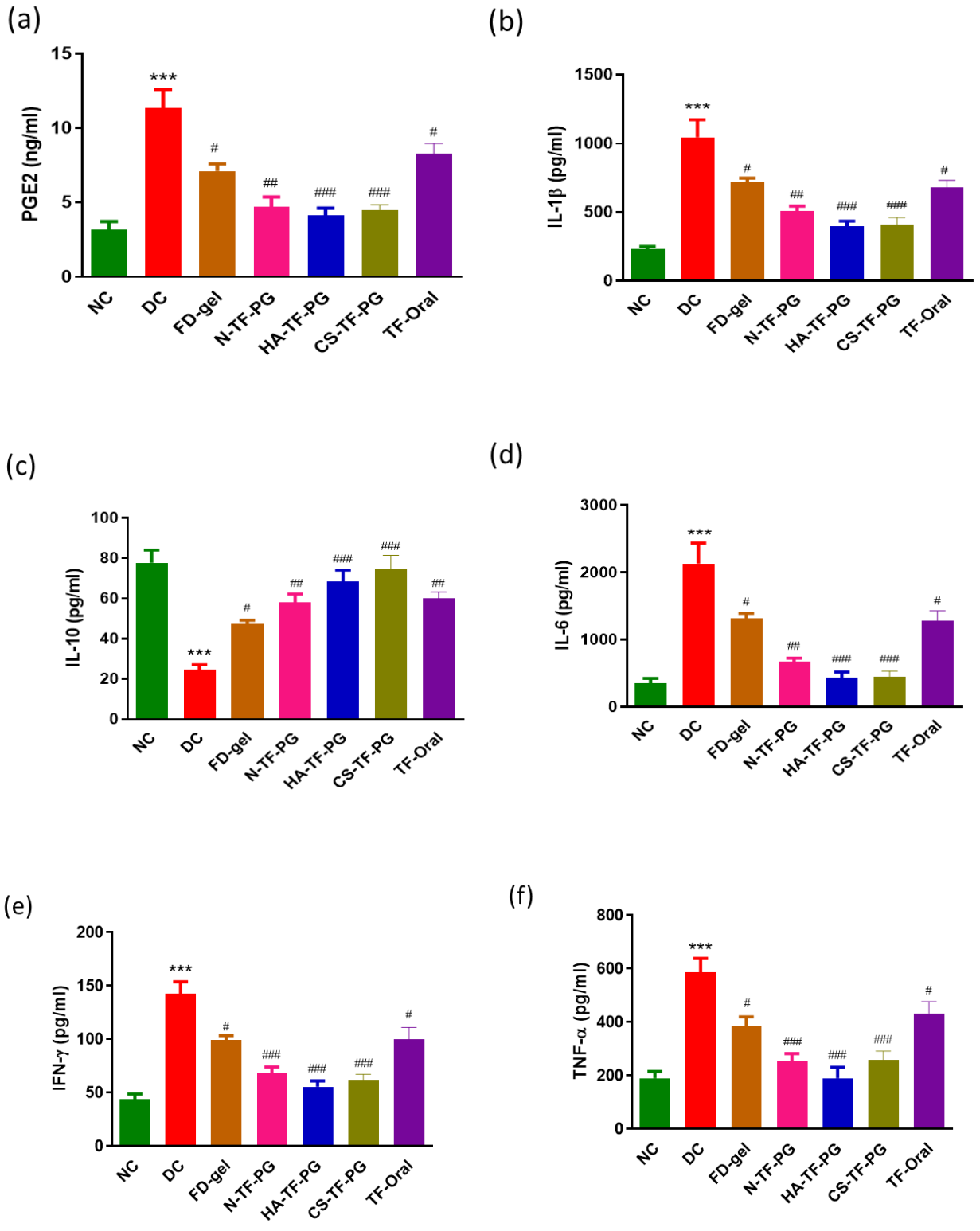

Figure 6.12. The levels of the inflammatory cytokines in serum after the treatment of CFA rats with CS-TF-PG gel, TF oral, and FD gel. (A) Level of PGE-2, (B) IL-1β b, (C) IL-6, (D) TNF-α, (E) IL-10, (F) IFN- γ, results are shown as mean ± SD *(n = 6, # p < 0.05, ## p < 0.01 ### p < 0.001 vs. disease control)*

6.7 Measurement of hematological parameters

The haematological parameters data i.e., Neutrophil count, RBC, hemoglobin count was presented in Figure 6.13. DC group treated with FD gel and TF oral showed only a partially increase in RBC and Hemoglobin i.e., 30% only. Whereas, the HA-TF-PG, CS-TF-PG treated group reversed the RBC and hemoglobin levels equal to NC group. Also, with respect to the neutrophils count no significant change was observed among the groups.

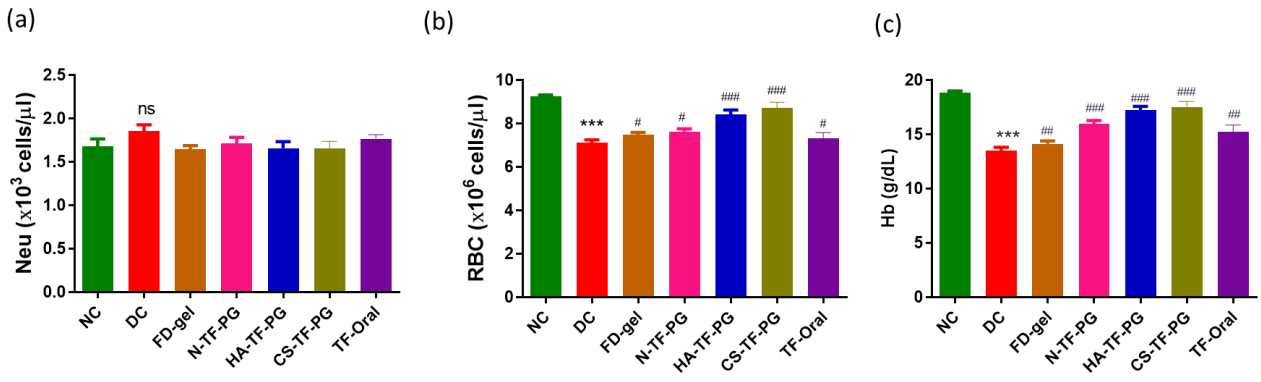

Figure 6.13. The assessment of (a) Neutrophil count (b) RBC (c) Hb count upon treatment with FD-gel, N-TF-PG, HA-TF-PG, CS-TF-PG gel and TF oral. All values were expressed as mean ± SEM (n = 6). *Statistical significance was determined by one-way ANOVA followed by Banferroni multiple comparison test. All the values were compared with disease control CFA group when #p < 0.05, ##p < 0.01, ###p < 0.001*

6.8 Histopathological observations of ankle joint

The histological assessment of all the groups was performed on the 29th day of study. The joint histopathology of the NC, DC, N-TF-PG, HA-TF-PG and CS-TF-PG, FD gel, and TF oral was illustrated in Figure 6.14. The DC group showed maximum infiltration of inflammatory cells, bone degradation, thickening of synovium, pannus formation, and articular inflammation. As per the results, HA-TF-PG and CS-TF-PG treated group showed minimal infiltrating cells count, pannus formation, synovial thickening whereas FD-gel and TF oral treated groups showed moderate infiltrating cells and pannus formation.

The final confirmation of radiological and histopathological analysis discloses that HA-TF-PG and CS-TF-PG treated group showed cartilage formation, reduction in joint space, lowered deformations and swelling in comparison to DC and other treatment groups. This could be due to the CD44 mediated active targeting of HA-TF-PG and CS-TF-PG to the specific inflammatory sites i.e., dermal and synovial regions.

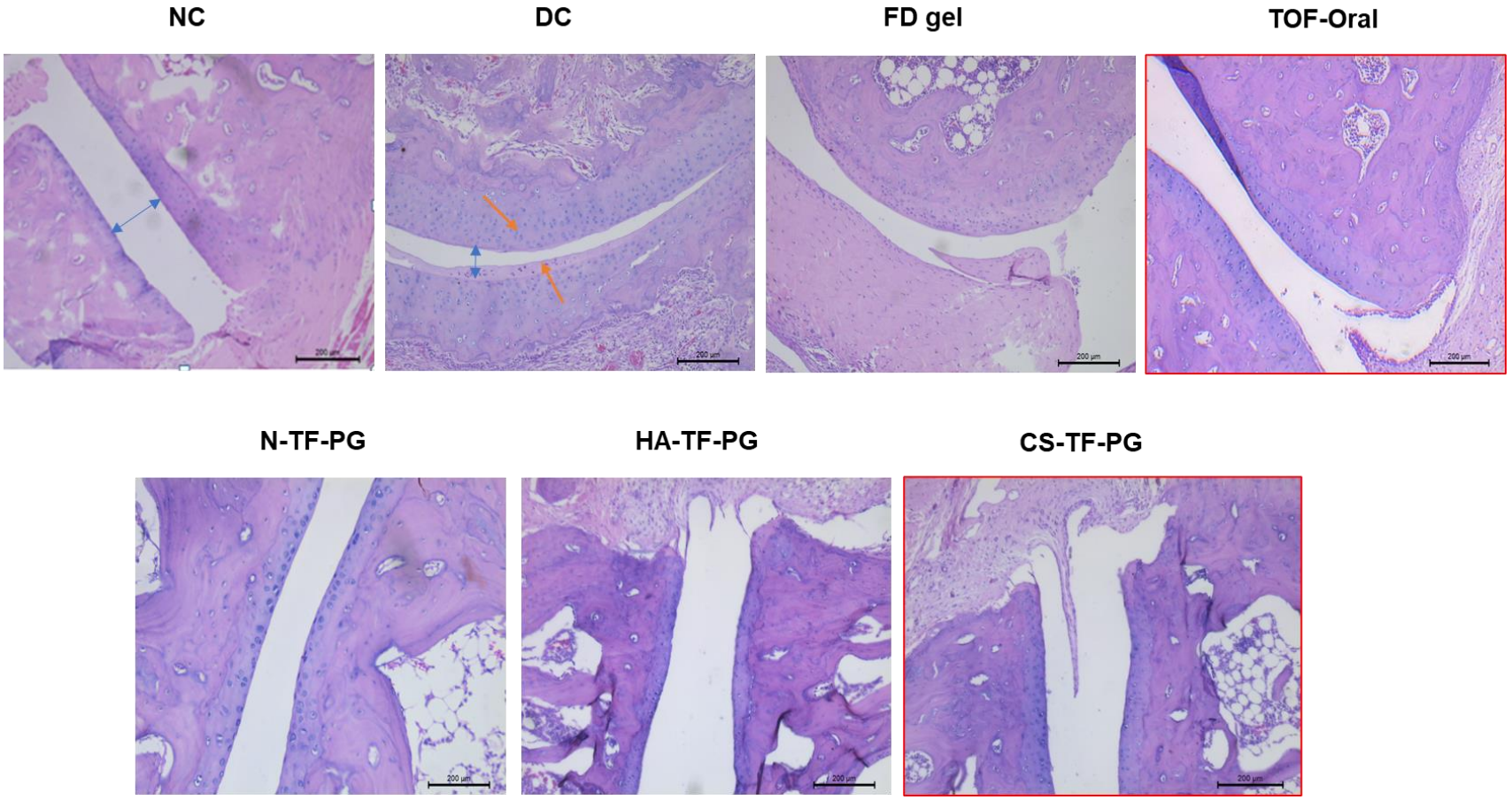

Figure 6.14. Histopathological examination of ankle joints from CFA rats treated with FD gel, TF oral, and CS-TF PG gel. The joint tissue sections were stained with haematoxylin–eosin (H&E). DC group showing synovial hyperplasia, edema, inflammatory cell infiltrate (→) and joint space narrowing (↔).

6.9 Conclusion

Based on the work and results, it was observed that TF was not detected in blood, till 6h, in case of developed formulations HA-TF-PG and CS-TF-PG gels whereas, in case of plain gel TF concentration in blood found to be 65.77 ± 2.45 ng/mL at 6h and in case of N-TF-PG gel concentration found to be 42.23 ± 1.78 ng/m. The results suggested that maximum amount of drug retained in skin in developed formulations HA-TF-PG and CS-TF-PG gels without reaching systemic circulation. The in-vivo efficacy study findings, upon treatment with HA-TF-PG and CS-TF-PG to CFA rats, suggested that the CD44 expression was significantly lowered upon treatment with these formulations and thus confirms that HA and CS has the potential to bind to the CD44 and lower its levels. In addition, CS and HA showed its positive effect by active targeting approach by anchoring to CD44, reduced inflammatory cytokines storm and repaired cartilage damage efficiently. The current study ensured that the HA-TF-PG and CS-TF-PG loaded sepineo P600 gels systems would provide a safe and effective formulation for localization of TF at the RA site and overcome the adverse effects associated with the TF.

References

1. Foyet HS, Tsala DE, Zogo ZE, Carine AN, Heroyne LT, Oben EK. Anti-inflammatory and anti-arthritic activity of a methanol extract from Vitellaria paradoxa stem bark. *Pharmacognosy Res.* 7(4), 367–377 (2014).

2. Sudha Yalamarthi S, Puppala ER, Abubakar M, *et al.* Perillyl alcohol inhibits keratinocyte proliferation and attenuates imiquimod-induced psoriasis like skin-inflammation by modulating NF-κB and STAT3 signaling pathways. *Int. Immunopharmacol.* 103, 108436 (2022).

3. Dey P, Puppala ER, Naidu VGM, Das G, Ramesh A. Multifunctional Synthetic Amphiphile for Niche Therapeutic Applications: Mitigation of MRSA Biofilms and Potential in Wound Healing. *ACS Appl. Bio Mater.* 3(12), 8830–8840 (2020).

4. Puppala ER, Jain S, Saha P, *et al.* Perillyl alcohol attenuates rheumatoid arthritis via regulating TLR4/NF-κB and Keap1/Nrf2 signaling pathways: A comprehensive study onin-vitro and in-vivo experimental models. *Phytomedicine.* 97, 153926 (2022).

5. Zhang Y, Xia Q, Li Y, *et al.* CD44 Assists the Topical Anti-Psoriatic Efficacy of Curcumin-Loaded Hyaluronan-Modified Ethosomes: A New Strategy for Clustering Drug in Inflammatory Skin. *Theranostics*. 9(1), 48–64 (2019).

6. Lindqvist U, Phil-LI. Dermal distribution of hyaluronan in psoriatic arthritis; coexistence of CD44, MMP3 and MMP9. *Acta Derm. Venereol.* 92(4), 372–7 (2012).

7 Summary and conclusion

RA is a ubiquitous chronic systemic inflammatory polyarthritis progressive autoimmune disorder that commonly affects wrists, proximal interphalangeal joints, metacarpophalangeal joints, knees, and ankles. The clinical presentation of RA includes articular manifestations (joint pain, swelling, and early morning stiffness) and extra-articular manifestations (myalgia, fatigue, and rheumatoid nodules). These affect the person's socioeconomic life and long-term outcomes such as physical disability reduced quality of life and increased mortality. Globally more than 14 million people are affected by RA and it was estimated that the global prevalence rate range from 0.24 to 1%. It can occur in any age group most likely in 20-45 years of age but it is 3 times more common in females than males.

The causes of RA are still under investigation. According to recent findings, it has been reported that lymphocytes play a key role in the pathogenesis of RA by releasing pro-inflammatory cytokines. Also, several signal transduction pathways have been incriminated in RA progression. TF is an orally available anti-rheumatoid agent approved by the FDA for the treatment of moderate to severe RA as a specific inhibitor of JAK 1 and JAK 3. Regardless of its significant efficacy to treat RA, concerns about TF dose-dependent adverse effects cause hyperlipidemia, and long-term safety studies showed higher rates of pulmonary embolism and death when using high doses of 10 mg bid. These limit the therapeutic applications of TF.

Therefore, the topical route might be a preferred approach to overcome the adverse effects associated with oral administration of TF and to enhance patient compliance by a non-invasive technique. The topical treatment of pain needs an improved concentration of TF in the synovial region and skin layers as compared to the plasma concentrations. Topically applied drugs may have a depot effect in skin layers and exhibit sustained release of the drug into the surrounding tissues. But the major challenge on the topical application of TF is penetration through the stratum corneum and permeation into the deeper layers to the inflamed joint.

To overcome these issues in recent days, few attempts have been made for the topical administration of TF including proposomes and microneedles to treat various skin disorders. Lipid-based topical drug delivery gained importance because of rapid penetration through the epidermis of the skin with low toxicity. The Liquid crystal nanoparticles and vesicular drug delivery systems can easily permeate through the skin, but the percutaneous permeability depends on the elasticity of vesicles. The modified liposomes with ethanol and propylene glycol have

shown more skin permeability compared to the conventional liposomal formulations. The major reasons for the preparation of modified liposomes using propylene glycol (PG) exhibited good solubility for TF, less volatile, high boiling point, and well used in skin moisturizers. In addition, in a research study, it was reported that the PG-incorporated liposomes showed superior skin deposition over the traditional liposomes, ethosomes, and deformable liposomes. Also, in consideration of the above-discussed points and RA pathophysiology, the targeted delivery of TF via ligands in RA condition could be a better approach to achieve better efficacy.

During the inflammatory condition, the macrophages exhibit CD44 on the surface of macrophages and fibroblasts. It has been investigated that CD44 can recognize and bind glycosaminoglycan-based biomaterials. CD44 consists of a variant stem fibrin region as a binding site for HA and CS. HA is a natural, water-soluble, linear, and non-sulphated anionic glycosaminoglycan. CS is a water-soluble, unbranched sulphated anionic glycosaminoglycan with virtuous biodegradability, biocompatibility, and less toxicity. It is present in cartilage, and ligament, and it is well recognized to decrease the joint space's discomfort and narrowing.

Thus, we have investigated TF delivery via developing liquid crystal nanoparticles gel and modified liposomes (proglycosomes) gel to treat RA. Also, developed HA and CS-coated TF-loaded proglycosomes a novel nano-topical drug delivery system for targeting CD44 in the inflamed skin layers as a vehicle for TF. The developed formulations were evaluated for particle size, zeta potential, entrapment efficiency, SEM, TEM, and *in vitro* release. Also, *Ex vivo* studies conducted to know the permeation and retention potential in the skin layer and dermal kinetics were evaluated. A complete Freund’s adjuvant (CFA) induced arthritis rat model was established, and TF delivery and anti-arthritic efficacy using un-coated proglycosomes were compared with HA-coated proglycosomes and CS-coated proglycosomes. Also, the possibility of the topical administration of HA-modified proglycosomes and CS-modified proglycosomes to target inflammatory arthritis conditions involving high CD44 expression was analyzed.

Analytical method development is the foremost step in drug product development. The developed spectrophotometric method was used to analyze the amount of TF in LCNP formulation whereas the proglycosomes and surface-coated proglycosomes were analyzed using the validated HPLC method. The optimized chromatogram conditions exhibited retention time (6.1 min), which is a time-saving RP-HPLC method. The obtained LOD and LOQ values were found to be 16.5 and 49.5 ng/mL, indicating that this method has a higher sensitivity than previously reported RP-HPLC methods for TF. The currently validated

method was validated as per ICH guidelines with respect to stability-indicating property, robustness, and specificity. The acceptable values of % RSD and % bias less than 2% indicated that the validated RP-HPLC method is reliable and precise and is in excellent accordance with the regulatory guidelines. The specificity study confirmed that the developed analytical method could quantify TF in the presence of formulation excipients. The appropriateness of the method was also confirmed in dermatokinetics studies on the topical administration of TF. Further, a simple reversed-phase HPLC method in rat plasma for the determination of TF was developed. The validated bioanalytical method could be widely used for the analysis of 100 µL plasma samples with 10 min runtime for their routine analysis for understanding the in-vivo pharmacokinetic-pharmacodynamic studies.

The development of TF-loaded lipid nanocarrier systems i.e., LCNP, Proglycosomes (N-TF-PG), HA-TF-PG, and CS-TF-PG. Tofacitinib-loaded liquid crystal nanoparticles (TF-LCNP) were developed with the QbD approach. The TF-loaded LCNP showed a uniform nano-size range (60-70 nm) and exhibited sustained release for 24 h. TF-LCNP demonstrated 2.81-fold higher retention of TF in the viable dermis layers than in conventional formulation. The *in-vivo* pharmacodynamic study, cytokines, and radiographic study on Complete Freud's adjuvant-induced arthritic rat model revealed that LCNP exhibited a significant ($P < 0.05$) reduction in inflammation in arthritic rat paw compared to the conventional TF.

The optimized N-TF-PG exhibited a particle size of 100 nm with a cationic charge on the surface of ~ +38.5 mV. This charge can favor the strong interaction with the anionic HA and CS and lead to significant changes on particle size, PDI, and entrapment efficiency. Also, a suitable amount of HA and CS needs to be added to obtain satisfactory HA and CS-coated proglycosomes. The NMR data and FTIR confirms the electrostatic interaction i.e., non-covalent ionic interaction between the CS and proglycosomes. The SEM and TEM analysis of HA-TF-PG and CS-TF-PG are viewed as spherical hard shapes surrounded by distinct shell-like structures and the size was also well correlated with the dynamic light scattering data. The shell-like structure may be due to the hydrophilic HA and CS which could absorb the moisture. The sustained release behavior of HA-TF-PG, and CS-TF-PG was due to the double-barrier effect offered by HA and CS coating and phospholipid membrane.

After loading LCNP, HA-TF-PG, and CS-TF-PG into the SEPINEO P600 gelling system, it revealed a non-newtonian shear thinning, and pseudoplastic flow behavior. This property of

gelling system makes it suitable for topical application and the amplitude and frequency tests confirmed the good stability and structural strength.

Further, the skin permeation of HA-TF-PG and CS-TOF-PG showed higher permeation compared to FD gel which might be due to the negative charge of formulation which could create channels due to the repulsion between the lipid constituents of the skin and negatively charged particles. The enhanced permeation and localization of HA-TF-PG and CS-TF-PG could be due to the PG in the nanovesicle structure and CS coating respectively.

In order to investigate the safety and efficiency of localization and site-specific delivery in RA patients, the formulations were tested in CFA administered diseased RA model. In the disease control model, based on the severity of inflammation the reduction in the body weight and increase in paw volume were observed. This could be due to lipids and protein metabolism alteration, stress, less food intake, and allodynia. Upon treatment with developed formulations, the weight was significantly increased. The order of weight gained upon treatment was HA-TF-PG = CS-TF-PG > FD gel > TF oral. The paw volume and arthritis score were found to be significantly reduced with the HA-TF-PG and CS-TOF-PG gel ($P<0.001$) whereas similar upon treatment with TF oral and FD gel.

The HA-TF-PG and CS-TF-PG gel exhibited a stronger downregulation of the assayed cytokines and CD44 expression marker on macrophages than the FD gel and TF oral group ($p < 0.001$). This could be due to the anchor of this CS to the surface of skin cells with high CD44 expression which lead to site-specific accumulation of TF at the inflammatory site on topical application. The findings confirm that HA and CS potentiate the anti-inflammatory activity of TF. The final confirmation of radiological and histopathological analysis discloses that surface coated proglycosomes treated group showed cartilage formation, reduction in joint space, lowered deformations, and swelling in comparison to DC and other treatment groups. This could be due to the CD44-mediated active targeting of HA-TF-PG and CS-TF-PG to the specific inflammatory sites i.e., dermal and synovial regions.

Future scope

Further studies based on the present outcomes could include

- The developed formulation can be explored for a clinical study
- Further scale-up to larger batch sizes can be explored for the industrial ~~approach~~ production
- The targeted delivery of LCNP by surface modification with ligands to target receptors in RA condition
- Modified liposomes preparation using other surfactants (penetration enhancers) and a combination of surfactants

Appendix I

PUBLICATIONS FROM THESIS

Research

1. **Gorantla S,** Saha RN, Singhvi G. Exploring the affluent potential of glyceryl mono oleate–myristol liquid crystal nanoparticles mediated localized topical delivery of Tofacitinib: Study of systematic QbD, skin deposition and dermal pharmacokinetics assessment. Journal of Molecular Liquids. 2022 Jan 15; 346:117053.
2. **Gorantla S,** Saha RN, Singhvi G. Spectrophotometric method to quantify tofacitinib in lyotropic liquid crystalline nanoparticles and skin layers: Application in ex vivo dermal distribution studies. Spectrochimica Acta Part A: Molecular and Biomolecular Spectroscopy. 2021 Jul 5; 255:119719.
3. **Gorantla S,** Saha RN, Singhvi G. Design of experiment-driven stability-indicating RP-HPLC method for the determination of tofacitinib in nanoparticles and skin matrix. Future Journal of Pharmaceutical Sciences. 2021 Dec;7(1):1-2.
4. **Gorantla S,** Eswar Rao P, Naidu VGM, Saha RN, Singhvi G. Hyaluronic acid-coated proglycosomes for topical delivery of tofacitinib in rheumatoid arthritis condition: Formulation design, in vitro, ex vivo characterization, and in vivo efficacy studies. 2023 Jan 1224:207-222.
5. **Gorantla S,** Eswar Rao P, Naidu VGM, Saha RN, Singhvi G. Design of chondroitin sulphate coated proglycosomes for localized delivery of tofacitinib for the treatment of rheumatoid arthritis. 2023 May186:43-54.

Review

1. Gorantla S, Singhvi G, Rapalli VK, Waghule T, Dubey SK, Saha RN. Targeted drug-delivery systems in the treatment of rheumatoid arthritis: recent advancement and clinical status. Therapeutic Delivery. 2020 Apr;11(4):269-84.
2. Gorantla S, Gorantla G, Saha RN, Singhvi G. CD44 receptor-targeted novel drug delivery strategies for rheumatoid arthritis therapy. Expert Opinion on Drug Delivery. 2021 Nov 2;18(11):1553-7.
3. Gorantla S, Batra U, Samshritha RN, Puppala ER, Waghule T, Naidu VG, Singhvi G. Emerging trends in microneedle-based drug delivery strategies for the treatment of rheumatoid arthritis. Expert Opinion on Drug Delivery. 2022 Apr 3;19(4):395-407.

4. Waghule T, Dabholkar N, Gorantla S, Rapalli VK, Saha RN, Singhvi G. Quality by design (QbD) in the formulation and optimization of liquid crystalline nanoparticles (LCNPs): A risk-based industrial approach. Biomedicine & Pharmacotherapy. 2021 Sep 1; 141:111940.

Book chapters

1. Jain S, Gorantla S, Singhvi G. Nanomaterials for Drug Delivery. In: Nanotoxicology. Daima, H.K., Kothari, S.L., & Suresh Kumar, B. (Eds.). (2021). Nanotoxicology: Toxicity Evaluation of Nanomedicine Applications (1st ed.). CRC Press. https://doi.org/10.1201/9780429299742

AWARDS AND CONFERENCES ATTENDED

- **Srividya Gorantla** received **'Research Award 2021-2022 Winner Position under the Jeevanam category** in the '22nd Annual Science Awards and Memorial Oration Function of Dr. K. V. Rao Scientific Society' for presenting the research work. under jeevanam category for presenting the Research work entitled as "Exploring the Affluent potential of Glyceryl Mono Oleate – Myristol Liquid Crystal Nanoparticles Mediated Localized Topical Delivery of Tofacitinib: Study of Systematic QbD, Skin Deposition and Dermal Pharmacokinetics Assessment." Held on **1st October 2022, Hyderabad, Telangana**
- **Srividya Gorantla secured 2nd prize at Disso India at zonal level:** DRPI 2022 in association with the American Association of Pharmaceutical Scientists (AAPS) and APTI under central zone topper for the best oral presentation for the topic "Topical active dermal targeting of tofacitinib loaded hyaluronic acid-coated proglycosomes to CD44 on activated macrophages in rheumatoid arthritis condition". **Held on 16th July 2022**

PATENTS

- Granted patent on the "Process for preparing a lipid-based nanocarrier composition" **(Patent No. 396280; Date of Grant:06/05/2022)** In the names of Gautam Singhvi, Vamshi Krishna Rapalli, Tejashree Waghule, Srividya Gorantla, Sunil Kumar Dubey, Ranendra Narayan Saha.
- Patent filed on the "Topical Formulation Comprising Tofacitinib and Preparation Thereof" **(202111017452)** in the names of Srividya Gorantla, Gautam Singhvi, Rajeev Taliyan, Ranendra Narayan Saha.

Dr. Gautam Singhvi Biography

Dr. Gautam Singhvi is faculty in the Department of Pharmacy, BITS, Pilani. He has 15 years of research and teaching experience. Currently, he is involved in industrially feasible nanocarrier-based formulation development and optimization for various therapeutic agents. His team is extensively working on the QbD-driven design of topical drug delivery systems for rheumatoid arthritis, psoriasis, and fungal infections. He has published more than 80 publications in reputed international peer-reviewed journals and 15 book chapters with international publishers such as Elsevier, Springer, and Willy. He is actively involved in sponsored research projects from government funding agencies and pharmaceutical industries. As an inventor, he has filed 8 formulation patents. He is also a peer reviewer of several international journals. Dr. Singhvi has been listed in the "World Top 2% Scientists" in the 2021 and 2022 databases (Published in the journal of PLOS Biology: 19 October 2021 & 11 October 2022) created by experts at Stanford University, USA. He is very passionate about practicing the newer teaching pedagogy in his classroom and motivating students to face the challenges of the new era.

Prof. Ranendra N. Saha Biography

Ranendra N. Saha is a Former Vice Chancellor (Acting) of BITS-Pilani, Pilani campus and Former director of BITS-Pilani, Dubai Campus, UAE. He is a senior professor in the Department of Pharmacy, BITS. He has more than 35 years of teaching, research, and administrative experience. He is an expert in pharmacokinetic and dosage form design. He has successfully completed several industrial and government-funded projects. He has transferred five product technologies to the pharma industry, one of which was released onto the Indian market in 2005. Currently, he is involved in the development of nanotechnology-based commercially feasible products for the treatment of cancer, central nervous system disorders, rheumatoid arthritis (RA), ophthalmic diseases, and skin diseases.

Ms. Srividya Gorantla Biography

Srividya Gorantla completed her M. Pharmacy from Sri Padmavati Mahila Visvavidyalayam (SPMVV), Tirupati, Andhra Pradesh. She has been selected for the DST-INSPIRE fellowship award (INSPIRE Fellowship Registration No. IF190259) during her Ph.D. She has research experience in the development and characterization of lipid-based nanoformulations for topical delivery, ophthalmic delivery, and targeted drug delivery systems for the treatment of rheumatoid arthritis. She has published reviews and research work in reputed international peer-reviewed journals.